

AD-A285 061



DREDGING RESEARCH PROGRAM

TECHNICAL REPORT DRP-94-3

PLUME MEASUREMENT SYSTEM (PLUMES)
CALIBRATION EXPERIMENT

by

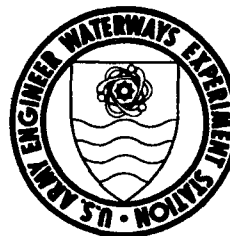
Atle Lohrmann

SonTek, Inc.
7940 Silverton Avenue, No. 105
San Diego, California 92126

and

Craig Huhta

JIMAR
University of Hawaii, Honolulu, Hawaii 96822



August 1994

Final Report

Approved for Public Release; Distribution Unlimited

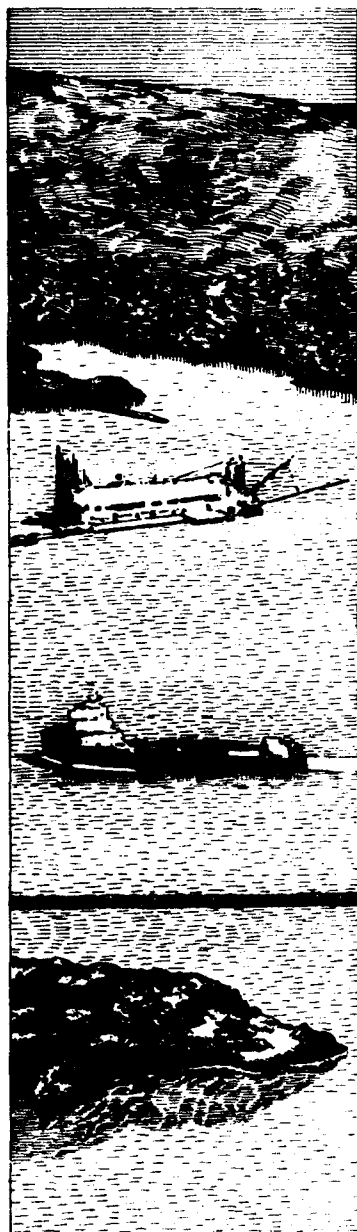
DTIC QUALITY INSPECTED 3

Prepared for DEPARTMENT OF THE ARMY
US Army Corps of Engineers
Washington, DC 20314-1000
Under Work Unit 32464

94 9 28 128



US Army Corps
of Engineers



94-31080



ISPR





US Army Corps
of Engineers
Waterways Experiment
Station

Dredging Research Program Report Summary



Plume Measurement System (PLUMES) Calibration Experiment (TR DRP-94-3)

ISSUE: Conducting dredging and dredged material disposal operations in an environmentally sustainable manner can require addressing issues that involve the amount of sediment in suspension, and the depth, movement, and settling of suspended material clouds. Acoustic instrumentation has been shown to be capable of producing near-synoptic measurements of currents and suspended sediments. Acoustic measurement of currents is well-established and documented. To apply acoustic technology to monitoring suspended sediments at dredging and disposal sites, the relationship between acoustic measurements and suspended sediment concentrations must also be determined.

RESEARCH: One of the primary objectives of the Dredging Research Program (DRP) work unit entitled "Measurement of Entrainment and Transport" is to develop methods, procedures, and equipment for monitoring sediment plumes associated with dredging and dredged material disposal operations in open water. The work unit has developed the acoustic PLUme MEasurement System (PLUMES) for this monitoring. To determine

the relationship between PLUMES acoustic measurements and suspended sediment concentrations, a laboratory sediment calibration experiment was conducted.

SUMMARY: An experimental laboratory study of acoustic backscattering from particles equivalent in size to those commonly found at dredging and dredged material disposal sites was conducted. A calibration chamber was designed and built. Particles were suspended in the chamber, and backscatter and attenuation measurements were made. The experiment was successful for particles ranging in size from 38-850 μm at nominal concentrations of 5 to 1,000 mg/l.

AVAILABILITY OF REPORT: Copies of the report are available through the Interlibrary Loan Service from the U.S. Army Engineer Waterways Experiment Station (WES) Library, telephone number (601) 634-2355. National Technical Information Service (NTIS) report numbers may be requested from WES Librarians. To purchase a copy of the report, call NTIS at (703) 487-4780.

DTIC QUALITY INSURED 3

About the Authors: Mr. Atle Lohmann is the Principal Oceanographer of SonTek, Inc., San Diego, CA. Mr. Craig Huhta is an Instrument Specialist with JIMAR at the University of Hawaii, Honolulu, HI.

Points of Contact: Mr. Michael Tubman, Coastal Engineering Research Center, CERC, Principal Investigator for this work unit; Dr. Billy Johnson, Technical Area Manager, WES.

Plume Measurement System (PLUMES) Calibration Experiment

by **Atle Lohrmann**

**SonTek, Inc.
7940 Silverton Avenue, No. 105
San Diego, CA 92126**

Craig Huhta

**JIMAR
University of Hawaii
Honolulu, HI 96822**

Accession For	
NTIS CRA&I	<input checked="" type="checkbox"/>
DTIC TAB	<input type="checkbox"/>
Unannounced	<input type="checkbox"/>
Justification	
By	
Distribution /	
Availability Codes	
Dist	Avail and/or Special
A-1	

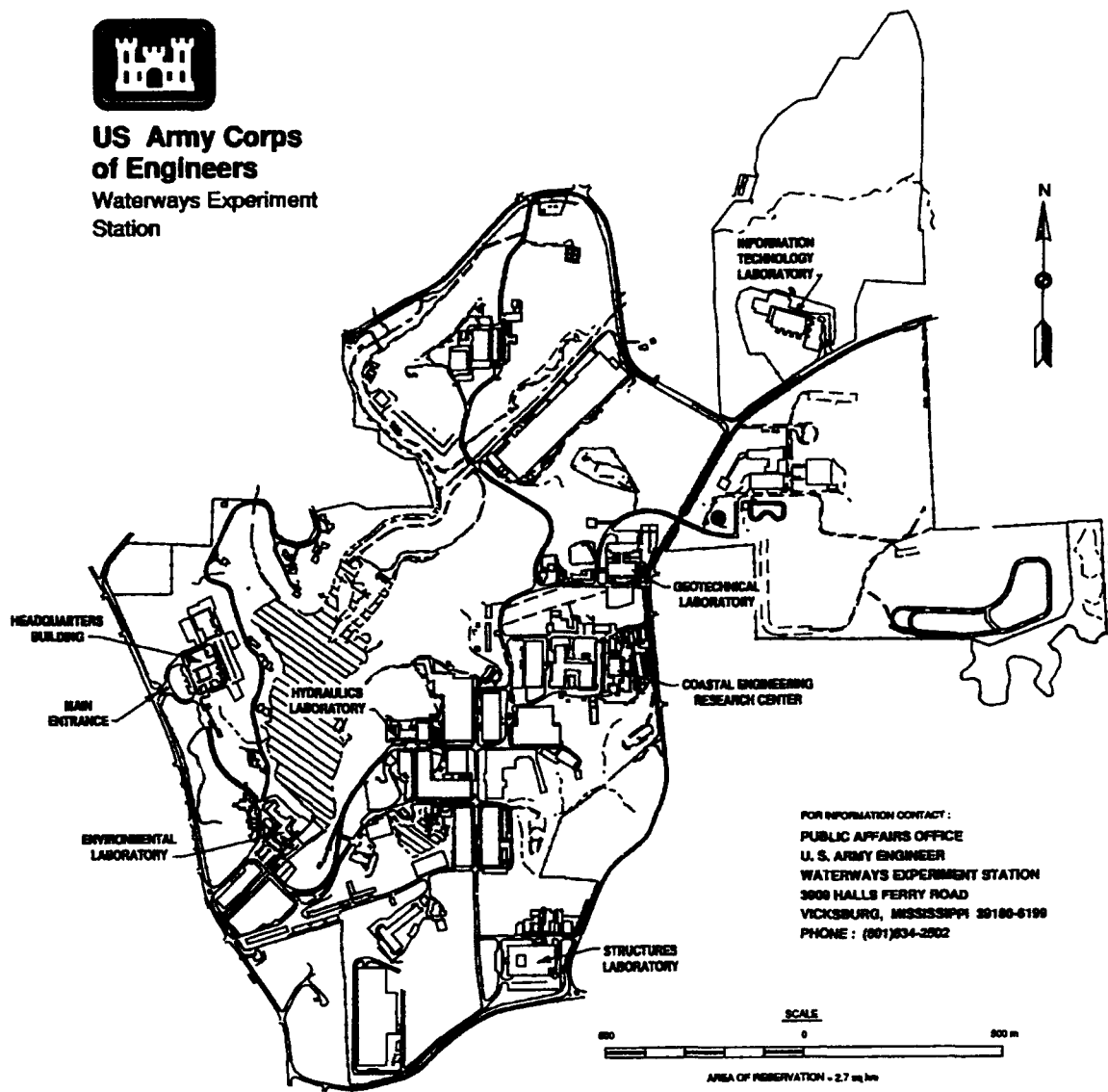
Final report

Approved for public release; distribution is unlimited

**Prepared for U.S. Army Corps of Engineers
Washington, DC 20314-1000**



**US Army Corps
of Engineers**
Waterways Experiment
Station



Waterways Experiment Station Cataloging-in-Publication Data

Lohrmann, Atle.

Plume Measurement System (PLUMES) calibration experiment / by
Atle Lohrmann, Craig Huhta ; prepared for U.S. Army Corps of
Engineers.

152 p. : ill. ; 28 cm. — (Technical report ; DRP-94-3)

Includes bibliographic references.

1. Suspended sediments — Measurement — Instruments. 2.
Dredging — Environmental aspects. 3. Acoustooptical devices — Cali-
bration. 4. Backscattering. I. Huhta, Craig. II. United States. Army.
Corps of Engineers. III. U.S. Army Engineer Waterways Experiment Sta-
tion. IV. Dredging Research Program. V. Title. VI. Series: Technical re-
port (U.S. Army Engineer Waterways Experiment Station) ; DRP-94-3.
TA7 W34 no.DRP-94-3

Contents

Preface	vii
1—Introduction	1
2—Description of Calibration Experiment	3
Calibration Chamber	3
Nominal Sediment Concentration	4
Separating Uniform Size Classes	5
Sediment Sample Preparation	6
Experimental Procedure	7
Water Sampling	7
Gravimetric Analysis	8
Description of Acoustic Systems	8
3—Experimental Accuracy and Repeatability	11
Uniform Concentration	11
Repeatability - Acoustics	15
Repeatability - Gravimetric Analysis	18
Repeatability - Water Sampling	21
Acoustic Contamination	24
Special Problems	25
4—Calibration	29
Modelling	30
Near Field	34
Receiver Response	38
Transmit and Receive Calibration	41
5—Data Analysis	46
Data Processing	46
Scattering Models	52
Model Comparisons	54
6—Conclusions	59
Main Results	59

Acknowledgements	60
References	61
Appendix A: File Summary Tables and Slope Information	A1
Appendix B: Uncorrected Mean Scattering Profiles	B1
Appendix C: Corrected Mean Scattering Profiles and Concentration	C1
SF 298	

Preface

The experiment described herein was conducted at RD Flow, Inc. in San Diego, CA, under contract with the Coastal Engineering Research Center (CERC), U.S. Army Engineer Waterways Experiment Station (WES). The work was performed under the Measurement of Entrainment and Transport Work Unit 32464 of DRP Technical Area 1 (TA1), "Analysis of Dredged Material Placed in Open Water." Messrs. Robert H. Campbell and Glenn R. Drummond were the HQUSACE Chief and TA1 Technical Monitors, respectively, for the DRP. Mr. E. Clark McNair, Jr., CERC, was the DRP Program Manager (PM), and Dr. Lyndell Z. Hales, CERC, was Assistant PM. Ms. Michelle M. Thevenot, CERC, was Principal Investigator of Work Unit 32464, and Dr. Nicholas C. Kraus was the TA1 Manager during the conduct of the experiment and preparation of the report. Mr. Michael Tubman was Principal Investigator of Work Unit 32464 during the editing of the final report.

Ms. Thevenot was under the general supervision of Mr. Bruce A. Ebersole, Chief, CPB. Mr. Tubman was under the direct supervision of William L. Preslan. This study was conducted under the general supervision of Dr. James R. Houston, Director, CERC, and Messrs. Charles C. Calhoun, Jr., Assistant Director, CERC, H. Lee Butler, Chief, RD, CERC, and Thomas W. Richardson.

At the time of publication of this report, Director of WES was Dr. Robert W. Whalin. Commander was COL Bruce K. Howard, EN.

For further information on this report or on the Dredging Research Program, contact Mr. E. Clark McNair, Jr., Program Manager, at (601) 634-2070.

The contents of this report are not to be used for advertising, publication, or promotional purposes. Citation of trade names does not constitute an official endorsement or approval of the use of such commercial products.

1 Introduction

The purpose of the Plume Measurement System (PLUMES) project is to develop instrumentation that can help determine the fate of sediments discharged during dredging and dredged material disposal operations. PLUMES uses acoustic backscatter instruments to provide near-synoptic data on the three-dimensional spatial distribution of suspended sediment. Advantages of acoustic systems in this context are: a) they are remote sensing and thereby non-interfering, b) they have long ranges (10-100 m), and c) they are suitable for mounting on surface vessels. The information provided by these systems is a significant improvement on that obtained using only water sampling and single-point measurement devices.

The disadvantage of using acoustic backscatter systems is that the backscattered signal is not a direct measurement of the concentration of suspended sediments. Instead, the strength of the backscattered signal is a function of size, density, and elasticity of the material. Size dependency poses the greatest problem since, unlike the density and elasticity of the sediment, it can rarely be determined a priori. The distribution of the sizes of sediment particles in suspension can exhibit temporal and spatial variations that undermine key assumptions incorporated in the equations used to calculate concentration.

To determine the relationship between PLUMES acoustic measurements and suspended sediment concentrations, a sediment calibration experiment was undertaken by RD Flow at their facility in San Diego, CA. A sediment calibration chamber was built, along with a pool for transducer calibration. Sand crystals and glass beads were sieved into different size classes and suspended in the sediment calibration chamber, at different concentration levels. The water was ensonified with short acoustic pulses at two frequencies (600 kHz and 2 MHz) and acoustic backscatter was measured. Acoustic backscatter was related to measurements of suspended sediment concentration in the chamber determined using water samples drawn from the chamber.

Details of the experimental setup and procedures are described in Chapter 2. Repeatability of the experiments and validity of the results are described in Chapter 3. In Chapter 4, the range calibration, including a numerical model to describe the acoustic near field, as well as the transmit

and receive calibrations of the systems, are described. In Chapter 5, the results of the calibration experiment are presented. Descriptions of how data were prepared and presented for analysis are given, along with example presentations. Complete data presentations are in Appendixes A, B, and C. Descriptions include details of the data processing procedures, as well as comparisons of the results with scattering models. Finally, in Chapter 6, main findings are summarized and implications for the performance of the PLUMES system in typical monitoring situations are discussed.

2 Description of Calibration Experiment

This chapter describes the calibration facility and the experimental procedures, with reference to the considerations that went into their design. The first two subsections give an overview of the calibration chamber and its characteristics. The remaining subsections describe the calibration procedures.

Calibration Chamber

The primary requirement for the design of the calibration facility was to create a region of uniformly distributed sediment over a sufficiently large volume for the instruments to make accurate measurements without being affected by the walls of the chamber. This was accomplished by taking advantage of the narrow beam width of the acoustic systems and the predictable fall velocities of the particles. Figure 1 shows a general overview of the calibration chamber. It is constructed from a piece of clear cast acrylic tubing 8 ft tall (2.4 m), with an outer diameter of 18 in. (0.46 m), and a wall thickness of 1/4 in. (6.4 mm). Sediments were injected at the top of the tube, fell through the water column to the bottom, and then were pumped back up to the inlets at the top. The bottom of the tube is fitted with a funnel that channels the sediment into a small tube for pumping. The sediment and water were pumped through 1/2-in. (12.7-mm) tubing, using a peristaltic pump to avoid entrainment of air into the circulation system.

At the top of the tank, the main return line is split into four separate lines and directed into the tank as shown in Figure 2. The pumping velocity in the main return line is about 1.7 m/sec. The main return line splits into four separate lines

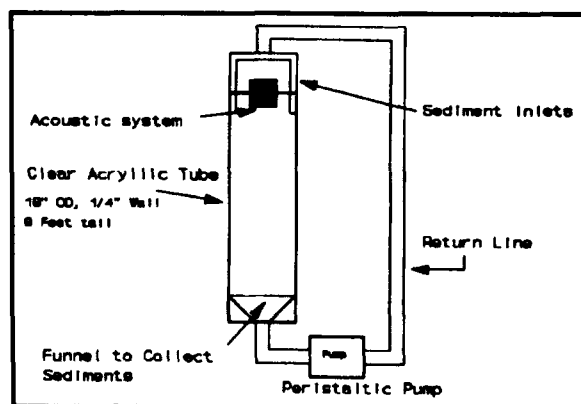


Figure 1. Overview of the calibration facility

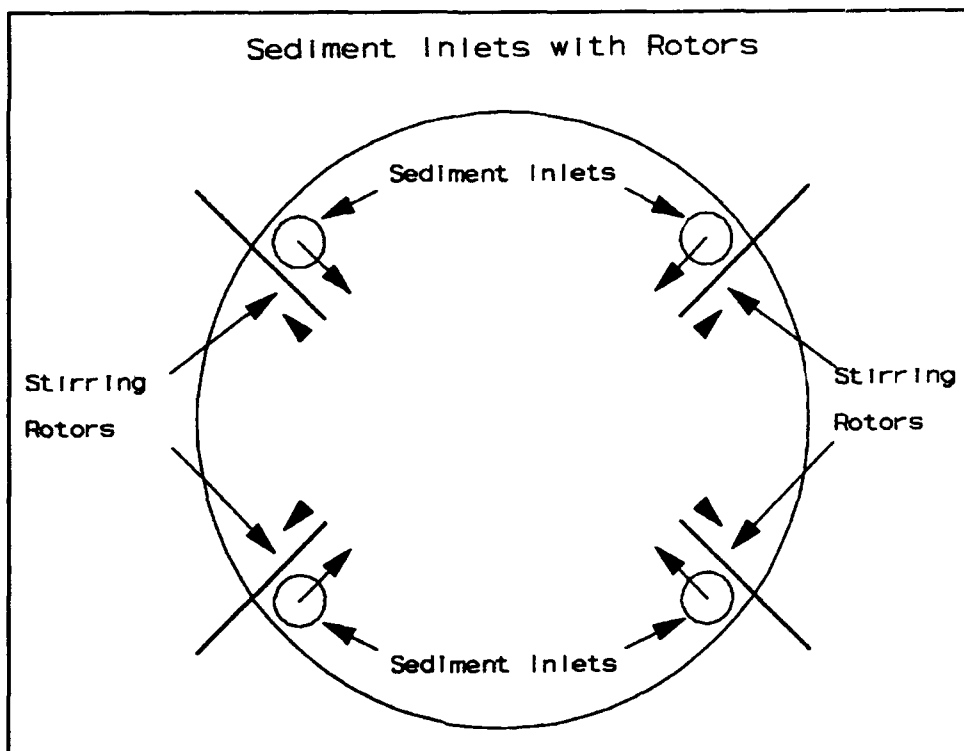


Figure 2. Calibration chamber recirculating and stirring system

feeding into four inlets at the top of the tank. The ends of these four inlets are 80 percent blocked to increase the velocity of the sediments at the inlets and thereby create more uniform mixing. When calibration runs were done using larger particles (greater than $150\ \mu\text{m}$), additional mixing was required. This was accomplished by using four mechanical rotors inserted next to each of the inlet tubes. These rotors produced a nearly uniform distribution of particles up to $850\ \mu\text{m}$ in diameter.

In addition to the normal sediment return line, the tank has a set of filters that can be switched in line to remove sediment from the system when data collection is complete. These are placed immediately after the pump, and controlled by a set of Y-valves. Filtering time varies with sediment size and type, requiring from 30 min to as long as 8 hr.

Nominal Sediment Concentration

The calibration facility is a closed system, mass is conserved, and concentration can be estimated using the geometry of the tank, the sediment fall velocities, and the flow velocity in the main return line. These parameters are described in Table 1.

Table 1 Calibration Chamber Parameters		
Parameter	Description	Value
A_1	Cross-sectional area of acrylic pipe	0.155 m ²
L_1	Effective length of acrylic pipe	2.35 m
V_1	Sediment fall velocity	0.9 cm/sec
A_2	Cross-sectional area of main return line	1.27 cm ²
L_2	Effective length of return line	7.32 m
V_2	Sediment velocity in main return line	1.7 m/sec
C_1	Sediment concentration in calibration chamber	0-2,000 mg/l

For the calibration facility, conservation of mass includes the requirement that no sediment is trapped in the system. An estimate of the concentration in the chamber can be made by assuming that the tank reaches an equilibrium where the sediment flux across any cross section is constant. If M is the total mass of sediment added, the estimated (or nominal) concentration can be expressed as:

$$C_1 = \frac{M}{(A_1) * (L_1 + L_2 * \frac{V_1}{V_2})} \quad (1)$$

where the dimensions of the subscripted parameters are given in Table 1. Equation 1 provides a general relationship between sediments added and concentration in the tank. It is sufficiently accurate to provide a guideline for how much material should be added to reach a desired concentration. To accurately measure the sediment concentrations in the calibration chamber, a pump-out water sampling system was used to provide water samples for gravimetric determination of sediment concentration. The pump-out system is described in the section titled "Water Sampling" in Chapter 2 and the section titled "Repeatability Gravimetric Analysis" in Chapter 3. Chapter 3 presents comparisons between nominal and measured concentrations for different types of sediments.

Separating Uniform Size Classes

A motorized sieving system, model CL-305A, made by Soiltest Inc., was used to separate the material into uniform size classes. Fourteen sieve sizes were used. A summary of materials and size classes tested is given in Table 2.

Table 2
Types and Classes of Materials Tested

Material	Size Classes, μm
Crystal White Silica Sand ("CWSS")	600-850 500-600 355-500 300-355 212-300 180-212 125-180 106-125 75-106
Sil-Co-Sil Ground Silica ("Silica")	125-180 75-106 63- 75 45- 63 38- 45
Glass Spheres ("Glass Beads" or "Beads")	590-840 500-600 355-500 300-355 210-297 149-210 105-149 74-105 53- 74 45- 53 38- 45

The two types of silica described in Table 2 were obtained from different manufacturers, and, before sieving, had different size distributions. After sieving, overlapping size classes were used for comparison. For the glass spheres, the original manufacturers' size classes were used with additional classes created by sieving.

When sieving material, up to six sieves were used at one time, stacked up in order of increasing size. A small amount of material (typically 150 g) was placed in the top (largest) sieve, and the machine ran for 10 to 15 min. The material was removed and stored by size class. Each sieve was brushed to remove trapped particles every time it was used. Sieving followed procedures recommended by the American Society for Testing and Materials.

Sediment Sample Preparation

Early experiments showed that adding sediments directly to the tank did not produce repeatable results. Small air bubbles entrained with the particles affected the acoustic measurements. A standard procedure was developed to prepare samples before they were added to the chamber.

First, the desired mass of a particular size class was weighed and added to a cup of water. The mixture was stirred thoroughly, then placed in a vacuum chamber for 5 min. The vacuum chamber was kept at approximately 29 in. (73.7 cm) of mercury, enough to vigorously boil the water without losing material. The samples were then added to the tank. Typically, all samples for a particular type and size class were prepared at the beginning of an experiment, then added as needed over the course of the experiment. For very fine sediments (less than 38 μm), the samples would be added to an electric blender and gently stirred to break up larger groups, then degassed for a period of 10 min. After degassing they were gently stirred in the blender, taking care not to entrain air into the mixture. Several experiments were performed with the fine sediments before determining that this procedure gave the most repeatable results.

Experimental Procedure

Table 3 shows the standard masses added for all sediment types, along with the nominal concentrations. These weights were used on all runs, except when there was insufficient material to achieve the highest concentrations. For some sediment types, particularly very small grain sizes, the concentrations were taken to a higher level than stated in the table.

Table 3 Standard Amounts of Sediments Added During Runs			
Run	Sediment Added, g	Total Sediment, g	Nominal Concentration, mg/l
00	0	0	0
01	2	2	5
02	3	5	13
03	5	10	25
04	10	20	50
05	30	50	125
06	50	100	250
07	100	200	500
08	200	400	1,000

Every run began with data collection in a clear tank, first with the 600-kHz system and then with the 2-MHz system. Both the backscatter and the reflected signal from the bottom of the tank were recorded. In addition, a water sample was collected to provide a background check of the concentration. Sediment was then added to the top of the tank, and allowed to mix and reach equilibrium after a period of between 10 and 25 min, depending on size and type. Another data set was then recorded, and a water sample collected. The procedure was repeated for all concentration levels. Each complete cycle of nine runs typically took 3 to 5 hr.

Water Sampling

Each water sample contained 4 L of water. Since the smallest nominal concentration was 5 mg/l, a 4-l sample had about 20 mg of sediment, allowing for reasonably accurate gravimetric analysis.

The samples were drawn through a 1/4-in. (6.4-mm) inner diameter J-tube placed approximately 1 in. (2.54 cm) from the center axis of the tank, approximately 0.7 m above the bottom, using a self-priming

peristaltic pump with approximately 2.8 l/min capacity. The J-tube ensures that the inlet to the tube is oriented into the direction of fall of the particles (Figure 3). The pump produces a fluid and sediment velocity in the tube of approximately 1.7 m/sec, sufficiently high to ensure accurate sampling (see the section titled "Repeatability - Gravimetric Analysis" in Chapter 3). After a 4-l sample was drawn from the tank, the sediment was allowed to settle. For larger sediments, excess water was poured off and the sediment was transferred to smaller containers. For smaller sediments (i.e., less than 75 μm), the samples were processed directly from the 4-l containers.

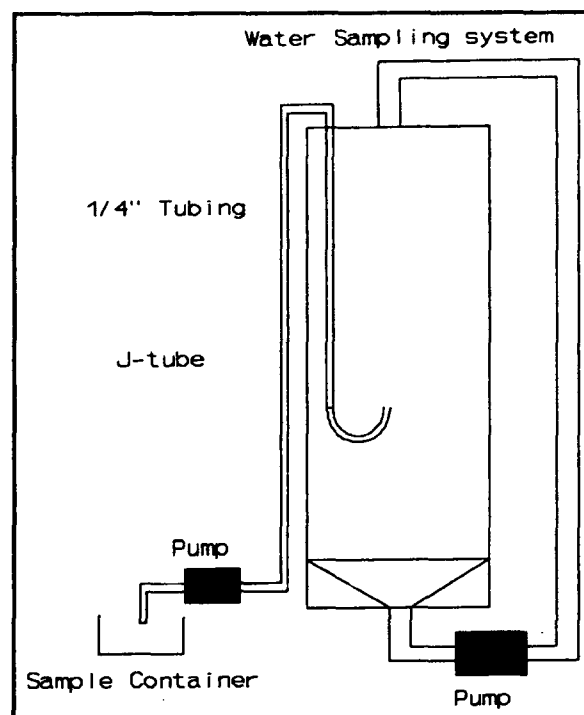


Figure 3. Overview of water-sampling system

Gravimetric Analysis

The samples were filtered through preweighed glass fiber filter paper manufactured for gravimetric analysis. Each filter was dried and weighed to determine total mass. A dual-range balance was used, with a stated accuracy of 1 mg for a maximum capacity of 40 g, and a stated accuracy of 10 mg for a maximum capacity of 400 g. Accuracy and repeatability of the analysis are discussed in the section titled "Repeatability - Water Sampling" in Chapter 3. Samples were typically processed within 48 hr of data collection.

Description of Acoustic Systems

Backscatter data were collected by the two acoustic systems. The 600-kHz system's actual operating frequency was 614.4 kHz. The systems used different signal processing schemes and transmit pulse configurations. System parameters are summarized in Table 4.

Table 4
System Parameters for the Two Acoustic Systems Used During the PLUMES Calibration Experiment

System Property	600-kHz System	2-MHz System
Frequency	614,400 Hz	2,000,000 Hz
Ceramic diameter	10.16 cm	3.175 cm
Beam width	1.46 deg	1.56 deg
Processing circuitry	Linear amplifier with A/D board	RSSI logarithmic processor
Dynamic range	100 dB total; 40 dB per data set	70 dB total; 70 dB per data set
Transmit code element length	2 carrier cycles (3.26 μ sec)	16 carrier cycles (8 μ sec)
Transmit pulse - backscatter mode	6.51 μ sec (2 code elements)	8 μ sec (1 code element)
Transmit pulse - attenuation mode	208 μ sec (64 code elements)	112 μ sec (14 code elements)

The 600-kHz system has a single circular transducer with a diameter of 10.16 cm, profiling vertically along the tank axis. This system collects vertical profiles of data in two transmit configurations. The two configurations are referred to as backscatter and bottom attenuation modes. In the backscatter mode, the system transmits two in-phase code elements (four carrier cycles, or 6.51 μ sec at 614.4 kHz), providing high resolution backscatter data. In the bottom attenuation mode, a resistor is used in line with the transmit pulse to reduce transmit power by approximately 35 dB, allowing the system to measure the bottom return without hard limiting. For bottom measurements, the system transmits 64 in-phase code elements (creating a total pulse length of 208 μ sec) to produce a repeatable and stable bottom return. This mode was included in the experiment to make a direct measurement of the attenuation of the acoustic signal in the tank. The section titled "Correction for particle attenuation" in Chapter 5 describes how attenuation data were used to correct the backscatter measurements. The section titled "Receiver Response" in Chapter 4 provides a detailed description of the processing circuitry. A detailed description of code elements and the acoustic signal, applicable to both systems, can be found in Brumley et. al. (1991).

Data from the 600-kHz system were processed to produce records of the relative backscatter level. First the raw 600-kHz data, sampled at 2 MHz, were reduced using a simple RMS filter to either 5-cm bins (for the backscatter profile), or 1-cm bins (to allow sufficient resolution of the bottom return). RMS levels were adjusted to account for the pre-amplifier gain setting and the sensitivity of the analog to digital (A/D) converter board. Linear profiles were averaged to produce a mean profile, and then converted to a decibel (dB) scale.

The 2-MHz system also has a single circular transducer. The diameter of the ceramic is 3.175 cm. As with the 600-kHz system, the 2-MHz system collects data in two different transmit configurations: the backscatter profile mode and the bottom attenuation. In the backscatter mode, the system alternates between a single code element pulse (1 code element equals 16 carrier cycles, or 8 sec at 2.00 MHz) for fine resolution backscatter information, and a series of two single pulses separated by a time lag to allow for Doppler velocity calculations. In the bottom attenuation mode, a 14-code element (112- μ sec) pulse produces a reproducible bottom return. Again, the bottom return is a measure of the integrated attenuation in the tank. The 2-MHz receiver circuitry provides amplitude information in logarithmic units every 16 μ sec, corresponding to 1.18-cm vertical resolution. Data from the 2-MHz system were stored in 1.18-cm increments in units of dB. Circuitry is described in detail in the section titled "Receiver Response" in Chapter 4.

3 Experimental Accuracy and Repeatability

Uniform Concentration

The primary concern at the beginning of the calibration experiment was whether uniform distributions of particles could be produced in the calibration chamber. For the larger particles, significant spatial variations in concentration were visually observed in early runs and a significant amount of time was spent rectifying the situation.

The first time large particles were used, visual and acoustical observations of the concentration distributions in the calibration chamber showed the situation to be unacceptable. Figure 4 shows the acoustic signature of what was observed. The figure shows the average (100 pings) signal levels on top of an "ideal" curve, representing an empirical model of the

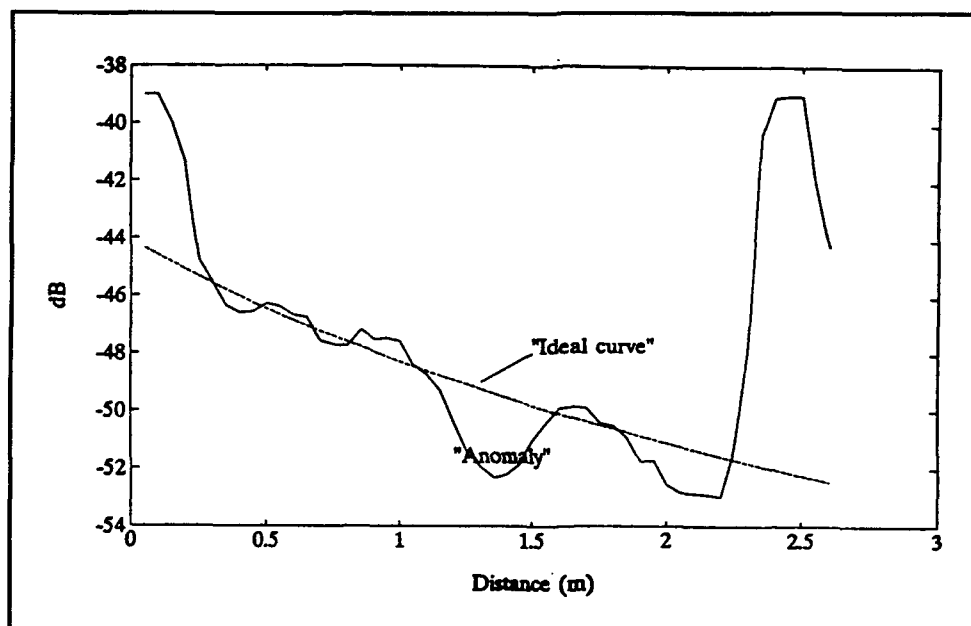


Figure 4. Initial anomalies in the intensity profile

transmission losses due to spreading and water absorption, but does not include particle attenuation (see the section titled "Modelling" in Chapter 4 for a discussion of the loss mechanisms). The figure shows anomalous "dips" in the measured vertical profile, representing significant vertical variations in the particle concentration along the center line of the calibration chamber. It was hypothesized that the inhomogeneous distribution was caused by a helical circulation pattern set up by the inlet jets.

Two experiments were conducted to test this hypothesis. In the first experiment, different inlet configurations were tried (500 pings for each of five different jet configurations). Each jet configuration either had a different orifice size (the larger the opening, the lower the inlet velocity) or the jets were pointing in slightly different directions. Every 500-ping file was separated into five ensembles of 100 pings each and the results are plotted in Figure 5. Data from each jet configuration have been offset by 15 dB in the plot. As can be seen in the figure, configurations 1 and 2 show strong anomalous areas between 50 and 150 cm from the transducer, whereas configurations 3-5 seem to be relatively stable and have a shape in general agreement with the "ideal" curve shown in Figure 4.

The second test looked at the temporal evolution of the scattering level in the calibration chamber. Five 300-ping data files were collected over a period of 30 min without changing the concentration or the jet configuration. The jets were set to minimize variations along the center line; these are referred to as "centered jets." In the time period between 30 and 45 min into the run, two additional 300-ping files were collected with a jet configuration known to create a helical circulation pattern; these are referred to as "skewed jets." After offsetting the two last runs from the first

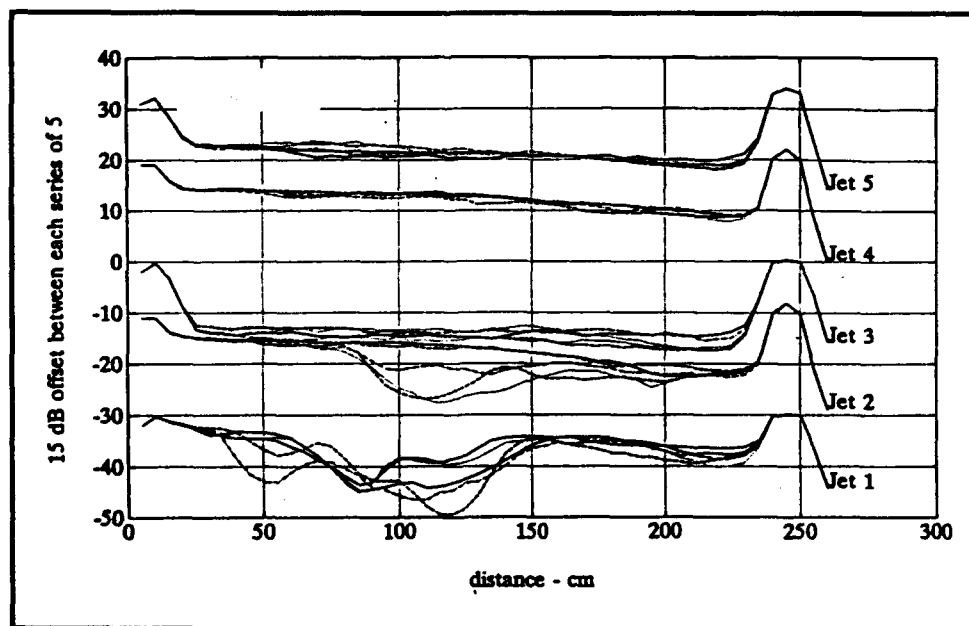


Figure 5. Five 100-ping ensembles collected with five different jet configurations

five runs by 10 dB, the data were plotted in Figure 6. In the first set of fifteen 100-ping averages with centered jets, only one profile (the last one) shows an indication of the "anomaly" around 80-100 cm from the transducer, whereas all six profiles taken with skewed jets show strong vertical variations.

The results of these two tests support the hypothesis that the inhomogeneous concentration distribution in the calibration chamber was caused by a helical circulation pattern set up by the inlet jets. To remedy the situation, mixing of sediments and water near the inlets needed to be increased without adversely affecting acoustic backscatter. After some preliminary experiments with different types of rotors, one electrical rotor was placed in front of each of the four inlets (Figure 2). With the rotors there was an immediate improvement in the distribution of the larger particles. The previously observed spatial patterns became much weaker, both as measured acoustically and as visually observed. On the negative side, it was noted that the electronic noise level went up by several dB for both systems (600-kHz, 2.5 dB; 2-MHz, 7 dB), and the rotors introduced additional contaminating particles. To minimize the adverse effect of the added noise, the rotors were not used for the smallest particles. Fortunately, the rotors were not needed for the smaller particles, because the lower fall velocities of the smaller particles (less than 150 μm) allowed the particles more time to disperse, creating a uniform sediment concentration distribution without using rotors.

The effectiveness of the system, reconfigured to include rotors in front of the inlet jets, was formally tested using silica sand of size 212-300 μm . Runs made with and without rotors were compared; these are shown in

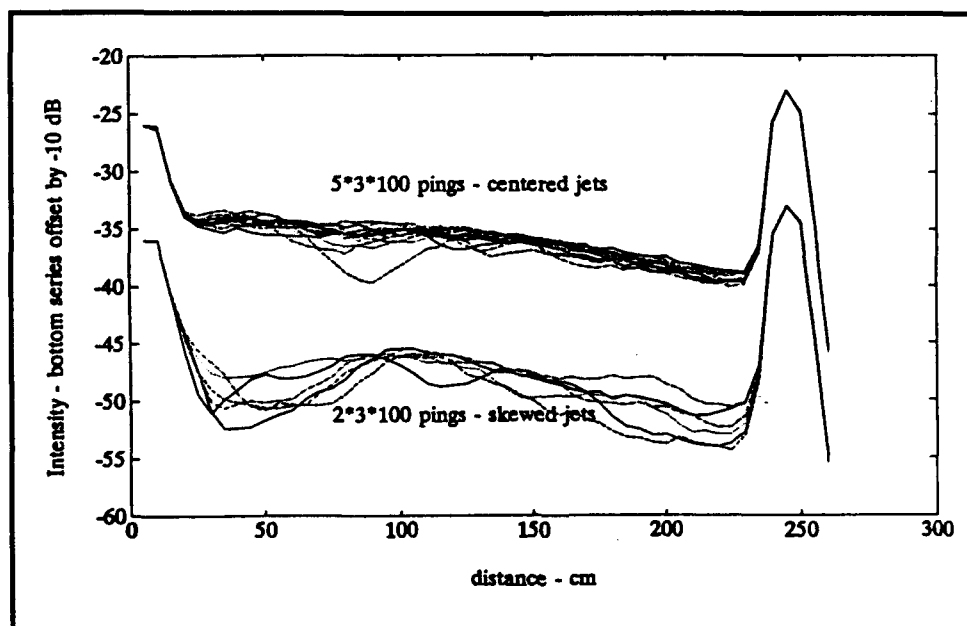


Figure 6. Data in upper half collected before inlets were skewed (data in lower half)

Figures 7 and 8. The runs were carried out in exactly the same way, using eight different concentrations varying from approximately 5 mg/l to 1,000 mg/l. Vertical profiles for each of the eight runs are shown in the figures. The figures show that the large anomalies present in the calibration chamber without rotors are no longer detectable when the rotors are used. It was concluded that the rotors effectively distribute the sediment uniformly in the calibration chamber.

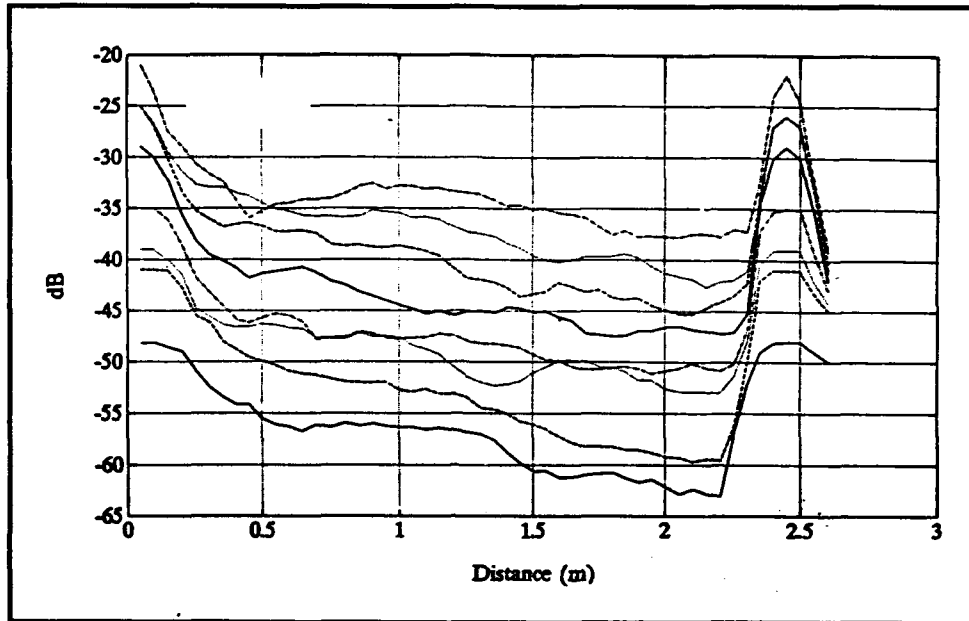


Figure 7. M17 Run A (600 kHz), 212-μm crystal white silica, no rotors

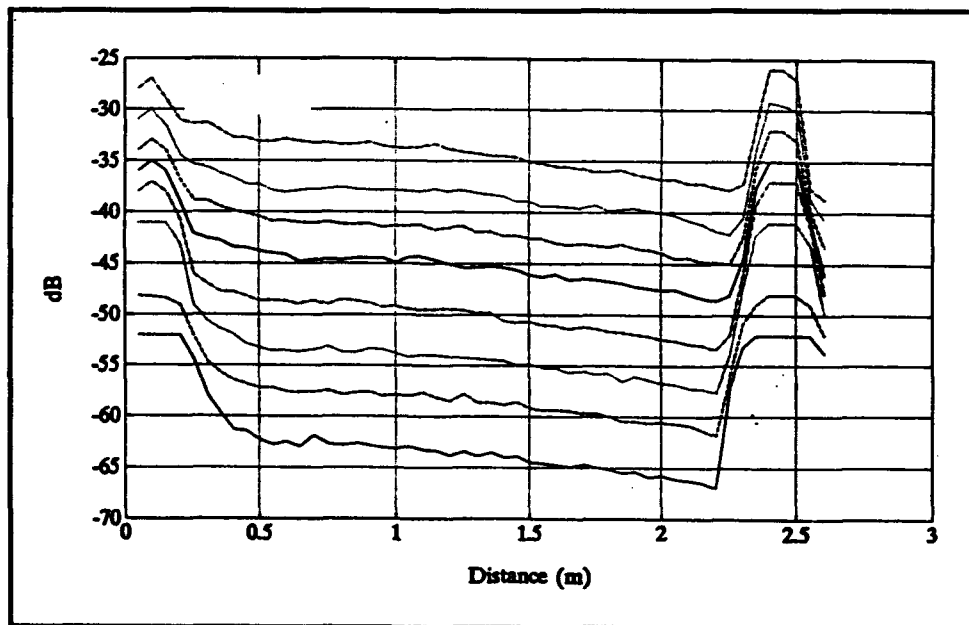


Figure 8. M17 Run A (600 kHz), 212-μm crystal white silica, rotors operating

Repeatability - Acoustics

A consequence of the limited time available to complete the calibration experiment was that the repeatability issue had to be addressed through a series of select tests rather than by reproducing every run. The identified areas of concern were (a) questions about the required waiting period before starting data collection, (b) temporal stability of the acoustic data, (c) sensitivity to transducer mounting position, and (d) repeatability of a complete run.

Temporal stability

An average backscatter profile was derived from a statistical mean of 100 ping ensembles (for a more complete description of data processing, see the section titled "Mean profiles" in Chapter 5). When the propellers were operating, intensity data were collected 10 min after the particles were added. For smaller particles, this waiting period was extended to between 15 and 25 min.

To test if the intensity profiles remained constant over time, a special test using 212- μm sand with the 600-kHz system was designed and carried out. First, a background data set was collected. Then, 20 g of sand were added to the calibration chamber and twelve 100-ping data sets were collected at 10-min intervals. Each 100-ping ensemble was averaged without range-dependent corrections (i.e., spreading, absorption, and attenuation). The mean profile from each of the 13 data sets is plotted in Figure 9. The figure shows that the 12 data sets collected with constant concentration

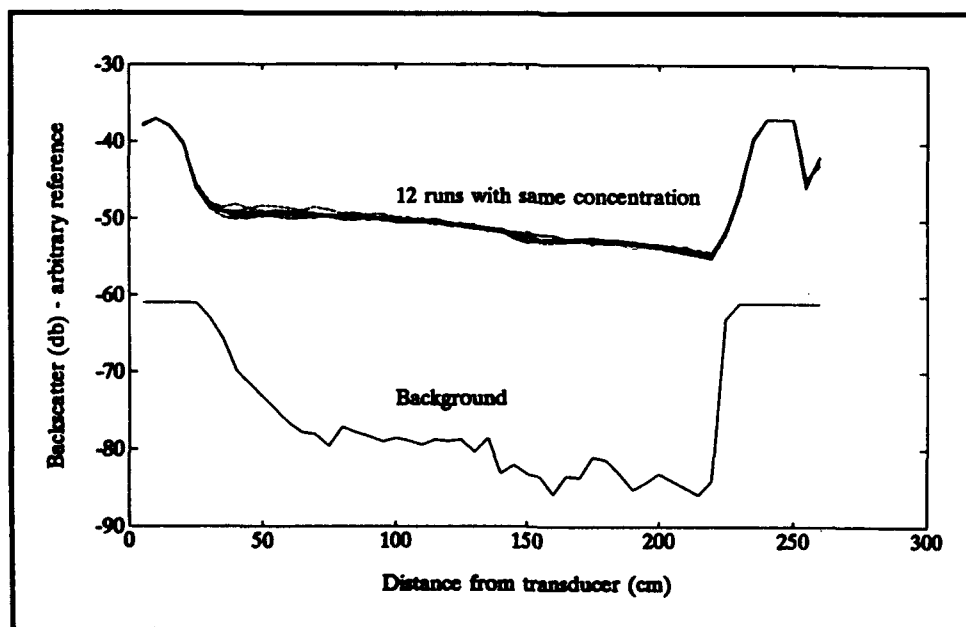


Figure 9. Temporal variation in the mean signal level (fixed amount of sand)

varied little in concentration over the 2-hr period. In Figure 10, each of the mean vertical profiles has been averaged over three range intervals (50-100 cm, 100-150 cm, and 150-200 cm). The three time series show no systematic trend and the standard deviation of the 12 data sets is less than 0.25 dB. It was concluded that a waiting period of 10-25 min is sufficient to reach a stable particle distribution.

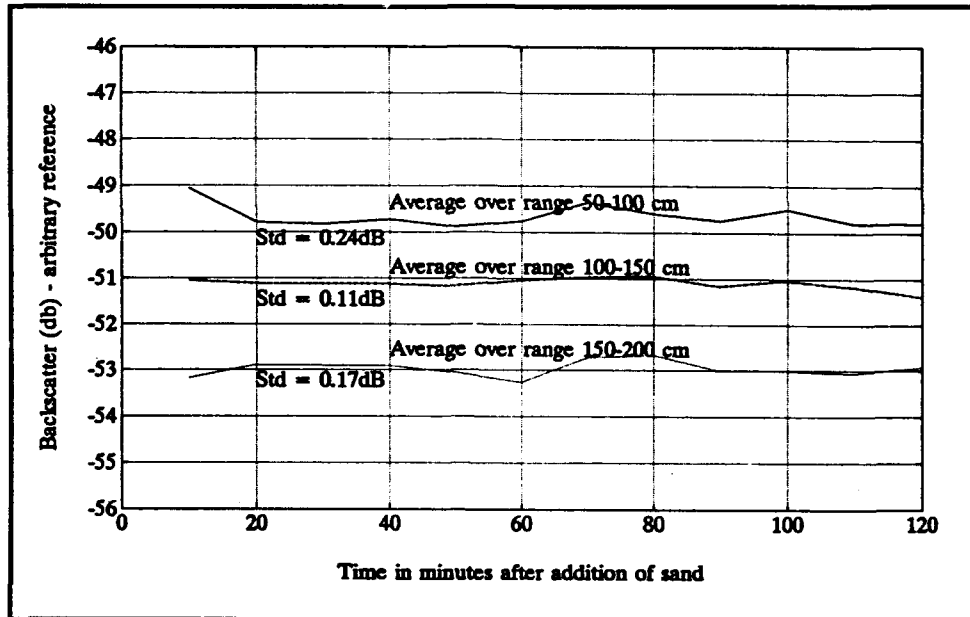


Figure 10. Standard deviation of the vertically averaged ensembles (fixed amount of sand)

Sensitivity to mounting position

The 600-kHz and 2-MHz transducers were removed and installed each time particles were added to the tank. Mounting fixtures were constructed in order to ensure repeatable positions, within 0.25 cm or ± 0.5 deg. To verify that the data are not sensitive to the exact position of the transducer, nine data sets at constant concentration were collected as the position of the 2-MHz transducer was systematically changed. For each of the nine configurations shown in Table 5, 100 pings were collected.

Table 5
Position of Transducer During
Mounting Test

Run Number	2-MHz Mounting Position
1	Transducer on center line
2	Transducer 1.25 cm off center line
3	Transducer 2.50 cm off center line
4	Transducer 3.75 cm off center line
5	Transducer 5.00 cm off center line
6	Transducer 6.25 cm off center line
7	Transducer 7.50 cm off center line
8	Transducer on center line, tilted 3
9	Transducer on center line, tilted 6

The vertical profiles derived when averaging over 100 pings are shown in Figure 11. For each run, the average scattering level (between 50 and 150 cm) was averaged and plotted in Figure 12. This figure shows the variation with transducer position to be small and the standard deviation between the runs to be 0.32 dB. It was concluded that backscatter data are unaffected by small changes in transducer position.

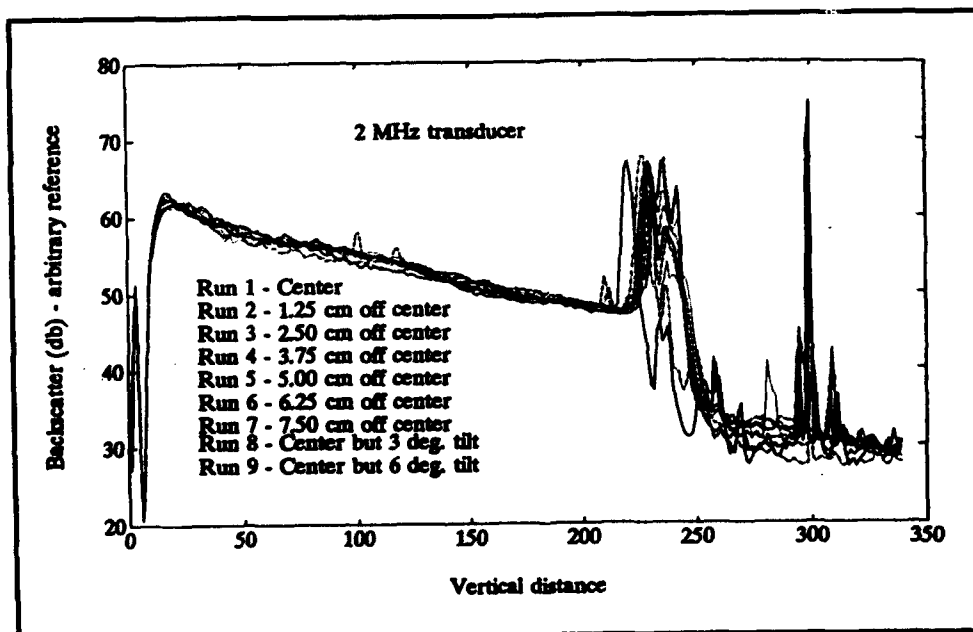


Figure 11. Variation in the mean signal level when the transducer position is changed

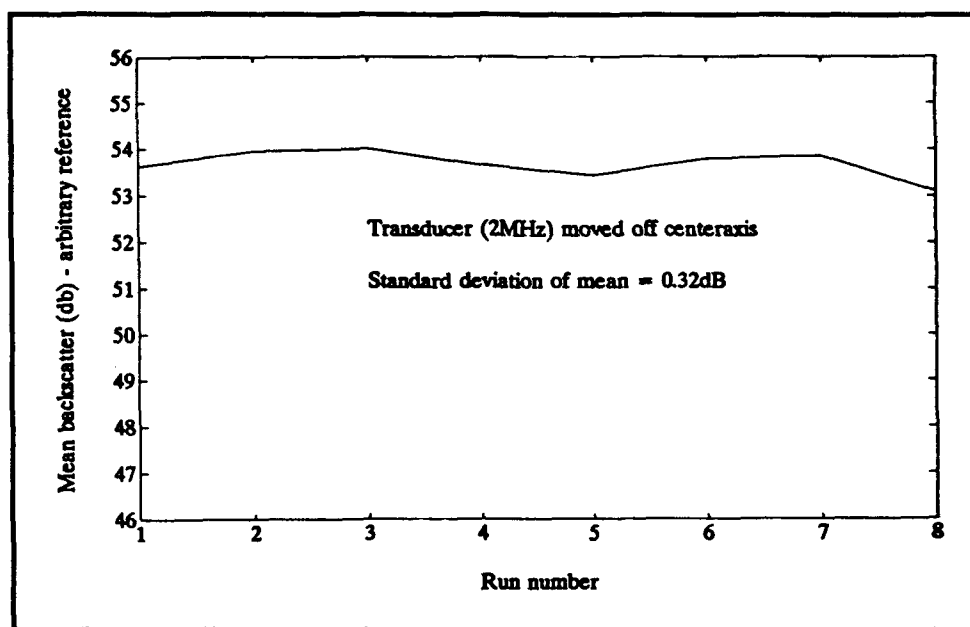


Figure 12. Standard deviation of the vertically averaged ensembles (changing transducer position)

Repeatability of a complete run

To determine whether results were repeatable, a "double run" was carried out with 212- to 300- μm silica sand. During this run, data were collected at each concentration, first with the 600-kHz system, then with the 2-MHz system, followed by a water sample, then at 600 kHz and again at 2 MHz, followed by a second water sample. This procedure was carried out for a full run (eight different concentrations) and generated two sets of backscatter data for each frequency. Results are shown in Figures 13 and 14; they show minimal backscatter variations.

In addition to the double run, two full runs with 212- to 300- μm sand were carried out on two different days with different persons operating the tank. The results of the test are shown in Figures 15 and 16 for the two acoustic systems. The relatively small variations in the acoustic scattering level support the conclusion that the acoustic measurements are repeatable, well within the overall project specification of 3 dB. Similar tests were conducted for very fine particles (less than 10 μm), with unusual results. These results are discussed in the section titled "Fine sediments."

Repeatability - Gravimetric Analysis

Using preweighed glass fiber filter paper recommended for gravimetric analysis, the samples were filtered, dried, and weighed to determine total mass. Numerous tests of the sample processing were performed with known amounts of sediment to determine its accuracy and repeatability

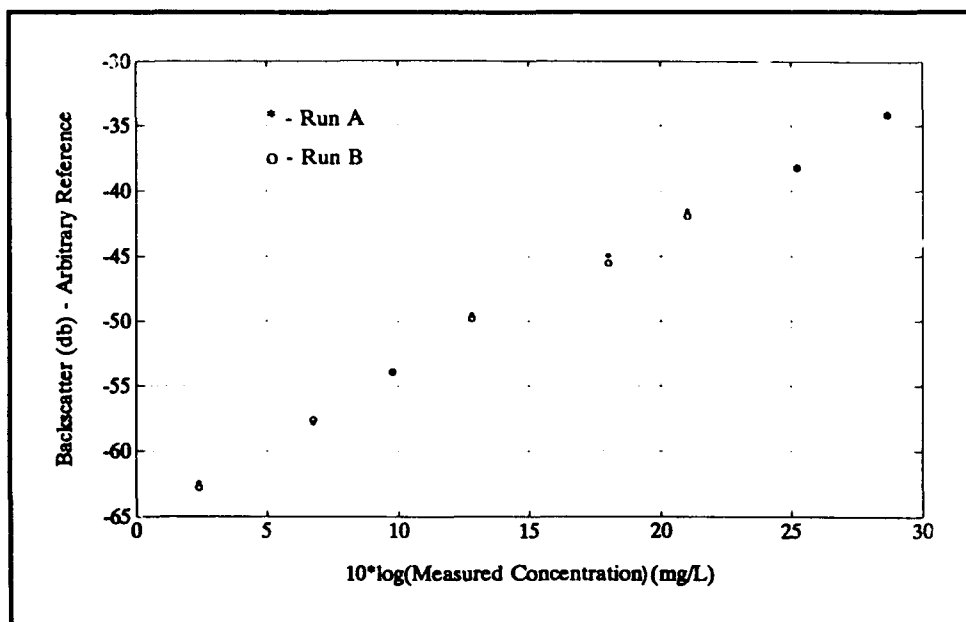


Figure 13. Repeatability test, 600 kHz - "Double run"

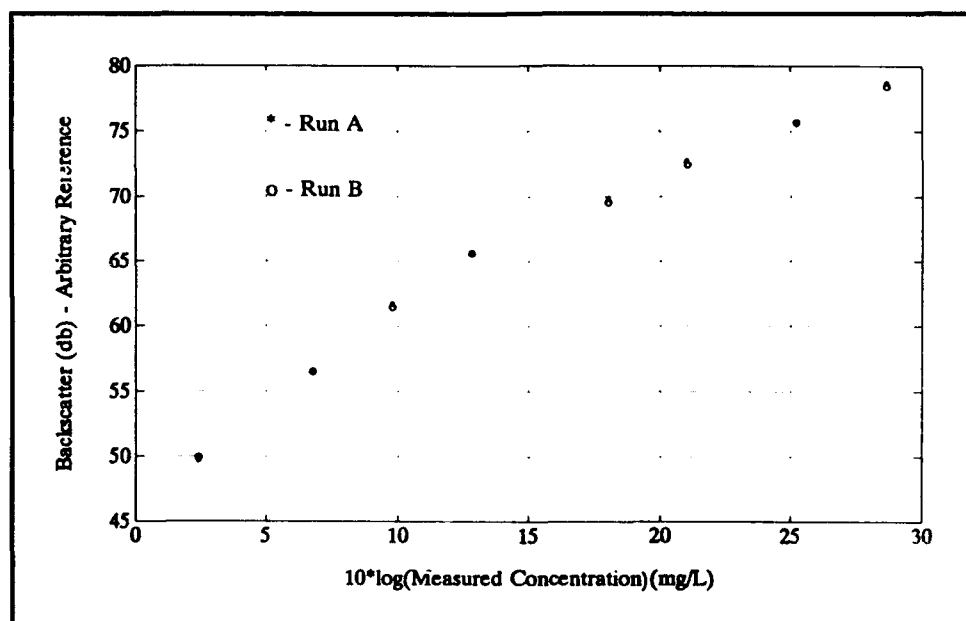


Figure 14. Repeatability test, 2 Mhz - "Double run"

(see Table 6). At lower weights (< 100 mg), the processing was repeatable to ± 3 mg. The main source of uncertainty appears to be the presence of additional water in the filter paper, a result of variable drying time, which depends on type and amount of sediment. At higher sediment amounts, the process was repeatable to ± 3 percent.

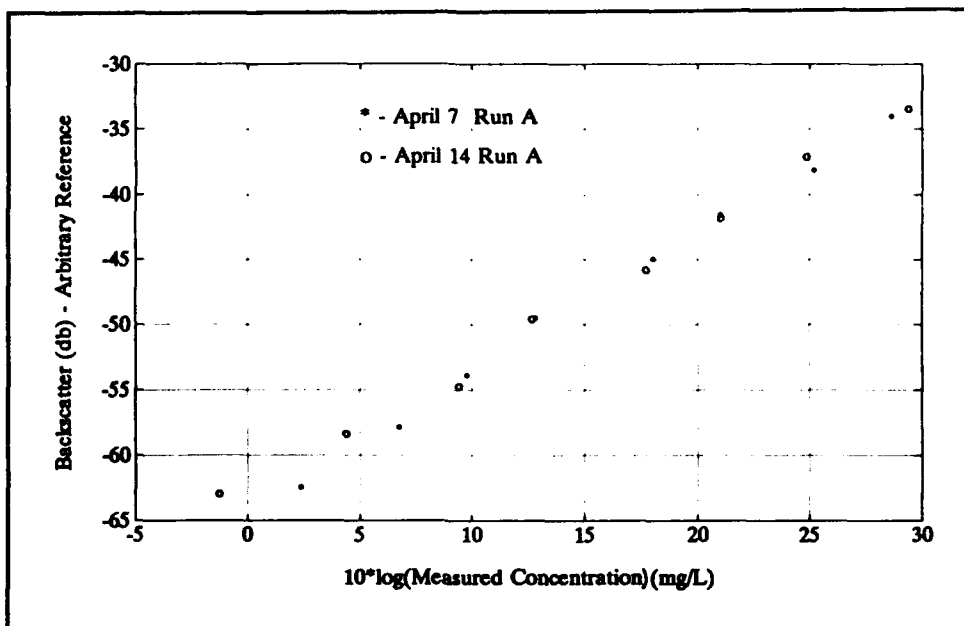


Figure 15. Repeatability test, 600 kHz

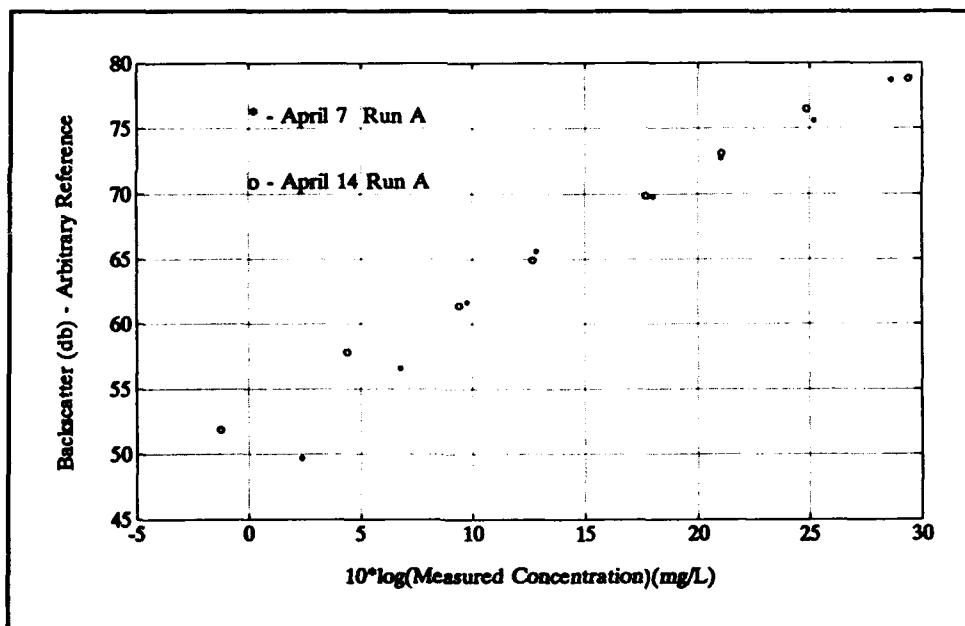


Figure 16. Repeatability test, 2 Mhz

Table 6
Weights of Samples of Known
Concentration

Sample Number	Sediment Present, mg	Measured Sediment, mg
1	27	28
2	6	7
3	40	44
4	18	21
5	107	109
6	32	34

Repeatability - Water Sampling

The system for water sampling was tailored after the recommendation described in an article by M.J Crickmore and R.F. Aked (1975). The motivation for their work was the need for a practical pump-out system. Through a series of laboratory and field experiments the authors showed that the water velocity at the inlet can be different from the oncoming velocity of the ambient fluid.

In sum, their experiments with 90- to 200- μ m diameter particles showed that:

- a. There is no significant bias as long as the inlet velocity is larger than 1.0 m/sec.
- b. Flow rate for the sampling system is immaterial.
- c. The inlet should be pointed into the flow to avoid the 18-percent underestimation of concentration observed when the inlet was pointed in the direction of the flow.

As described in Chapter 2, the pump-out system meets all of these criteria.

To quantify the extent to which the pump-out system produces consistent samples, five water samples were drawn at constant concentration from the area in the tank where the water samples were drawn during standard data runs. The test was carried out twice with slightly different concentrations of 212- to 300- μ m silica sand. The results are shown in Table 7. These results indicate that the water sampling results were repeatable to within a standard deviation of approximately 10 percent.

Table 7
Weights of Pump-Out Samples

Sample Number	Run 1	Run 2
Sample 1	83 mg	116 mg
Sample 2	92 mg	128 mg
Sample 3	74 mg	105 mg
Sample 4	79 mg	115 mg
Sample 5	90 mg	108 mg
Mean	84 mg	114 mg
Standard deviation	7 mg	8 mg

Table 8
Samples Taken from Different Vertical and Horizontal Positions in the Tank

Position	Run 1, mg	Run 2, mg
Mean at "normal spot" (center line)	84	114
Half way to wall	88	58
Close to wall	21	221
1 ft above "normal spot" (center line)	17	114
2 ft above "normal spot" (center line)	166	93

Water samples taken from different positions in the calibration chamber showed significant variations. During a run with 212- to 300- μ m sand, pump-out samples were taken at various locations in the tank to quantify these variations, and results are shown in Table 8. The initial reaction after run 1 was that something had gone wrong during the test. Run 2 shows more consistent data along the vertical center line (114 mg, 114 mg, and 93 mg) but there still is considerable variation in the horizontal plane. Given the repeatability of the pump-out samples established by the data shown in Tables 6 and 7, the data presented in Table 8 probably show that there were still significant local variations in the tank, at least for the time scale defined by the time it took to draw a water sample (100 sec). Within the time constraints of the experiment, no further tests were conducted to establish alternative explanations for the variations reported in Table 8.

Comparisons between measured and nominal concentration (see the section titled "Nominal Sediment Concentration" in Chapter 2) are shown in Figures 17 and 18. Figure 17 shows the results for 300- to 355- μ m silica sand, and Figure 18 shows the results using field samples from the James River in Virginia. The

mean diameter of the sediments from this location is approximately 6 μ m. As expected, measured concentrations are lower than the nominal values, due to material trapped in the return lines, collecting on the funnel at the bottom of tank, or otherwise caught in the system. The differences between nominal and observed values are smaller for the fine field samples than they are for the large sand particles. This is consistent with visual observation showing a significant aggregation of particles on the funnel for the larger size classes.

From the figures, it can also be observed that the relative difference between nominal and measured concentration becomes smaller at high concentrations. This may reflect that the relative amount of material being trapped in the system is reduced at high concentrations.

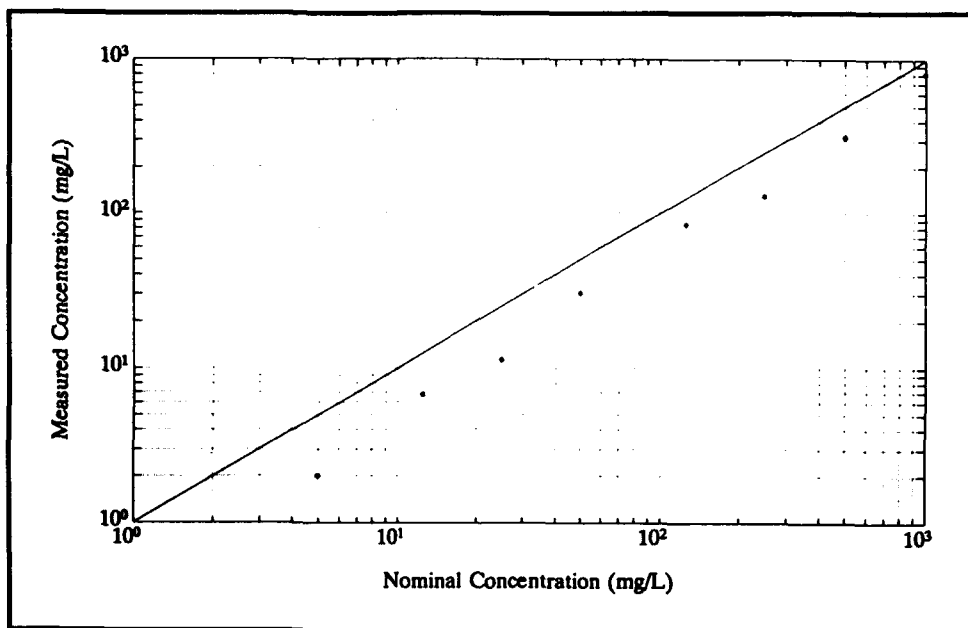


Figure 17. Run A06B - nominal versus measured concentration

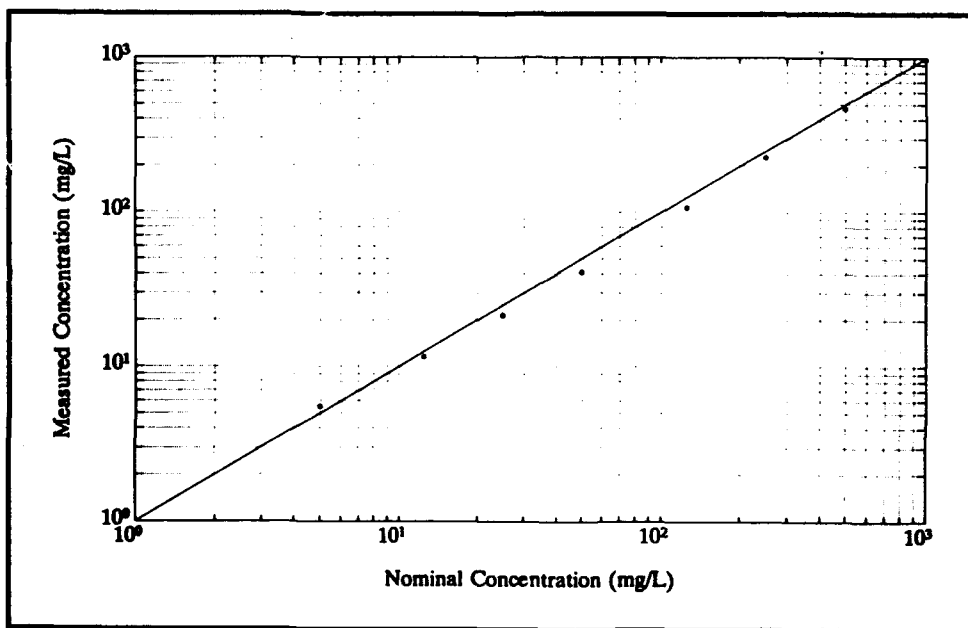


Figure 18. Run M27A - nominal versus measured concentration

Acoustic Contamination

One of the most critical and most difficult aspects of the experiment was to maintain a sufficient level of cleanliness within the calibration chamber, especially with smaller sediments, since a very small amount of foreign material is sufficient to bias the acoustic data significantly. A careful routine was developed, using the chamber's in-line filter system, to keep contaminating material to a minimum.

As a reference, background files were taken with every data set to show the acoustic return levels prior to the addition of sediments. In these files, the tank was placed in a fully operational condition, with the pump on and filters out of line for data collection. During some runs, contaminating material was unavoidable and scattering values were affected at lower concentrations.

At several points during the course of the experiment, there was concern over the potential presence of micro bubbles in the water column. These bubbles could affect both backscattering and signal attenuation. Numerous experiments were performed to look for specific evidence relating to bubbles; none of these experiments provided evidence to confirm a significant effect. As a precaution, several steps (based on practical experience) were taken to avoid contamination from small bubbles. They were:

- a.* Only water that had been standing still for some time and effectively degassed was used when the calibration chamber was replenished. Normally, water from the larger tank was used. Tap water required a delay of approximately 3 days for natural degassing to occur.
- b.* Every run started with a check of the background scattering level. No run was started before the background level was close to the electronic noise level. With few exceptions, this procedure was followed successfully.
- c.* Particles were mixed with water, degassed in a vacuum chamber, and usually left standing for more than an hour before the mixture was added to the tank. Additionally, data were not collected for a minimum of 10 min after the mixture was added. These procedures imposed waiting periods so that bubbles entrained with the mixture, or that resulted from changing transducers, would have a chance to rise to the surface.

Special Problems

Temperature sensitivity

During data analysis, it was noted that the attenuation data measured with the 600-kHz single-beam system varied in a manner inconsistent with theory, which predicts increasing attenuation with increasing concentration. The unexpected variation was investigated further.

After several failed hypotheses (e.g., change in scattering off the funnel due to accumulation of sediments), the problem was found to originate in temperature-sensitive pre-amplifiers, especially at low amplification levels (high echo levels). During most of the runs carried out during March, the air temperature was constant during the day and sensitivity did not manifest itself. During a heat wave in April, however, the temperature around the transducers was estimated to have varied from 20 °C in the morning to 30-35 °C in the afternoon.

A temperature sensitivity calibration was performed in an environmental chamber and the results for the 600-kHz system are shown in Figure 19. As can be seen, the problem mostly affects the low preamplifier settings. The low preamplifier settings are required to measure the strong bottom reflections used to calculate the attenuation. When measuring the backscatter signal, the preamplifier settings were 32 or higher and the temperature effect would have been at most 1.5 dB for a ± 5 °C temperature change at 25 °C. The receive circuitry of the 2-Mhz system is less sensitive to temperature than the 600-kHz system.

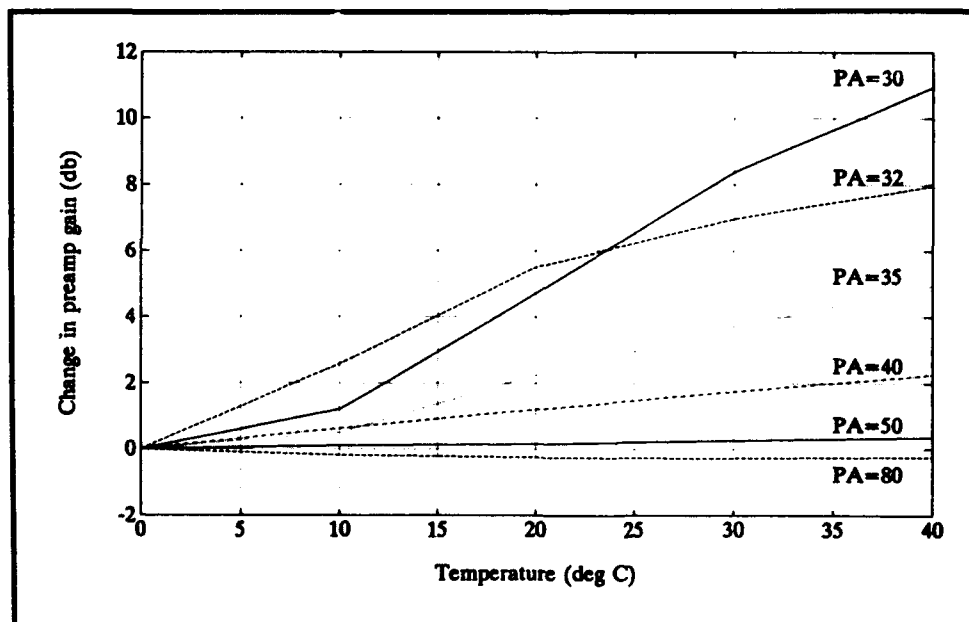


Figure 19. Temperature sensitivity of 600-kHz receivers

Fine sediments

The sieving equipment achieved uniform size classes ranging from 38 to 850 μm . Several attempts were made to calibrate the return signal for smaller size classes, leading to some unusual results. Two materials in particular produced similar, but inconsistent, results. The materials were silica sand, ranging from approximately 1 to 10 μm in diameter (referred to by the manufacturer as 15- μm Sil-co-sil), and pulverized kaolinite, which has a mean particle size of approximately 1.5 μm and a very broad distribution (from 0.2 to 50 μm).

A large concentration (typically 500-1,000 mg/l) of these materials was added to the calibration chamber at the beginning of each run. Acoustic backscattering and sediment concentration data were collected approximately every 30 min. Figures 20 and 21 show the results for kaolinite and 15- μm silica, respectively, using data from the 2-MHz system. The horizontal axis shows measured sediment concentration, and the vertical axis shows mean backscattering level. Elapsed time between data points has been noted on the figures. Figure 20 shows that scattering levels for the kaolinite changes by approximately 20 dB, while the measured concentration only changes by approximately a factor of 2 (3 dB) during the same interval. Similarly, for the 15- μm silica, scattering levels change by approximately 10 dB, while again the concentration only changes by a factor of 2. The same pattern was observed with the 600-kHz system. Thus, the decrease in backscattering level with time far exceeded the corresponding decrease in sediment concentration.

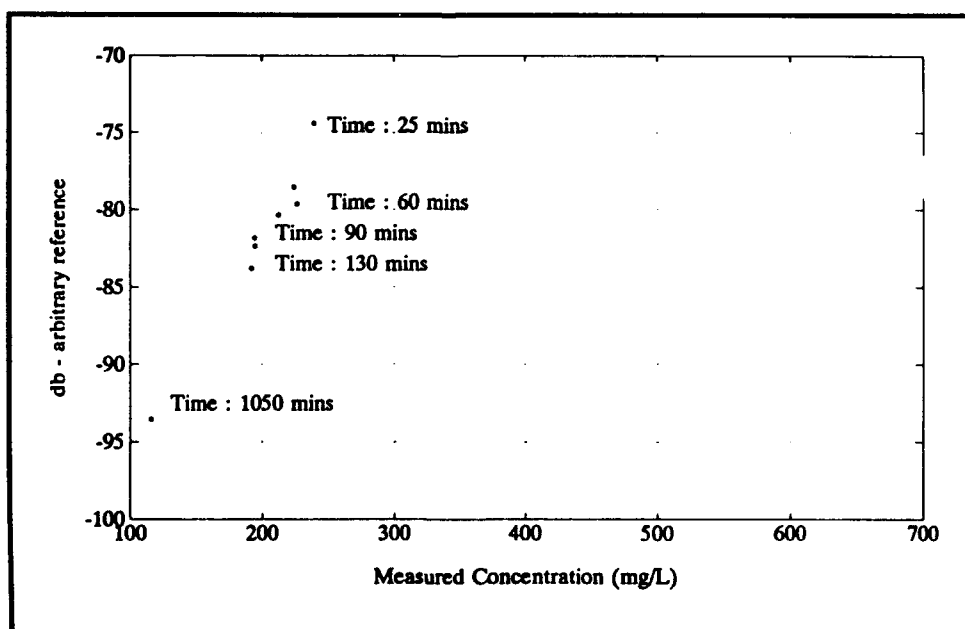


Figure 20. Run J01A - temporal variability of scattering level from kaolinite (2 MHz/long pulse)

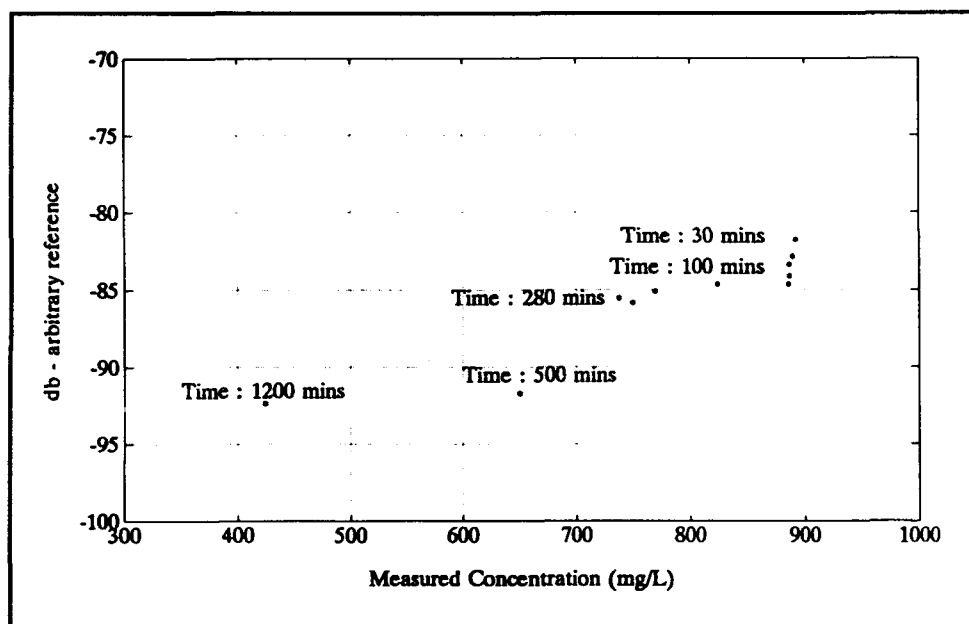


Figure 21. Run J18A - temporal variability of scattering level from 15- μ m silica (2 MHz/long pulse)

The original hypothesis for the large change in scattering was that the size distribution was changing through cohesion between the particles - or lack thereof. Several tests were run with and without deflocculant and increasing levels of mixing, blending, and degassing. The test results shown in Figure 21, for example, were collected using 15- μ m silica and a deflocculant. No change in results was observed in any of the tests, and the hypothesis was finally discarded.

The second and final hypothesis was based on the mechanisms by which sediment becomes trapped in the system. Most is either caught on the funnel, or passes by the upper edge of the funnel and is trapped beneath the funnel. Conceivably, these trapping mechanisms could be biased for different particle sizes, effectively changing the size distribution with time. Since the largest particles, which dominate the backscatter, have higher fall velocity than the smaller particles, their residence time in the tank is shorter and they are more prone to being trapped.

A test of this hypothesis started with the calibration chamber having been run for 24 hr with 400 mg/l of 15- μ m silica. This initial concentration is shown in Figure 22 as the concentration at time zero. Then, 800 mg/l of 15- μ m silica was added (to a total of 1,200 mg/l), increasing the scattering level by approximately 5 dB. Finally, approximately 400 mg/l of 45- to 63- μ m silica sand was added and the larger particles completely dominated the scattering level (15-dB increase). This mixture was left running over 48 hr, at which point the concentration was about 700 mg/l and the scattering level returned to the level originally seen when there were only 15- μ m silica particles.

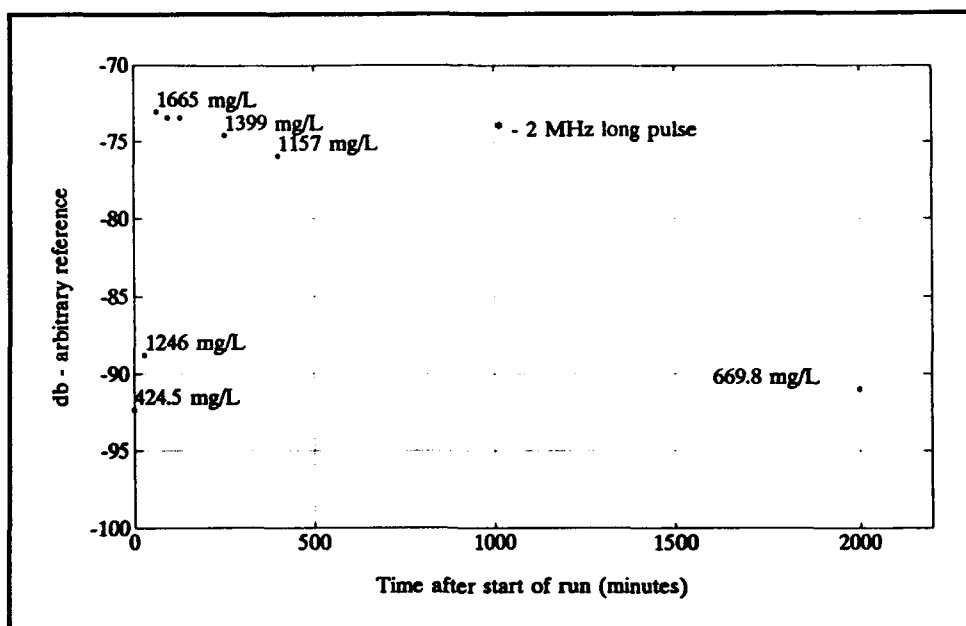


Figure 22. Run J19A - scattering level from 15- μ m and 45- to 63- μ m silica

The data fit the hypothesis of selective trapping of sediments, since the larger size class had completely disappeared after 48 hr. It was concluded that this phenomena was the major cause for observed changes in scattering levels. As a consequence of this selective trapping mechanism, the calibration facility was unable to be used to calibrate the acoustic systems for sediment sizes less than 10 μ m. Material in the 10- to 38- μ m range was not available for testing.

4 Calibration

The acoustic systems were individually calibrated to ensure that the results of the experiment can be applied to any other experiment carried out with calibrated acoustic systems. In addition to knowing the exact instrument characteristics, an accurate description of the propagating pulse is required to calculate the parameters that describe the scattering process. In describing the propagation, there is a distinction between the transducer near and far field. The separation can be made at a near field distance d^2/λ where d is the transducer diameter and λ is the acoustic wavelength. For a 600-kHz system with 10-cm transducers, the separation distance is 4 m. In the far field, acoustic pressure decreases with distance r by a factor $1/r$ as a result of the spherical spreading. In the near field, this equation is not valid and can only be evaluated through numerical integration of the governing equations.

For low-frequency transducers (<1 MHz) applied in open-water operations, the distinction between near and far field is normally not significant. The range of the system is much longer than the near-field distance and nearly all the significant processes take place in the far field. For tank experiments, however, narrow beam transducers do not generate a well-behaved acoustic pressure field within the length of the tank. A range-dependent correction term that includes near-field effects must be included to describe that backscatter data correctly.

In the following sections, the overall model for the transmit signal, volume scattering, and receive response are described. The model is described in the section titled "Modelling" below. In the section titled "Near Field," the particular characteristics of volume scattering in the near field are described. The section titled "Receiver Response" describes the relative receive responses of the systems. The last section of this chapter, titled "Transmit and Receive Calibration," deals with transmit and receive calibration and reports the results.

Modelling

There are two basic elements in the calibration of an acoustic system: transmit calibration, i.e., pressure generated in the water column, and receive calibration, i.e., the system output for a given pressure in front of the transducer. In addition, when modelling volume scattering, appropriate expressions for the beam pattern and the scattering must be included. Suspended sediment concentrations in the calibration chamber are assumed to be homogeneous, thereby simplifying the range-dependent corrections. The corrected data are referred to as range-normalized. The system is referred to as calibrated when all the parameters describing transmit and receive are known.

For acoustic backscatter applications, the transducer typically has the shape of a piston. For modelling purposes, the transducer can be thought of as having an infinite number of elements that all are radiating energy in spherical shells. Defining a scaling parameter B_0 with units of $Pa \cdot m$, the transmitted rms pressure p at a point \mathbf{r} (bold characters signify vectors) in the water can be expressed as an integral over all the individual transducer elements (Ma et al. 1987) as:

$$p(\mathbf{r}) = \frac{B_0}{A} \left| \int_A \int \frac{e^{ik|\mathbf{r}-\mathbf{r}'|} e^{-\alpha_w \mathbf{r}} e^{-\int \alpha_s d\mathbf{r}}}{|\mathbf{r}-\mathbf{r}'|} dA \right| = B_0 \Psi(\mathbf{r}, \theta) X(\mathbf{r}) \quad (2)$$

where

$$\Psi(\mathbf{r}, \theta) = \frac{1}{A} \left| \iint_A \frac{e^{ik|\mathbf{r}-\mathbf{r}'|}}{|\mathbf{r}-\mathbf{r}'|} dA \right|$$

$$X(\mathbf{r}) = e^{-\alpha_w \mathbf{r} - \int \alpha_s(\mathbf{r}) d\mathbf{r}}$$

where k is the acoustic wave number and \mathbf{r}' is a point on a circular transducer of area A and radius a , Ψ is the range-dependent beam pattern in units of inverse meters. Media-dependent transmission losses are collected in the factor $X(\mathbf{r})$. The term for water absorption is α_w (units of nepers/meter). Losses caused by scatterers present in the water column are collected in the attenuation coefficient α_s . The latter is expressed in its most general form as an integral where the concentration and the size distribution can vary along the transmit path.

As indicated in Equation 2, the expression for $p(\mathbf{r})$ can be expressed in terms of the distance (r) along the center axis and the angle (θ) off the axis when the transducer is symmetrical. To the first order, the far-field approximation ($r \gg a$) of $p(\mathbf{r})$ can be expressed as:

$$p(r, \theta=0)_{far} = \frac{B_0}{r} X(r) \quad (3)$$

since

$$\lim_{r/a \rightarrow \infty} \Psi(r, \theta=0) = \frac{1}{r}$$

When the piston transducer is calibrated for transmit level, the pressure in clear water ($\alpha_s = 0$) is measured at a distance r'' along the center axis and then reduced to a reference distance of 1 m. The reference pressure p_0 (units of Pa*m) is used to normalize Equation 2 as follows:

$$p_0 = \frac{r'' p(r'')_{far}}{X(r'')} = \frac{r''}{X(r'')} \left[\frac{B_0}{r''} X(r'') \right] \Leftrightarrow B_0 = p_0 \quad (4)$$

As the transmit pulse propagates outward, a fraction of the energy is scattered by the individual particles present in the water column. The acoustic cross section s_v per unit volume per steradian in the backscatter direction can be defined in terms of the incident pressure p_i and the scattered pressure p_r at a distance r_0 from the scattering volume as follows:

$$s_v = \left(\frac{p_r r_0}{p_i} \right)^2 d\Phi^{-1} \quad (5)$$

where

$$d\Phi = (r^2 d\Omega) \left(\frac{1}{2} c d\tau \right)$$

$\tau =$ pulse length (sec)

$c =$ speed of sound (m/sec)

The term $d\Phi$ is the differential scattering volume and needs to be integrated over the cross section of the beam pattern $d\Omega$ and over the transmit pulse $d\tau$.

When the scattered pressure wave is received by the transducer, it is preferentially treated with respect to direction and the angular response function is equal to the transmit dependency expressed in Equation 2. Taking the case of an individual particle located at a position r_0 from the transducer, the receiver output (disregarding noise terms) is:

$$V_m * C = \int_A \int p_r r_0 \frac{e^{ik|r_0-r'|}}{|r_0-r'|} X(r_0) dA = p_r r_0 \Psi(r_0, \theta) X(r_0) \quad (6)$$

where V_m is the measured output at the transducer terminals and C' is a calibration coefficient. This assumes that the spherical wave generated by the scattering process has no angular dependency within the sector that bisects the transducer. While this assumption of quasi-isotropic scattering may not be accurate for an individual particle, the average scattering pattern can be assumed to be broad at small angles around the backscatter direction.

The data for the receive calibration is obtained in an experimental setup that approximates the condition where a plane wave is transmitted toward and along the center line of the transducer. Pressure (p_{echo}) is measured just in front of the transducer and the receiver rms output (V_m) is measured. The calibration coefficient C' is the plane wave sensitivity coefficient and it models both the receiver response and the transducer efficiency. C' is not a constant but may vary as a function of acoustic pressure if the receivers are nonlinear:

$$V_m * C' (p_{echo}) = p_{echo} \quad (7)$$

The measured term p_{echo} , the equivalent plane wave response to a spherical wave, is:

$$p_{echo} = p_r r_0 \Psi(r_0) X(r_0) \quad (8)$$

The beam forming at transmit, expressed by Equation 2, the scattering expressed by Equation 5, and the receive response, expressed by Equation 6, can be integrated over the scattering volume under the assumption of linear superposition, i.e., the order of integration can be changed, which results in the following:

$$V_m^2 * C'^2 = p_0^2 \int_{\Omega} \int_{\tau} s_v \Psi^4(r, \theta) X^4(r) (\frac{1}{2} c d \tau) (r^2 d \Omega) \quad (9)$$

$$(receive) (xmit) \quad (scatt) \quad (beam) \quad (loss) \quad (volume)$$

Assuming that the acoustic scattering cross section only varies slowly over the size of the transmit pulse, the logarithm of Equation 9 can be expressed as:

$$10 \log_{10} (V_m^2 * C'^2) = 10 \log_{10} (p_0^2) + 10 \log_{10} (I) + 10 \log_{10} (s_v) + \quad (10)$$

$$10 \log_{10} \int_{\Omega} \Psi^4(r, \theta) r^2 d \Omega + 40 \log_{10} (X)$$

where l is the two-way length of the transmit pulse in units of meter. Assuming a homogeneous concentration and grain-size distribution along the beam path, for which α_s is constant, the far-field approximation of Equation 9 is the usual sonar equation for volume scattering. After rearranging the terms, it is:

$$S_v = 10 \log_{10}(s_v) = 20 \log_{10} \left(\frac{V_m * C}{p_0} \right) - 10 \log_{10}(l) + 20 \log_{10}(r) + \quad (11)$$

$$2 \alpha' r - 10 \log_{10} \int_{\Omega} b^2(\theta) d\Omega, \quad b(\theta) = \Psi^2(\theta), \quad \alpha'(dB/m) =$$

$$(\alpha_w + \alpha_s) * 20 \log_{10}(e)$$

where $b(\theta)$ is the classical definition of the range-independent beam pattern and α' in units of dB/m represents the losses from water absorption and particle-dependent attenuation.

The term for water absorption, α_w , is given by Fisher and Simmons (1977) as:

$$\alpha_w = 10^{-15} f^2 (55.9 - 2.37 T + 4.77 * 10^{-2} T^2 - 3.48 * 10^{-4} T^3) \quad (12)$$

in dB/m, where T is in degrees Celsius and f is in hertz. Francois and Garrison (1982) determined a somewhat different relationship as follows:

$$\text{For } T \leq 20 \text{ }^\circ\text{C} \quad (13)$$

$$\alpha_w = 10^{-15} f^2 (493.7 - 25.9 * T + 9.11 * 10^{-1} * T^2 - 1.50 * 10^{-2} T^3)$$

$$\text{For } T > 20 \text{ }^\circ\text{C}$$

$$\alpha_w = 10^{-15} f^2 (396.4 - 11.46 * T + 1.45 * 10^{-1} * T^2 - 6.5 * 10^{-4} * T^3)$$

In the data analysis α_w is 0.8 dB/m for the 2-Mhz system and 0.08 dB/m for the 600-kHz system. These values are the mean result of the two algorithms (Equations 11 and 12). It is assumed that both systems operate in clean water and at a temperature of 20-25 °C. The attenuation coefficient α_s was measured directly in the experiment, as described in the section titled "Correction for particle attenuation" in Chapter 5.

Near Field

The function Ψ^2 , or the range-dependent intensity of the transmitted pressure field, was evaluated analytically along the center axis of the transducer (Ma et al. 1987). The results are shown in Figures 23 and 24 for the 600-kHz and the 2-MHz systems, respectively. There is a significant discrepancy (>1 dB) between the exact model and the far-field response function ($1/r^2$) over a distance that roughly corresponds to half of

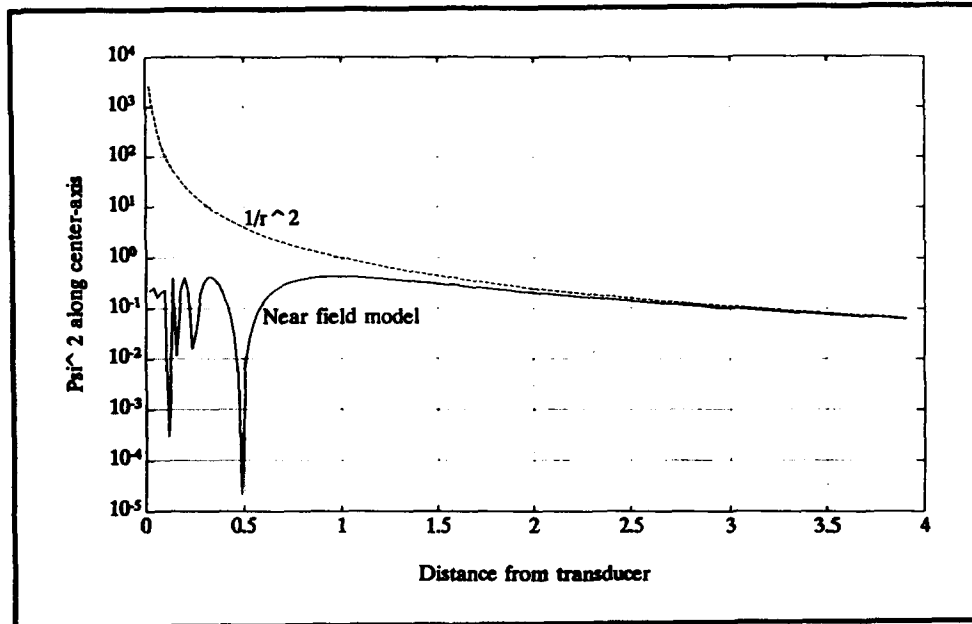


Figure 23. Intensity of the pressure field along the center axis, 600 kHz

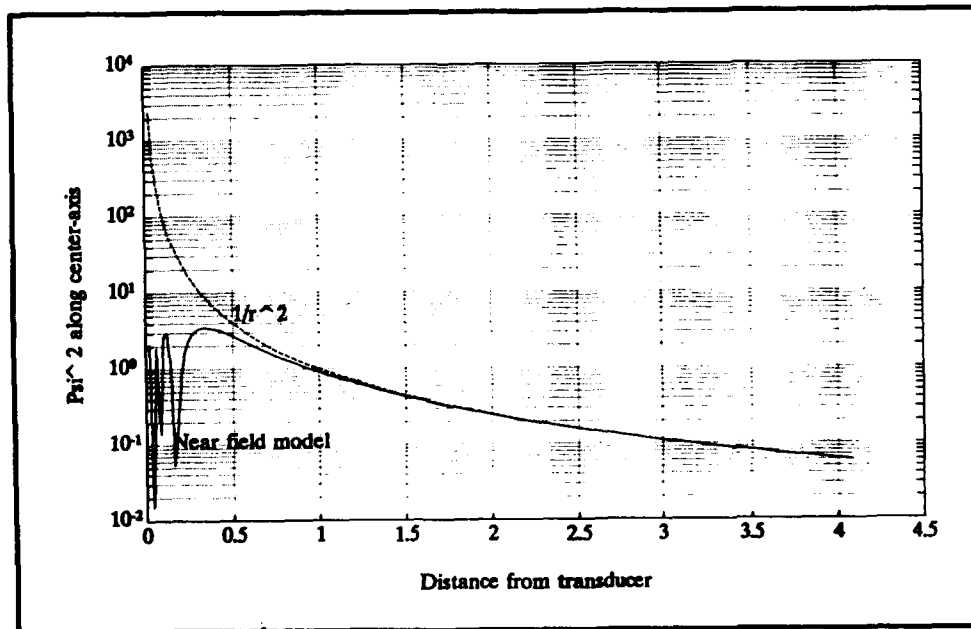


Figure 24. Intensity of the pressure field along the center axis, 2 MHz

the previously defined near-field distance. The figures also show the intensity of the pressure field to exhibit nodal features. These features can be interpreted as the interference pattern generated by the individual elements of the transducer. The last minimum occurs at a distance equal to one eighth of the near-field distance. These features have caused concern amongst other researchers (Ma et al. 1987) because these minima are "blind spots," where particles cannot be seen. To suppress these nodes, acoustic shading techniques can be implemented. Acoustic shading, in this case, is implemented by using transducers that do not respond uniformly to the driving electrical current but have a tapered response toward the edges of the transducer. As will be seen later, the concern about nodes may have been unwarranted.

The integral of Ψ^4 will converge toward the product of the far-field spreading loss, i.e., $1/r^2$, and the integral of the range-normalized beam pattern. A final check of the numeric integrations can thus be done by comparing the results with the far-field beam pattern. For a piston-shaped transducer, the far-field approximation can be evaluated analytically and the results are shown in Figures 25 and 26. The numerically evaluated integral converges asymptotically to the far-field solution.

Finally, the solution of the integral of Ψ^4 over the beam is shown along with the far-field approximation in Figures 27 and 28. Model results are depicted as a solid line and show the range dependency of the backscattered power, excluding absorption and particle attenuation losses, for the 600-kHz and the 2-MHz systems, respectively. In the area close to the transducer the difference between the two solutions is more than 10 dB. For the 600-kHz system, the use of the near-field solution is important over the full length of the 2.5-m calibration chamber. The 2-MHz system has a shorter near-field distance and the near-field model is only required for distances closer than 1 m.

Two observations can be made from Figures 27 and 28. First, the range dependency has a characteristic peak close to last axial maximum of the transmitted pressure field. This is in contrast to the results reported by Libicki et al. (1989), where the same model produced a monotonically decreasing function. The cause for this discrepancy is not known, but may be related to shading techniques employed in their 3-MHz system. The particular shape of the range correction in the near field may also account for the difficulty in interpreting the backscatter profiles reported by Tamura and Hanes (1986), as part of their attempt to calibrate a 3-MHz system for sand particles. Secondly, it should be noted that the nodal structure observed in the transmitted pressure field is no longer present in the range-dependent response. The reason for this is that volume scattering represents, by definition, a spatial average of the backscattering level. The nodal structure thus disappears when averaged over the cross section of the beam. The implication is that transducer shading is not necessary for this reason alone, and instead may increase the complexity of the near-field modelling. Shading suppresses the nodes but it also affects the system by suppressing side lobes and widening the main lobe. This is

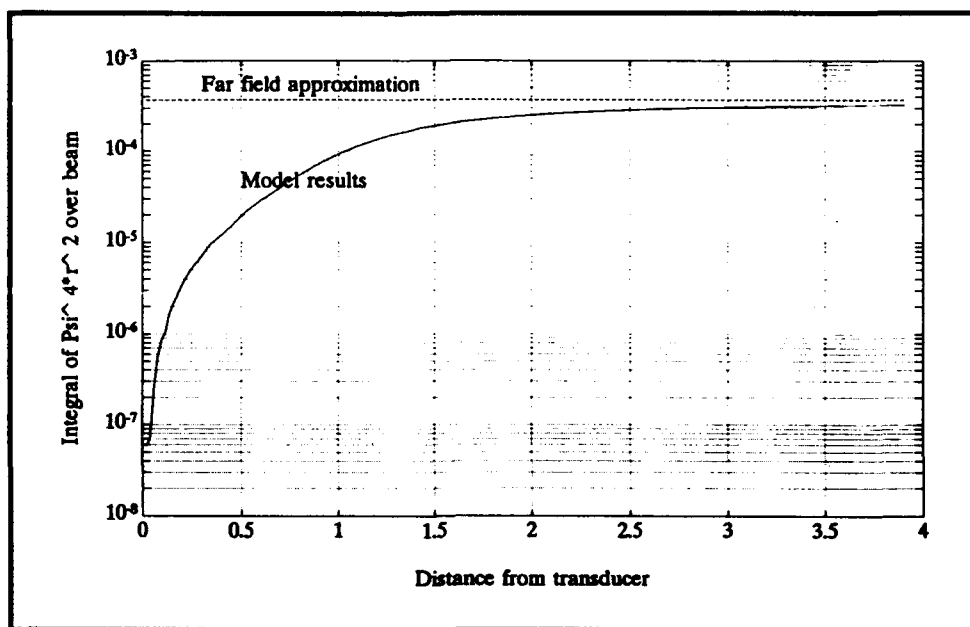


Figure 25. Equivalent beam pattern as a function of range, 600 kHz

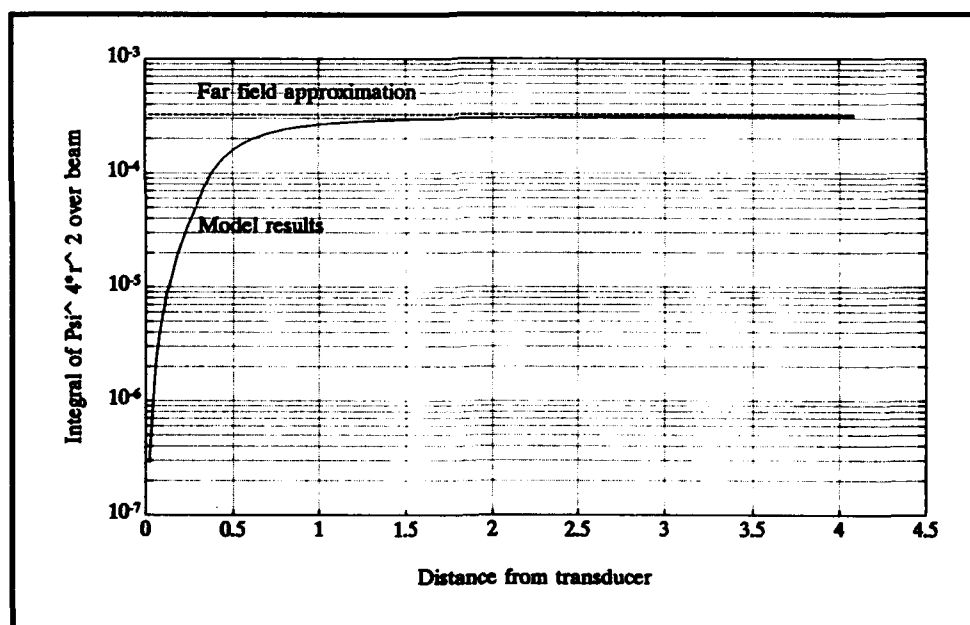


Figure 26. Equivalent beam pattern as a function of range, 2 MHz

important in conjunction with the definition of the “effective” transducer area that is used in the near-field model. The 600-kHz transducer, which has no shading, has a measured full beam width of 1.46 deg in the far field. This corresponds to an effective diameter of 9.7 cm, which is close to the physical size of 10.16 cm. The 2-Mhz transducer, however, was originally built for Doppler velocity measurements and is effectively shaded. The measured two-sided beam width (1.56 deg) is thus not a good measure of the effective transducer size. In the absence of a model

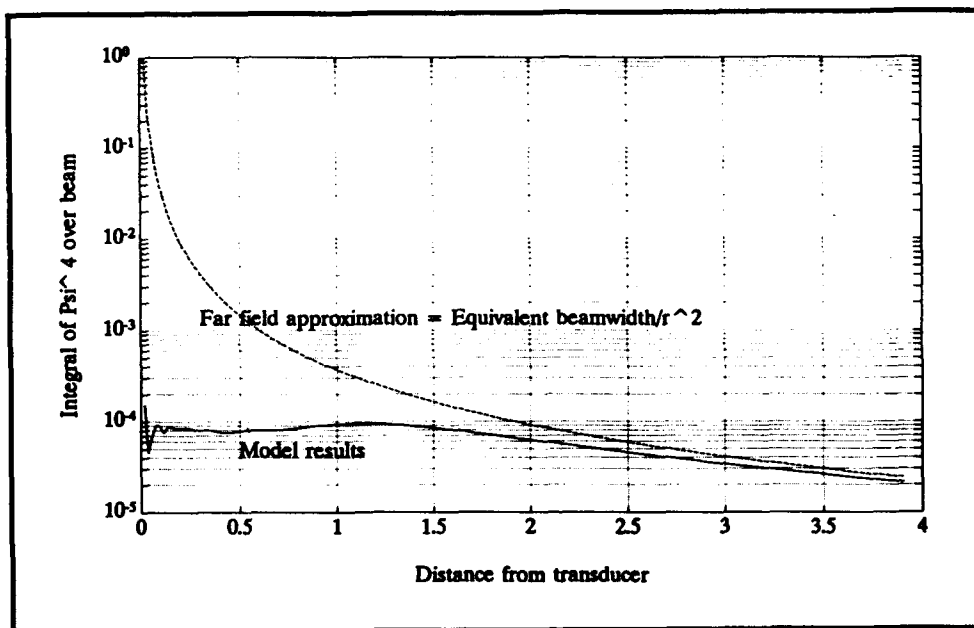


Figure 27. The range-dependent signal level (assuming constant concentration), 600 kHz

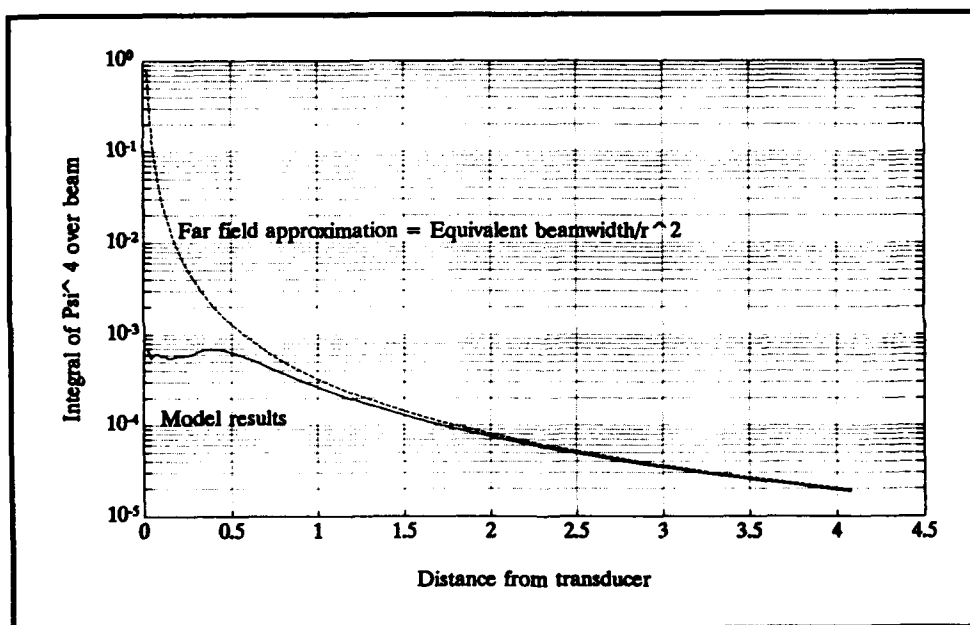


Figure 28. The range-dependent signal level (assuming constant concentration), 2 MHz

for the exact transducer response, the physical transducer size (i.e., 3.175 cm) is used for modelling purposes.

Before a comparison can be made between the model and the measured data, the integral over Ψ^4 must be digitally filtered in the same way as the analog filters in the acoustic systems modify the signals. The 600-kHz system has very wide band filters (of order 500 kHz) and filtering has no

effect on a narrow band signal. In the 2-Mhz system, the amplitude signal generated by the Receive Signal Strength Indicator (RSSI) chip (see the section titled "Receiver Response" below) is filtered twice by a 20-kHz single-pole RC filter, which slightly alters the vertical profile.

Finally, comparisons between model results and actual data are shown in Figures 29 and 30. Water absorption has been accounted for in these figures, but not particle attenuation. The data were selected from event Y29 (63- to 75- μ m silica). The mean over the three highest concentrations is shown because the profiles collected at high concentration (>100 mg/l) are the most stable. The first 0.4 m of the profile for the 600-kHz system and the first 0.25 m of the profile for the 2-Mhz system should be disregarded because of acoustic and electronic ringing. Additionally, it is not certain that the scattering field can be characterized as uniform in the upper part of the tank. Note that the vertical scale is arbitrary, and the measured data profiles have been moved around to obtain the best overall fit. It should also be noted that the data reproduce the vertical maximum at the position predicted by the near-field model. Overall fit between the model and the data is quite good. The effect of particle attenuation can be seen at 2 MHz, where the measured profile decreases with range to a greater extent than the model profile.

Receiver Response

The two acoustic systems employ significantly different methods for processing the receiver signal. The 600-KHz system processes all information linearly, with about 42 dB of dynamic range in any one configuration, and a total range of approximately 100 dB. The 2-MHz system uses a logarithmic response circuit with a total dynamic range of approximately 70 dB. For the purpose of describing the derivation of the parameter C in Equation 6, both receivers are described in detail.

Signal processing in the 600-KHz system provides considerable flexibility and has a large total range. The return signal from the transducer is fed into a linear preamplifier, providing between 0 and 60 dB of gain. The preamplifier gain is software selectable and is adjusted before each period of data collection. After the preamplifier, the signal is fed into an 8-bit A/D converter, sampling at 2 MHz. The output from the A/D has 48 dB of dynamic range and is stored directly onto the computer hard drive. The high sampling rate allows for complete resolution of the return signal and considerable flexibility in post-processing. By varying the preamplifier setting, a total dynamic range of approximately 100 dB is obtained. Since the A/D has a limited dynamic range during any particular run, the 600-kHz system is not able to resolve backscattering from the water column and return from the bottom in a single data file. The processing scheme is computationally intensive, typically producing 700 kB for a single data file.

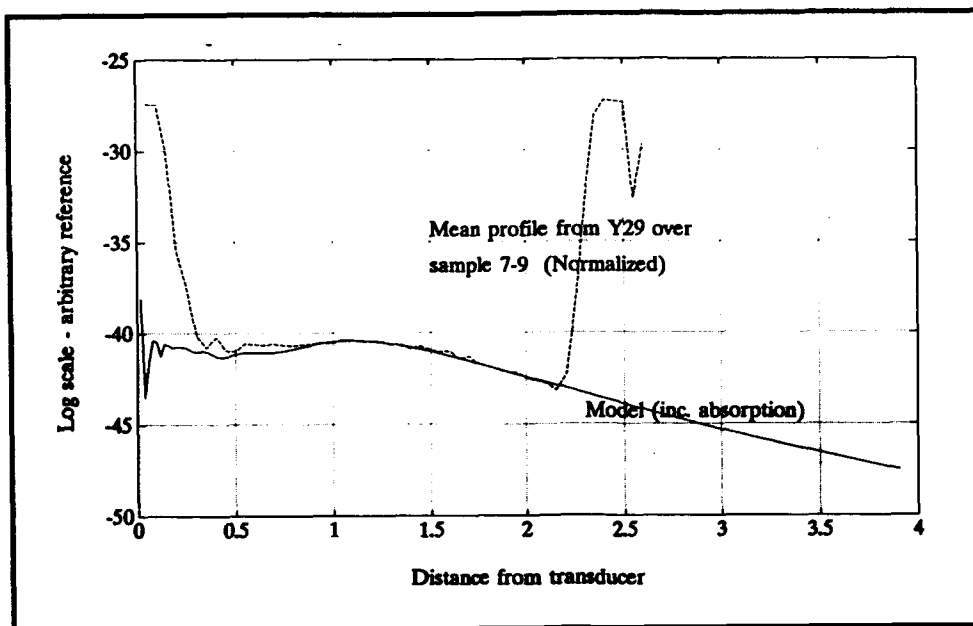


Figure 29. Comparison between measured echo level and the near-field model, 600 kHz

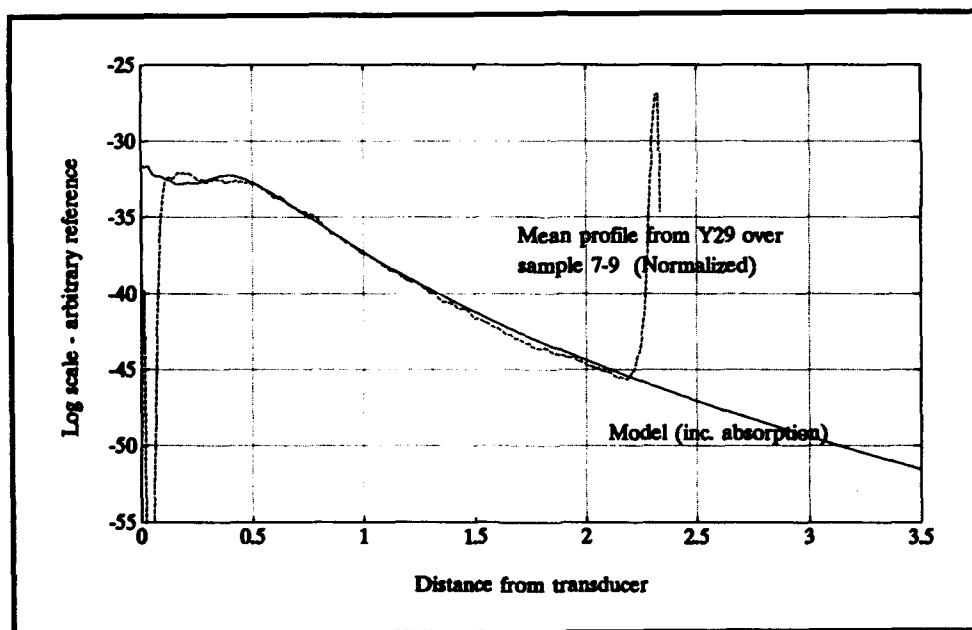


Figure 30. Comparison between measured echo level and the near-field model, 2 Mhz

The critical step in analyzing data from the 600-kHz system was obtaining a relative calibration of the preamplifier gain. This was done using a calibrated transmit hydrophone (Model E27 from the Naval Research Laboratory). The hydrophone transmitted a signal of known power, and the 600-kHz system received the signal using different preamplifier gains. The gain is set in software to an integer value between 28 and 115, which is sent to an 8-bit digital to analog converter and provides a driving

voltage to the amplifier circuit. The limits on gain settings are determined by the power requirements and saturation limits of the circuit. Figure 31 shows the calibration curve for the preamplifier, which is used for comparison of data recorded at different preamplifier settings. The curve shows strong changes in gain at lower settings (28-40), but levels off as the setting approaches saturation voltage. The receive circuitry for the 600-kHz signal is linear, so post processing is also done on a linear scale, and converted to decibels as the last step. In converting the signal level to decibels, a fixed but unknown reference is used. In other words, the preamplifier calibration provides the relative shape of the function C' but the absolute value of C' remains to be determined.

The acoustic return signal from the 2-MHz system is processed using the RSSI logarithmic response circuit. Output from the transducers is fed into the RSSI, producing two output signals. The first is an amplitude-normalized signal that maintains the phase information of the input, and is used for Doppler velocity calculations. The second is a 0- to 5-V DC output, which is proportional to the logarithm of the amplitude of the input signal. The DC output passes twice through a low-pass filter with cutoff frequency of 20 kHz (corresponding to a maximum vertical resolution of 3.75 cm) to produce a smoother profile. After the filter, the output signal is fed into an 8-bit analog to digital converter, producing a signal strength from 0 to 255 "counts." The A/D converter samples the RSSI amplitude signal every 16 μ sec, corresponding to a vertical resolution of approximately 1.18 cm (using 1,481 m/sec as the speed of sound, and accounting for two-way travel). The final amplitude information, in 1.18-cm bins, is stored in logarithmic units.

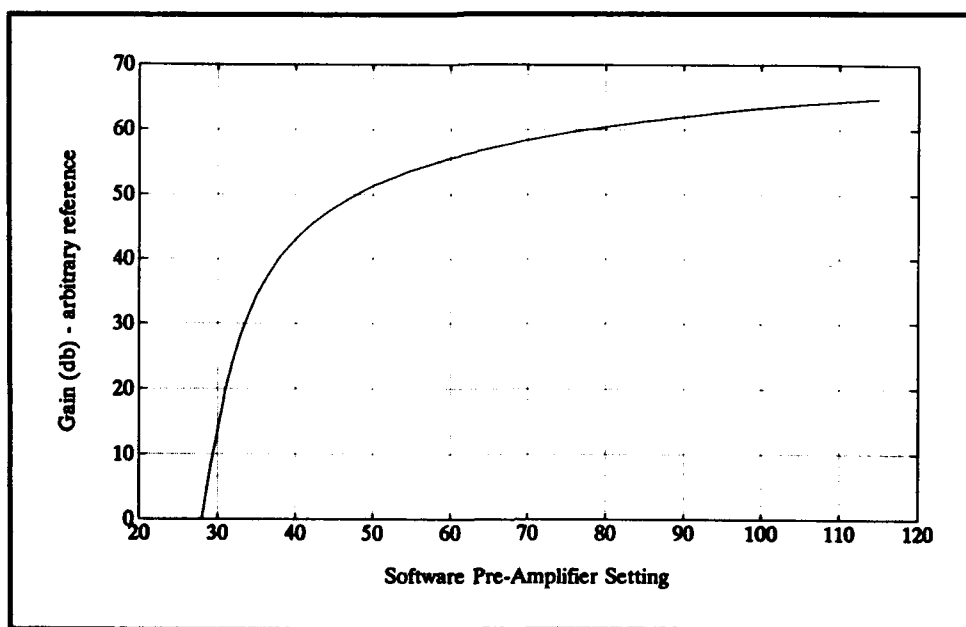


Figure 31. 600-kHz preamplifier calibration

To obtain an accurate calibration of the RSSI response, three different ceramic elements were used to feed a signal directly to the 2-MHz transducer. The three resulting curves were fit together to provide an overall conversion between RSSI counts and signal strength. A linear interpolation between adjacent points was used when calibration information was unavailable. The final calibration curve can be seen in Figure 32. A best fit line to the data points results in a slope of 0.47 dB per count. However, to accurately reproduce the small oscillations seen in the calibration data, a conversion table was made relating a signal input level to a particular RSSI count. This table was used in converting the data from counts to dB. The choice of input level is made with respect to an arbitrary but constant reference. As for the 600-kHz system, the receive calibration of the 2-MHz system only provides the relative shape of C' and the absolute reference level remains to be determined. This reference level is discussed in the section titled "Self-reciprocity calibration."

Transmit and Receive Calibration

Calibration of the single-beam 2-MHz and 600-kHz systems was carried out in a tank measuring 4.8 m by 1.8 m by 1.8 m. Calibrated hydrophones leased from the Naval Research Laboratory (Models E27 and E8) were available for the calibration and the procedure was roughly the same for both systems. In the description to follow, the E8 and the E27 are referred to as "the hydrophone" and the 2-MHz/600-kHz systems are referred to as "the transducer."

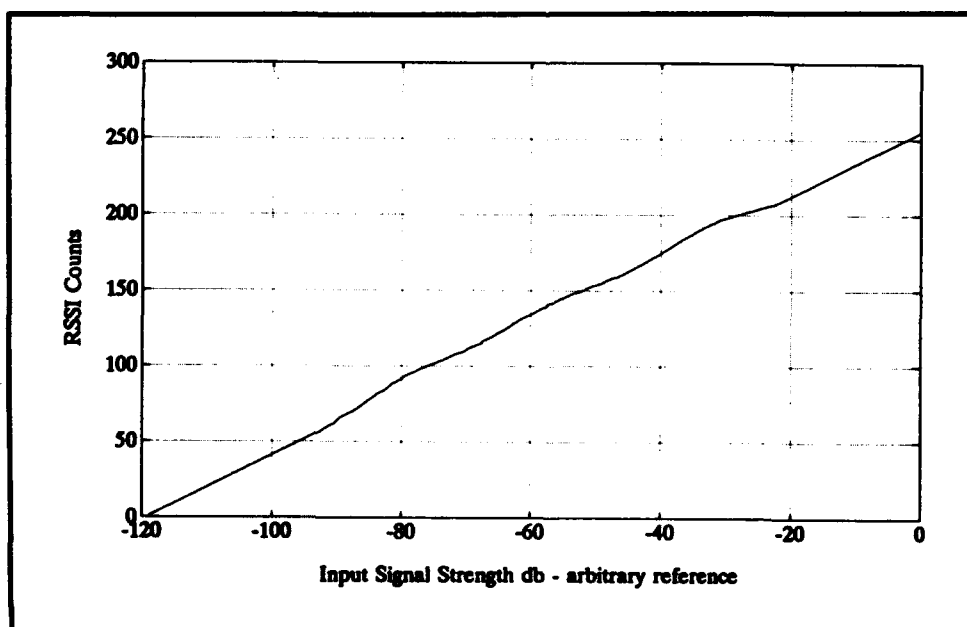


Figure 32. 2-MHz receiver calibration (RSSI output versus input signal strength)

The hydrophones from the Naval Research Laboratory are characterized by receive and transmit response curves. These curves show how voltage output or input at the terminals of the hydrophone is related to the acoustic pressure in the water. Receive response of the hydrophones is guaranteed to be within 1 dB of the calibration. The transmit response calibrations, however, are less reliable and are not provided with the E8 hydrophone (serial No. 57).

For this reason alone, it was desirable to use a calibration procedure that does not rely on the transmit calibration of hydrophone. It was also desirable to develop a methodology that has the potential of being used in the field or at least does not require dedicated calibration facilities. This was attempted as part of the project and, although not successful, holds some promise for the future if the necessary hardware modifications are made.

Self-reciprocity calibration

The essential element of a self-reciprocity calibration is a wall (or a surface or a bottom) that reflects acoustic energy with known loss characteristics. By receiving the echo of the transmit pulse as it bounces off a wall (Figure 33), the strength of the echo relative to the transmit pulse can be measured and the relative receive response easily calculated. In the case of a wall, it can be regarded as a perfect acoustic mirror with no loss. If effective, the method would require only a rudimentary calibration facility, and as a possible future extension, rough field calibrations could be achieved by passing over a bottom with known characteristics.

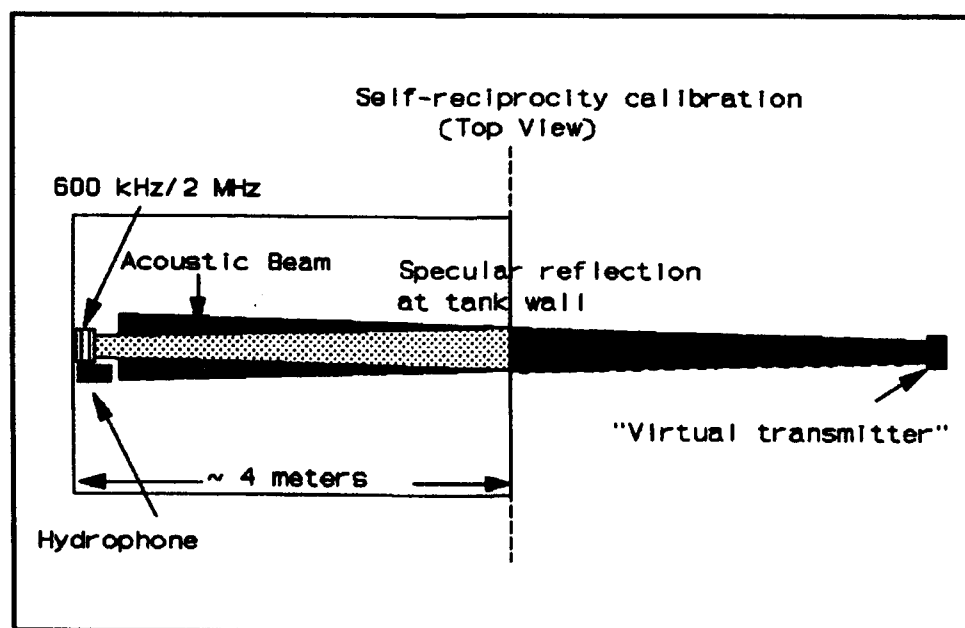


Figure 33. Self-reciprocity calibration

The biggest impediment to implementation of the self-reciprocity method was the lack of dynamic range in the acoustic systems. The acoustic systems (and the all-important receivers) were designed primarily for low signal levels. The echo bouncing from a wall located only 3-5 m from the transducers is several orders of magnitude stronger than the signal normally encountered in velocity profiling applications. As a result, several intermediary steps had to be introduced in order to measure the correct signal level. Examples are resistors in line with the transmit line, lossy materials hanging in the path of the beam, etc. In addition, the high end of the operating range of the 600-kHz receivers was quite temperature sensitive and not recognized as such until late in the project.

Finally, narrow acoustic beams severely restrict the accuracy of self-reciprocity calibration. If, for example, the transmitting 600-kHz system and hydrophone were located 4 m from, and pointing toward, the far wall, the pulse will bounce off the wall and come back toward the hydrophone. In the x/z -plane, the two-dimensional pressure field, measured as the voltage output from the hydrophone, will look like the contour plot shown in Figure 34. The gradients in the pressure fields are relatively weak and it is difficult to find the exact position of the maximum pressure. When the 600-kHz system is set to both transmit and receive, the relevant field strength is the two-way beam pattern (Figure 35). The gradients are quite strong and the error introduced is considerable unless the exact position of the peak pressure is found when mapping the field with the hydrophone. As can be seen in the figures, a 10- to 15-cm error in position (over a propagation distance of 8 m) will imply a 5- to 10-dB underestimation of the peak signal strength. In sum, the narrow beams and limited dynamic ranges of the acoustic systems used in the experiment make them unsuitable for self-reciprocity calibrations and initial attempts led to calibration errors of more than 10 dB. The beam width should be increased by a factor of 5-10 for this method to work properly. Also, to properly measure the reflected echo, the dynamic range of the acoustic systems should be increased by 20-30 dB at the high end.

Absolute calibration

For the absolute calibration, hydrophone E-8 (serial Nos. 67 and 57) was used. Characteristics of the hydrophone are shown in Table 9. To calculate the reference pressure p_0 , the transducer was set to transmit while readings were taken with the hydrophone at different distances (1-4 m) from the transducer and along the center line of the beam. Using the hydrophone receive sensitivity (see Table 9), the measured voltage levels were converted to pressure. The values of p_0 were calculated for both systems by reducing the pressure readings to a reference distance of 1 m. In the calculations, the theoretical pressure along the center line was used, with water absorption taken into account.

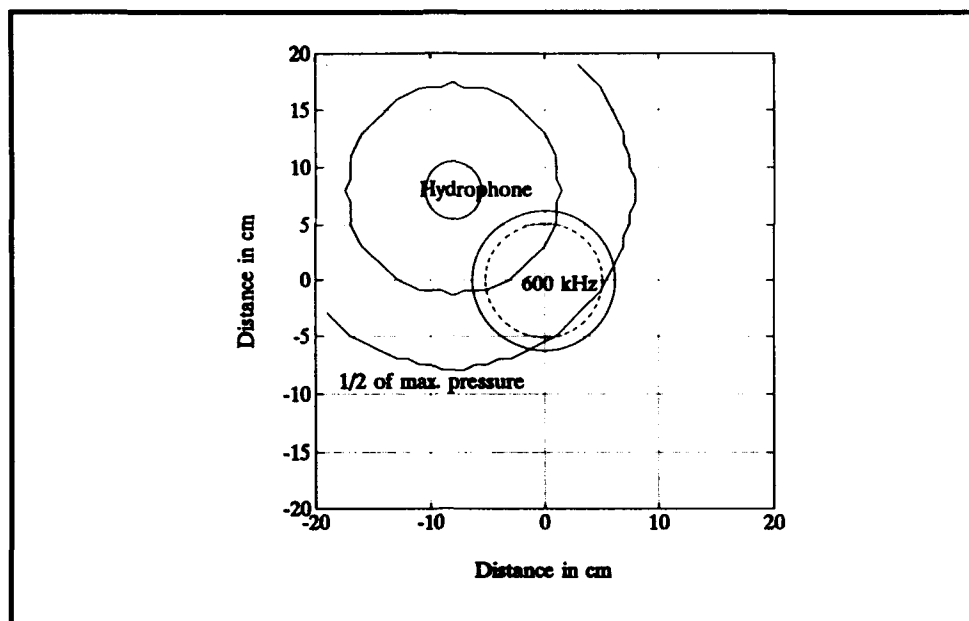


Figure 34. Contour plot of the 2-D pressure field at the position of the receiving hydrophone

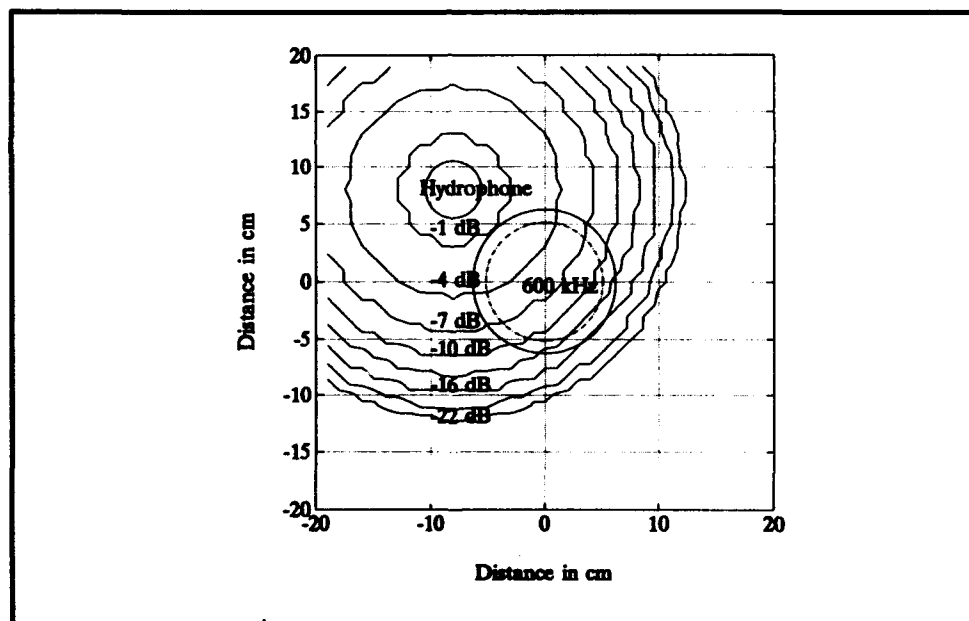


Figure 35. Contour plot of the two-way beam pattern at the position of the hydrophone

Table 9
Calibration Constants for the Hydrophones and the Transducers

Constant	600-kHz System (E8/#67)	2-MHz System (E8/#57)
Hydrophone receive sensitivity (reference = 1 V and 10^{-6} Pa)	216 dB	216 dB
Hydrophone transmit level (reference = 1 V and 10^{-6} Pa)	146.5 dB	156.5 dB (estimate)
Transducer transmit pressure (p_0)	101 kPa	25.7 kPa
$20 \log_{10} (C \cdot V_m / p_0)$ of transducer (arbitrary reference scale used in the preamplifier calibration)	-56.1 dB	-24.9 dB

In the second part of the calibration, the hydrophone and the transducer were positioned 4 m apart. The hydrophone was set to transmit and the transducer was set to receive. The systems were aligned to maximize the receive level in the transducer, thereby ensuring that the hydrophone was located on the center line of the transducer. The transmit level calibration for E-8, No. 67 was 146.5 dB, as shown in the table. The transmit calibration for E-8, No. 57 was not available. Since the two hydrophones are of the same kind, however, it was assumed that they had the same relative transmit/receive response at 2 MHz.

Using the hydrophone transmit response furnished by the Naval Research Laboratory, the pressure level was known at a distance 1 m from, and along the center line of the hydrophone. The pressure level 1 m in front of the receiving transducer was calculated using the far field approximation for spreading and the standard value for water absorption. The pressure in the water was thus known and can be related directly to the output of the transducers. This implies that an absolute reference level for the value of $C \cdot V_m$ was obtained. For simplicity, this value was combined with the reference pressure V_m and expressed as an offset to the arbitrary scale established after the receive calibration (Equation 11 and the section in this chapter titled "Receiver Response.") The absolute calibration of the acoustic system was then complete.

5 Data Analysis

This chapter is included to explain processing of backscatter data that were collected with the two acoustic systems, the 600-kHz system and the 2-MHz system. For each main stage of processing, a typical set of vertical profiles is presented as an example.

Data Processing

Raw data files

As described in the section of Chapter 4 titled "Receiver Response," analog processing in the two acoustic systems is not the same. The 600-kHz system processes the signal linearly, whereas the 2-MHz system uses a logarithmic amplifier in the receiver to extract the signal strength. Data files generated by the two systems also differ, but both systems store raw data in binary files to conserve disk space.

The 600-kHz system stores the output from the 8-bit A/D converter directly. A total of 7,000 samples collected at 2 MHz are stored for each data ping, with each sample requiring 1 byte. Thus, a typical 100-ping ensemble will create a file of 700 kB. Seven thousand samples at 2 MHz corresponds to profiling over a range of 2.59 m, providing information slightly beyond the bottom of the tank. Along with the raw data, a file header is written to each file containing the preamplifier setting, A/D board sensitivity, transmit pulse length, and other critical information. Time from the PC clock is written with each ping.

The 2-MHz system stores the scattering level in counts, sampled every 16 μ sec (1.18-cm resolution), with each point occupying 1 byte. Additionally, the 2-MHz system stores velocity information, along with the correlation coefficient, in 10-cm bins. For amplitude information, 290 samples at 1.18-cm resolution are stored, providing information well past the bottom of the tank. As with the 600-kHz system, the 2-MHz system produces a file header with all critical data collection information and writes the time from the PC clock with each ping.

Initial data conversion

All data processing was done using Matlab, so raw data files were first converted into a compatible ASCII format. For the 600-kHz system, this involved averaging the data into 1- or 5-cm cells using a block RMS filter. The long cells (5 cm) were used for backscattering profiles, and the short (1-cm) cells were used to resolve the bottom when transmitting with reduced power. These RMS values were scaled to account for the preamplifier setting and A/D sensitivity, and converted to a relative scale in decibels. The internal scale is set such that 0 dB corresponds to the largest signal the 600-kHz system can resolve.

With the 2-MHz system, data are read from the binary form and written directly to ASCII files. Four different files are created for each 2-MHz raw file: amplitude profiles, velocity profiles, correlation profiles, and a configuration file showing data collection parameters.

Mean profiles

Despite efforts to maintain cleanliness in the calibration chamber, some contamination by foreign particles was unavoidable. These particles would appear as "spikes" in the acoustic data, with return levels much higher than the sediments. In order to minimize the effects of these spikes, a data processing scheme was devised to filter the 100-ping data ensembles, and produce a single mean profile to represent the scattering from the sediments being tested.

The first step in processing the 2-MHz data was to convert data from RSSI counts to a decibel scale. This is done using a calibration table, relating each RSSI count level to a particular signal input level in decibels (see section titled "Receiver Response" in Chapter 4). The 2-MHz data system is more prone to electromagnetic interference and additional despiking was implemented to remove all data profiles that are obviously erroneous.

The 100-ping ensembles were extracted in the same manner for both systems. The individual profiles were stored as a matrix, and then sorted in ascending order. From this sorted version, the middle halves of the profiles were selected, eliminating extreme signal levels. At this point, different processing procedures were used for each system. Since the receivers for the 600-kHz system operate entirely on a linear basis, a linear mean of this middle half of the data was computed, and then the data were converted to log space with the same decibel scale as before. For the 2-MHz system, the mean of the logarithmic values from the middle half of the profiles was calculated to be consistent with the logarithmic averaging performed by the log amplifier. Because a subset of the data was removed, the distribution was changed and the estimated mean no longer represented the statistically correct value. In addition, internal processing of the signal in the 2-MHz system had to be taken into account. The RSSI is

the logarithm of the rectified signal, and is different from the rms value of the intensity. These two effects combine and were included as an offset in the calibration (Table 10).

Table 10
Offset Required to Compensate for Error Introduced in Estimating Mean Scattering Profile

System	Offset Error	Type
600-kHz	+1.3 dB	Linear mean of middle 50 percent (filter out large values)
2-MHz	+1.7 dB	Receive voltage level rectified, logarithmic mean of middle 50 percent

The final result is a single mean profile for each 100-ping ensemble and for each system. The mean profile was calculated for each concentration of a particular sediment size class, providing a set of profiles as shown in Figure 36. The material used in the test run in Figure 36 was Crystal White Silica Sand, 300 to 355 μm in size. The figure shows nine profiles, starting with the background at the bottom and moving up with increasing concentration. Each profile represents one of the nominal concentrations given in Table 3. This test run is used as an example throughout Chapter 5. Mean profiles for all data runs are shown in Appendix B.

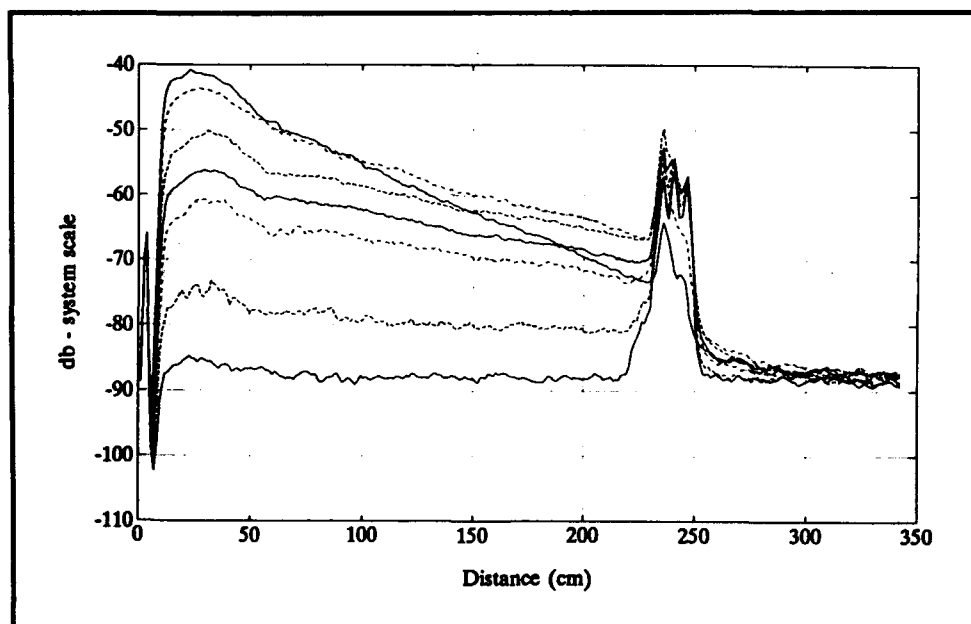


Figure 36. 2-MHz data from Run A06B, mean profiles

System noise correction

For low concentrations (and particularly for smaller particles), the backscattering level is close to the electronic noise level. Measurements are corrected for electronic noise level by subtracting it from all the mean profiles.

For the 600-kHz system, the noise level remains relatively constant from run to run, so a constant value was subtracted from the profiles. This constant was found by recording the system output after the bottom reflection had been received. The 2-MHz system is more susceptible to electromagnetic interference and the noise level changes somewhat from run to run. For each size class, the noise level was determined from the background profile.

Figure 37 shows the same data as Figure 36, after being corrected for system electronic noise. In this plot, the background scattering level has been removed, leaving eight profiles associated with the eight concentration levels above the background profile.

Correction for particle attenuation

A correction for particle attenuation was applied to each set of mean profiles for both acoustic systems. Particle attenuation is a combination of viscous and scattering losses and is proportional in magnitude to the concentration. An absolute measure of the attenuation in the calibration chamber can be made by comparing the magnitude of the bottom echo at all concentrations with the bottom echo in clear water. The reduction in

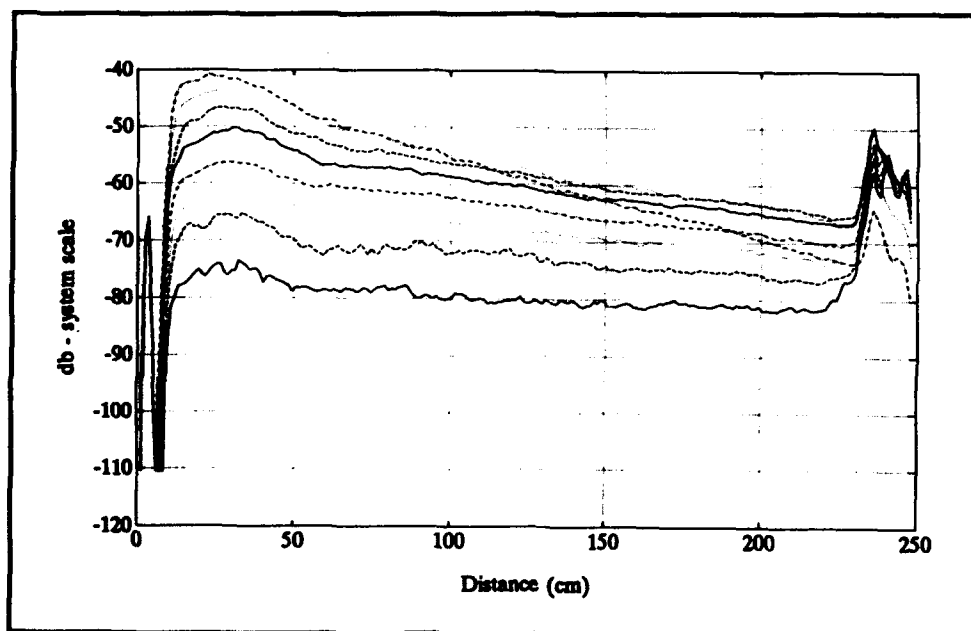


Figure 37. 2-MHz data from Run A06B, noise subtracted

bottom echo is a measure of the integrated attenuation over the length of the chamber caused by the particles. If the concentrations in the chamber are homogeneous, the scattering curves should show constant linear attenuation with range above that caused by absorption and spreading, and can be corrected for the particle attenuation.

Both acoustic systems collected data from the bottom echo. These are shown in Figure 37 as peaks in return levels starting at around 225 cm. In general, attenuation was only significant for the three highest concentrations (nominally 250, 500, and 1,000 mg/l) and for the assumption of homogeneous concentrations in the chamber; therefore, constant linear decay with range was generally valid for these concentrations. It was also found that the best results, as evidenced by the final success in removing range-dependent variation in return signals, were obtained by using the average of the bottom returns from the six lowest concentrations as the "clear water" echo for correcting the three highest concentrations.

Results of the procedure are shown in Figure 38. Figure 38 shows final profiles after applying the absorption, attenuation, and spreading losses. As can be seen in Figure 38, the procedure was reasonably successful in removing significant range-dependent variations in the return signals for the three highest concentrations.

Conversion to volume scattering

Using the near-field modeling and preamplifier calibration described in the section titled "Near Field" in Chapter 4, and the receive and transmit calibration in the section of Chapter 4 titled "Receiver Response," the

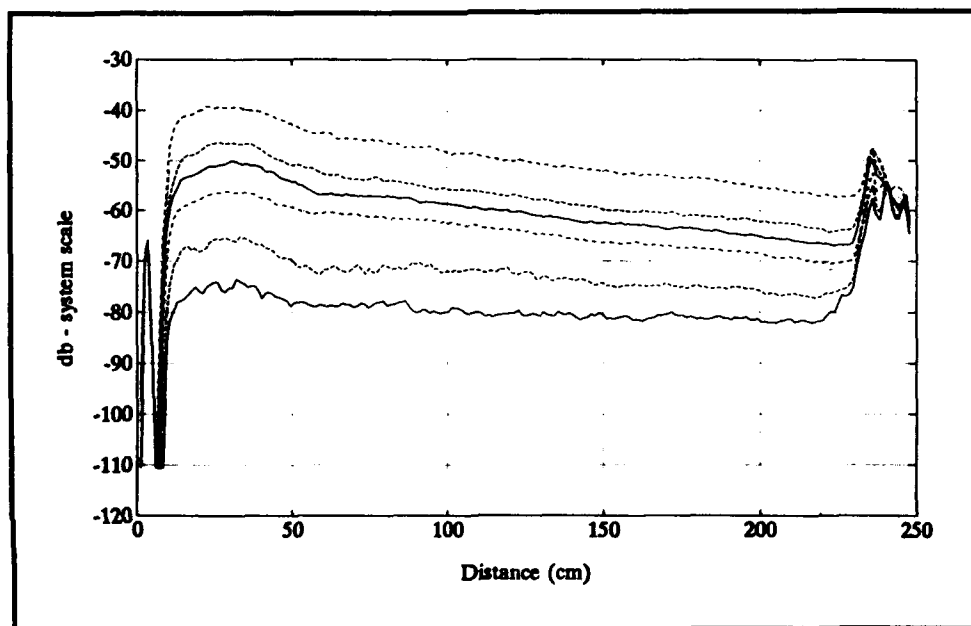


Figure 38. 2-MHz data from Run A06B, corrected for attenuation and noise

echo level can be normalized with respect to range (near and far field), pulse length, beam pattern, and transducer transmit and receive response. This makes it possible to convert all measured scattering levels from system-dependent scales to volume-scattering strength. After introducing the system corrections, and correcting for range, particle attenuation and noise, a set of profiles remain which show volume backscattering strength (S_v) over the length of the sediment chamber. Figure 39 shows the final profiles. The higher concentrations show uniform volume scattering with range. The reason for the increasing levels with range at lower concentrations is assumed to be the result of a vertical gradient in sediment distribution, but this has not been independently verified. If a particle attenuation correction had been applied to these low concentration profiles, the increases with range would have been larger.

Mean scattering levels and averaging interval

From the range- and system-normalized profiles, a series of mean scattering levels for each sediment concentration were extracted. From the profiles of S_v , a 50-cm region centered around the area where the water samples were collected was chosen for further processing; i.e., at approximately 155 cm from the transducers. Volume scattering over this region is averaged to produce data sets of concentration and volume scattering for each acoustic system. These data points can be compared directly with the scattering models, and the example data set is shown in Figure 40.

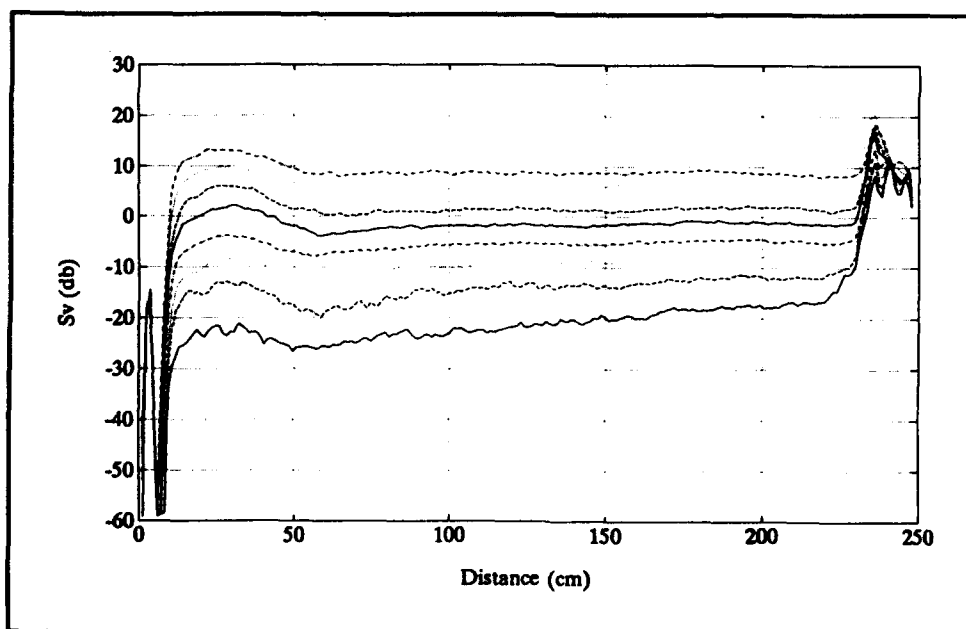


Figure 39. 2-MHz data from Run A06B, corrected for noise, attenuation, and range

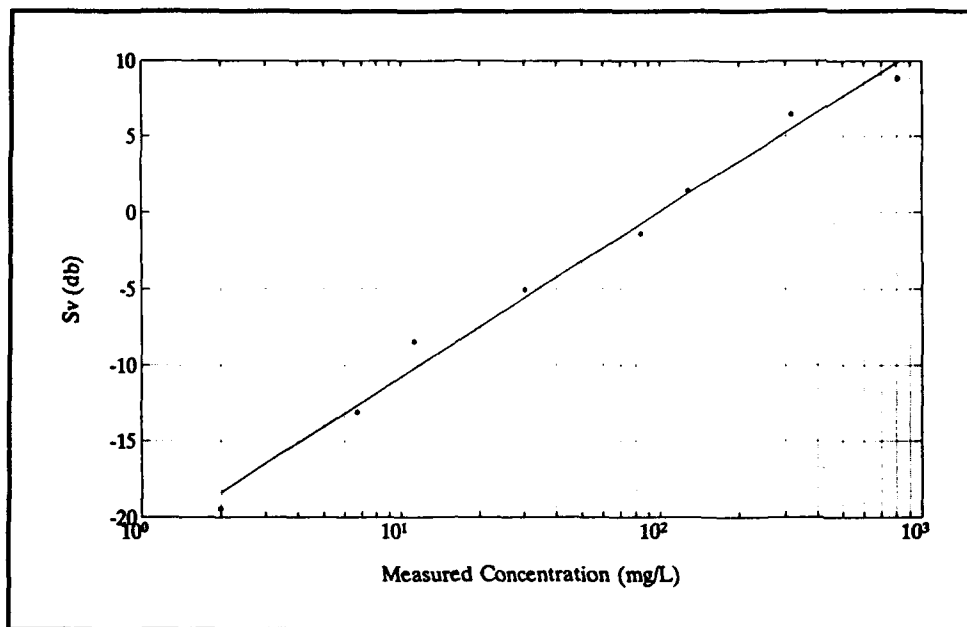


Figure 40. 2-MHz data from Run A06B, mean signal strength versus measured concentration

Additional plots and figures derived from the analysis described in this section and the above section titled "Conversion to volume scattering" are shown in Appendix C. The slope of the linear regression between S_v and concentration is listed in Table A3 (Appendix A). The slope between concentration and S_v (both in log units) for a fixed grain-size distribution should be 1.00 if particle attenuation is accounted for and multiple scattering is insignificant. A slope of 1.00 means that the scattering level is proportional to the number of suspended particles. Table A3 shows the mean slope from all data runs. For the 600-kHz system, the maximum value is 1.30 and the minimum is 0.97. For the 2-MHz system, the maximum slope is 1.71 and the minimum is 0.91. The mean for all runs regardless of frequency is 1.06 with a standard deviation of approximately 0.14. The mean measured correlation coefficient indicates that about half of the contribution (i.e., 0.06) is a consequence of statistical uncertainty. This does not, however, explain the bias toward slopes greater than 1 observed in the data.

Scattering Models

Data were collected during the calibration experiment to ascertain the extent to which acoustic measurements can be used to measure concentrations of suspended sediments. Dredging and dredged material disposal operations involve relatively large variations in suspended sediment concentrations and grain sizes, varying both spatially and temporally. The calibration experiment measured only a small number of the possible combinations of factors affecting the determination of concentrations from

acoustic backscatter measurements and a scattering model is needed to generally apply the results.

The frequencies for acoustic systems with sufficient ranges to be useful for most dredging and dredged material placement sites are such that the wave lengths are often greater than or nearly equal to the diameters of the sediment particles. The scattering model for small nonresonant spheres was first derived by Rayleigh (1945) (see also Clay and Medwin (1977)). Rayleigh's model predicts that the backscatter for spheres much smaller than the wave length is proportional to the fourth power of the frequency and the sixth power of the sphere's diameter. The volume backscattering strength S_v for Rayleigh scattering for spheres can be expressed in decibels as follows:

$$S_v = 10 \log_{10} (C_v k^4 a^3) + 10 \log_{10} (k_1) \quad (14)$$

where

- C_v = volume concentration of scatterers
- k = wave number (i.e., $2\pi/\text{wave length}$)
- a = sphere radius
- k_1 = constant

The constant k_1 is a function of the relative density and elasticity of the spheres and is given by:

$$k_1 = \frac{3}{4} \pi \left(\frac{e-1}{3e} + \frac{g-1}{2g+1} \right)^2$$

where

- e = ratio of sphere/water elasticity
- g = ratio of sphere/water density

This model is theoretically valid to first order when $(ka)^2 \ll ka$. When the ratio of the sphere's radius to the wave length is greater than 2π , but within the range of sizes equivalent to the maximum sediment sizes expected to be suspended during dredging and dredged material placement operations, spheres exhibit resonant oscillations. A model for this region was derived by Faran (1951) (see also Clay and Medwin (1977)).

Contemporaneously with the calibration experiment described in this report, the results of two significant experimental laboratory studies of the relationship between acoustic backscatter and suspended sediment concentrations were published. These are described in a paper by Hay (1991), who conducted multifrequency (1-, 2.25-, and 5-MHz) experiments using a free turbulent water jet carrying material in suspension, and two papers

by Thorne (1992 and 1993), who conducted tank studies similar to one described in this report using a 3-MHz system. Both studies found good agreement between Rayleigh scattering theory and the results of their experiments in the region of grain sizes where the model is predicted to be valid. Hay observed resonant scattering for glass spheres of the appropriate size, as predicted by theory, but found that natural sand with equivalent diameters did not display this resonant behavior. He attributed this absence of resonant behavior to the irregular shape of the sand. Hay also derived the theoretical prediction that at some point when the concentrations are great enough multiple scattering will make it impossible to determine the concentration from the backscatter. Hay's experimental results seemed to show that at 5 MHz, multiple scattering was not significant until the concentrations reached 2,500 mg/l.

Model Comparisons

Scattering models for small particles

To compare results with the scattering models it is customary (Hay 1991) to present the data in terms of a form factor f . In terms of S_v , the form factor is defined as:

$$f_{\infty} = 10^{S_v/20} * \sqrt{\left(\frac{4}{N * a^2}\right)} \quad (15)$$

where S_v and a are defined in Equation 14 and N is the number of particles inside a reference volume of 1 m^3 . The form factor describes the extent to which the scattering strength departs from being proportional to the area of the particles. In Figure 41, the mean form factors derived from data sets in the experiment are plotted with the results of Faran's (dashed line) and Rayleigh's models (solid line) for spheres with the density and elasticity of the glass beads. The circles are from the 600-kHz system and the asterisks are from the 2-MHz system. The horizontal scale is ka . For the model, the form factor is defined as $2|p|/a$ where $|p|$ is the absolute value of the scattered pressure from an individual particle. No screening, other than the processing described in the section titled "Data Processing" in this chapter, was performed. All data points have been plotted using concentrations derived from the water samples. The numbers of particles inside a reference volume were estimated from the true density of the particles.

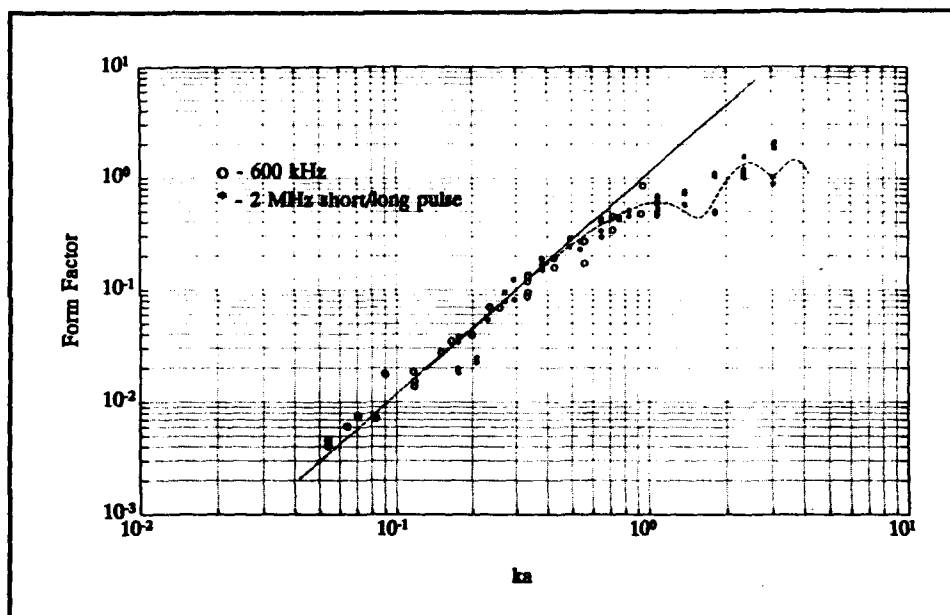


Figure 41. Measured form factor for all data and for both acoustic systems

Correction terms

Using the scattering models, the data can be corrected for the effects of finite bandwidth and distribution of sediments inside a size class. These effects (see Table 11) are relatively small for the systems and suspended material samples used in the experiment.

Table 11 Effect of Correcting for Bandwidth and Size Distribution		
Parameter	600-kHz System	2-MHz System
Size distribution (change in effective scattering frequency)	<5% (not included)	<5% (not included)
Bandwidth (transmit pulse for 600 kHz is four carrier cycles)	6%	—
Outlying data points (output power/run y23a and y24a)	—	+ 3 dB in Sv

The size classes used during the experiment were quite narrow with a typical maximum width of 15 percent. For the Rayleigh scattering regime, the effect of a uniform distribution inside the size class is to increase the effective ka value by no more than 5 percent. Since most size classes have a width of only 7 percent, the overall effect of size distribution is negligible.

The 600-kHz system transmitted short pulses. The pulses consisted of four carrier cycles, corresponding to 25 percent bandwidth. In the Rayleigh scattering regime, the high frequency components of the

transmit pulse are scattered more effectively and the effective scattering level is increased. Alternatively, this can be shown through numerical integration to be equivalent to a 6-percent increase in the center frequency for the 600-kHz system.

Finally, two of the outlying points for the 2-MHz system in Figure 41 were caused by an accidental change in the transmit power during the experiment. Based on the bottom echo, the transmit power used during runs Y23a and Y24 is estimated to be about 3 dB below the normal power level. With these three minor effects included, the data in Figure 41 were replotted in Figure 42. In Figures 43 and 44 data collected with glass beads are plotted separately from data collected with sand particles (i.e., CWSS). The overall fit with the model is quite good.

For $ka < 1$, there is little difference between scattering from glass beads and from sand. This implies that the particle shape is irrelevant for small particles, at least as long as the irregularities are modest, such as is the case for sand. For $ka > 1$, the scattering from sand departs from the model for glass beads; this is true even if the beads are modeled with density and elasticity identical to crystal silica. This agrees with the results of Hay (1991) and is probably a result of the irregular shapes of the sand particles.

Dependence on particle size

Comparisons with the scattering models as shown in Figures 40-44 are convenient because the form factor can be plotted on the same horizontal scale (ka) for both systems, making quantitative judgments about the comparisons between model and data relatively simple. In Figure 45, S_v has

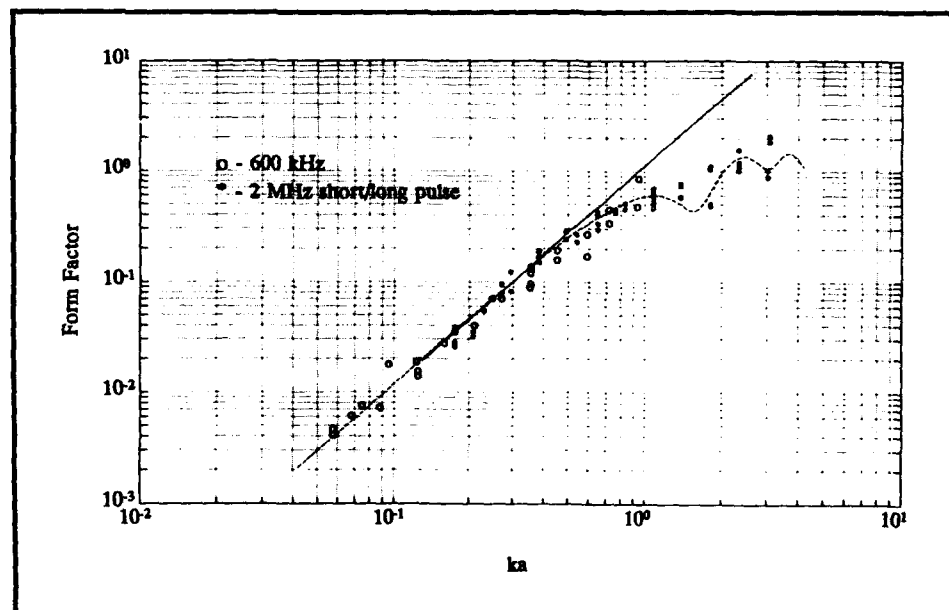


Figure 42. Same as Figure 41 but after correction for bandwidth

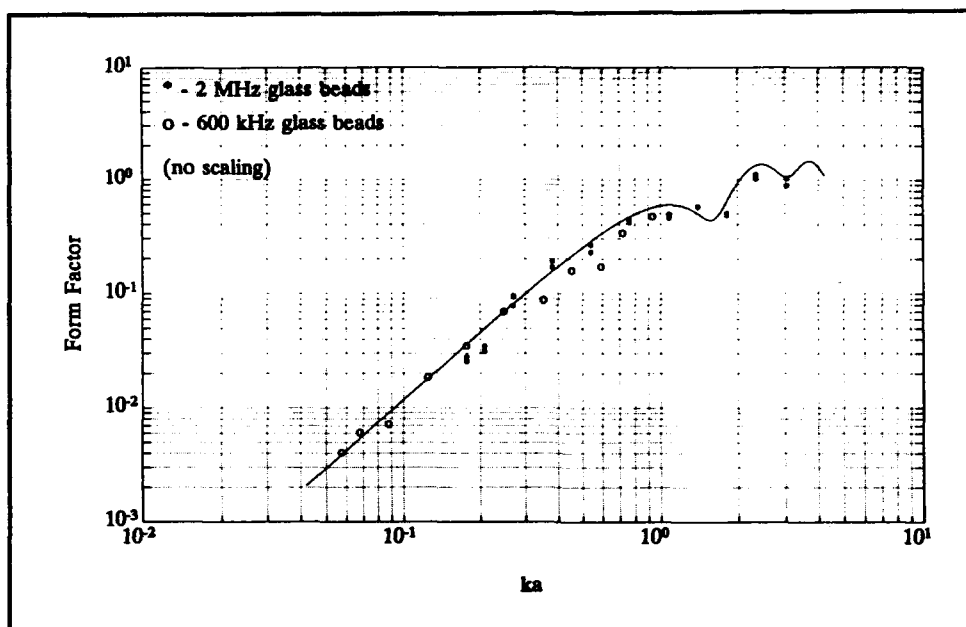


Figure 43. Measured form factor - glass beads only

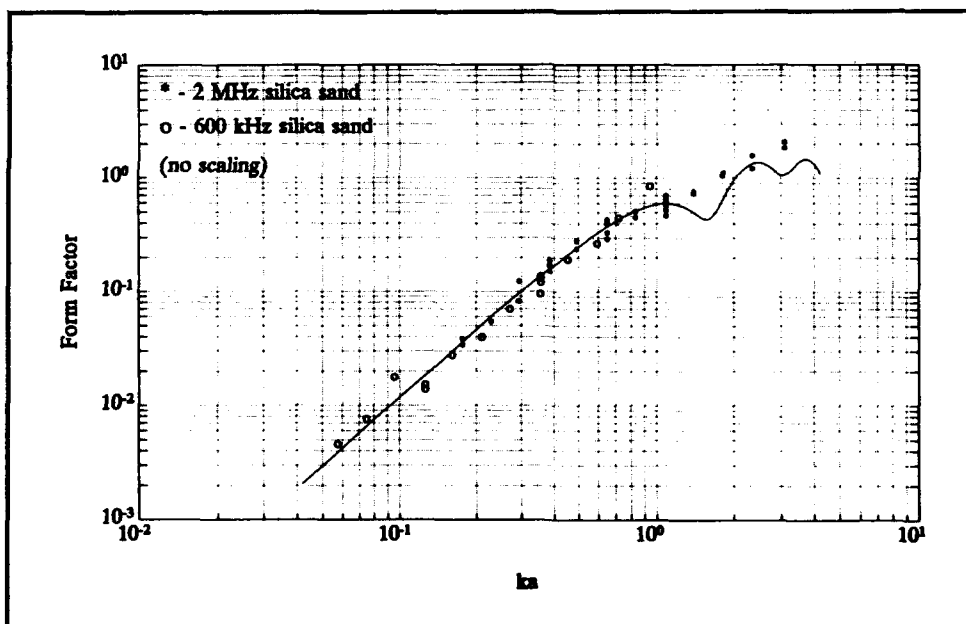


Figure 44. Measured form factor - sand only

been normalized for concentration, and plotted as a function of the log of the particle radius. These data are for CWSS and silica only. This normalized data set shows the size sensitivity of the backscatter data as defined by Clark, Proni, and Craynock (1984).

Figure 45 shows that the volume backscattering strength normalized with concentration varies as the third power of the radius for the 2-MHz system up to a radius of approximately $60 \mu\text{m}$, or $ka = 0.5$. Extending the

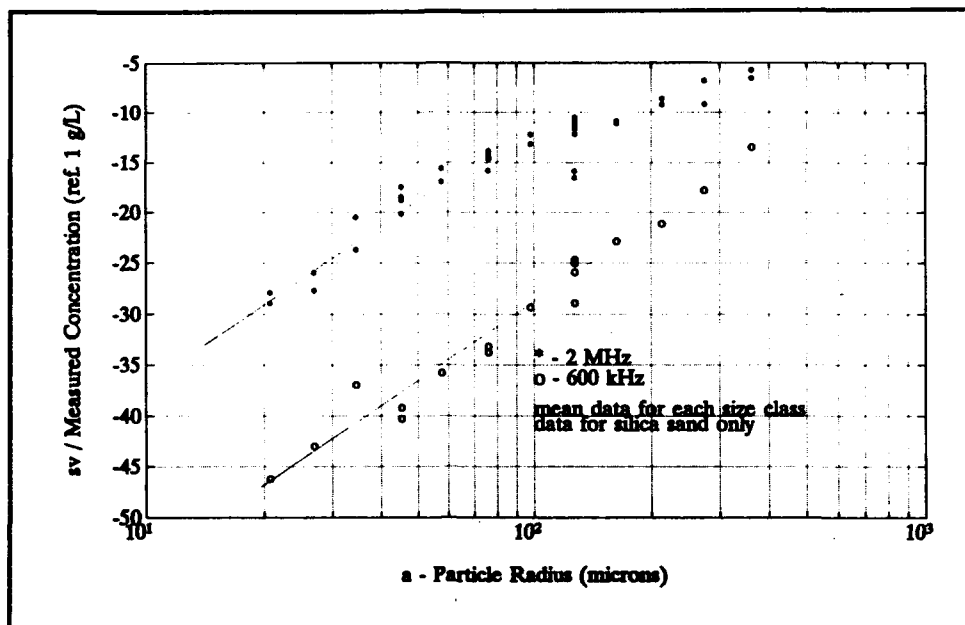


Figure 45. Sensitivity of the backscatter strength with particle size

third power dependence up to $ka = 1$, or 120 μm , would result in approximately a 5-dB error for the largest grain sizes. Above 60 μm , until the limit of the data points, i.e., approximately $ka = 3$, the dependence is to the 1.3 power of radius with no obvious resonant oscillations.

Figure 45 also shows data for the 600-kHz system. If the data point for a nominal radius of approximately 41 μm is disregarded, the values of S_v are correct relative to the 2-MHz data for a k^4 dependence on frequency. The size dependency is to the third power for all of the remaining data points, which for 600 kHz, is up to approximately $ka = 0.95$. The results agree well with a Rayleigh scattering model given by Equation 14 and there is no evidence of resonance. This agrees with Hay (1991) and Thorne (1992 and 1993).

6 Conclusions

An experimental laboratory study of acoustic backscattering from particles equivalent in size to those potentially found at dredging and dredged material disposal sites was conducted. The objective of the study was to determine the relationship between acoustic backscatter and sediment size, composition, and concentration to be used to analyze and interpret field data from PLUMES. To achieve the objective, a calibration chamber was designed and built. Particles of uniform size were suspended in the calibration chamber and backscatter and attenuation measurements were made using two different acoustic systems, one operating at a nominal frequency of 600 kHz and one operating at 2 MHz.

Main Results

The experiment was successful for glass beads and sand particles ranging in size from 38-850 μm at nominal concentrations of 5 to 1,000 mg/l. The average slope between concentration (in log units) and backscatter intensity (in log units) was measured to be 1.07 for a fixed grain size distribution. Part of the deviation from the theoretical slope of 1.00 is due to statistical error. It was concluded that, within the accuracy of the experiment, backscatter is proportional to concentration for a fixed size distribution.

The data show the same dependency on particle size and frequency as predicted by a Rayleigh scattering model for the appropriate range of grain sizes. This has independently been confirmed by Hay (1991) in his work at 1, 2.25, and 5 MHz and later by Thorne and Campbell (1992) and Thorne, Hardcastle, and Soulsby (1993). At 2 MHz, the Rayleigh model predicts the volume backscattering strength well for particles with diameters less than 120 μm . When the ratio of the particle radius to the acoustic wave length is greater than 2π , scattering from sand particles departs from the Faran (1951) model and does not exhibit resonances. This was previously observed by Hay (1991) and may be due to the irregularity of the particles. For the 600-kHz system, the Rayleigh model works well for all particles, including the largest particles with a nominal diameter of 760 μm .

The experiment was unsuccessful for particles that were less than 10 μm in size. It was determined that selective trapping of smaller grain sizes in the calibration system made it impossible to accurately make the required measurements for these small particles.

Calibration of the system parameters was carried out using a calibrated hydrophone. Calibration using the hydrophone was found to be the most accurate method for determining the acoustic performance of the 600-kHz and 2-MHz systems. An attempt was made to develop a simpler and more robust calibration method based on the self-reciprocity principle. The attempt failed, partly because of lack of dynamic range in the two acoustic systems at the high end and partly because the transducer beam widths were too narrow.

In terms of PLUMES, these results show that the PLUMES acoustic performance needs laboratory calibration and that a Rayleigh scattering model should be used to analyze and interpret field data for nearly all sediments of interest at sites of dredging and dredged material placement operations.

Acknowledgments

The calibration experiment was carried out under phase II of the PLUMES contract with the U.S. Army Engineer Waterways Experiment Station, Vicksburg, MS. The project was funded as part of the Dredging Research Program, Technical Area 1. We would like to thank Dr. Nicholas C. Kraus and Ms. Michelle Thevenot of the Coastal Engineering Research Center for their support and practical guidance. We would also like to thank Keith Bedford, Paul Ogushwitz, John Proni, Mark Skarbek, and Orson Smith of the PLUMES Technical Review Committee for providing valuable input in the design phase of the experiment. Last, we would like to extend our gratitude to Ramon Cabrera, Cedric Mallinckrodt, Mike Mulvany, and Jaime Hogan for dedicating their time and effort to getting the work done.

References

- Brumley, B. H., Cabrera, R. G., Deines, K. L., and Terray, E. A. (1991). "Performance of a broad-band acoustic Doppler current profiler," *IEEE J. Oceanic Eng.* 16(4), 402-7.
- Clarke, T. L., Proni, J. R., and Craynock, J. F. (1984). "A simple model for the acoustic cross section of sand grains," *J. Acoust. Soc. Am.* 76, 1580-2.
- Clay, C. S., and Medwin, H. (1977). *Acoustical oceanography: Principals and applications*. John Wiley and Sons, New York.
- Crickmore, M. J., and Aked, R. F. (1975). "Pump samplers for measuring sand transport in tidal waters." *Conference on instrumentation in oceanography*. University College of North Wales, Bangor, IERE Conference Proceeding No. 32, 311-26.
- Faran, J. J. (1951). "Sound scattering by solid cylinders and spheres," *J. Acoust. Soc. Am.* 23, 405-18.
- Francois, R. E., and Garrison, G. R. (1982). "Sound absorption based on ocean measurements; Part II: Boric acid contribution and equation for total absorption," *J. Acoust. Soc. Am.*, 72, 1879-90.
- Hay, A. E. (1991). "Sound scattering from a particle-laden, turbulent jet," *J. Acoust. Soc. Am.*, 90, 2055-74.
- Libicki, C., Bedford, K. W., and Lynch, J. F. (1989). "The interpretation and evaluation of a 3-MHz acoustic backscatter device for measuring benthic boundary layer sediment dynamics," *J. Acoust. Soc. Am.*, 85, 1501-11.
- Ma, Y., Varadan, V. V., and Varadan, V. K. (1987). "Acoustic response of sedimentary particles in the near field of high-frequency transducers," *IEEE, UFFC-34*, 3-7.
- Rayleigh, Lord (J. W. Strutt). (1945). *The theory of sound*, Vols. 1 and 2 (2nd eds., 1894 and 1896), published in one volume by Dover, New York.

Simmons, V. P. and Fisher, F. H. (1977). "Sound absorption in sea water," *J. Acoust. Soc. Am.* 62, 558-64.

Tamura, T., and Hanes, D. M. (1986). "Laboratory calibration of a 3 megahertz acoustic concentration meter to measure suspended sand concentration," *University of Miami, Rosenstiel School of Marine and Atmospheric Science Technical Report*, 86-004.

Thorne, P. D., and Cambell, S. C. (1992). "Backscattering by a suspension of spheres," *J. Acoust. Soc. Am.*, 92, 978-986.

Thorne, P. D., Hardcastle, P. J., and Soulsby, R. (1993). "Analysis of acoustic measurements of suspended sediments," *Journal of Geophysical Research*, 98, C1, 899-910.

Appendix A

File Summary Tables and Slope Information

Table A1 is a complete listing of all tests associated with the PLUMES calibration experiment, covering March 17 through July 2, 1992. This includes all sediment runs, as well as special tests as calibration efforts.

Table A2 is a listing of successful sediment calibration runs. The listing is organized by sediment size class, and lists all runs for which data are presented in Appendix B.

Table A3 is a listing of the slope and correlation coefficient from a linear regression of concentration and volume scattering data. Data are presented for all successful runs with uniform sediment size classes. Regressions are performed using $10 \cdot \log_{10}(\text{concentration})$, and the volume-scattering level in decibels.

Table A1
Summary of Data Runs

Date	Run	Experiment	Comments
March 17	A	212-300 CWSS	
March 18	A	590-840 micron glass beads	No 2-MHz attenuation files
March 18	B	2 MHz attenuation testing	
March 19	A	590-840 micron glass beads	
March 19	B	500-600 micron glass beads	600 attenuation/pulse to 64
March 20	A	355-500 micron glass beads	
March 20	B	210-297 micron glass beads	
March 21	A	149-210 micron glass beads	
March 21	B	38-45 micron glass beads	Noise problems
March 23	A	105-149 micron glass beads	
March 23	B	38-45 micron glass beads started	Sample degassing
March 24	A	74-105 micron glass beads	
March 24	B	53-74 micron glass beads	
March 25	A	45-53 micron glass beads	
March 25	B	Norfolk project samples	Run aborted
March 26	A	500-600 micron glass beads	Uneven distribution
March 27	A	Norfolk project samples	Incl 2.4 MHz
March 30	A	600-850 CWSS	Uneven distribution
March 30	B	500-600 CWSS	Uneven distribution
March 31	A	355-500 CWSS	Jets aligned
April 1	A	Particle Distribution Testing	Changing jets
April 2	A	Test for bubbles and jet alignment	
April 2	B	Added drills - test with 600-850 micron CWSS	
April 3	A	600-850 micron CWSS	Using drills
April 6	A	Testing noise effects of drills	
April 6	B	300-355 micron CWSS	Drills 65%
April 7	A&B	212-300 micron CWSS, double run	Drills 60%
April 8	A	180-212 micron CWSS	Drills 60%
April 8	B	125-180 micron CWSS	Drills 60%
April 9	A	106-125 micron CWSS	Drills 50%
April 10	A	Anchorage Alaska samples	Noise problems
April 14	A	212-300 micron CWSS, repeat	Drills 60%
April 15	A	212-300 micron CWSS, 20 grams	Single conc. tests
April 16	A	212-300 micron CWSS, 20 grams	bottom changes
April 17	A	212-300 micron CWSS, 20 grams	bottom changes
April 20	A	clean tank, then sand	temp. changes
April 21	A	using 600 kHz log receiver	temp. changes
April 21	B	Trying to control system temperature	
April 22	A&B	2 MHz - looking for positioning errors	
April 22	C&D	2 MHz - temperature testing	
April 27	—	Direct feed in 600 kHz preamp calibration	
April 27	A	2 MHz looking at horizontal distribution	

(Continued)

Table A1 (Concluded)

Date	Run	Experiment	Comments
April 28	—	600 kHz preamp temperature calibration	
April 29	—	2 MHz RSSI calibration with hockey pucks	
May 5-7, 11	—	2 MHz absolute calibration (E8 hydrophone)	
May 12	—	600 kHz absolute calibration (E27 hydrophone)	
May 12	A	212-300 micron CWSS	New 600 xdcr
May 13	A	Kaolinite	To 2500 mg/l
May 15	A	212-300 micron CWSS Bottle sampling test	
May 15	B	Kaolinite testing 600 kHz (Data lost?)	No samples
May 23	A	45-53 micron glass beads	
May 24	A	38-45 micron glass beads	
May 27	A	38-45 micron Silica	
May 28	A	45-63 micron Silica	
May 29	A	63-75 micron Silica	
June 1	A	Kaolinite testing (2 MHz) - with bottle samples	
June 7	A	75-106 micron Silica	
June 8	A	125-180 micron Silica	Not a full run
June 8	B	75-106 micron CWSS	Not a full run
June 9	A	Silica Mix #1 (212/125 micron)	Drills 65%
June 9	B	590-840 micron beads	Drills 65%
June 10	A	15 micron silica	Testing - unsuccessful
June 10	B	15 micron silica	Testing - unsuccessful
June 11	A	500-600 micron glass beads	Drills 65%
June 12	A	355-500 micron glass beads	Drills 65%
June 15	A	300-355 micron glass beads	Drills 65%
June 16	A	210-297 micron glass beads	Drills 65%
June 16	B	500-600 micron CWSS	Drills 65%
June 17	A	355-500 micron CWSS	Drills 65%
June 18	A	15 micron silica testing	
June 19	A	15 micron silica testing - with larger silica	
June 29	A	Silica Mix #2 (180 / 75 - different order)	Drills 65%
June 30	A	600 kHz 5 beam absolute calibration (E27)	

Table A2
Data Run by Sediment Type and Size Class

Material	Date	Run
600-850 micron CWSS	April 3	A
500-600 micron CWSS	June 16	B
355-500 micron CWSS	June 17	A
300-355 micron CWSS	April 6	B
212-300 micron CWSS	April 7 April 14 May 12	A,B A A
180-212 micron CWSS	April 8	A
125-180 micron CWSS	April 8	B
106-125 micron CWSS	April 9	A
75-106 micron CWSS	June 8	B
125-180 micron Silica	June 8	A
75-106 micron Silica	June 7	A
63-75 micron Silica	May 29	A
45-63 micron Silica	May 28	A
38-45 micron Silica	May 27	A
Silica Mix #1 (Mix 220 g 212-300 micron CWSS with 210 g 125-180 micron CWSS and 10 g 125-180 micron silica. Normal concentration levels using mix of sizes)	June 9	A
Silica Mix #2 (Add 20 g 180-212 micron CWSS to tank - record data. Begin adding 75-106 micron silica in {10 10 30 50 100 127} g increments. Watching as small sediments gradually dominate scattering)	June 29	A
15 micron Silica	June 18 June 19	A A
Norfolk project samples	March 27	A
Kaolinite	June 1	A
590-840 micron glass beads	June 9	B
500-600 micron glass beads	June 11	A
355-500 micron glass beads	June 12	A
300-355 micron glass beads	June 15	A
210-297 micron glass beads	June 16	A
149-210 micron glass beads	March 21	A
105-149 micron glass beads	March 23	A
74-105 micron glass beads	March 24	A
53-74 micron glass beads	March 24	B
45-53 micron glass beads	May 23	A
38-45 micron glass beads	May 24	A

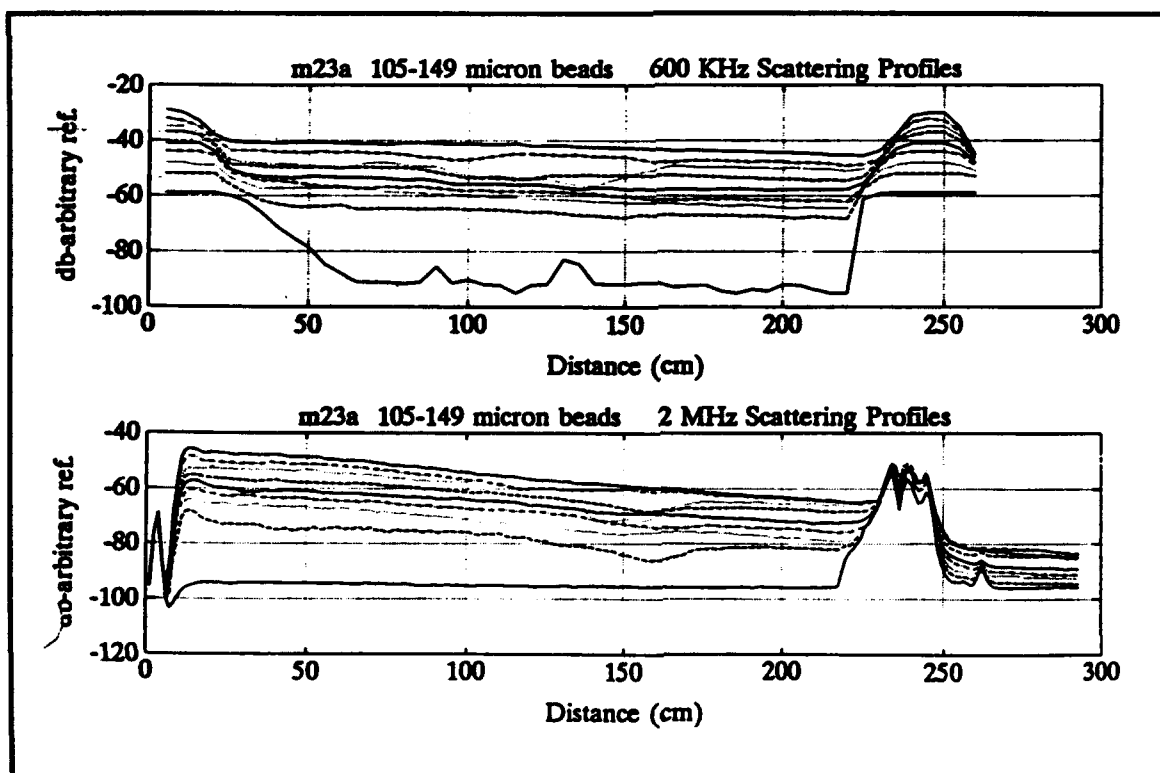
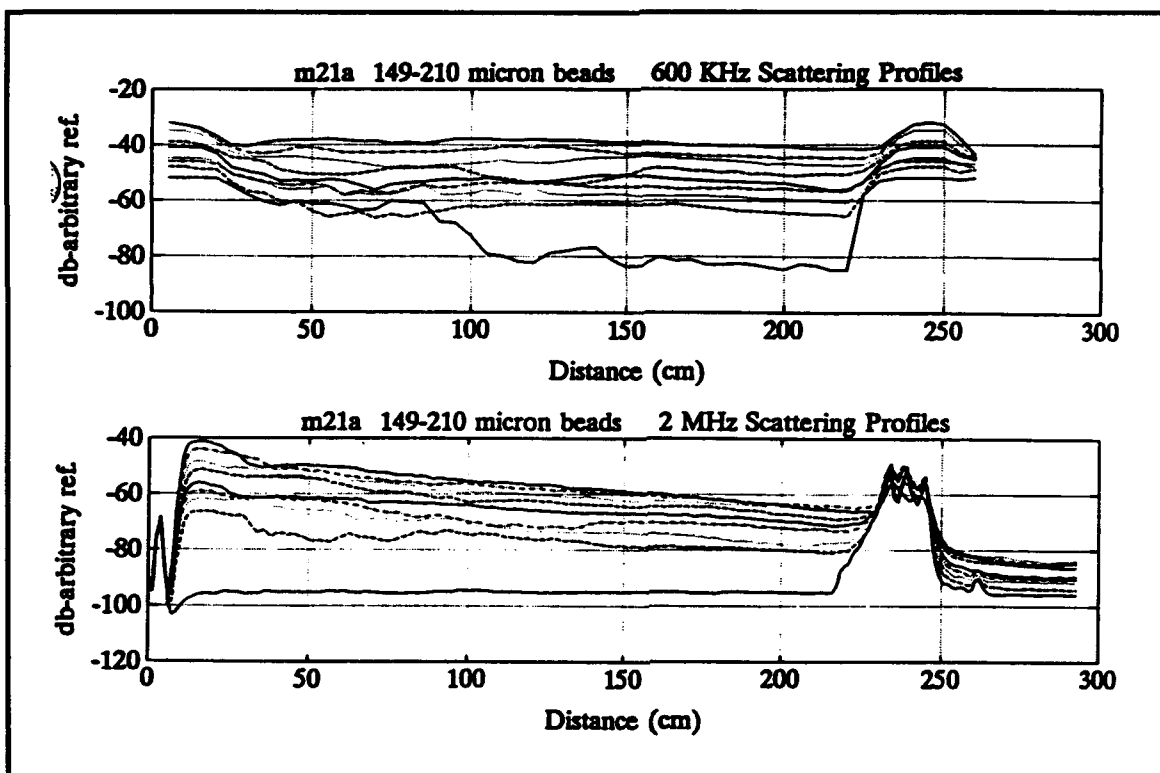
Table A3
Summary Results of All Slope and Correlation Coefficients (Concentration Versus Mean Scattering Level)

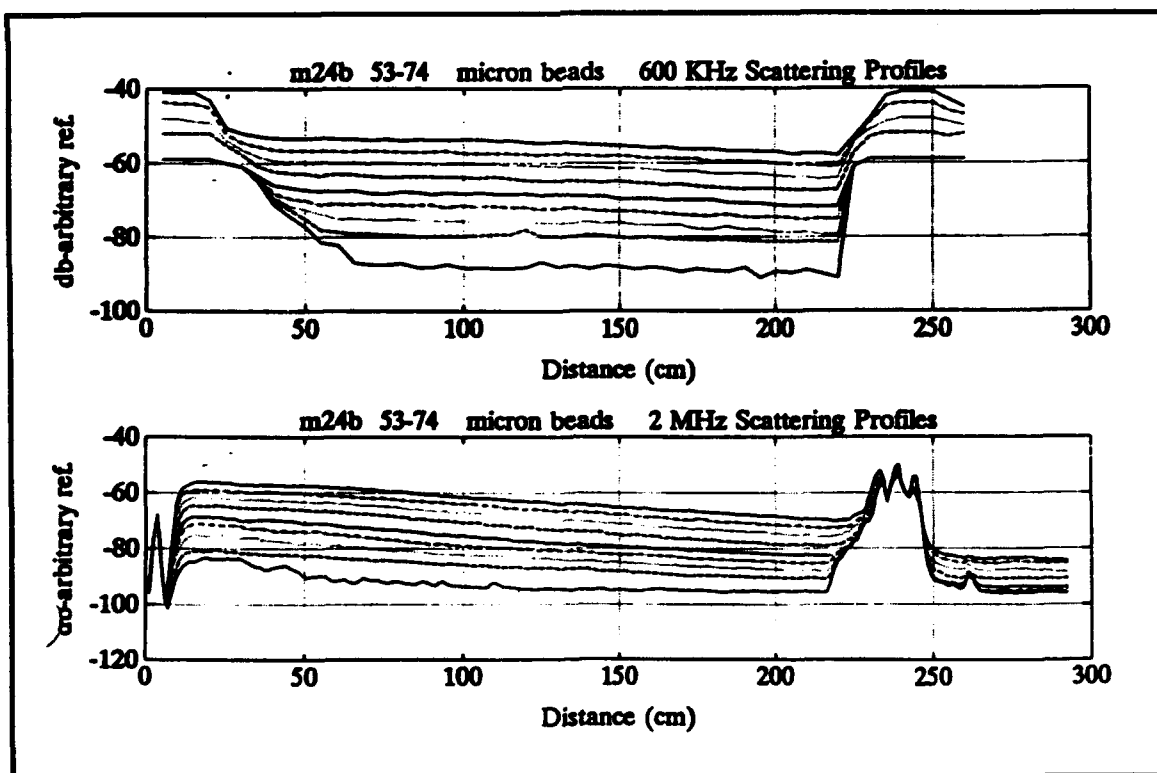
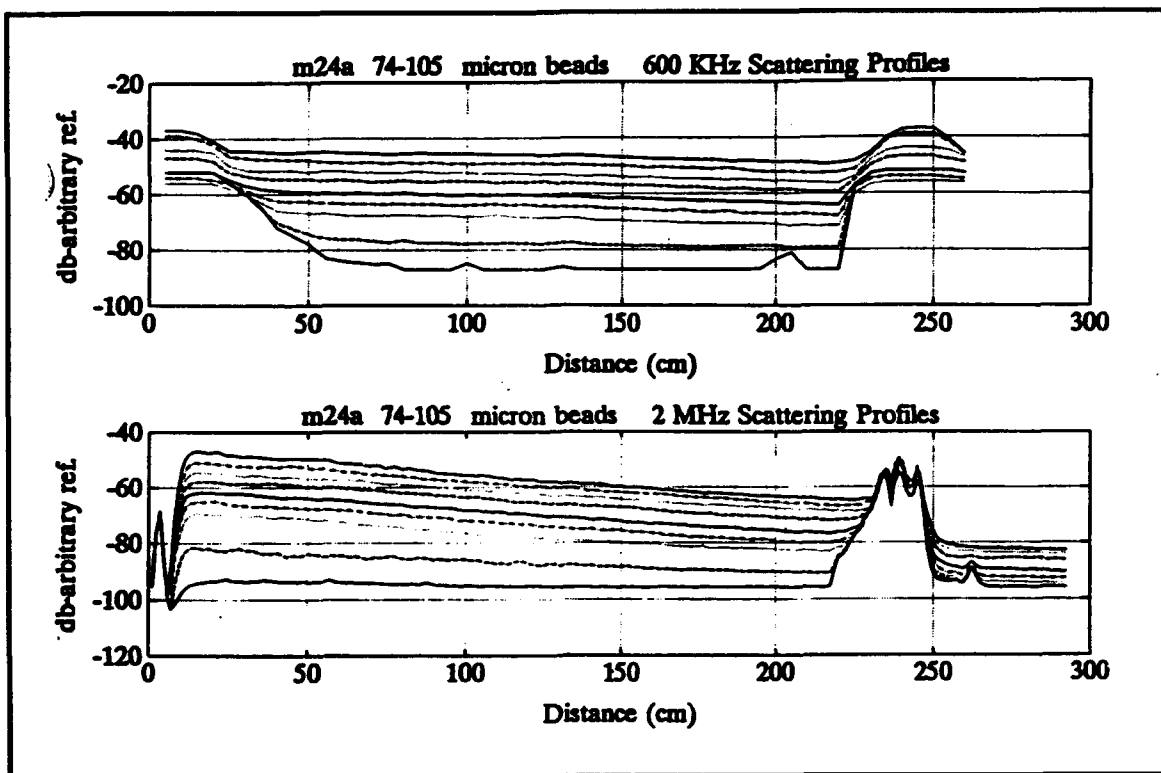
Data run	Material	600 kHz Slope/Corr	2 MHz Short Pulse Slope/Corr	2 MHz Long Pulse Slope/Corr
m21a	149-210 micron beads	0.966/0.994	1.064/0.998	1.041/0.997
m23a	105-149 micron beads	1.065/0.991	1.110/0.974	0.966/0.928
m24a	74-105 micron beads	1.082/0.999	1.085/0.999	1.114/0.997
m24b	53-74 micron beads	0.872/0.997	0.942/0.989	0.980/0.997
m27a	Norfolk sample	1.094/0.969	1.270/0.992	1.284/0.989
a03a	600-850 micron CWSS	0.876/0.984	0.954/0.992	0.765/0.991
a06b	300-355 micron CWSS	1.192/0.998	1.087/0.994	0.997/0.995
a07a	212-300 micron CWSS	1.047/0.993	0.900/0.985	0.860/0.993
a07b	212-300 micron CWSS	1.143/0.989	0.955/0.963	0.924/0.983
a08a	180-212 micron CWSS	0.985/0.997	0.847/0.992	0.876/0.995
a08b	125-180 micron CWSS	1.074/0.999	0.876/0.995	0.867/0.995
a09a	106-125 micron CWSS	0.889/0.965	0.770/0.974	0.768/0.981
a14a	212-300 micron CWSS	1.048/0.998	1.099/0.999	1.076/0.997
y12a	212-300 micron CWSS	1.390/0.970	1.712/0.932	1.669/0.941
y23a	45-53 micron beads	0.846/0.991	0.987/0.998	0.993/0.996
y24a	38-45 micron beads	0.957/0.998	1.065/1.000	1.108/0.999
y27a	38-45 micron Silica	1.012/0.999	1.090/0.999	1.113/0.999
y28a	45-63 micron Silica	1.034/0.996	1.410/0.930	1.126/0.999
y29a	63-75 micron Silica	0.876/0.988	0.968/0.958	1.116/0.989
j07a	75-106 micron Silica 125-180 micron	1.048/0.984	1.109/0.976	1.172/0.970
j08a	Silica	1.116/0.957	1.133/0.906	1.127/0.918
j08b	75-106 micron CWSS	0.947/0.998	0.983/0.992	1.001/0.991
j09a	Silica Mix #1	1.297/0.999	1.073/0.987	1.082/0.994
j09b	590-840 micron beads	1.132/0.981	1.106/0.948	0.885/0.975
j11a	500-600 micron beads	1.133/0.986	1.160/0.976	0.975/0.990
j12a	355-500 micron beads	1.210/0.991	1.180/0.996	1.070/0.997
j15a	300-355 micron beads	0.981/0.980	1.033/0.986	0.960/0.975
j16a	210-297 micron beads	1.145/0.997	1.050/0.995	1.036/0.998
j16b	500-600 micron CWSS	1.124/0.998	1.146/0.988	0.890/0.990
j17a	355-500 micron CWSS	1.161/0.998	1.151/0.988	1.032/0.997
Mean Slope		1.06	1.08	1.03

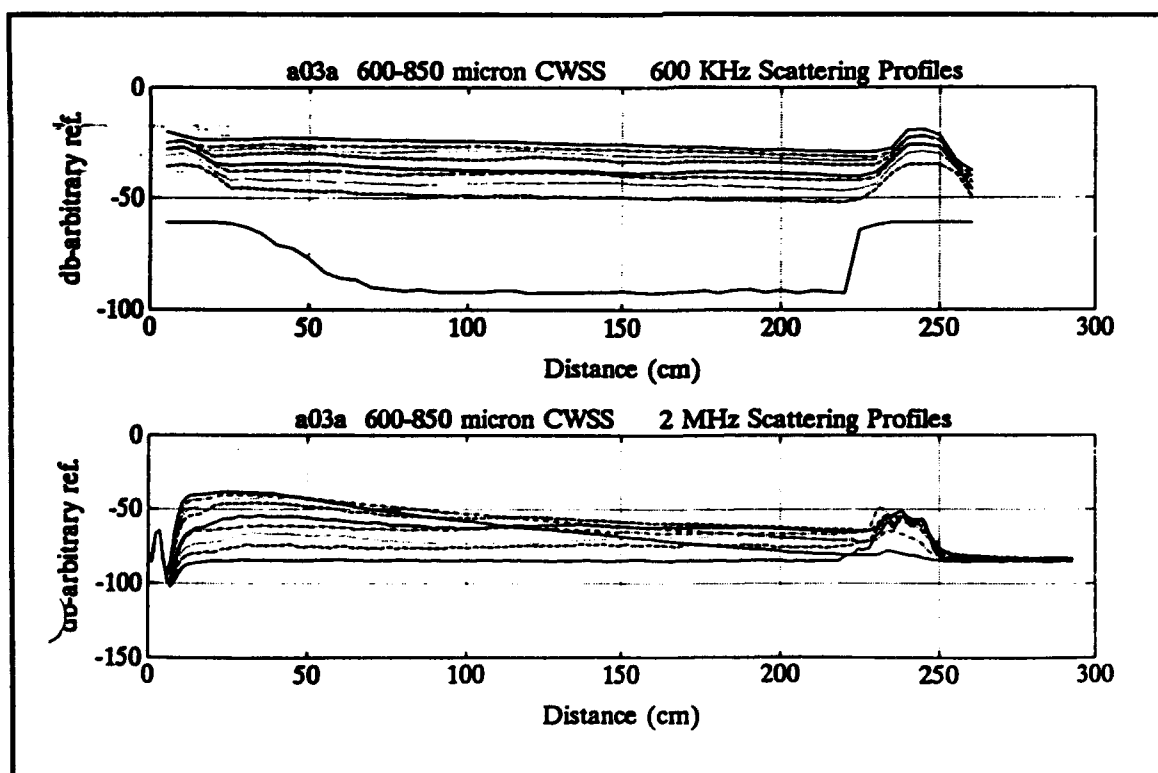
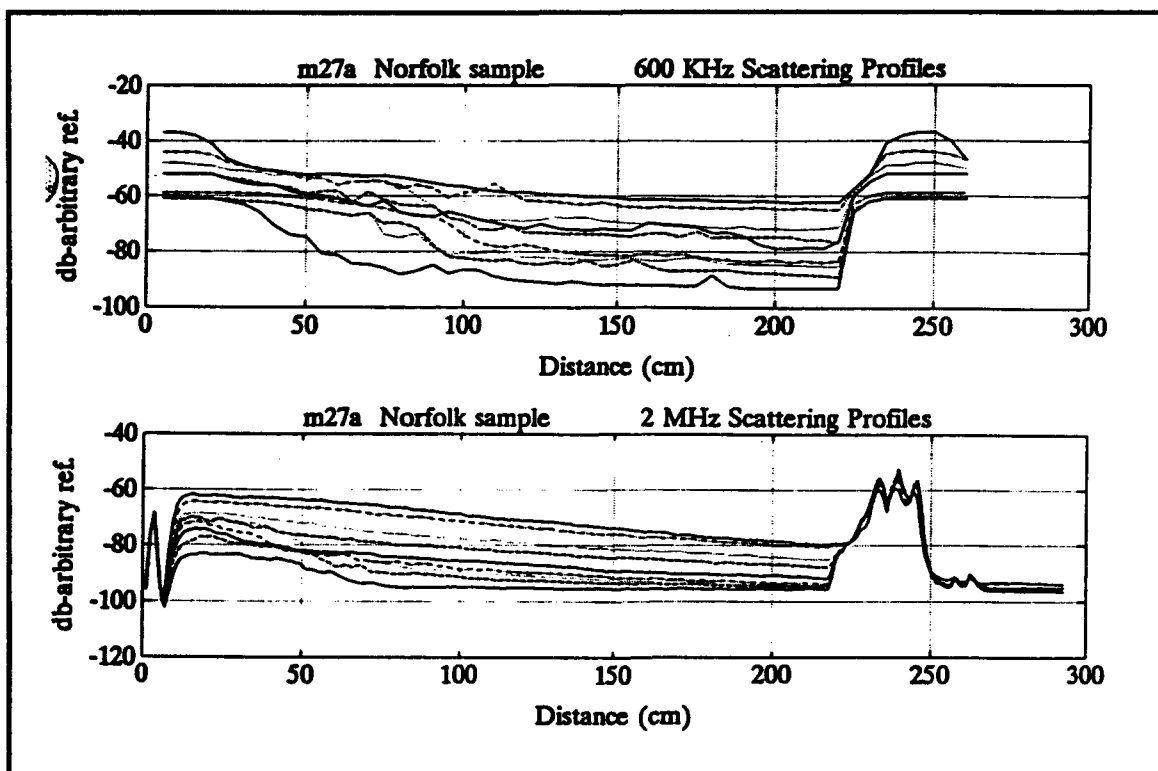
Appendix B

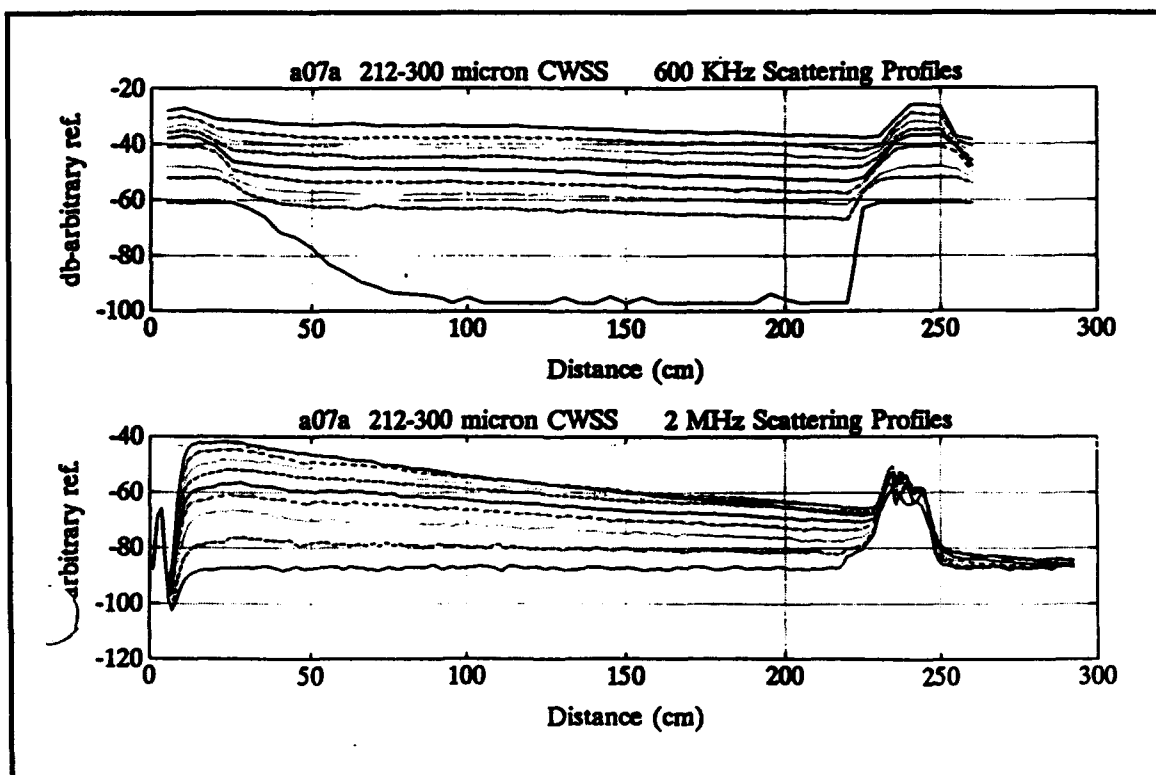
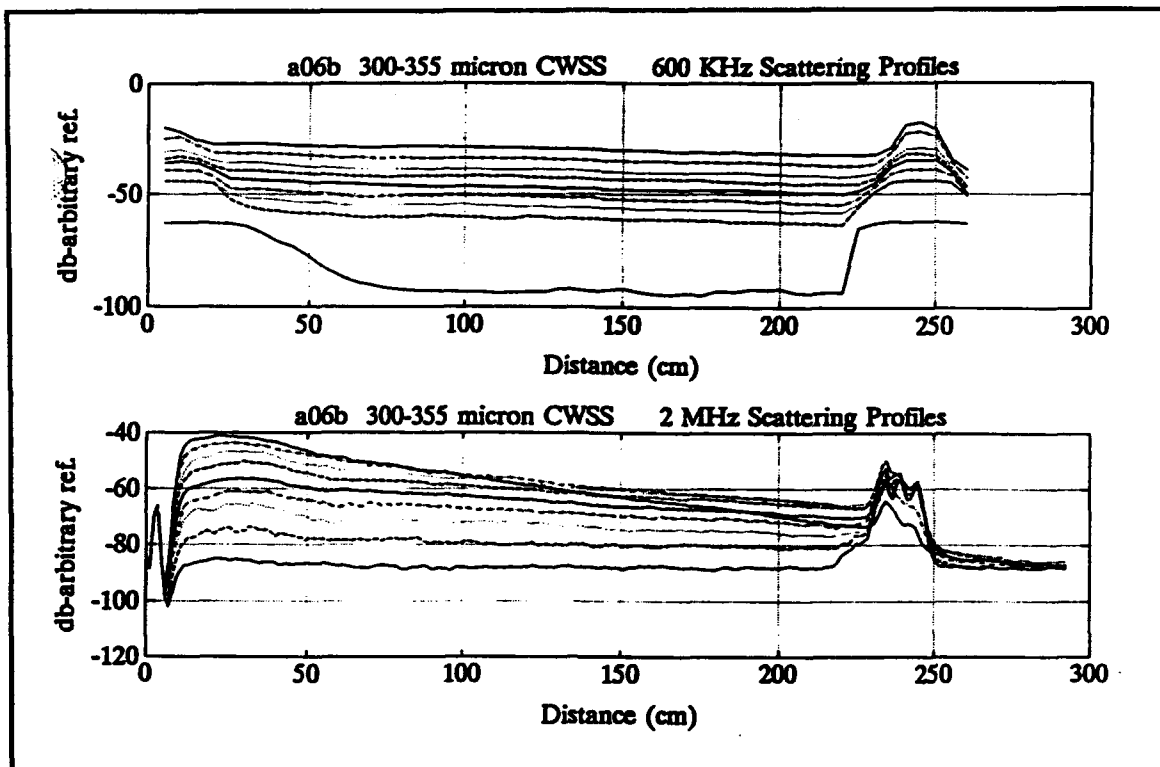
Uncorrected Mean Scattering Profiles

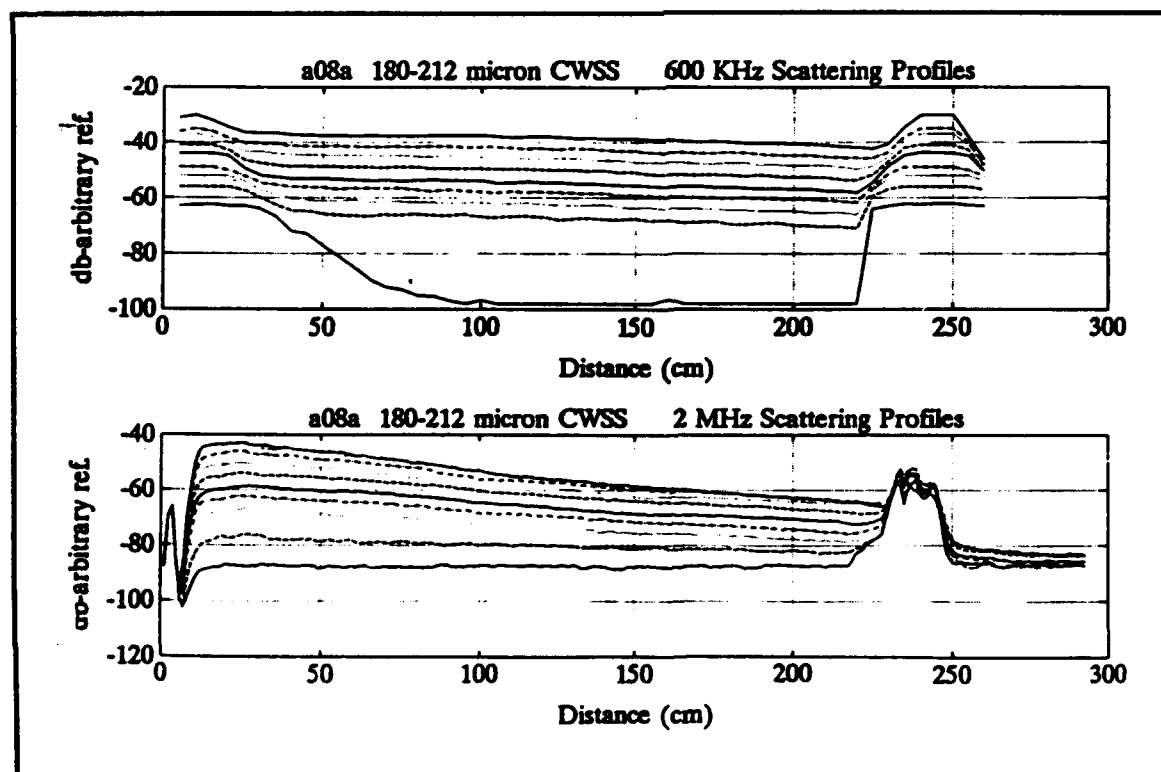
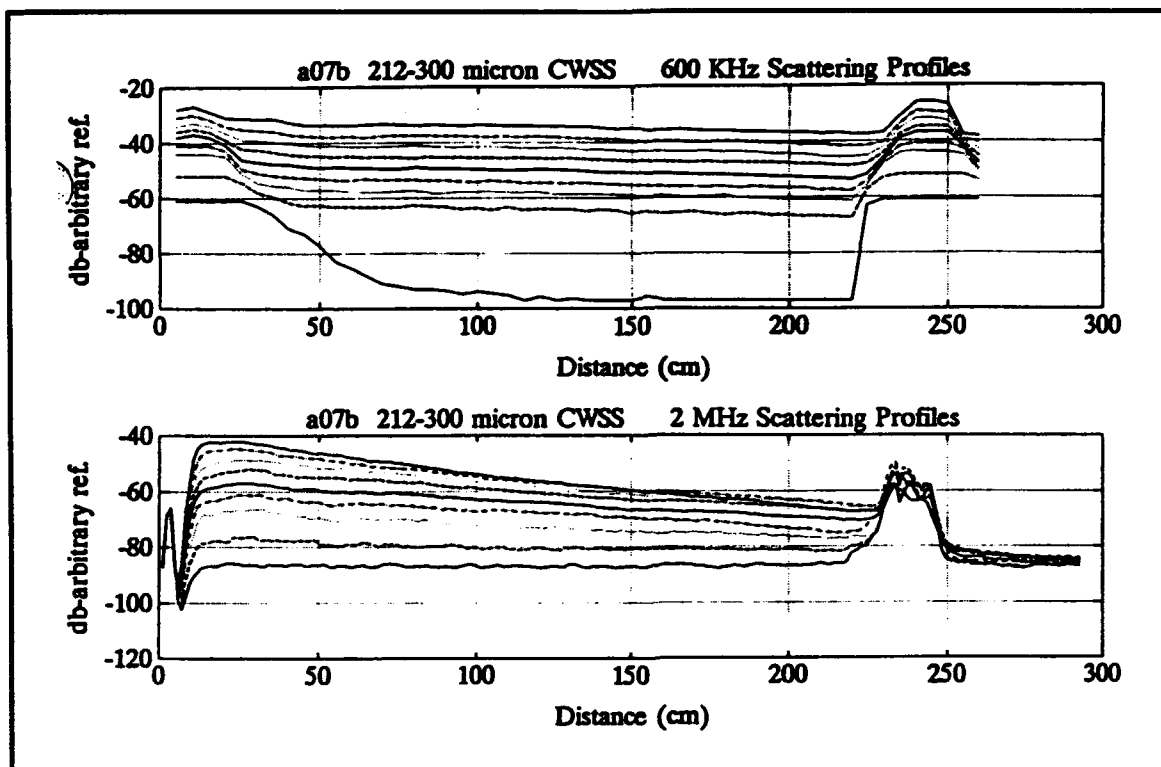
The following series of plots shows the mean scattering profiles, before any corrections. For each successful run, the mean profiles from the 600-kHz data and the 2-MHz short pulse data are presented. Please note that for special tests (i.e., very fine sediments and silica mixtures) the profiles will not necessarily follow a progression of scattering levels.

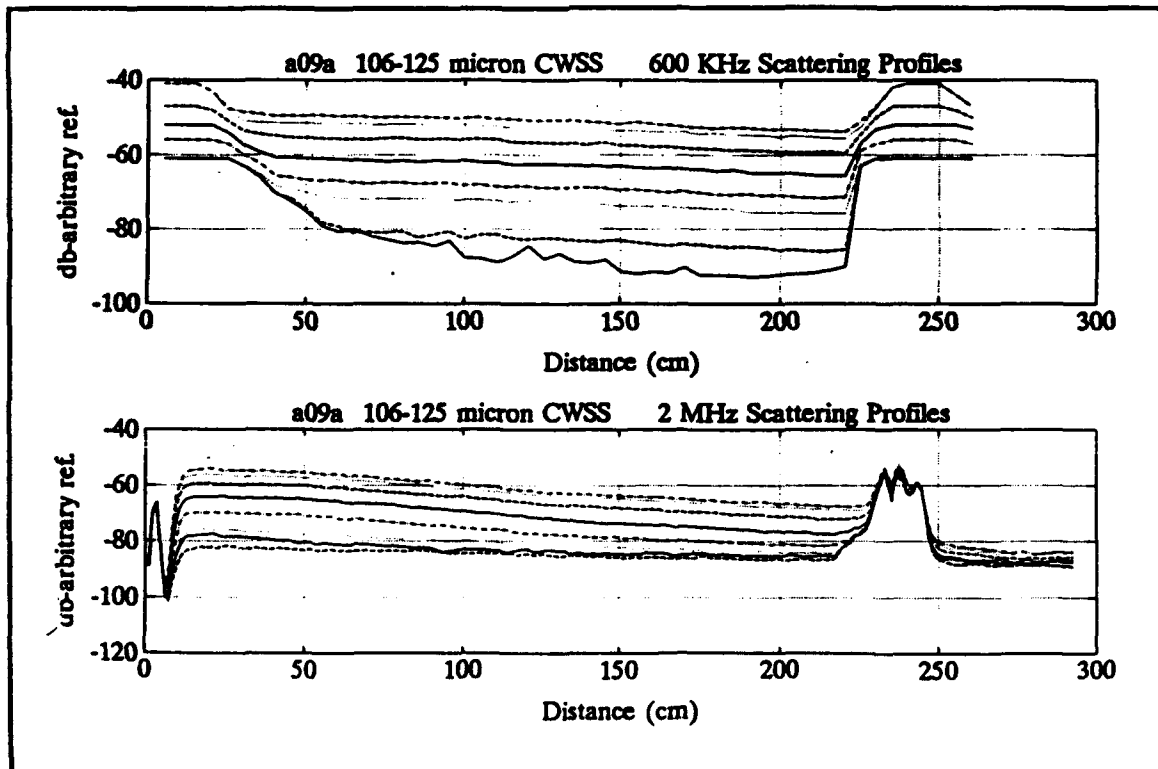
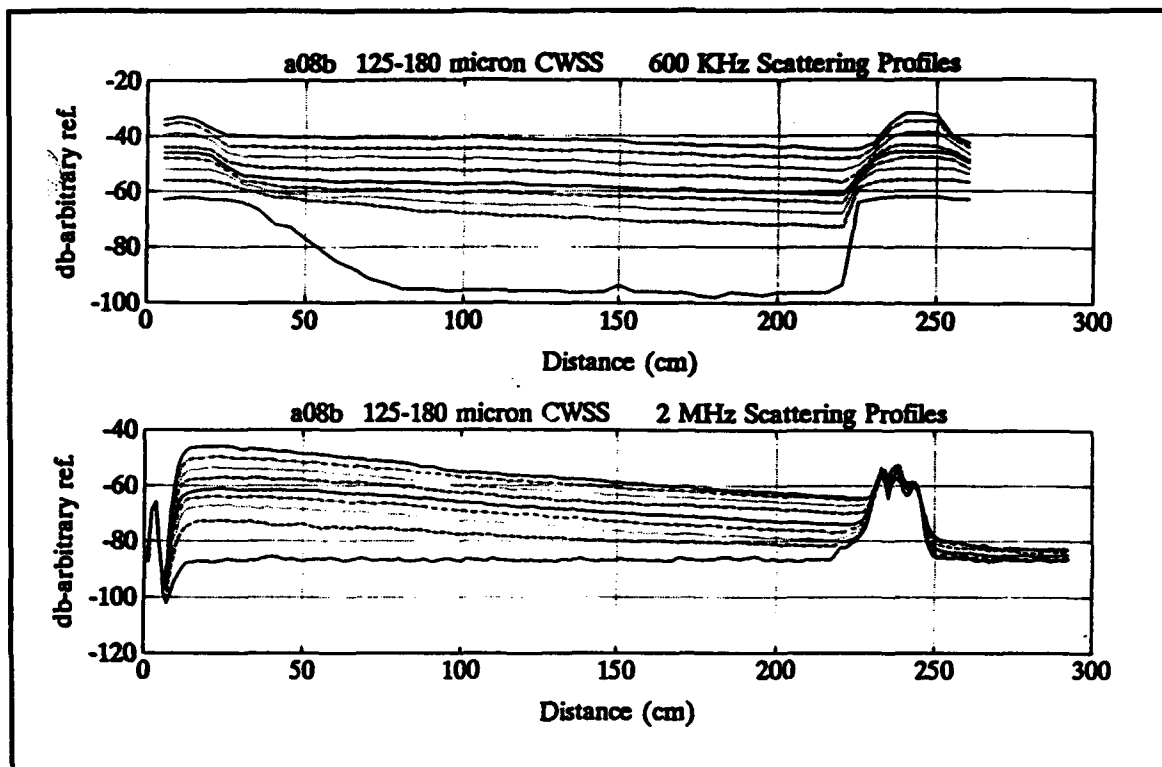


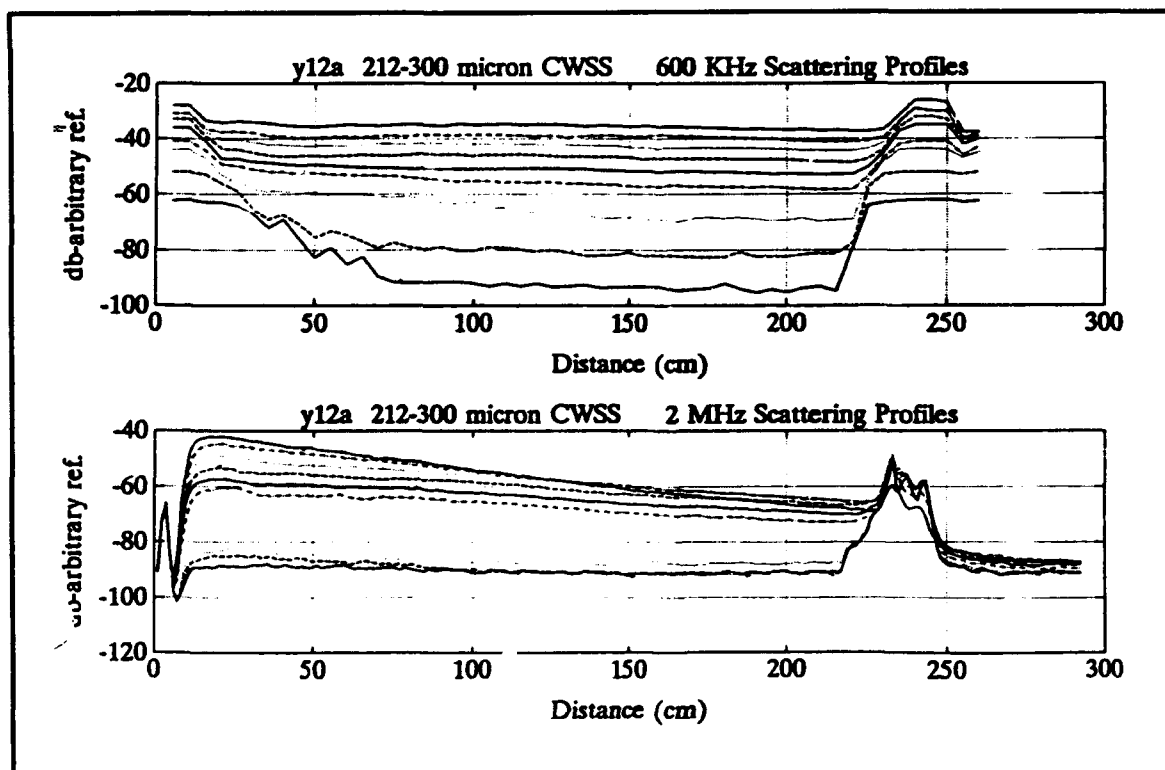
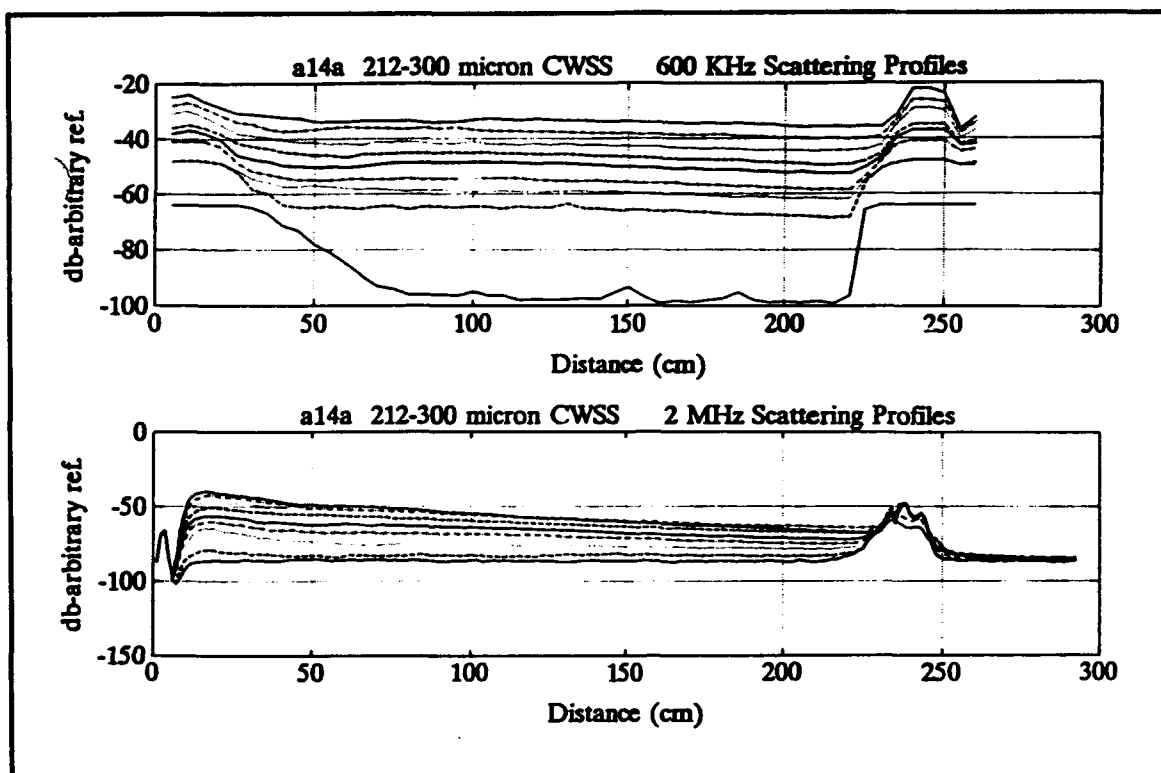


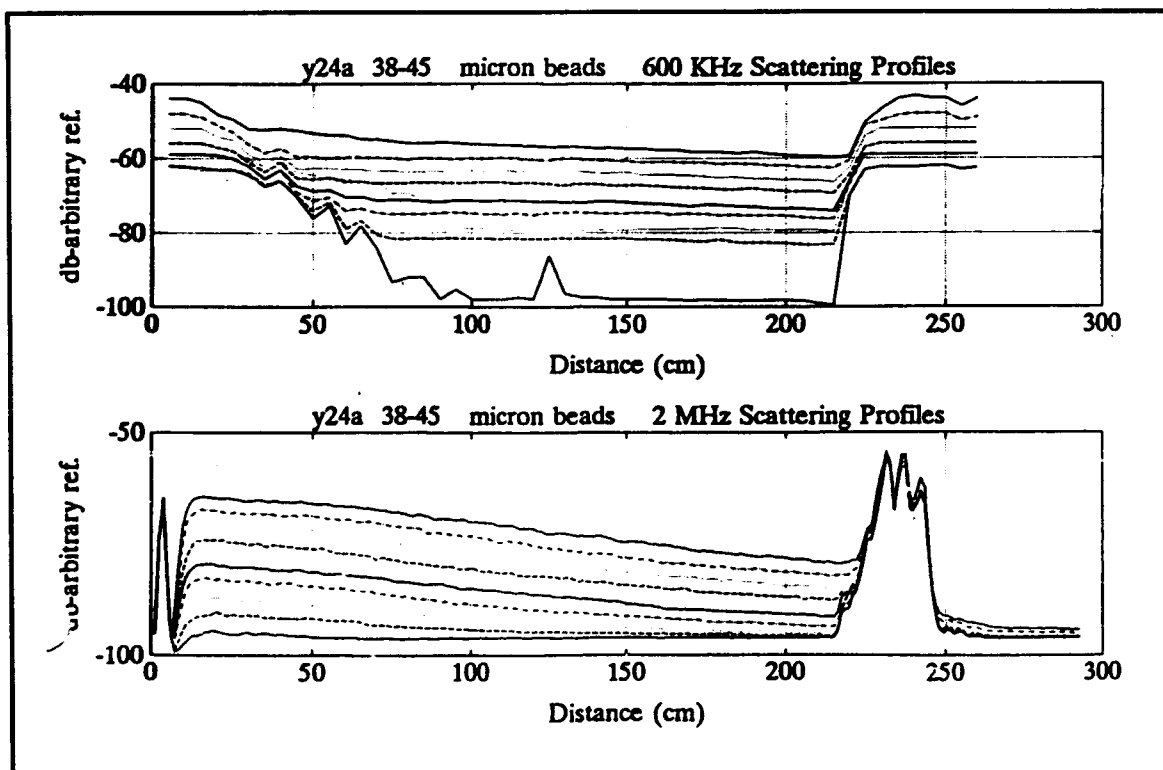
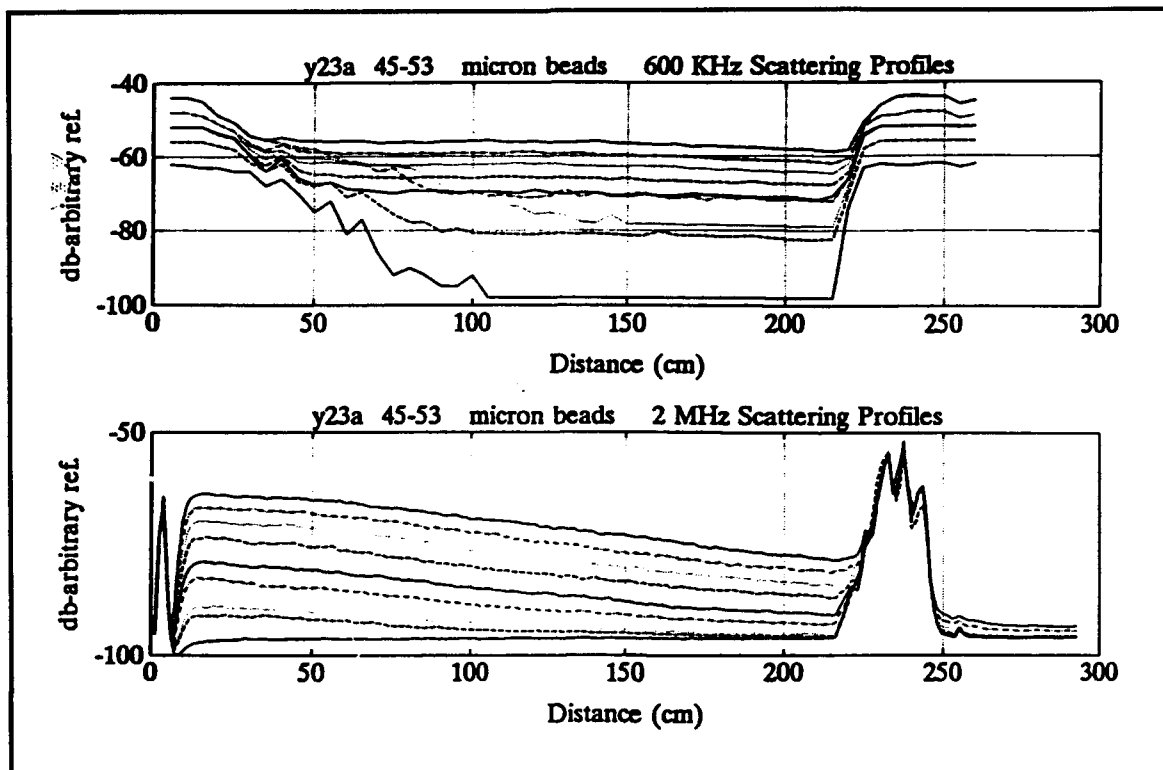


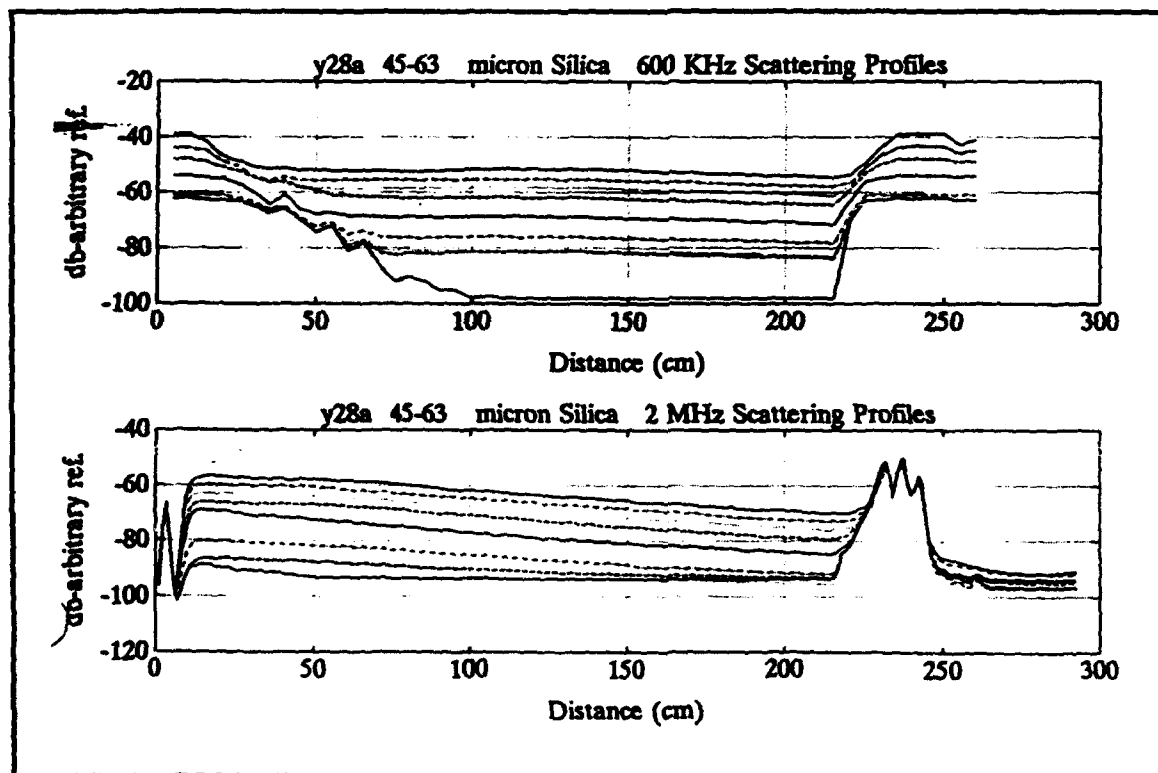
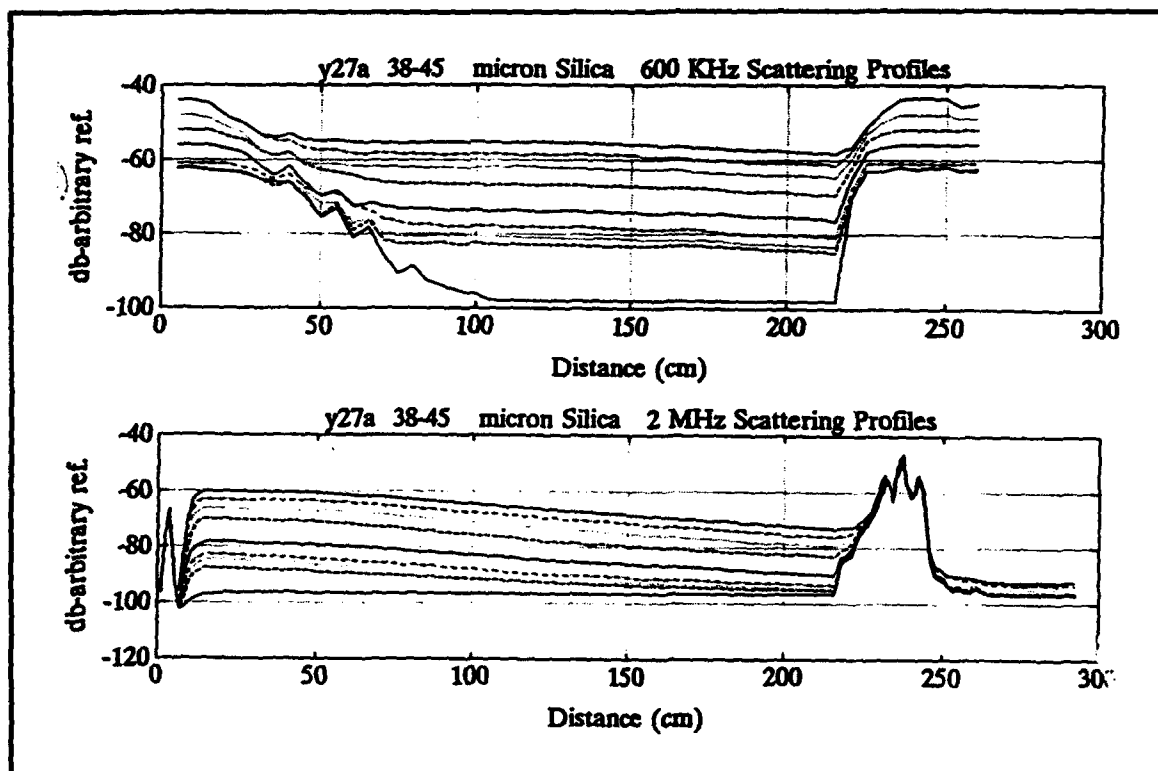


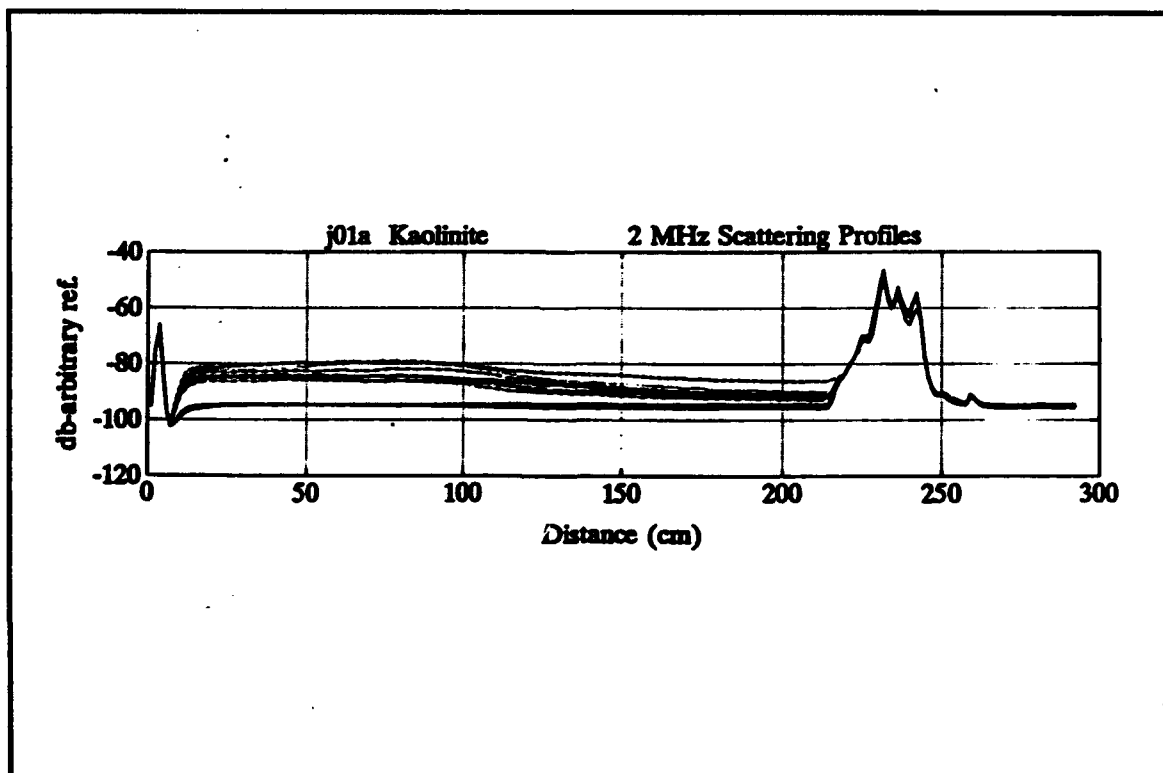
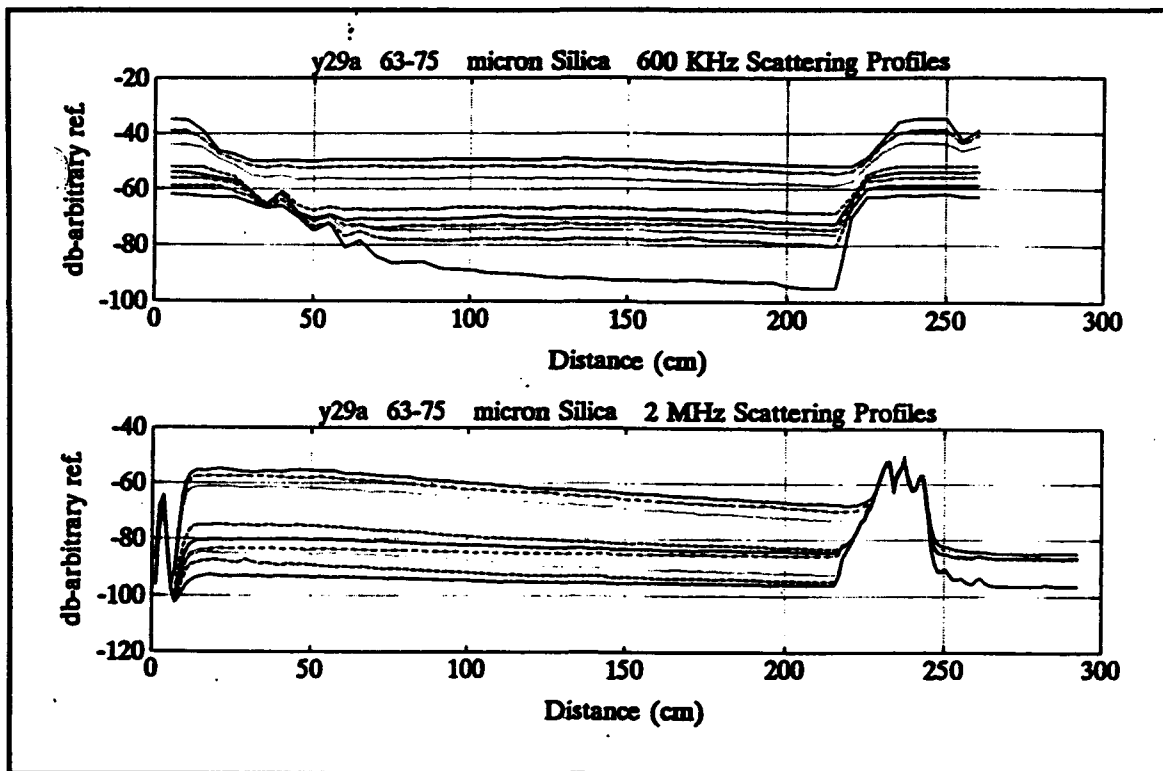


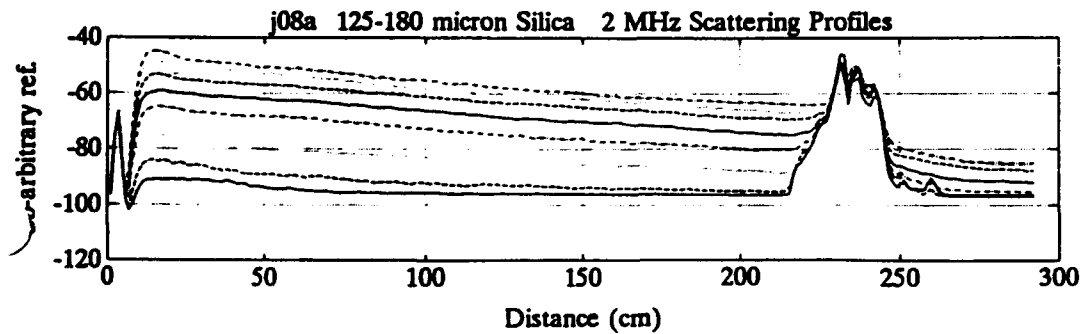
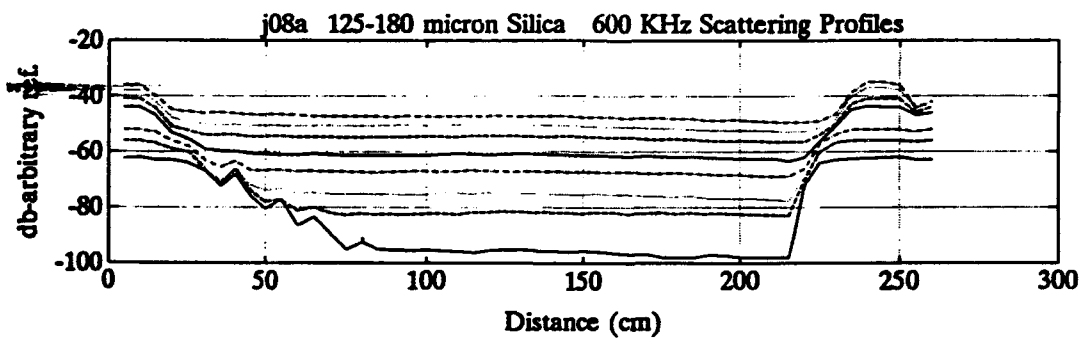
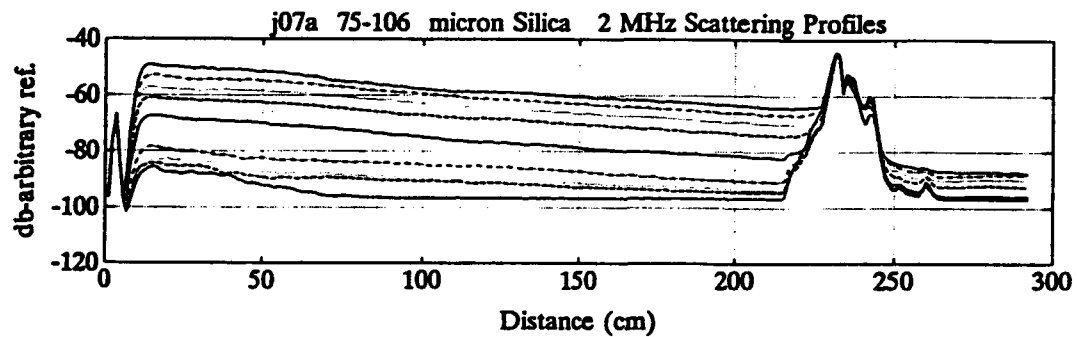
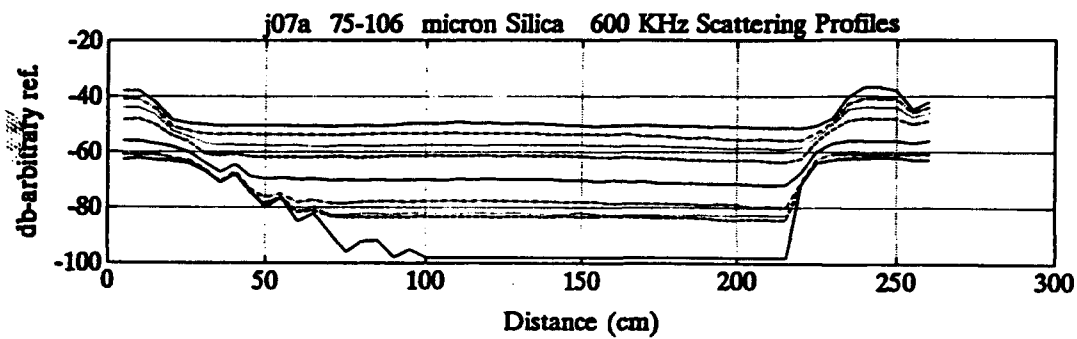


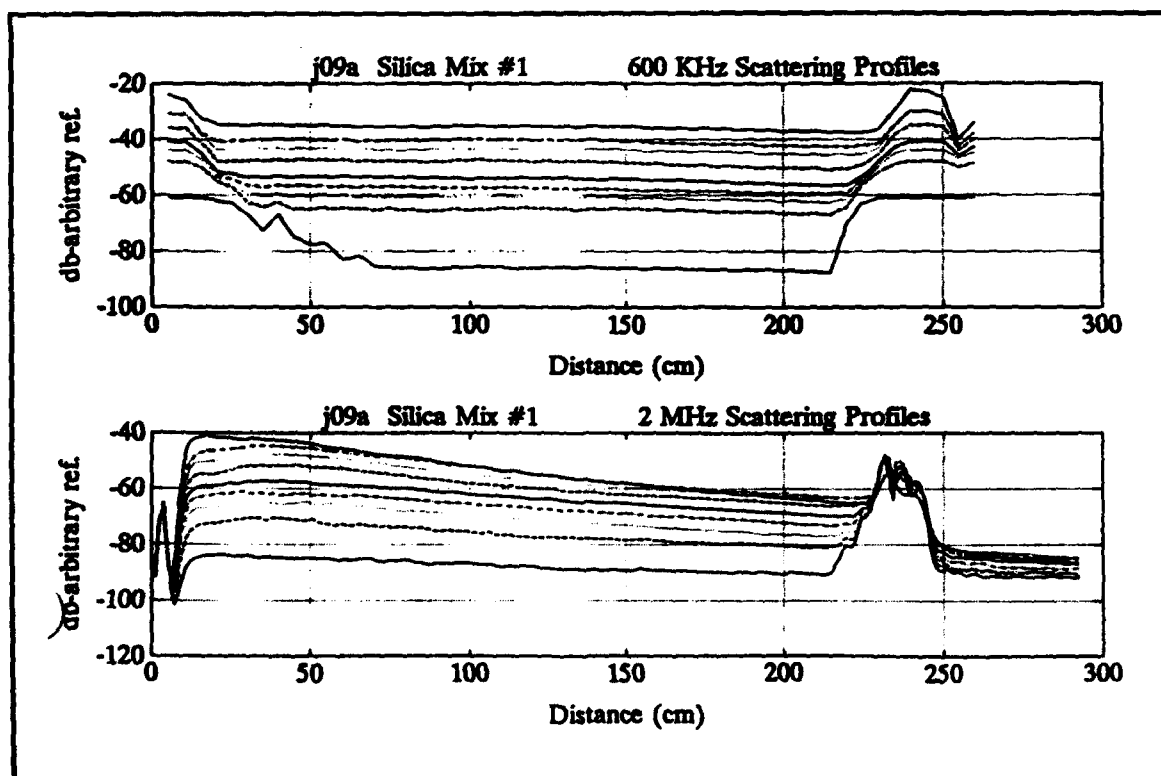
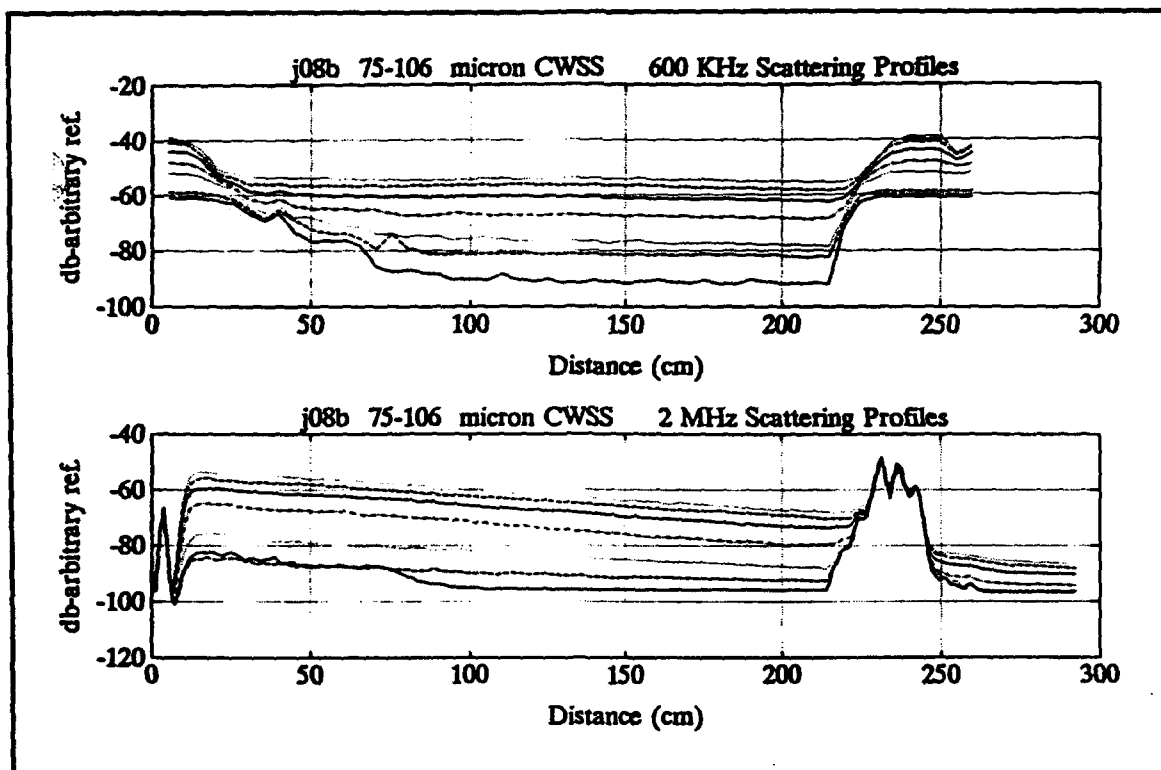


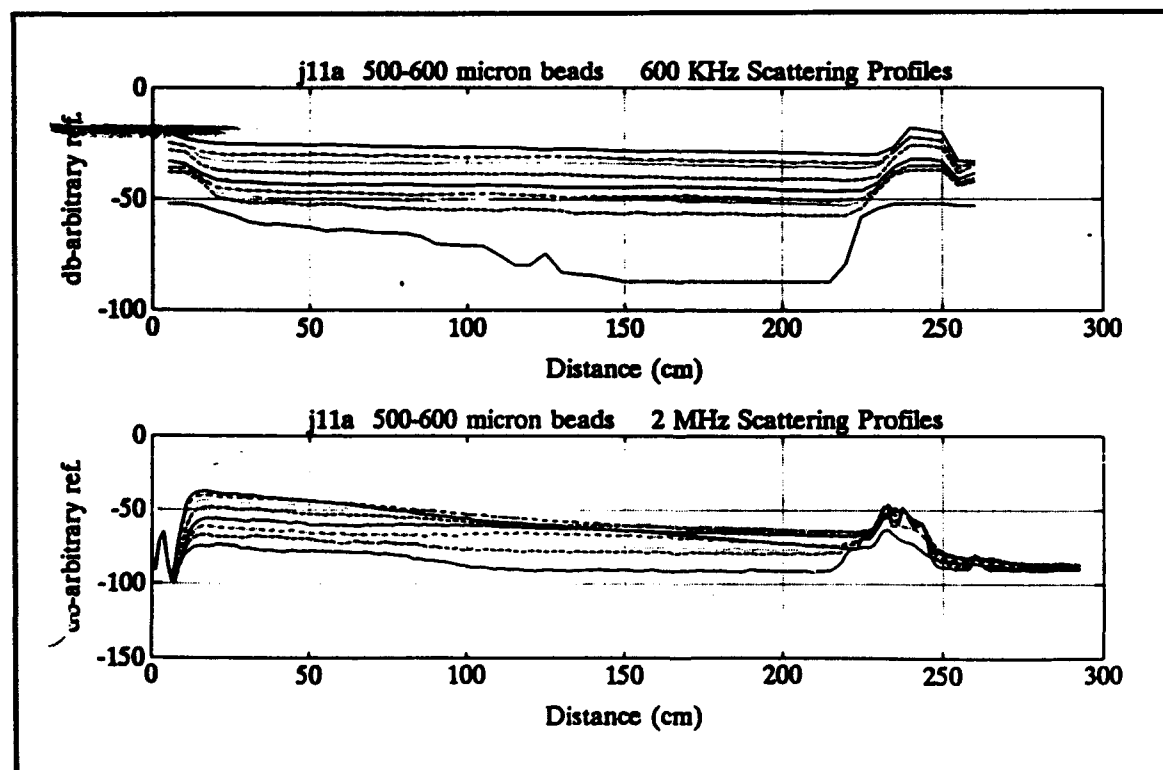
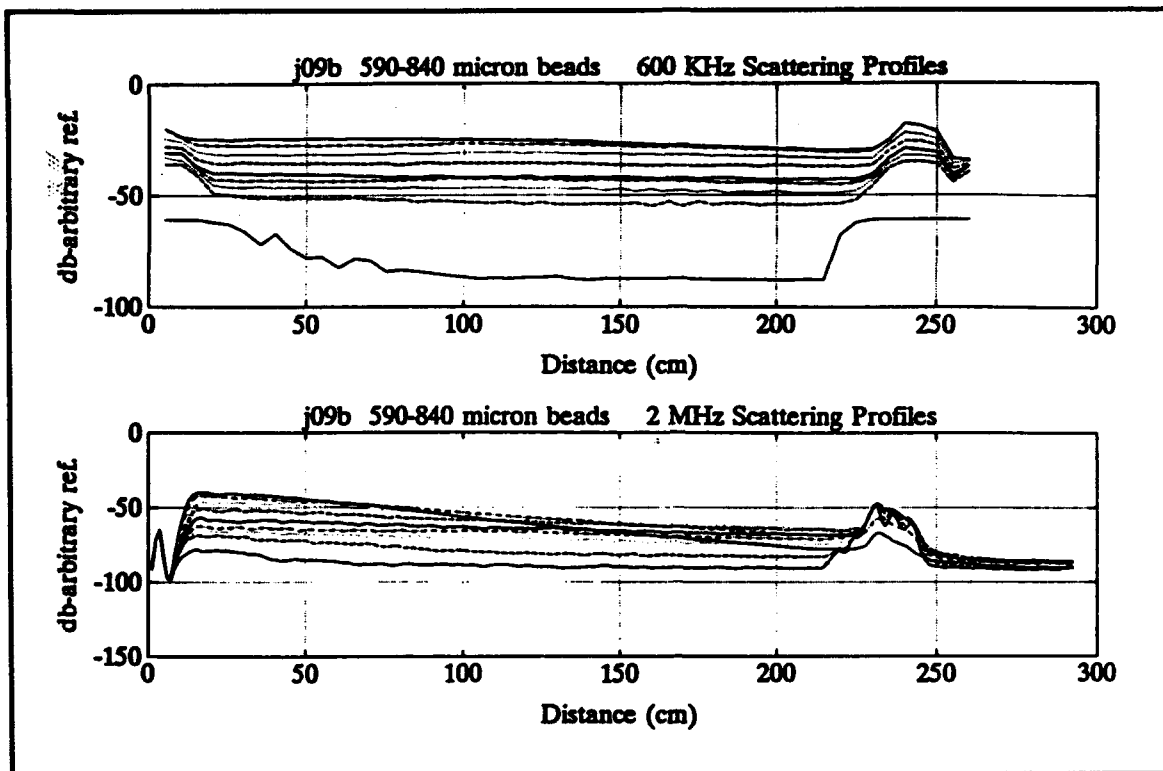


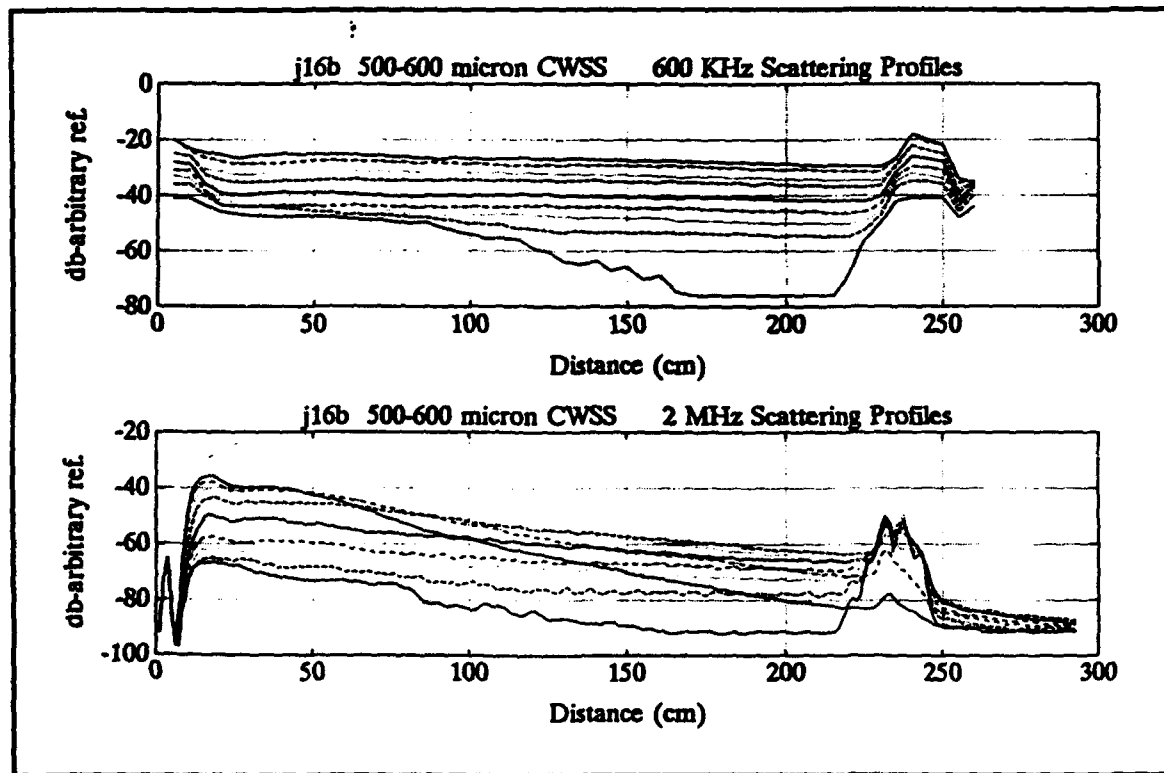
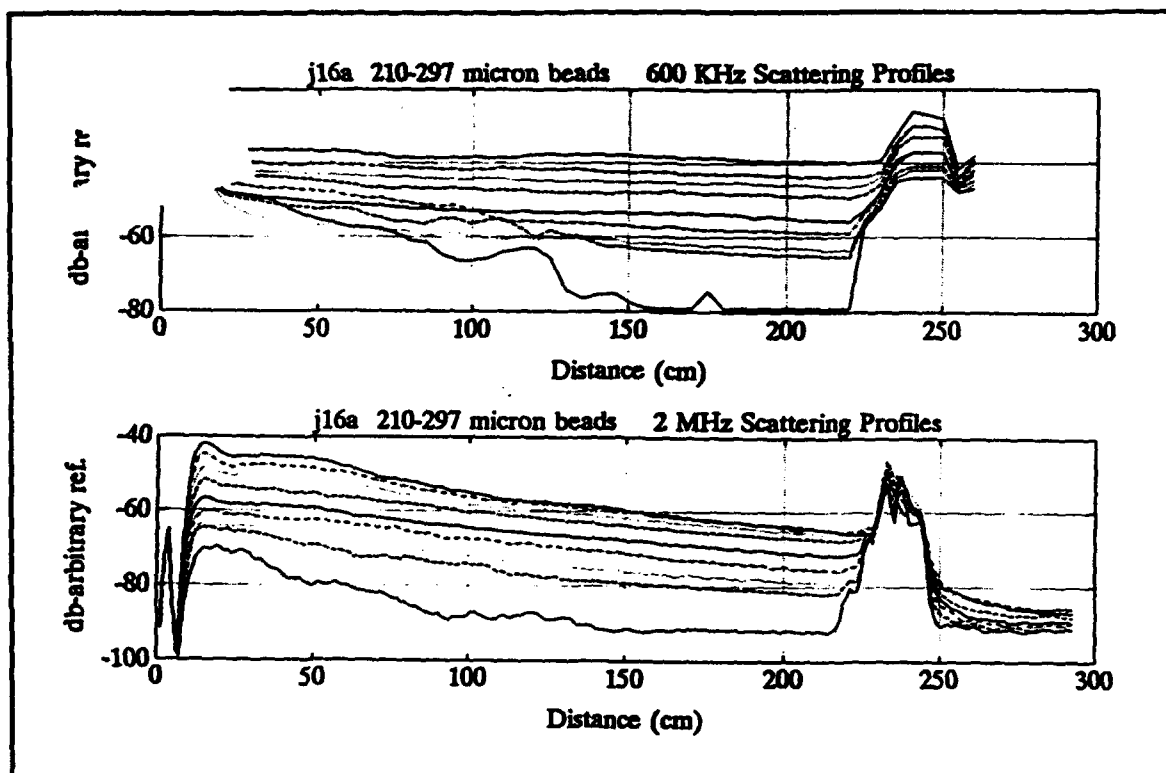


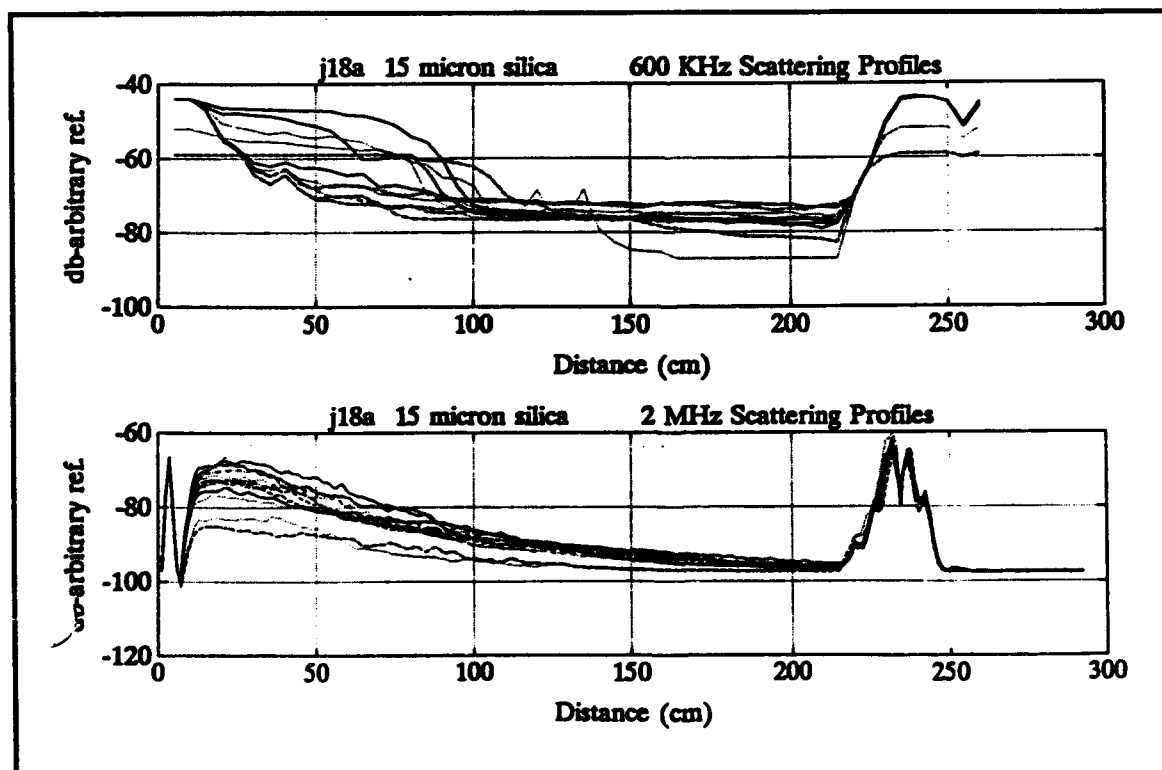
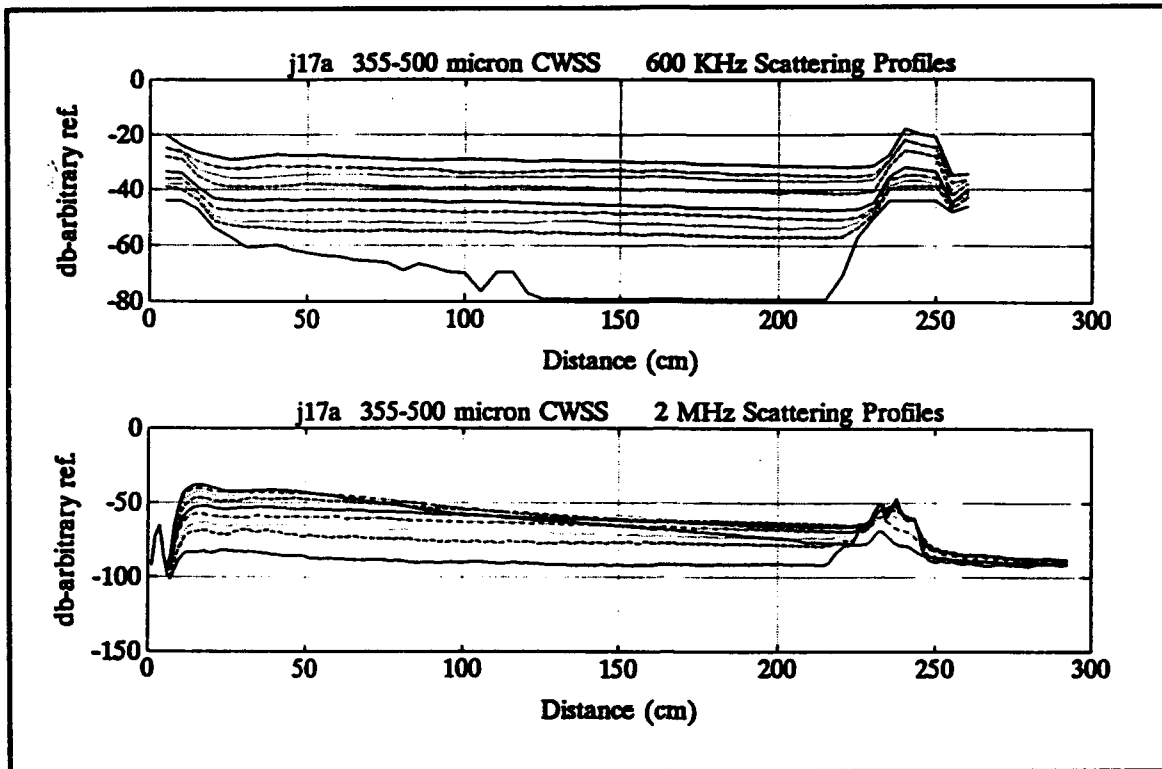


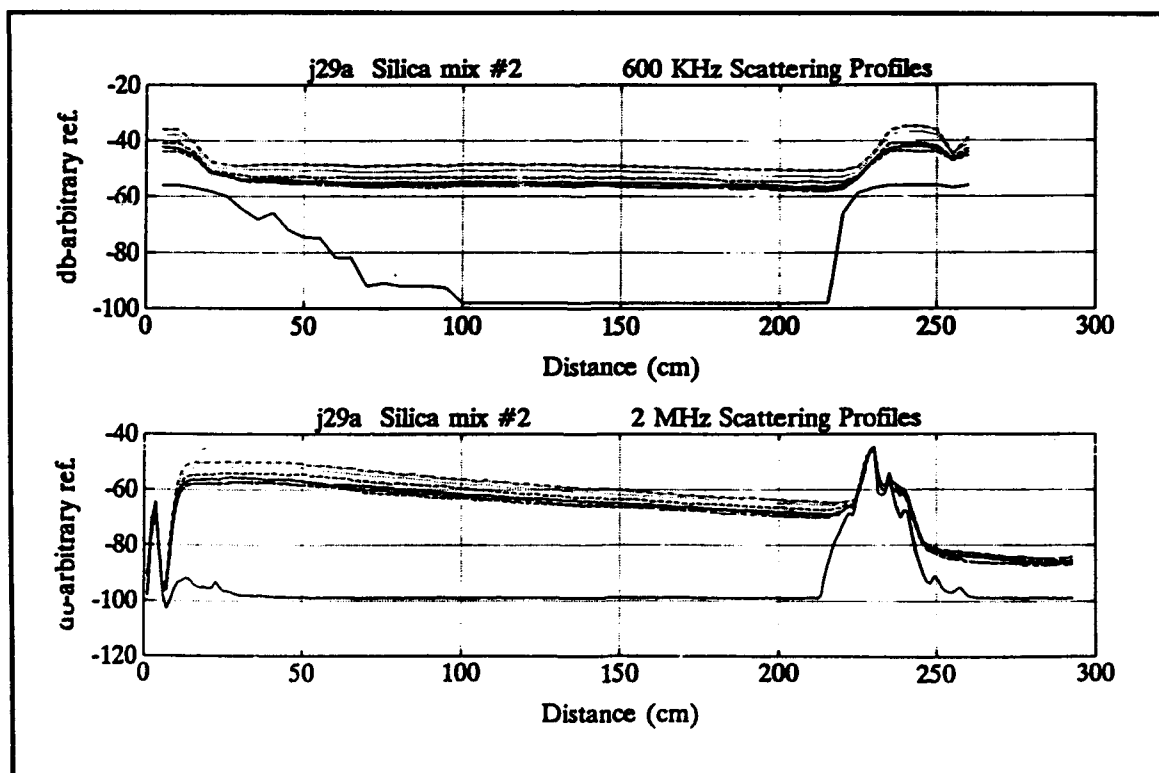
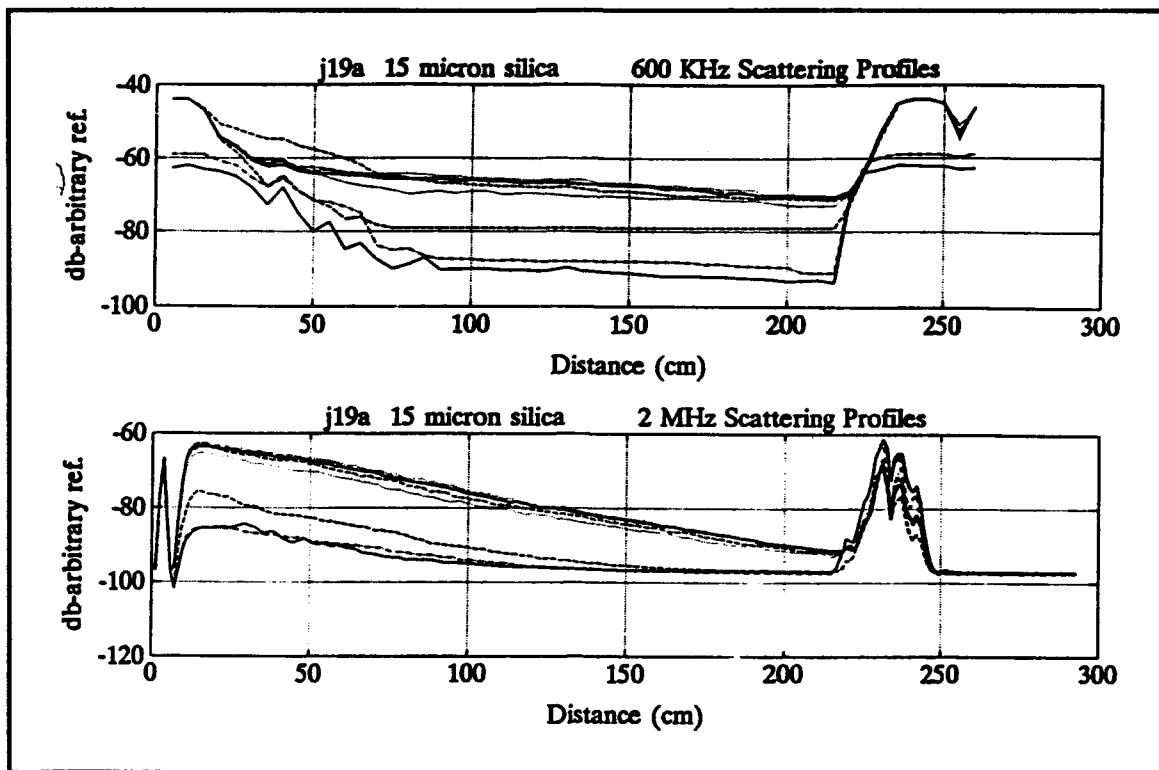








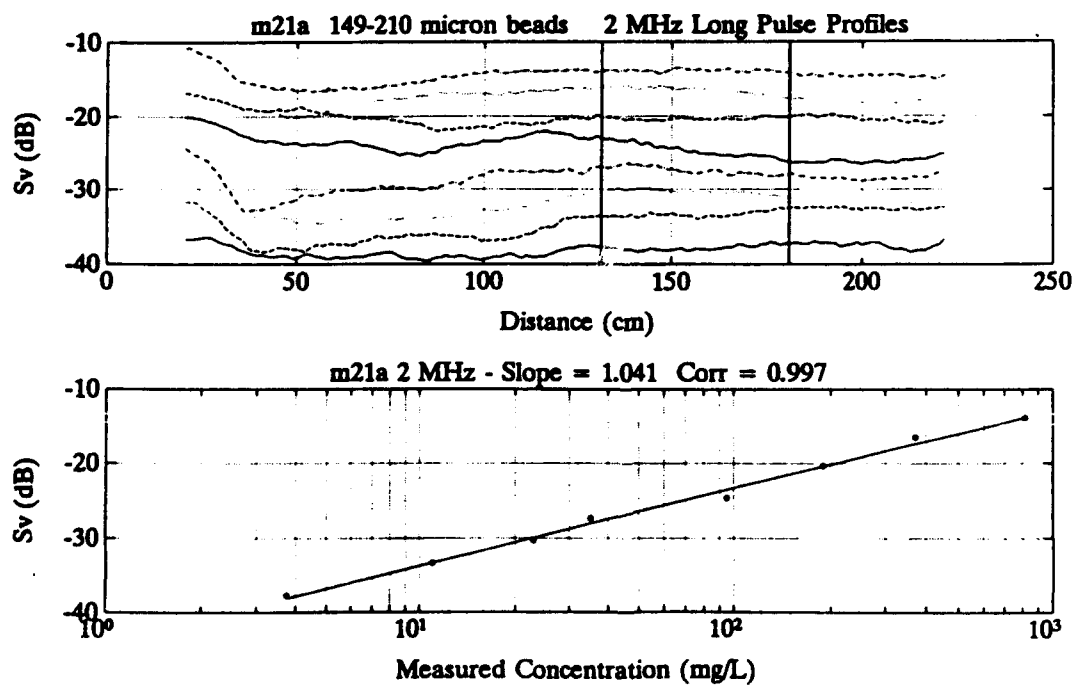
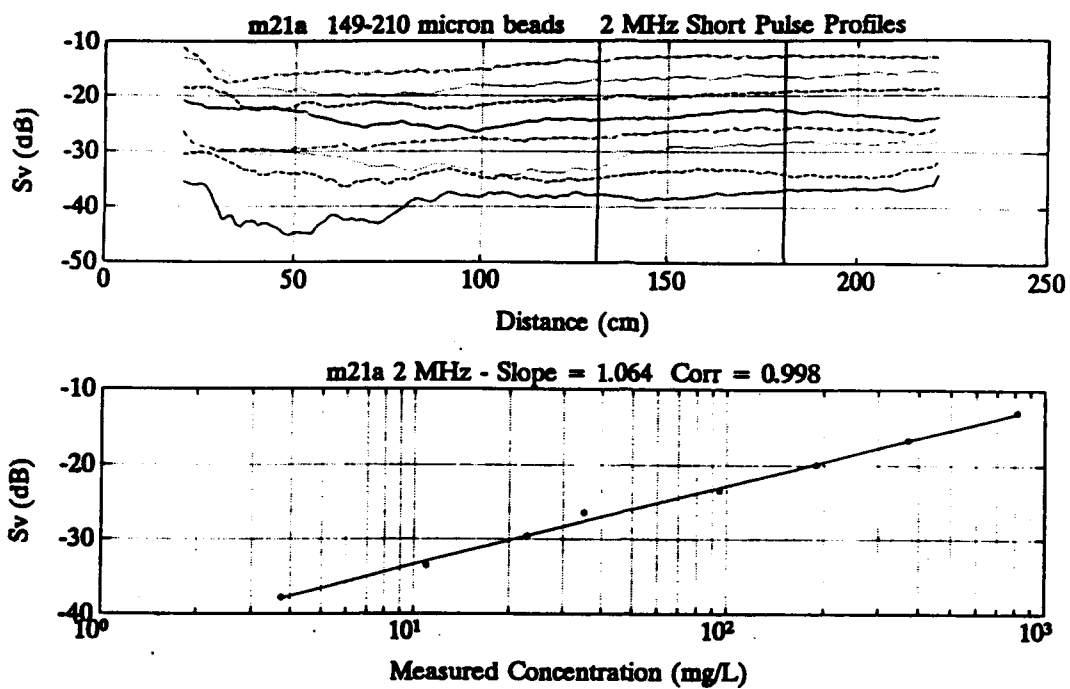


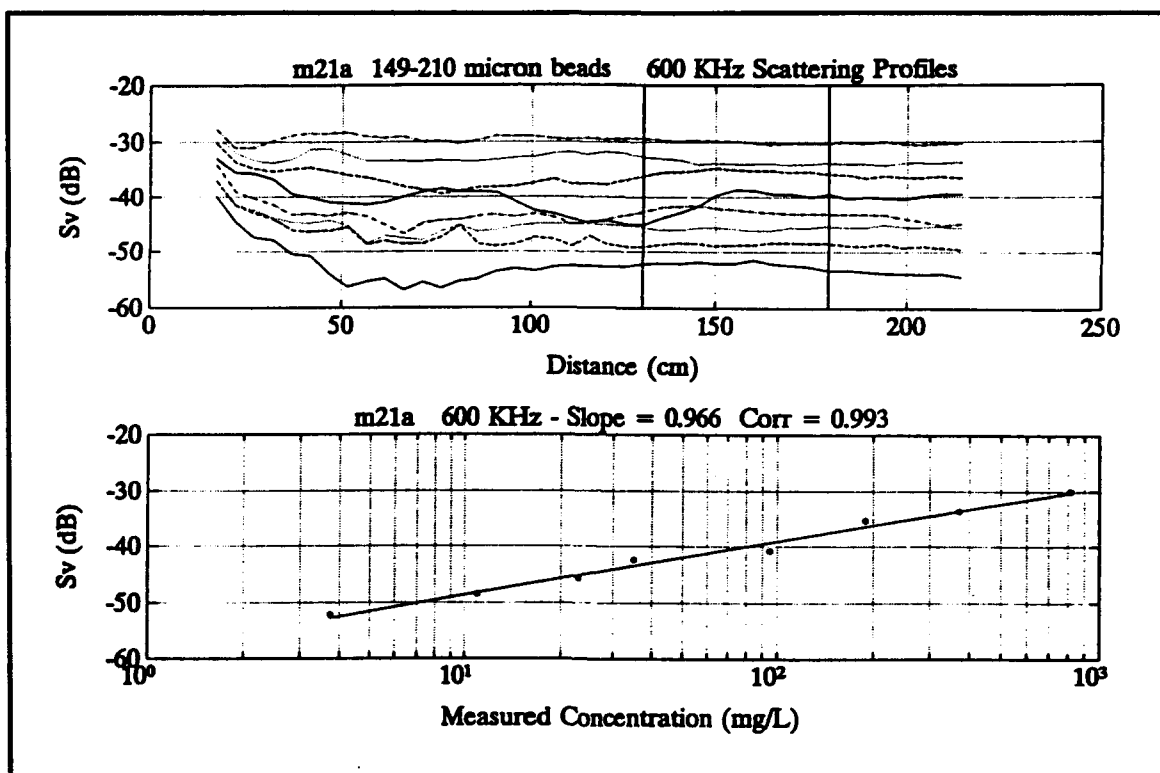


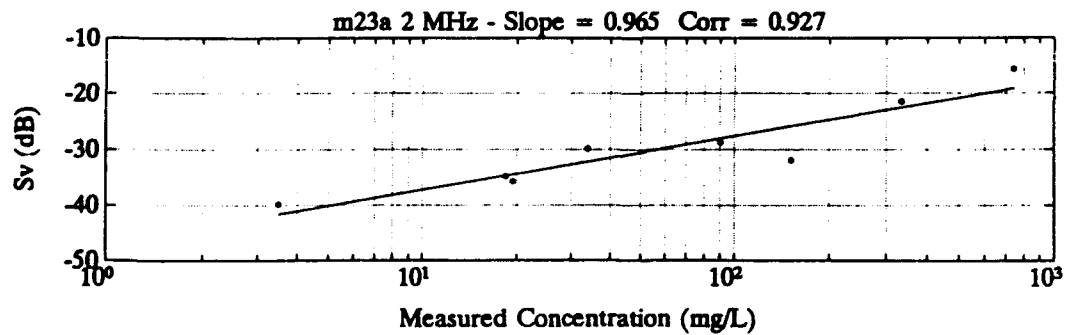
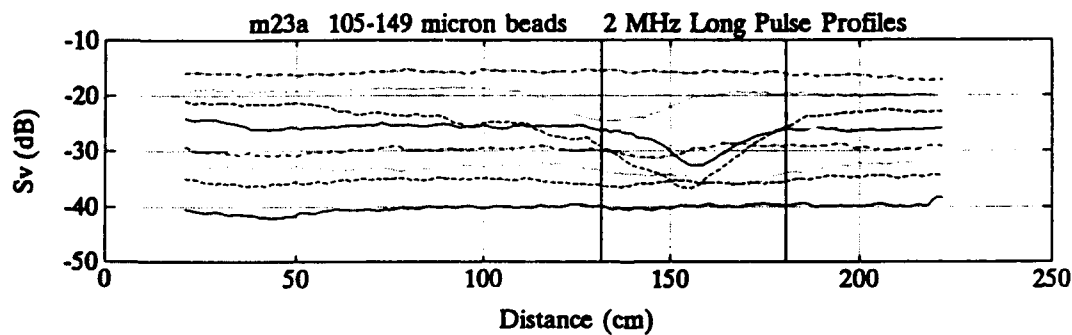
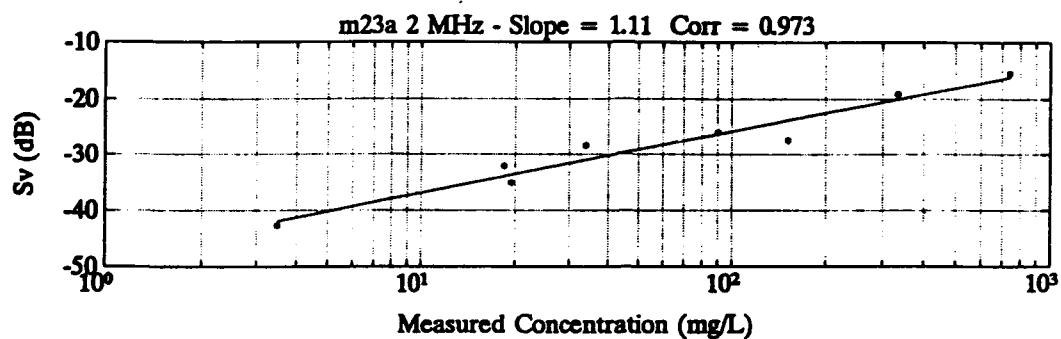
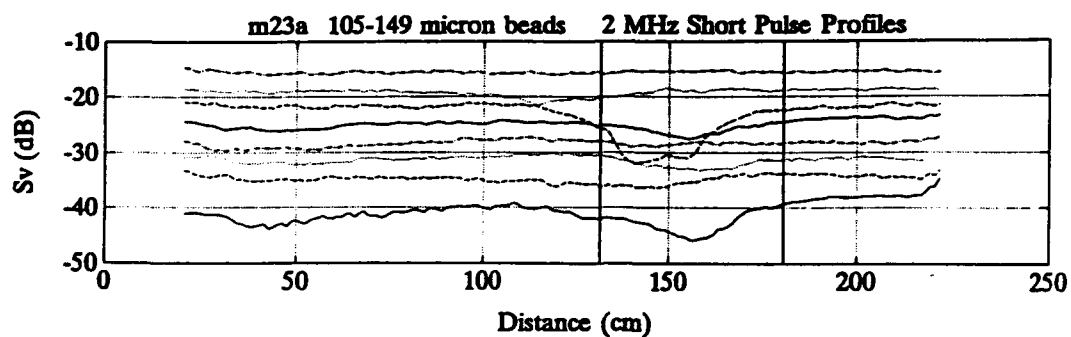
Appendix C

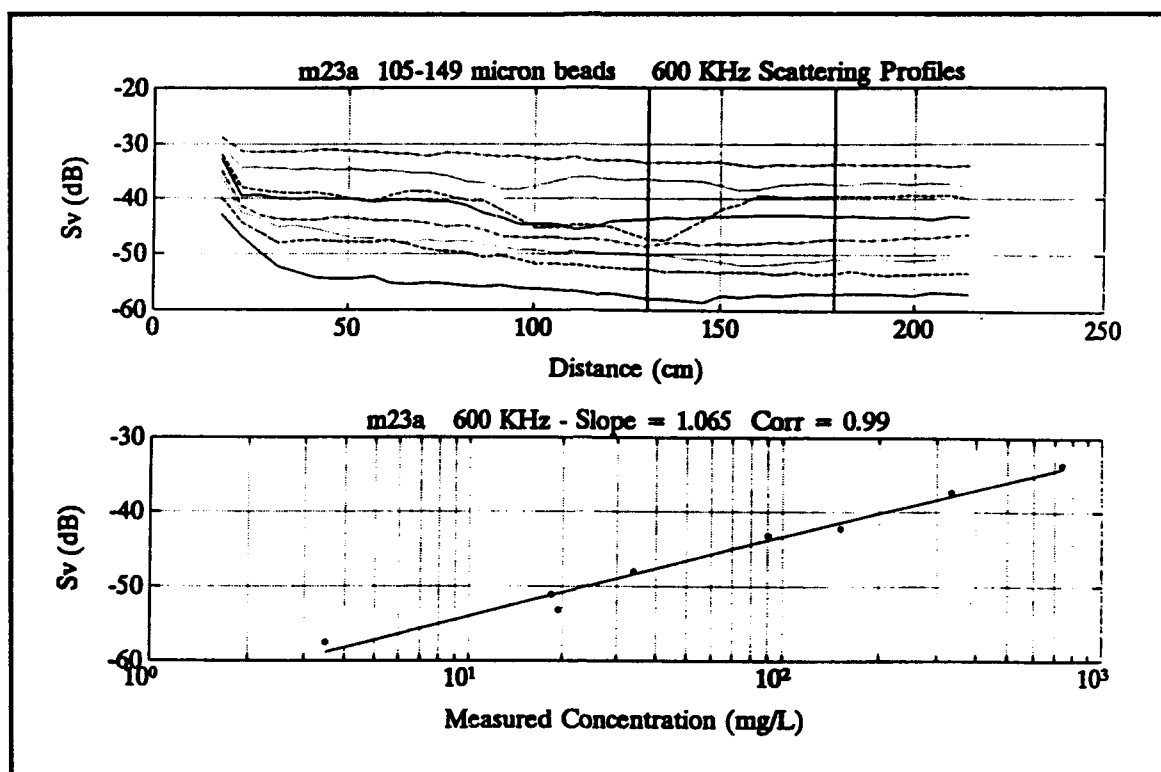
Corrected Mean Scattering Profiles and Concentration

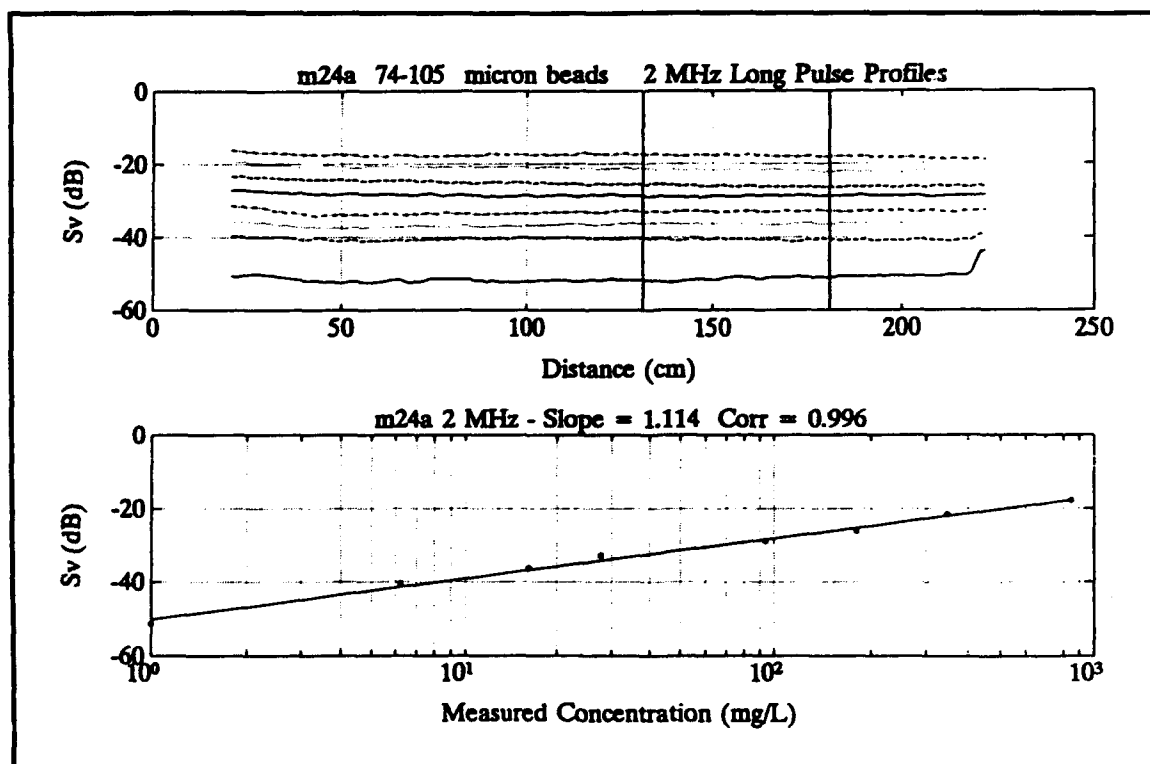
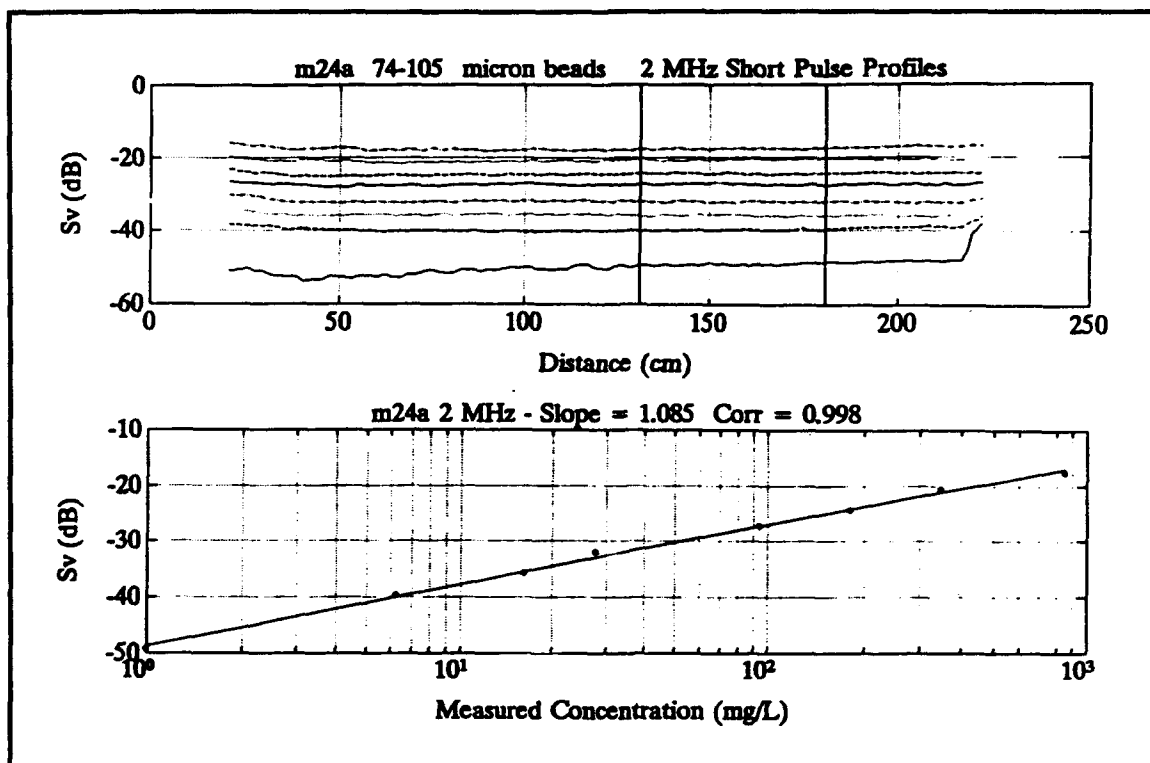
The following series of plots show the mean scattering profiles after correction for noise, attenuation and range. The vertical lines on the scattering profile show the averaging interval used for the mean scattering level. Additionally, a plot showing measured concentration versus mean scattering level is shown with a best fit linear regression. Profile and regression plots are presented for the 600-kHz data, and for the 2-MHz short and long pulse data sets. This appendix only contains these plots for uniform sediment size classes, data from the Norfolk samples and silica mixture No. 1.

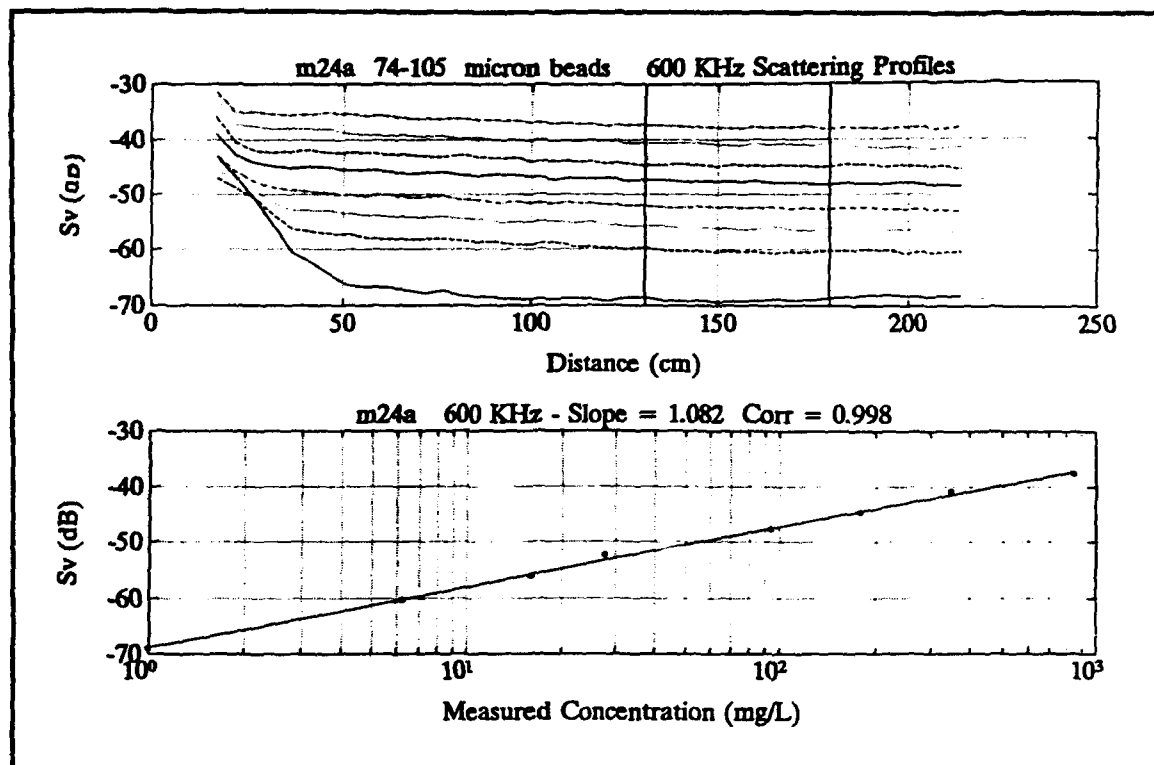


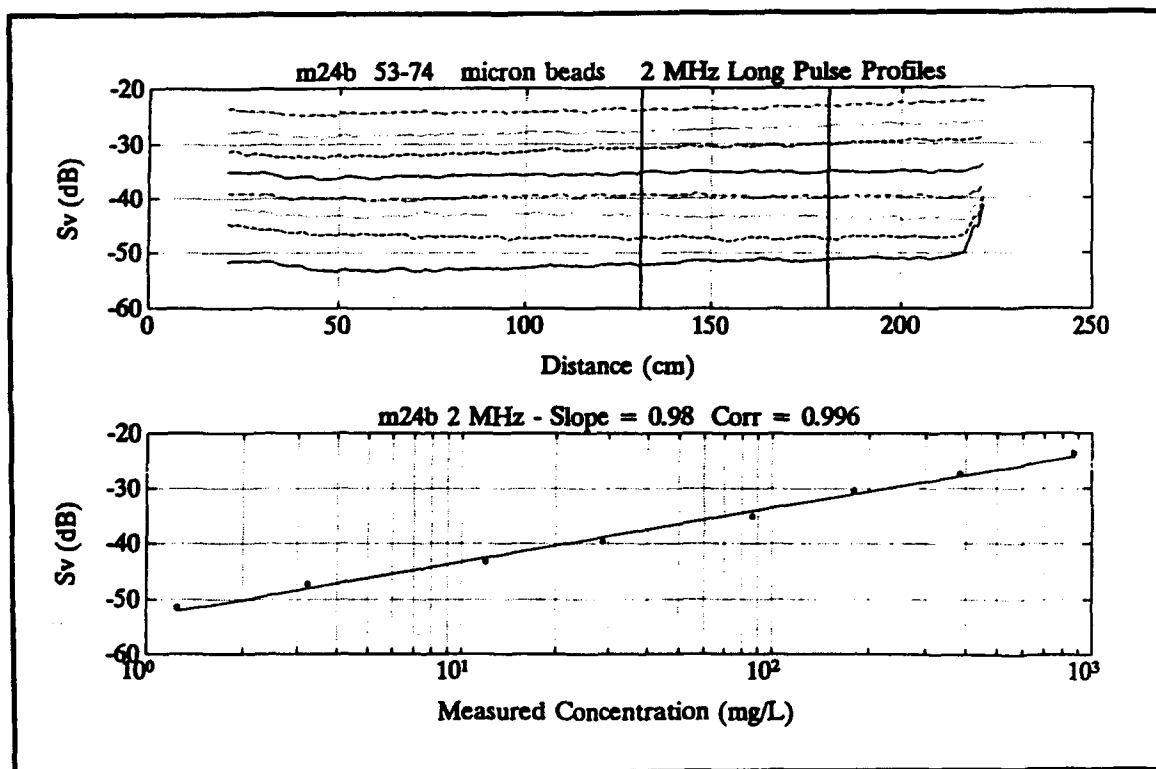
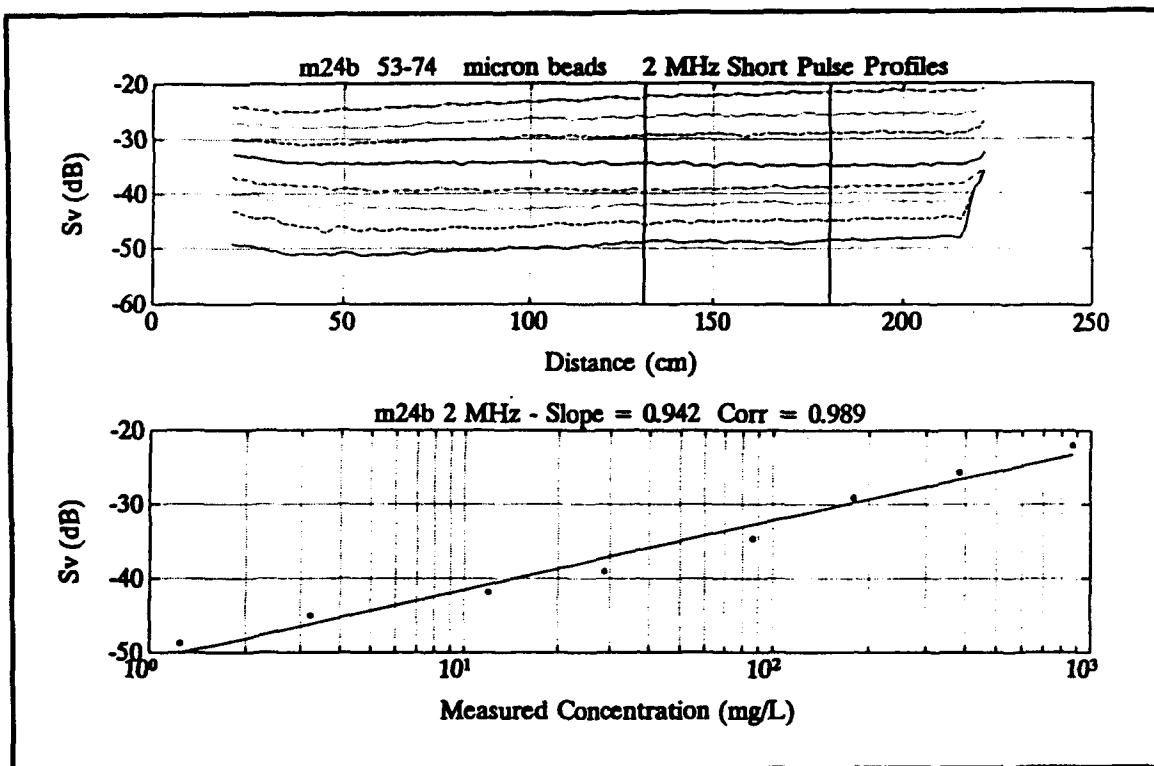


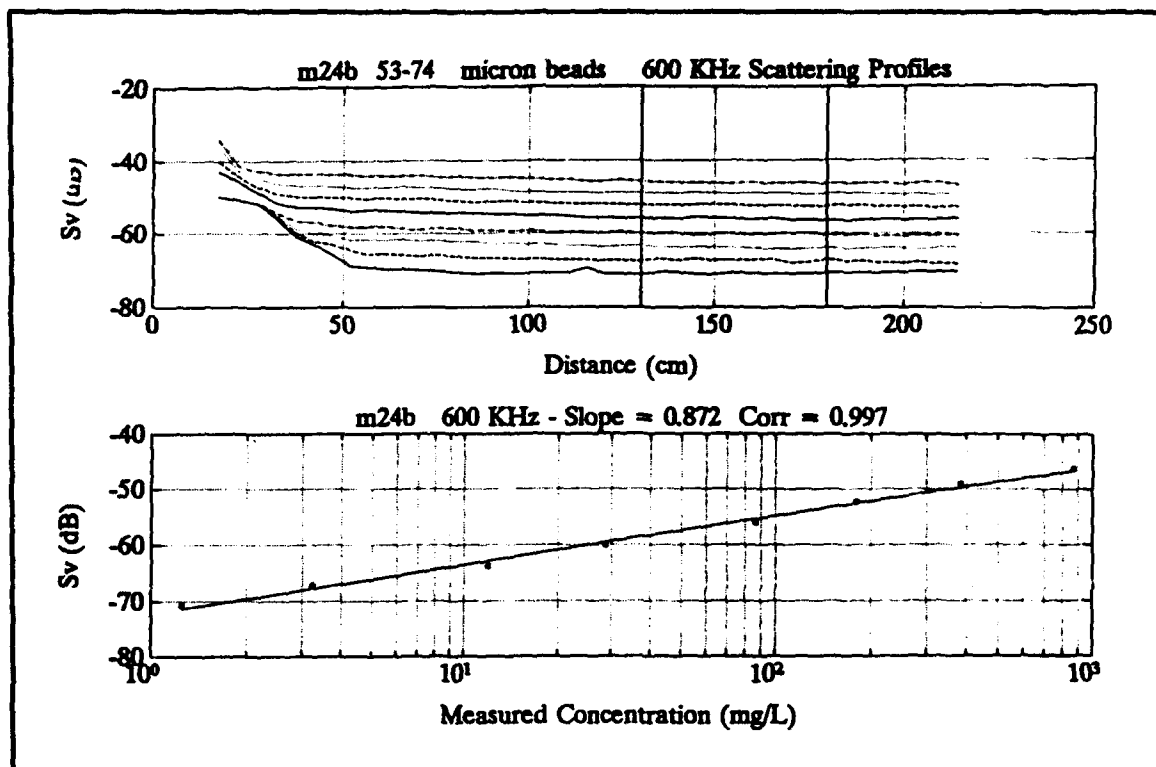


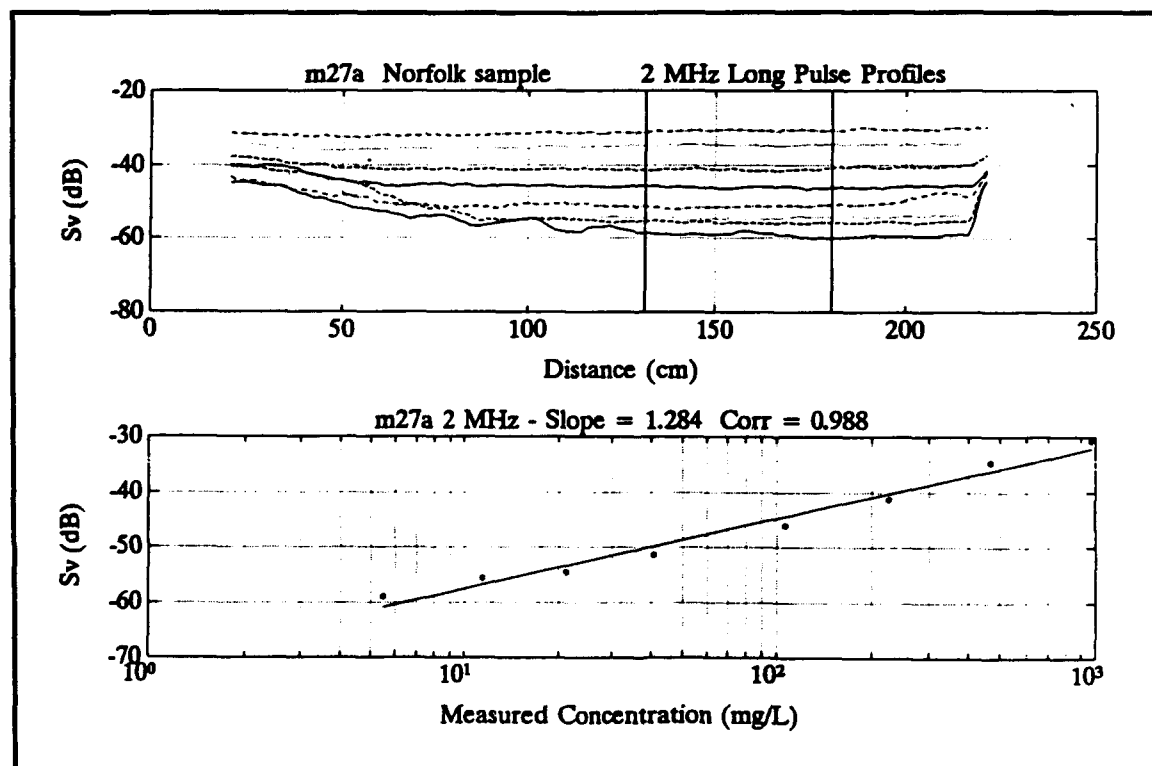
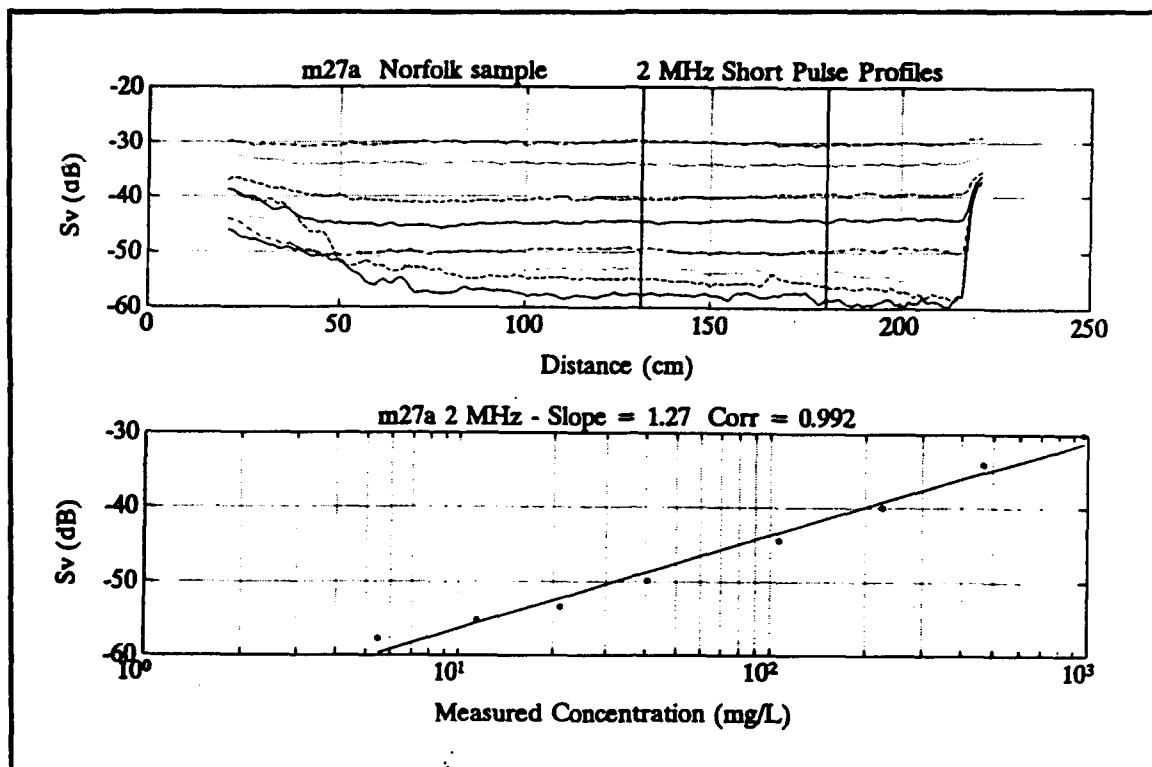


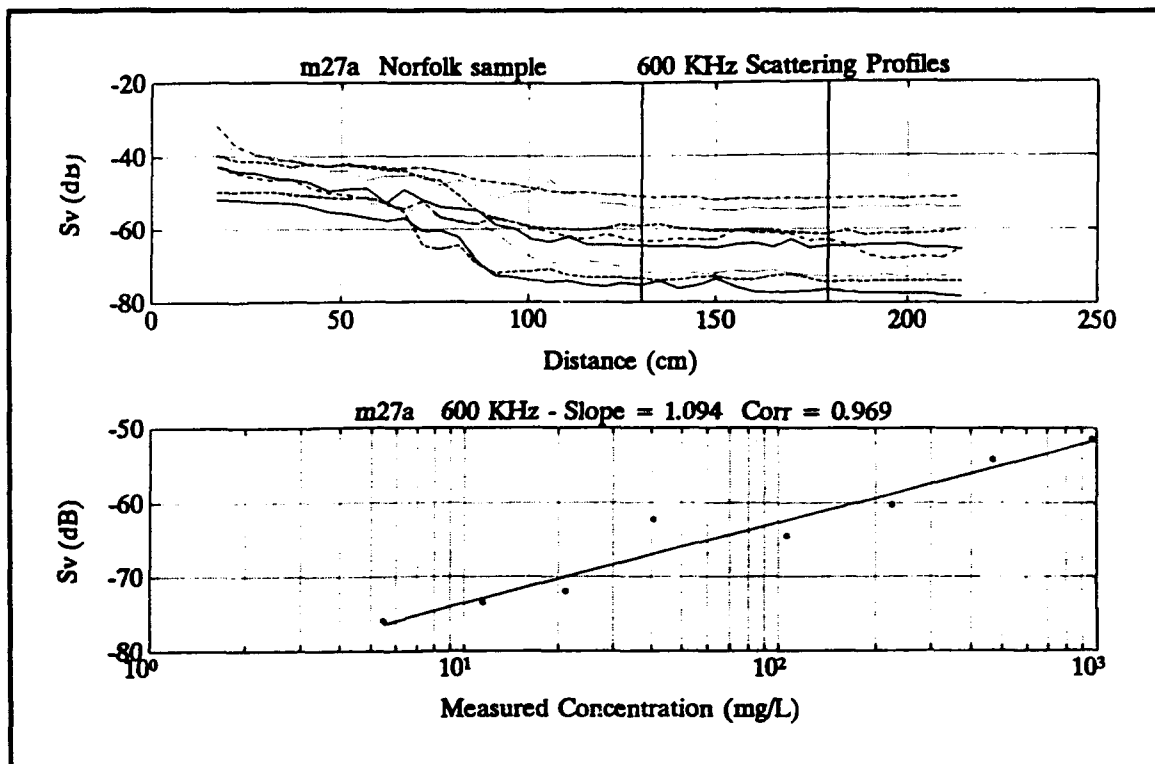


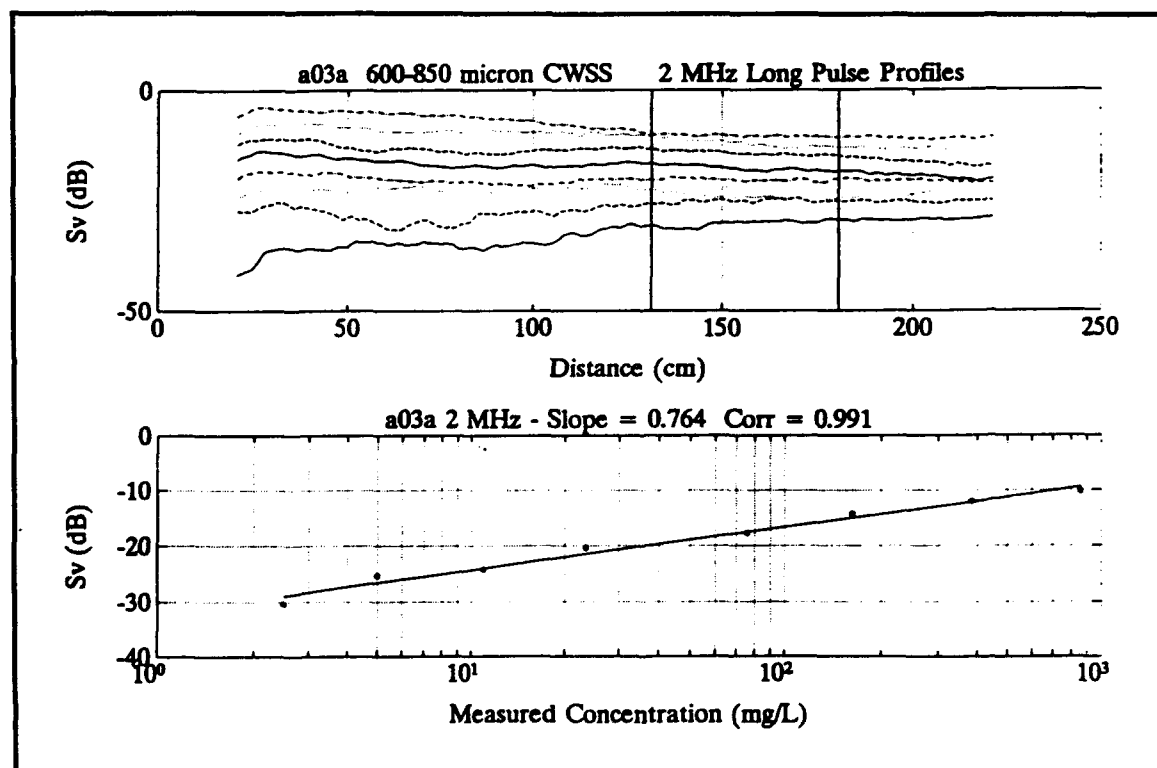
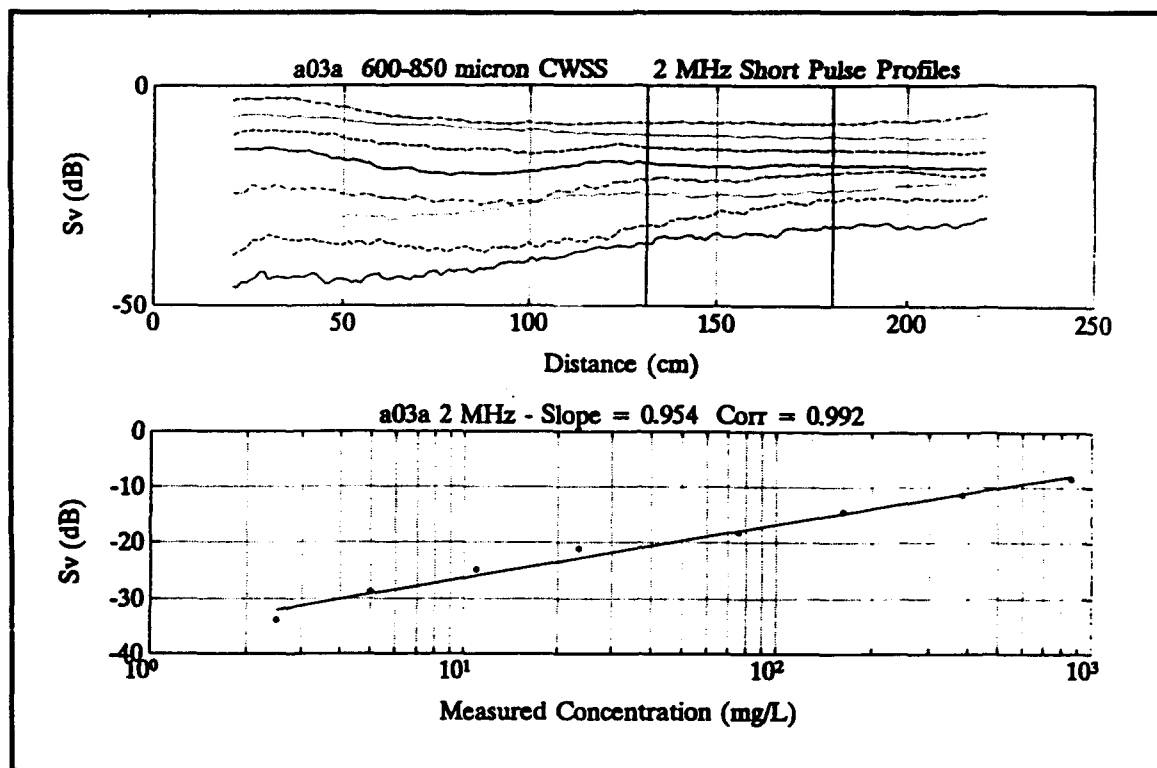


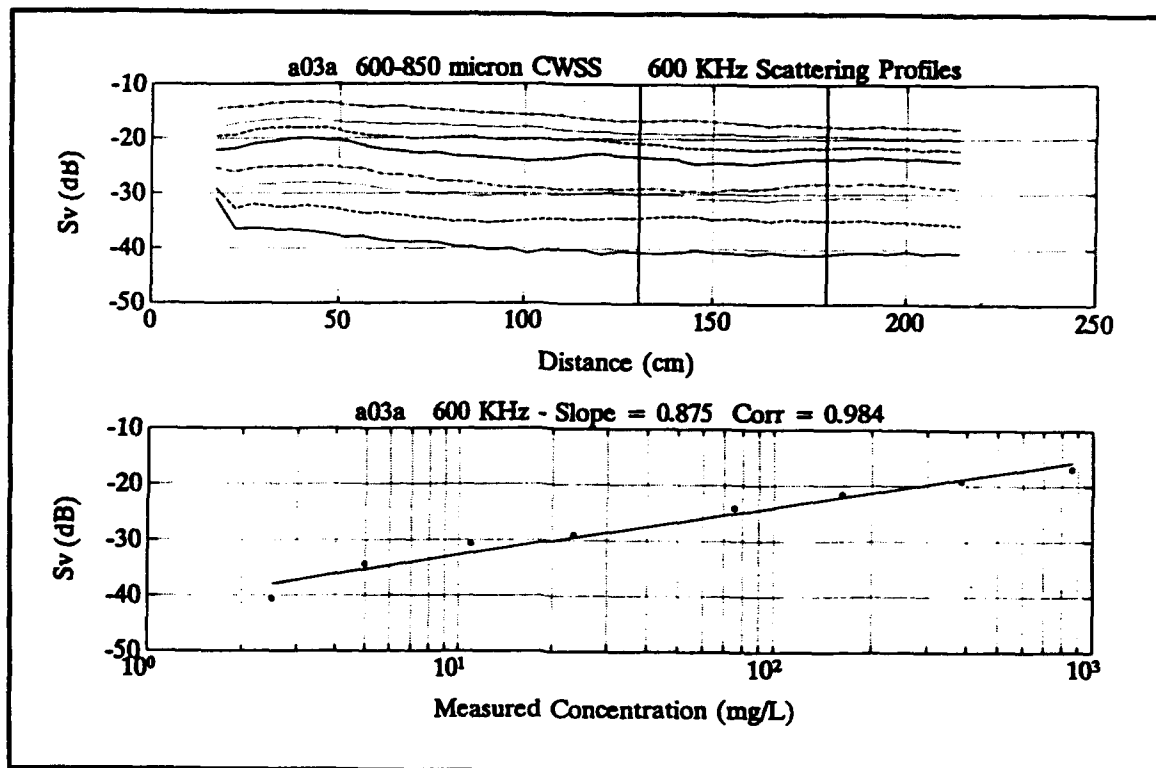


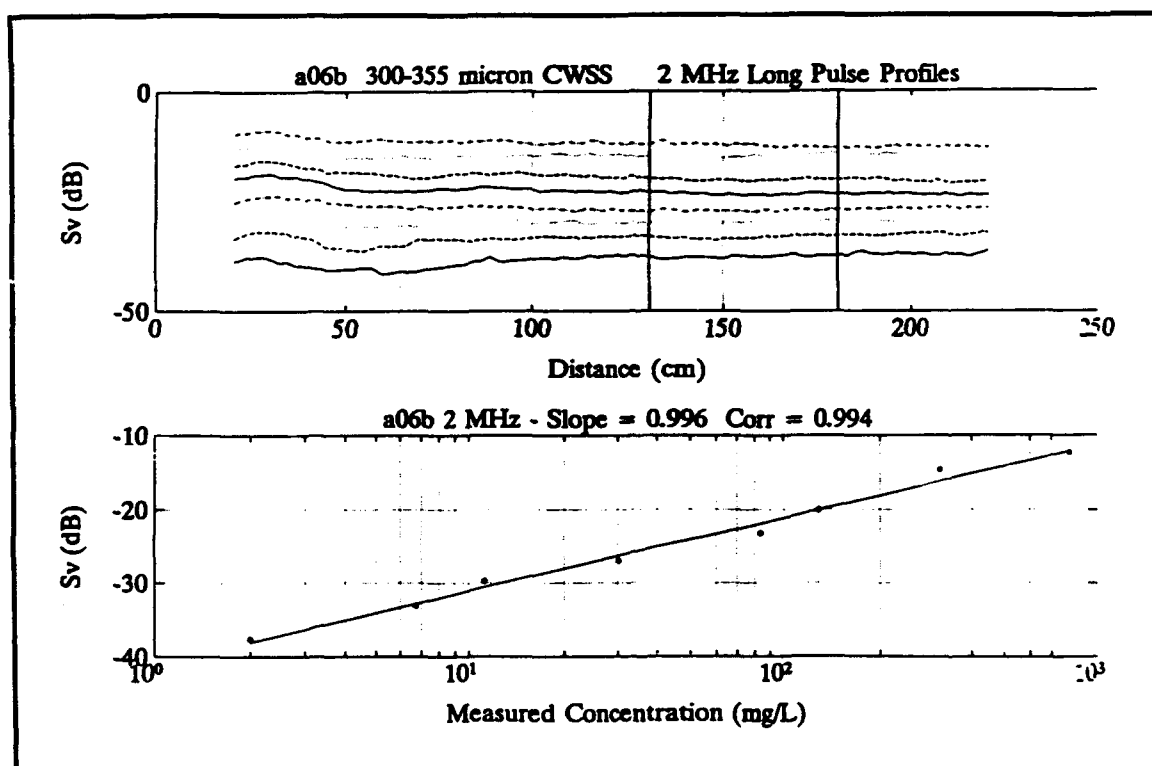
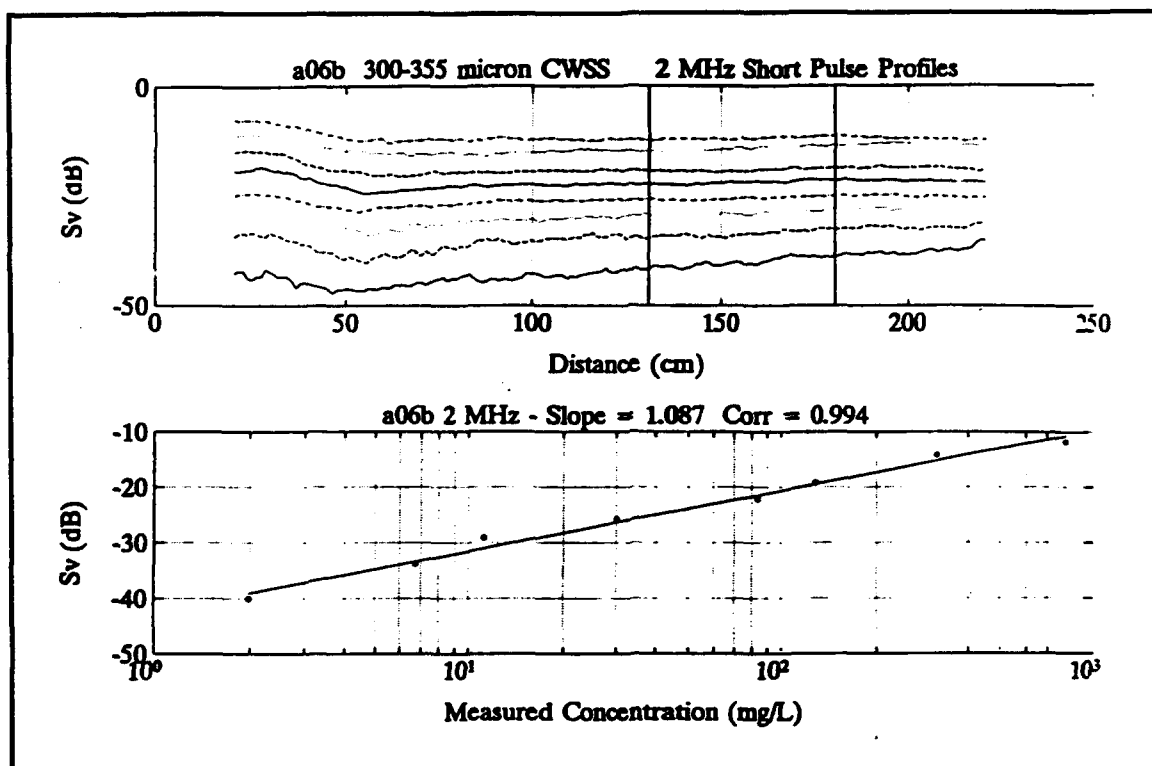


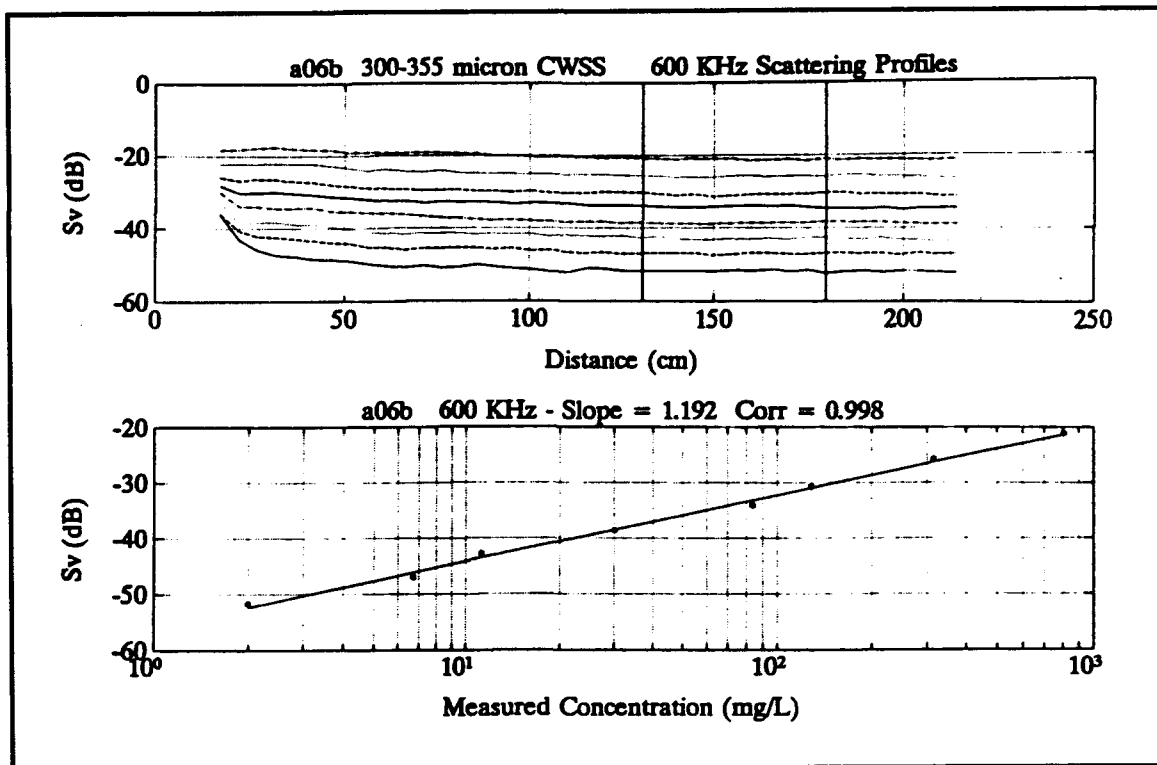


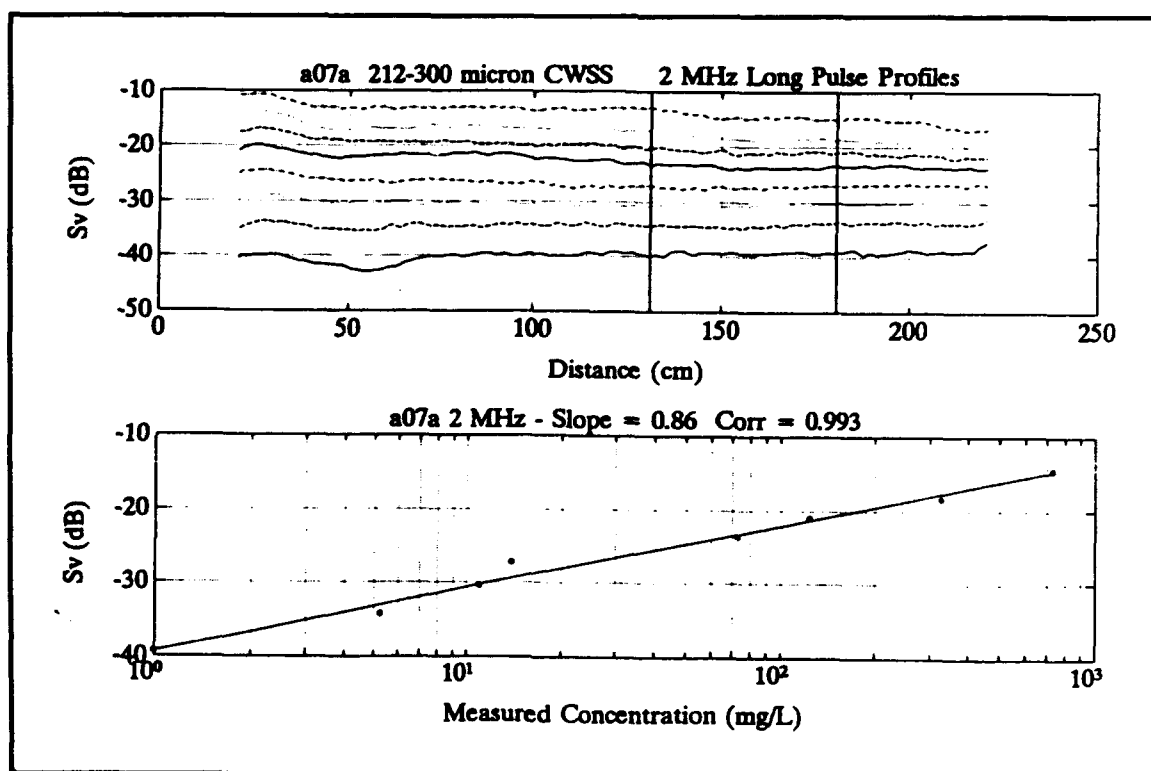
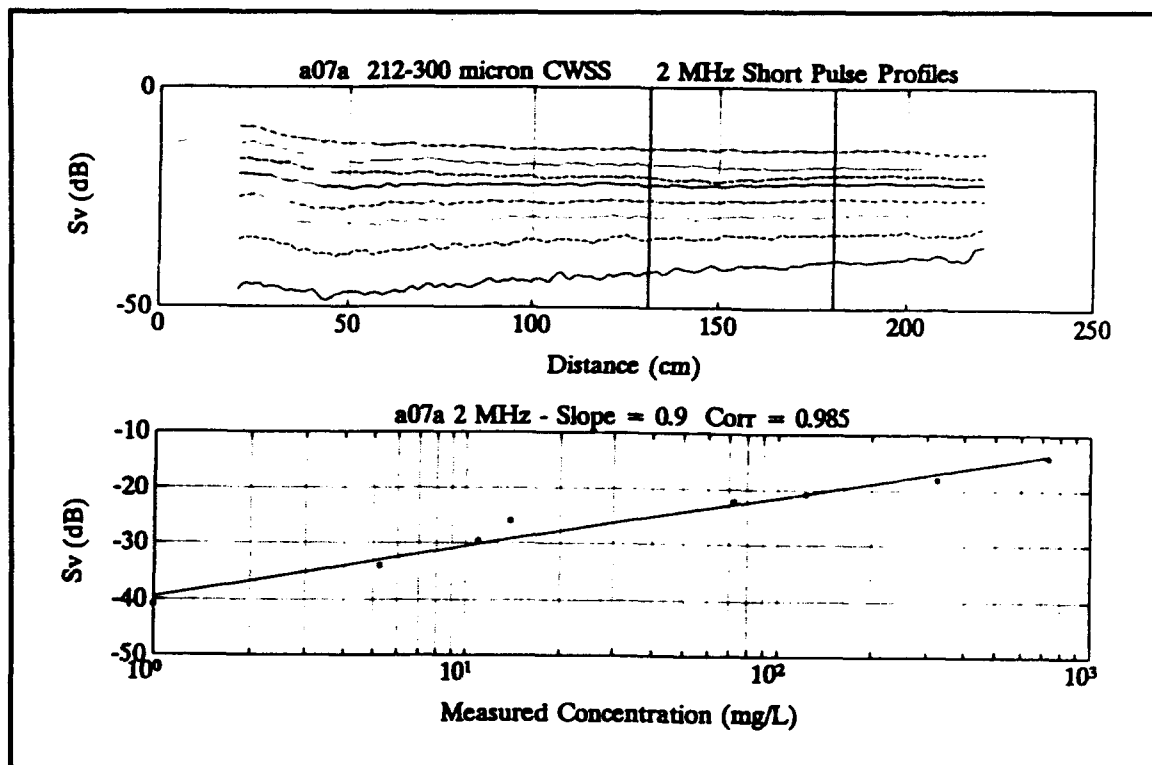


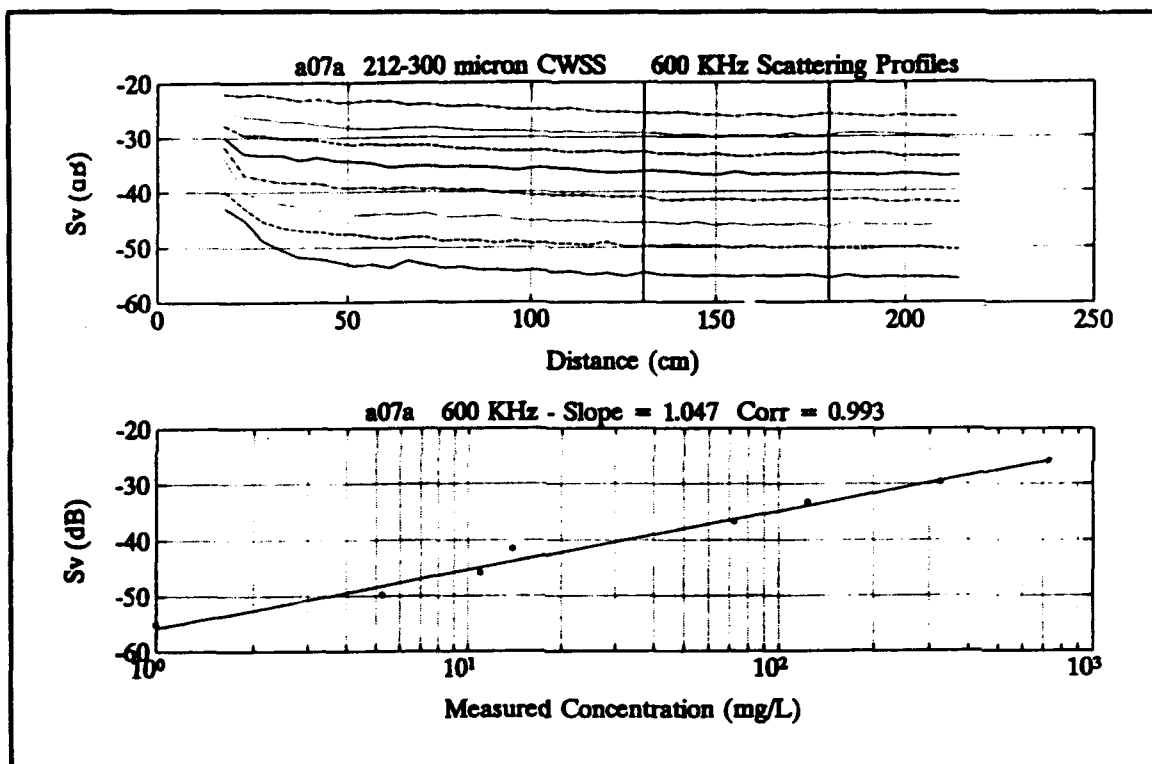


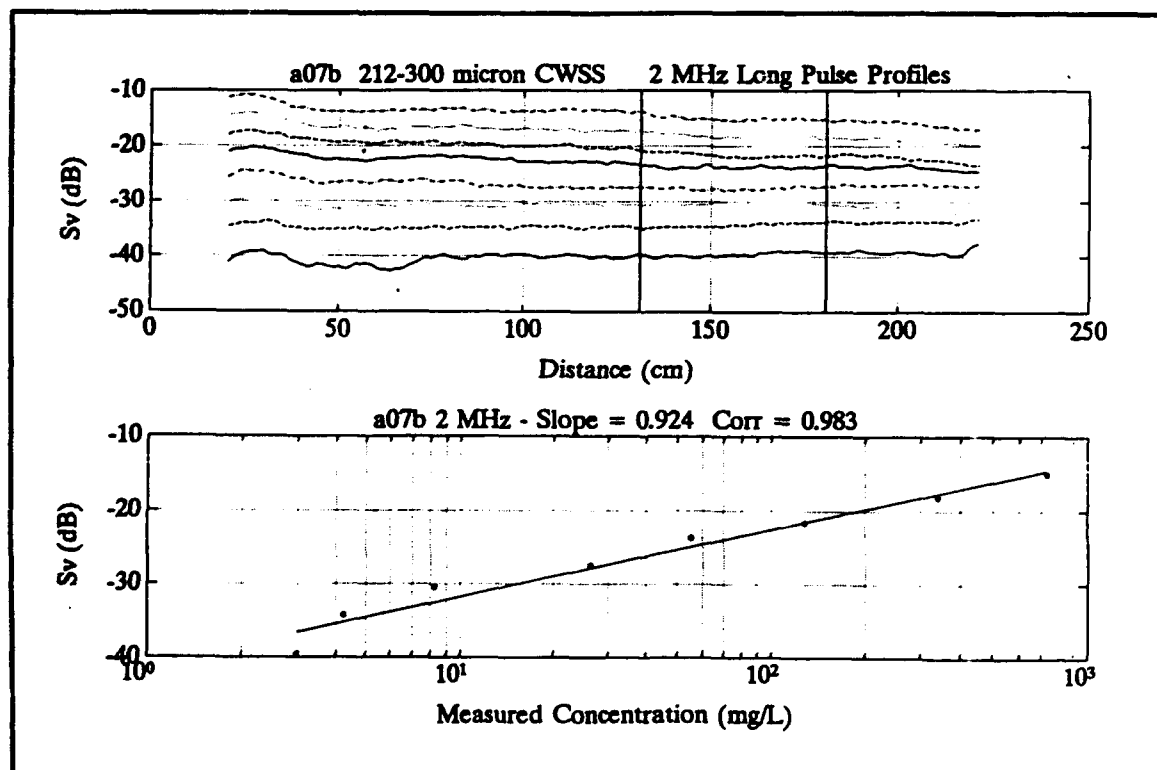
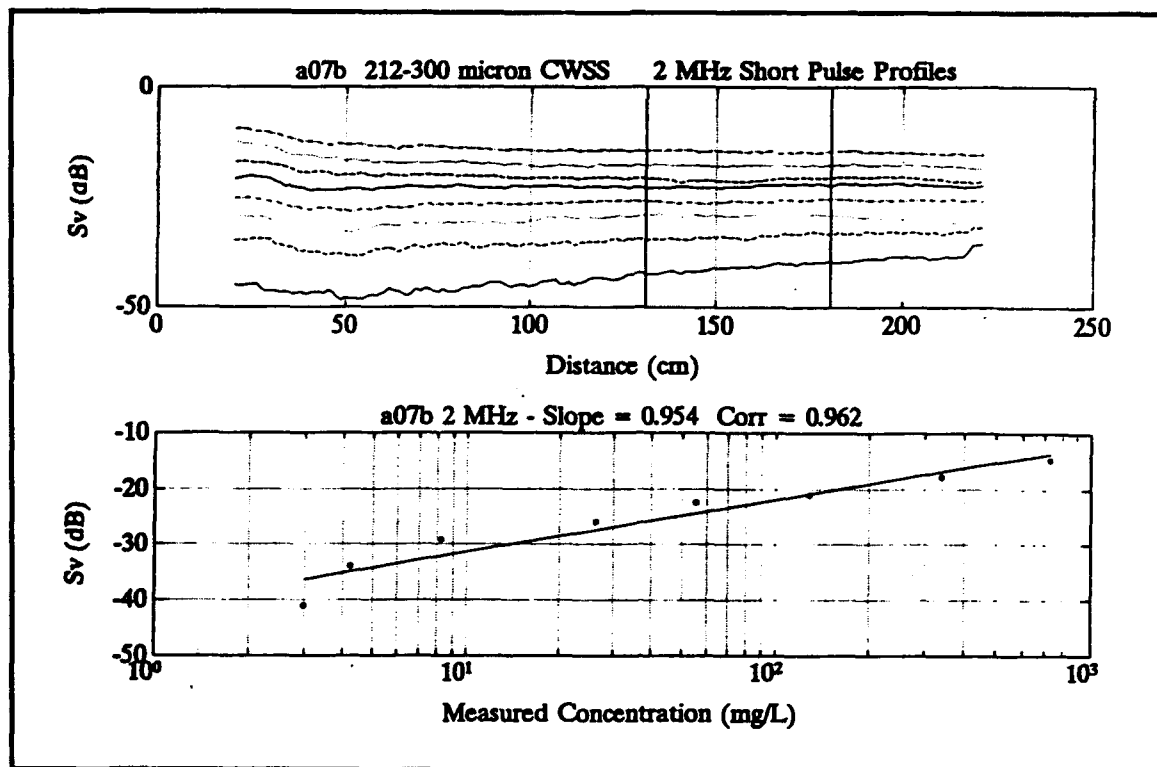


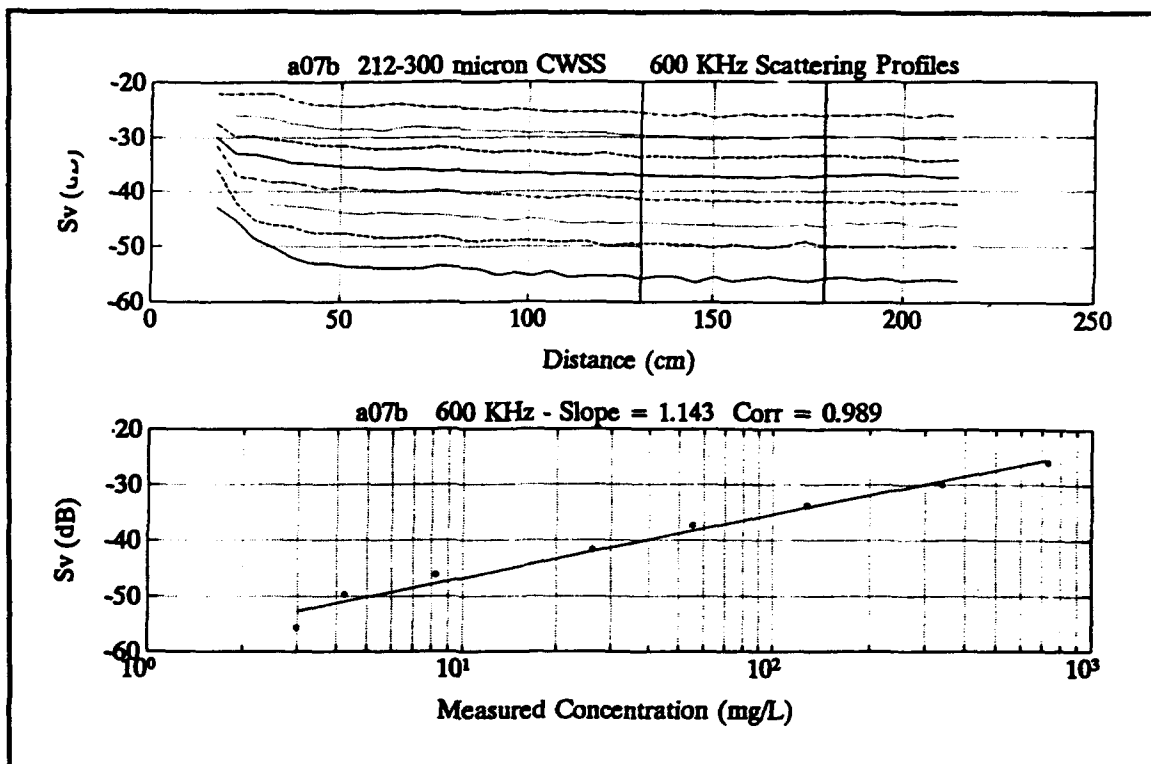


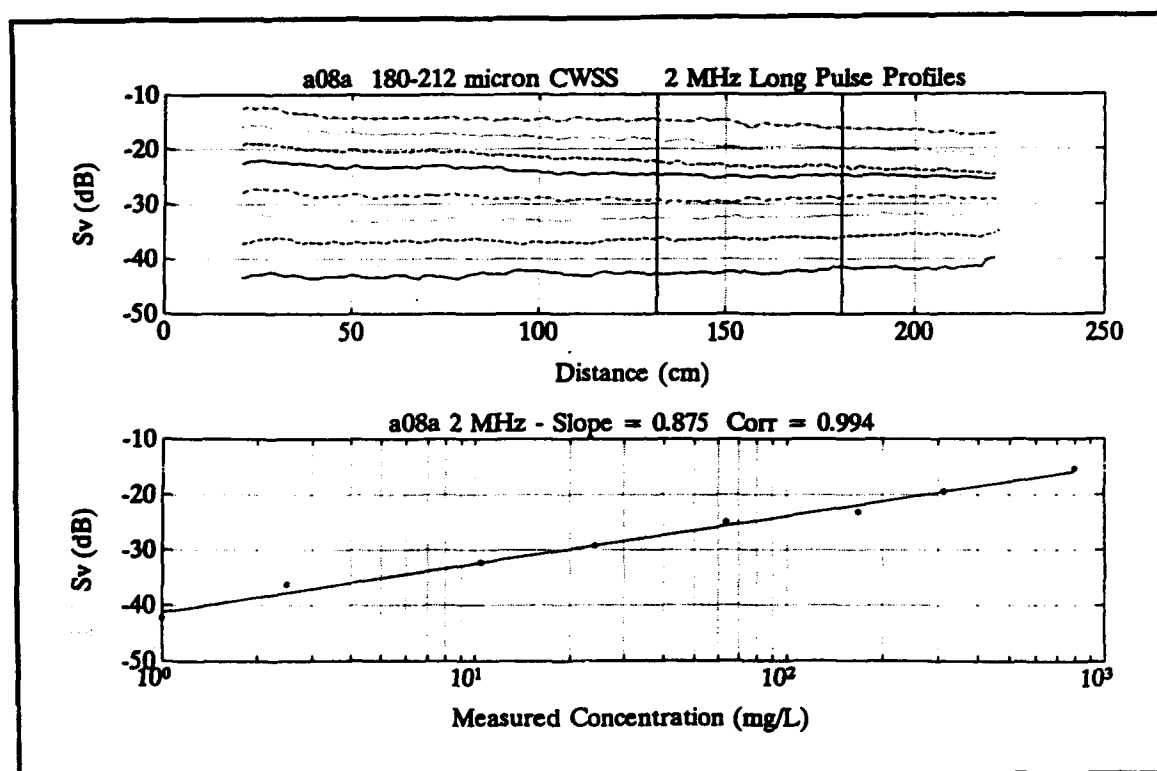
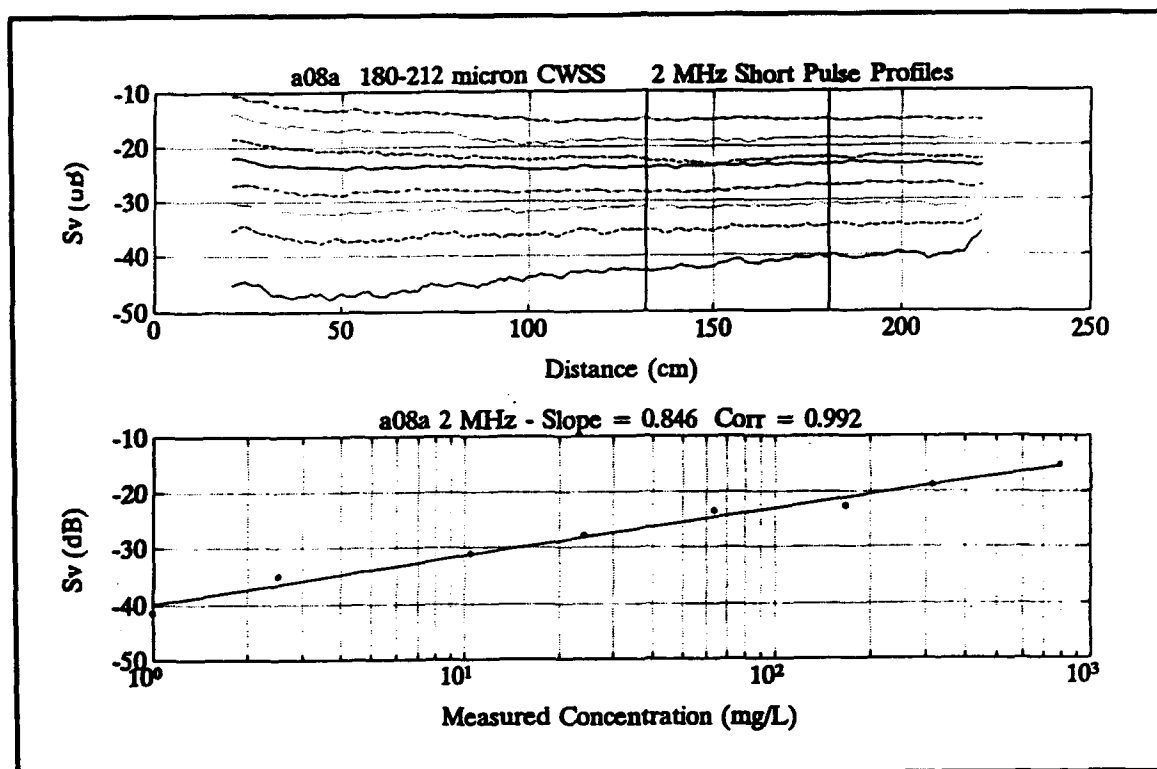


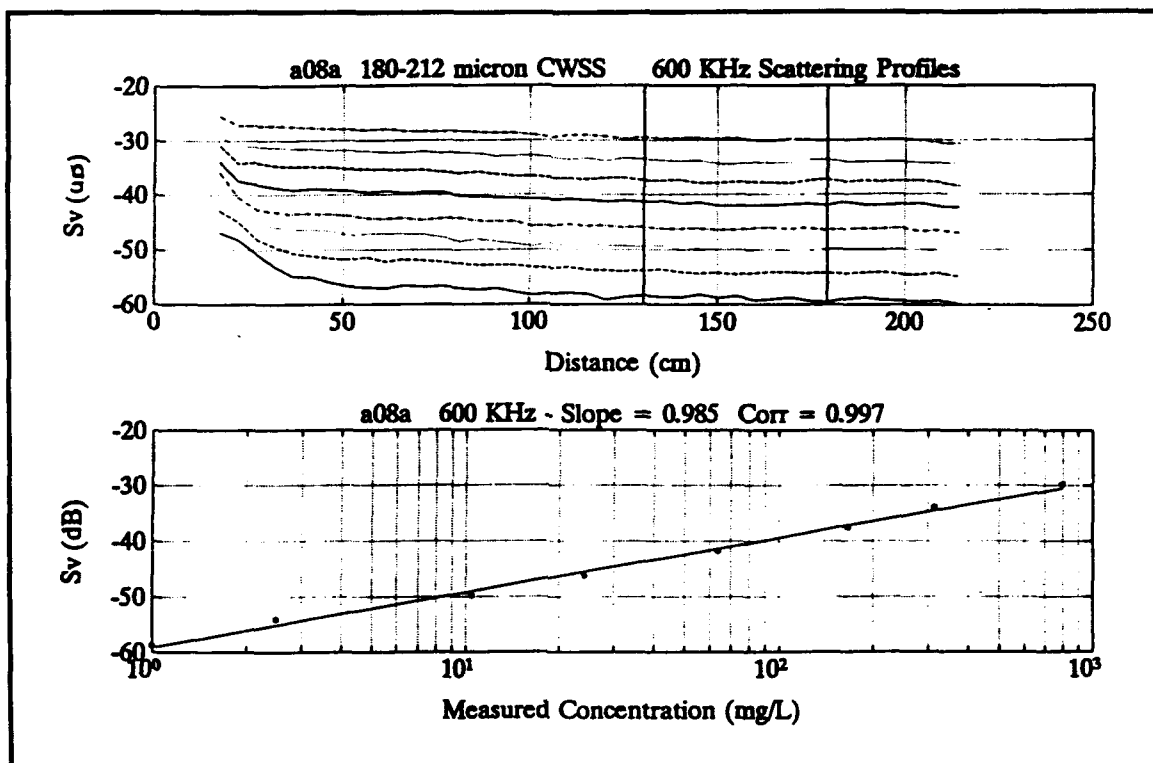


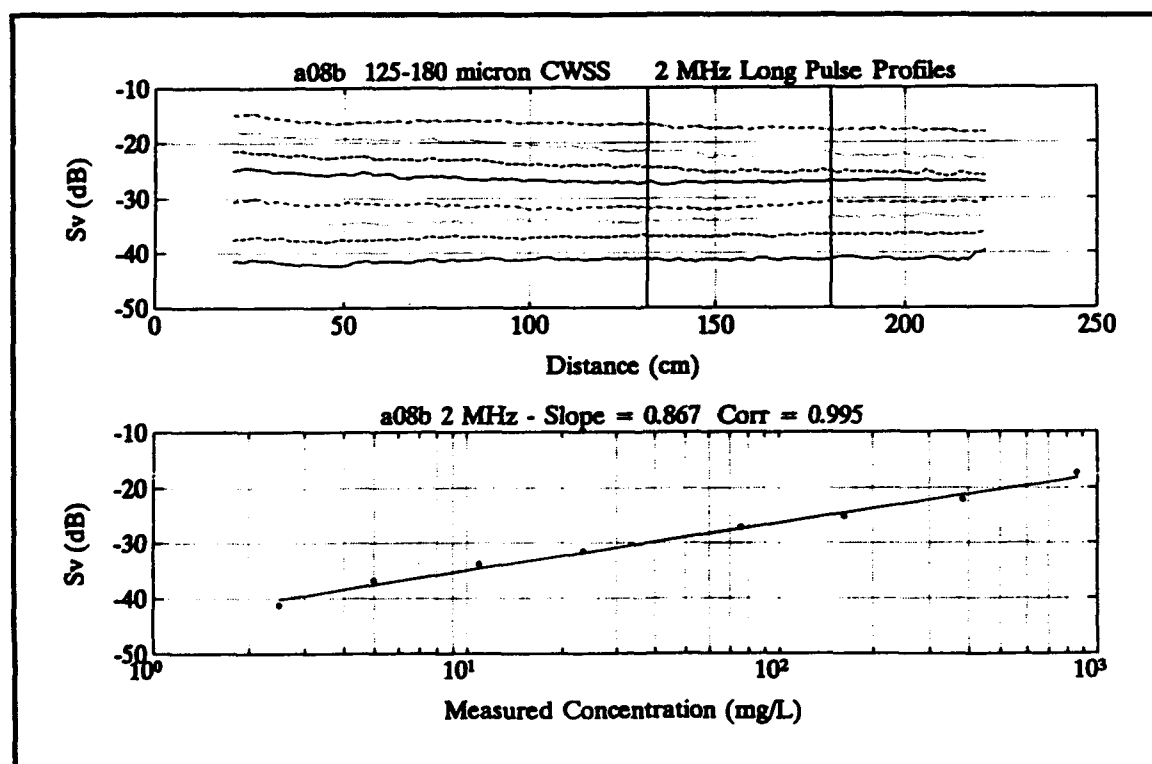
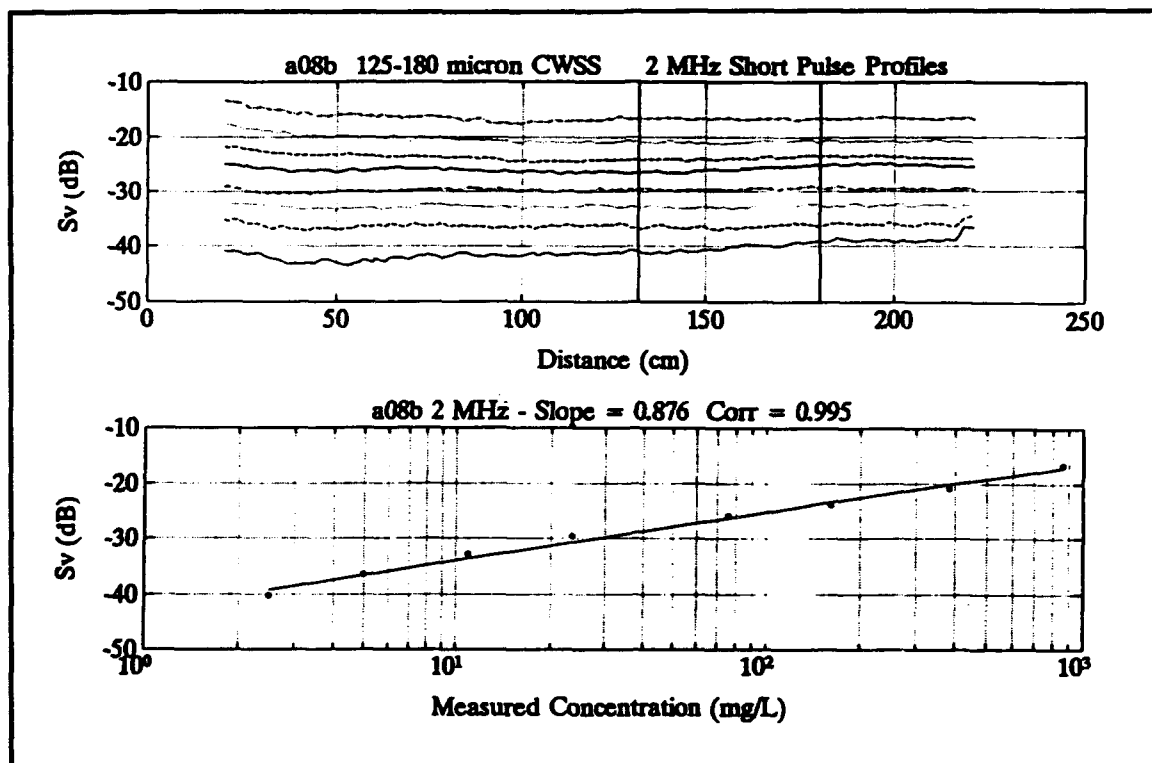


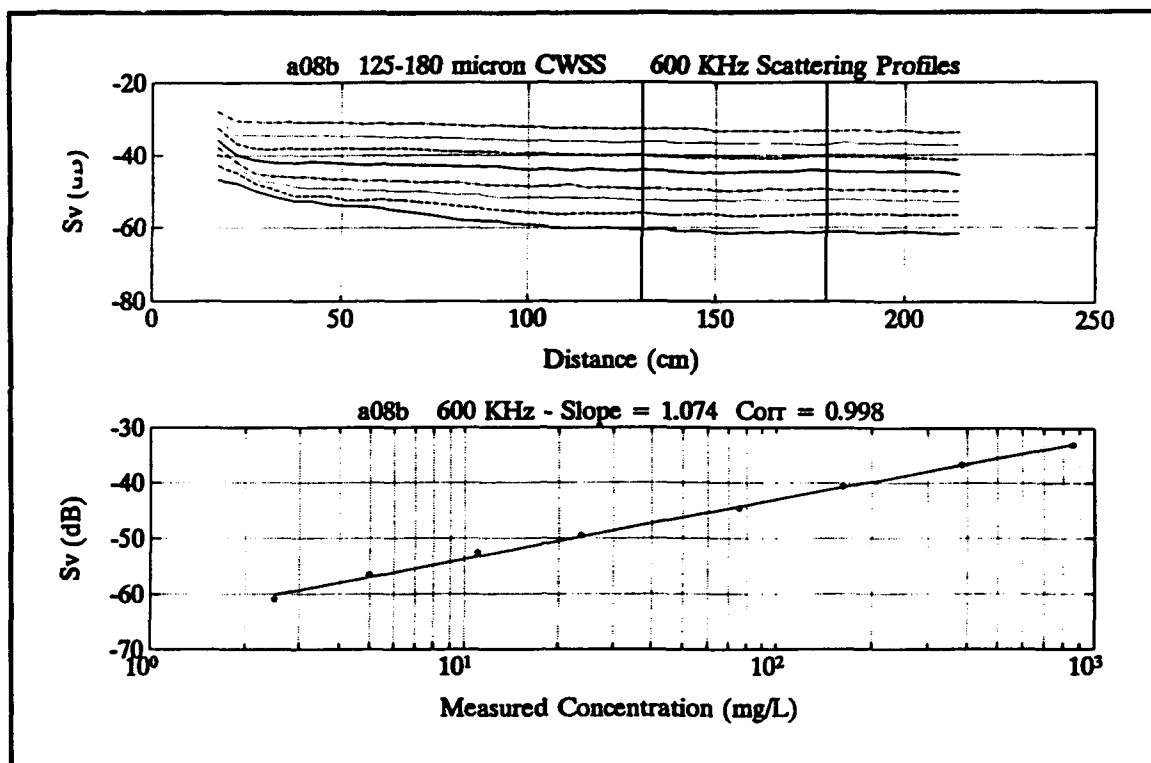


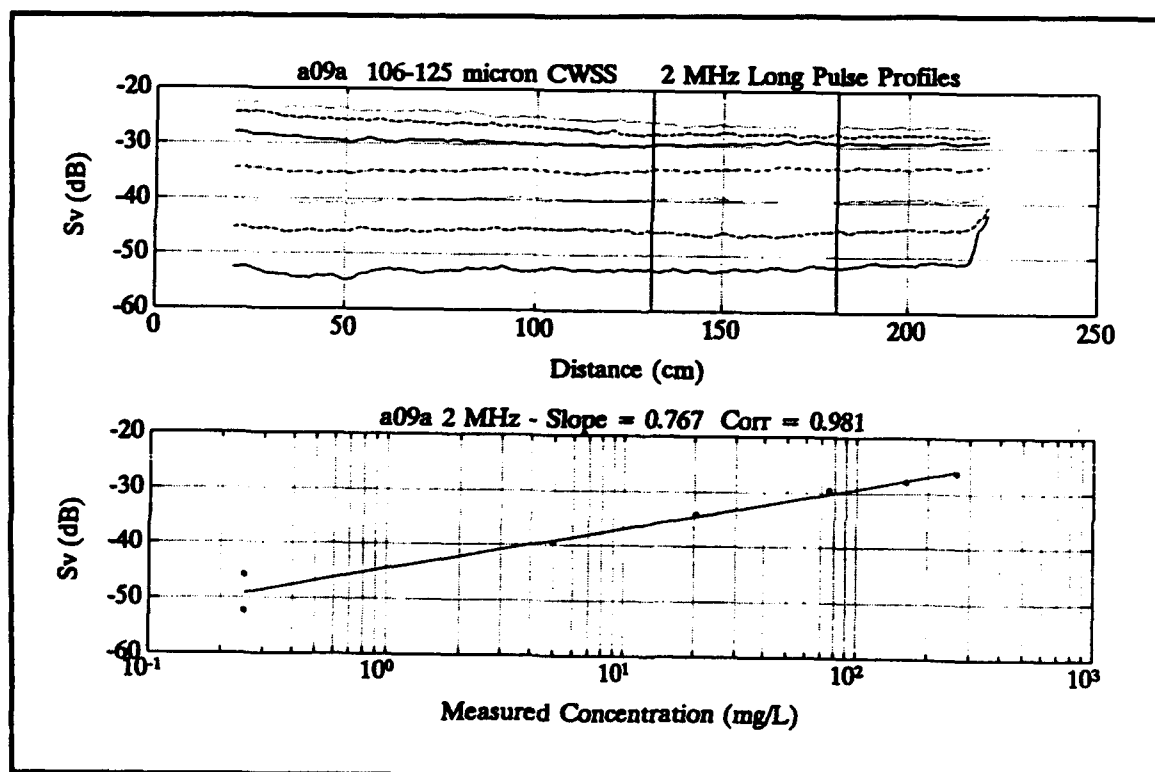
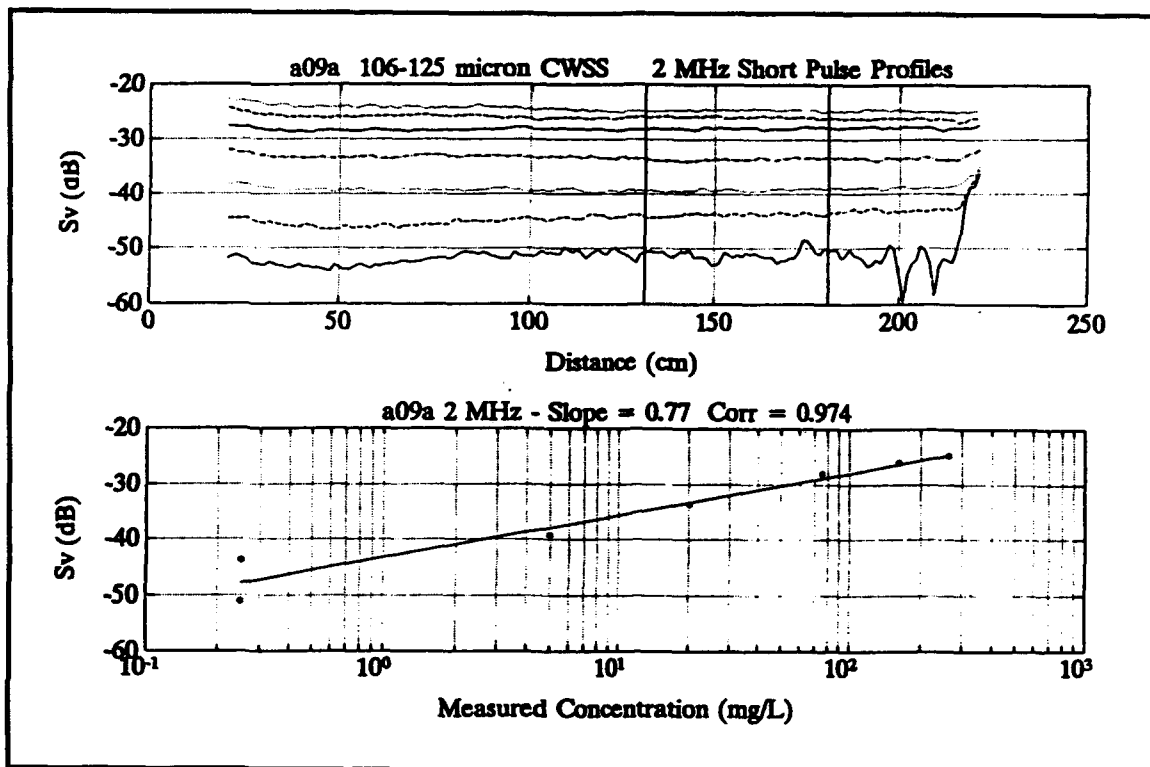


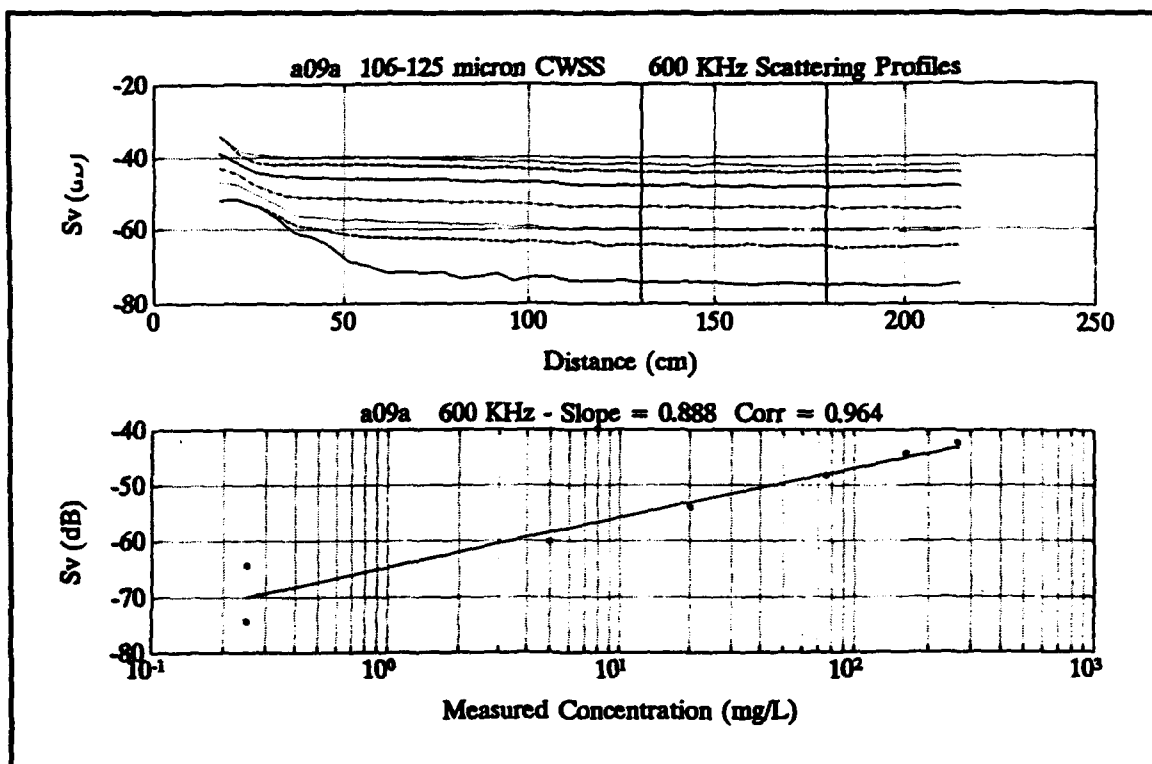


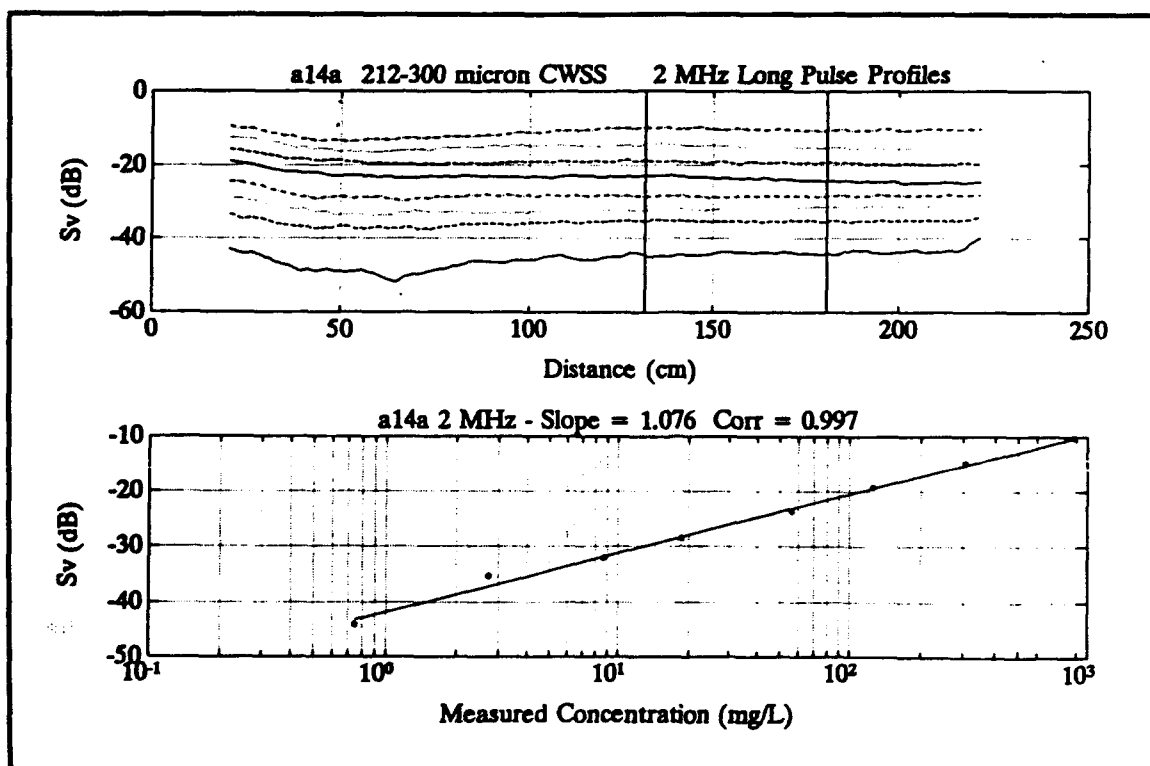
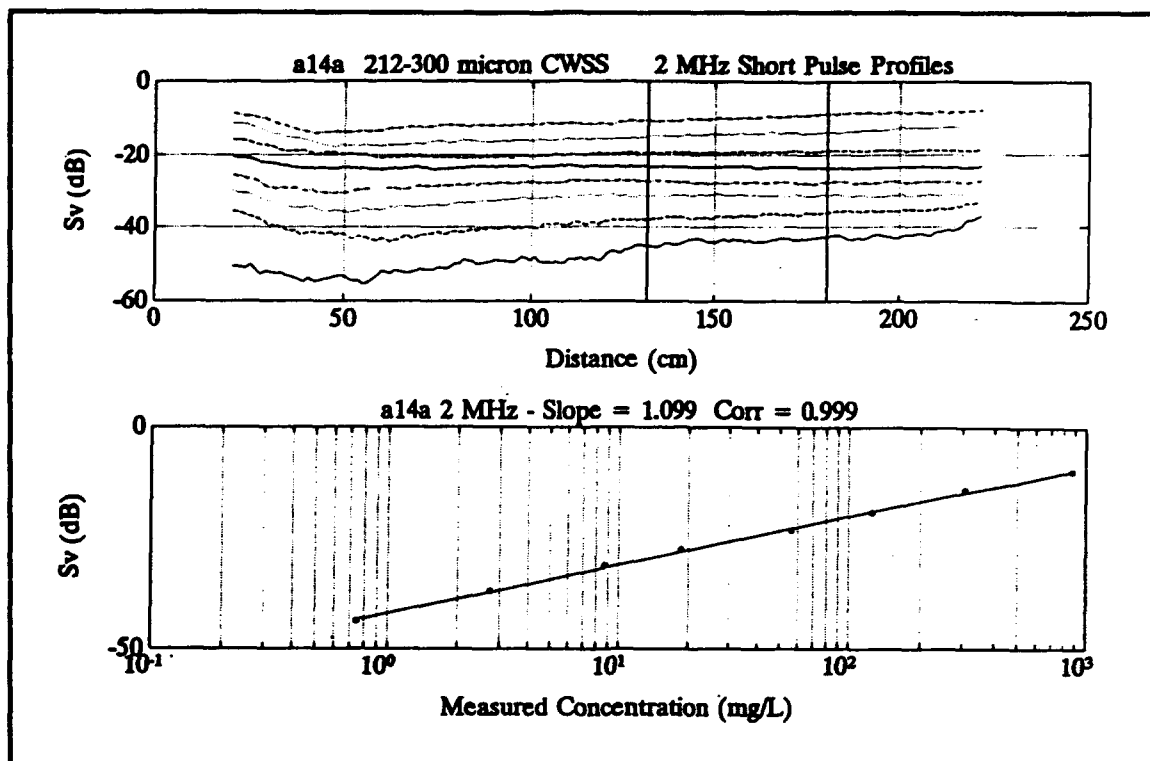


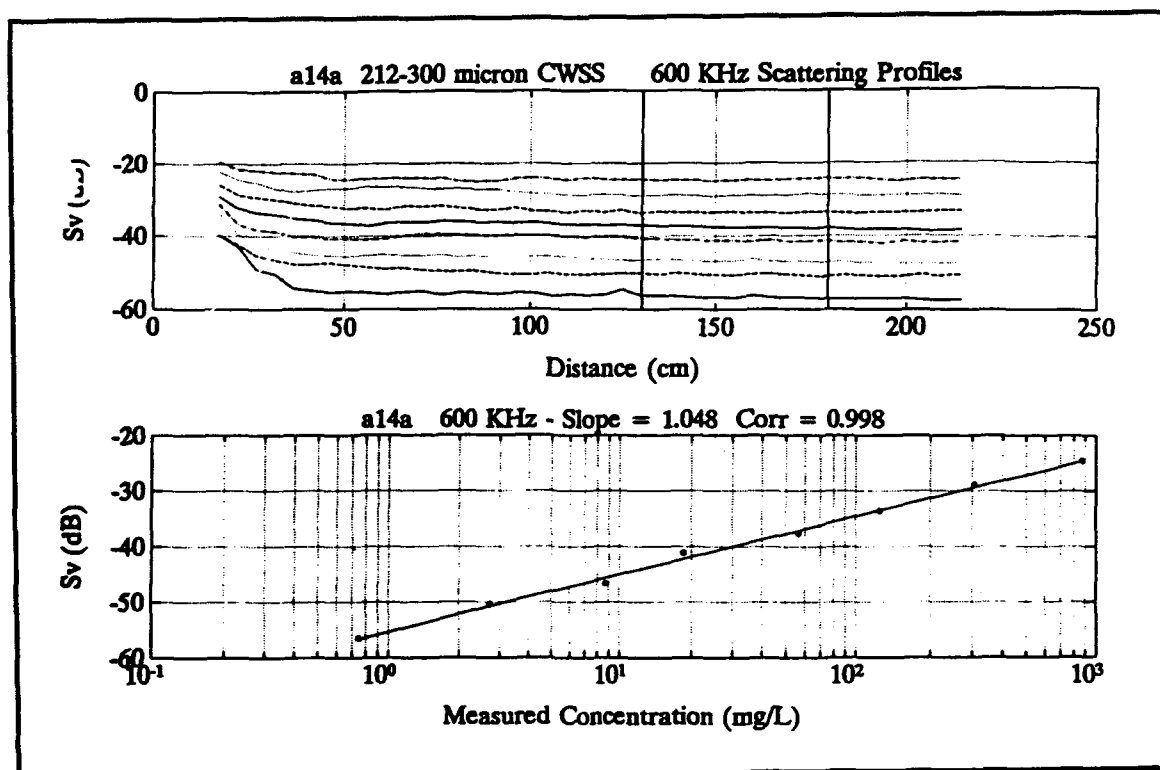


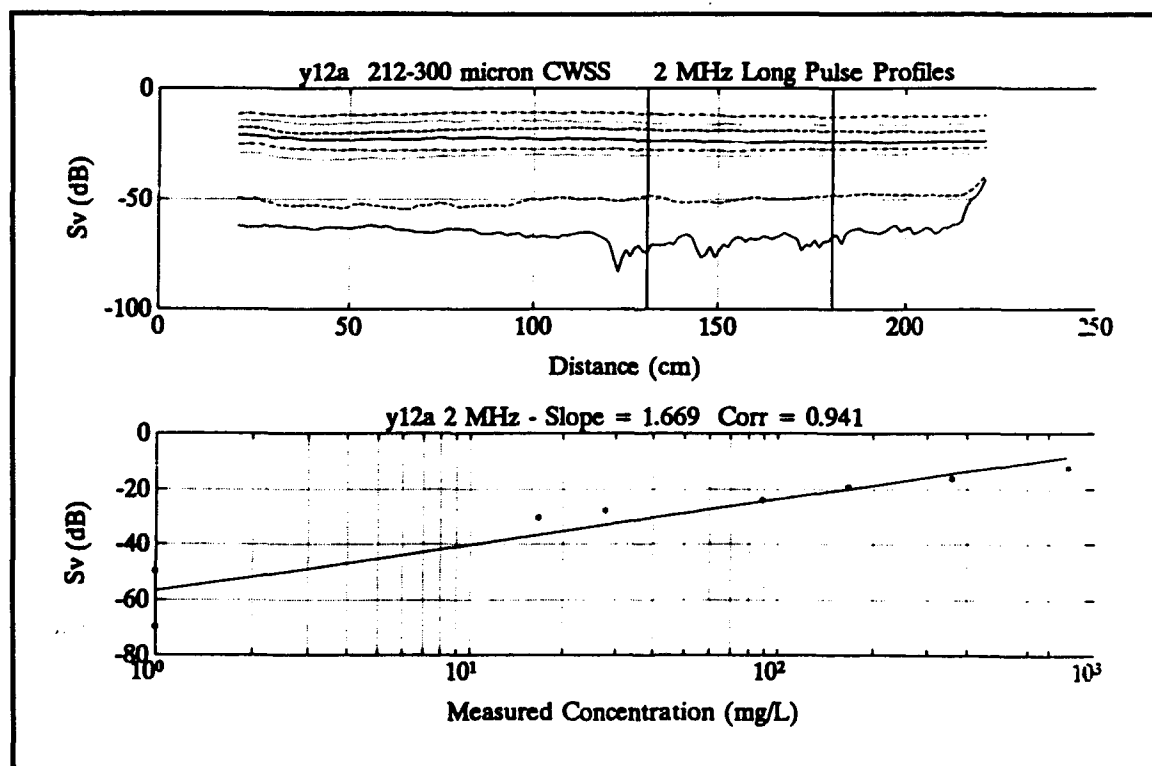
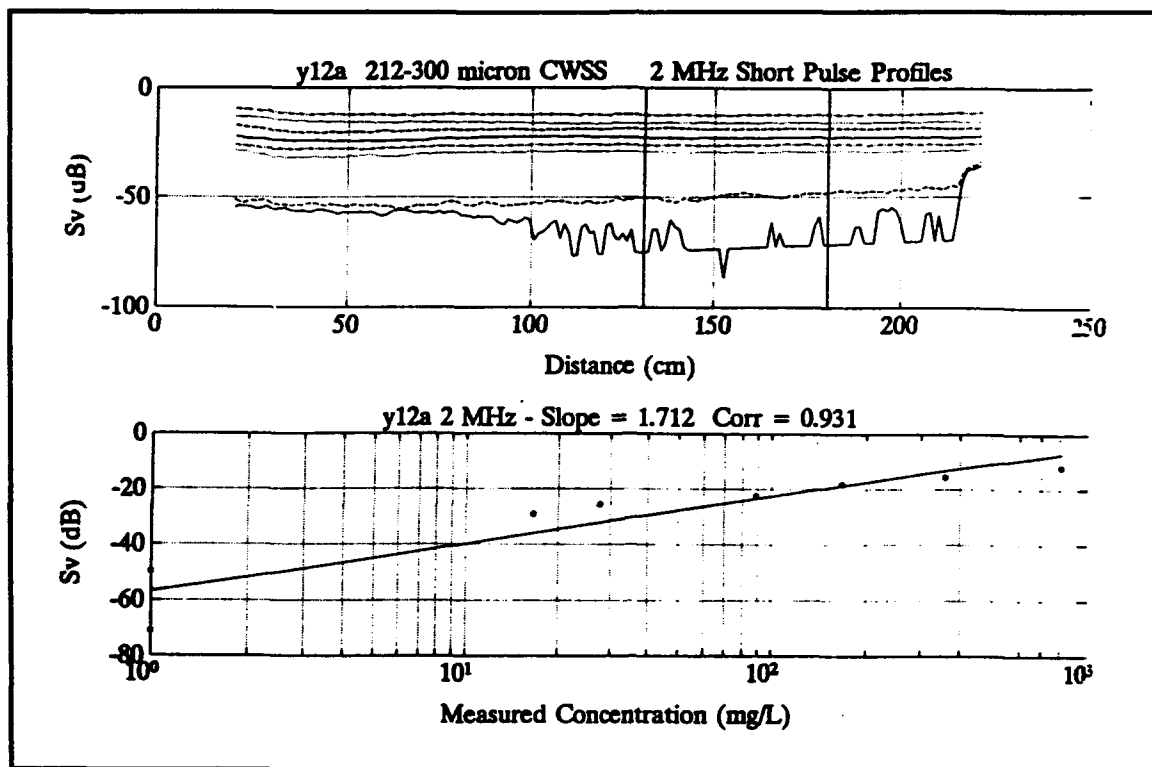


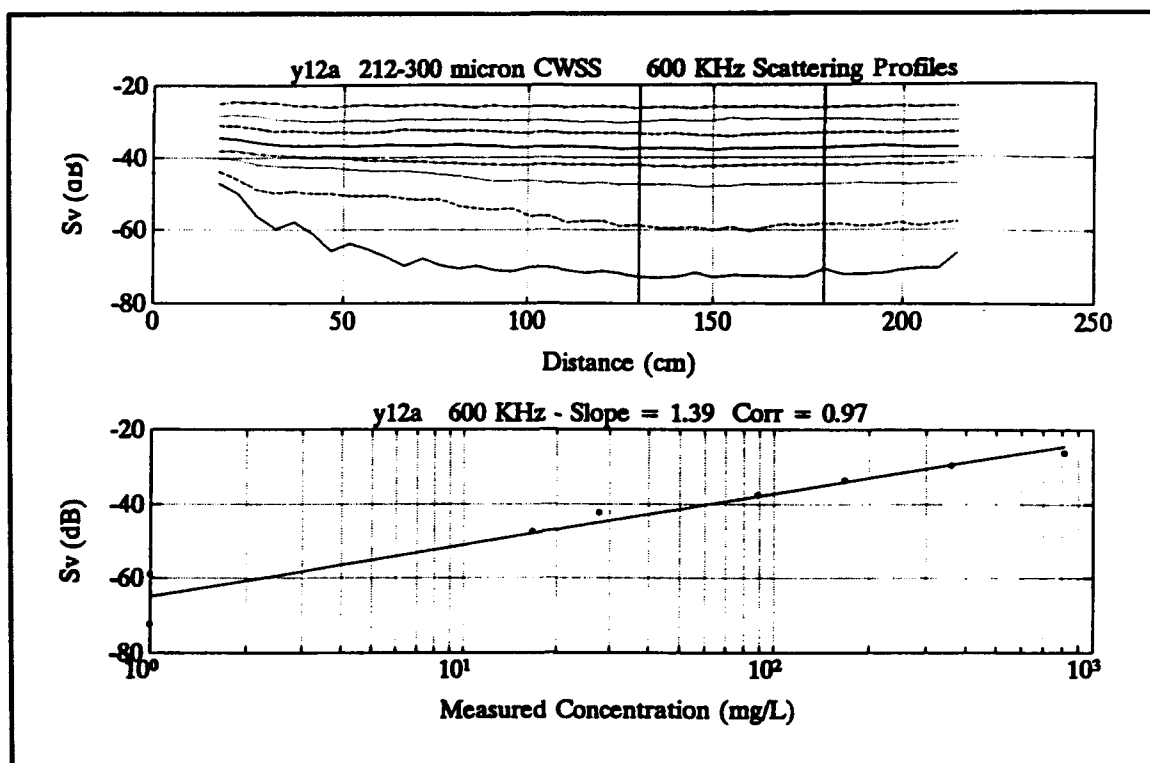


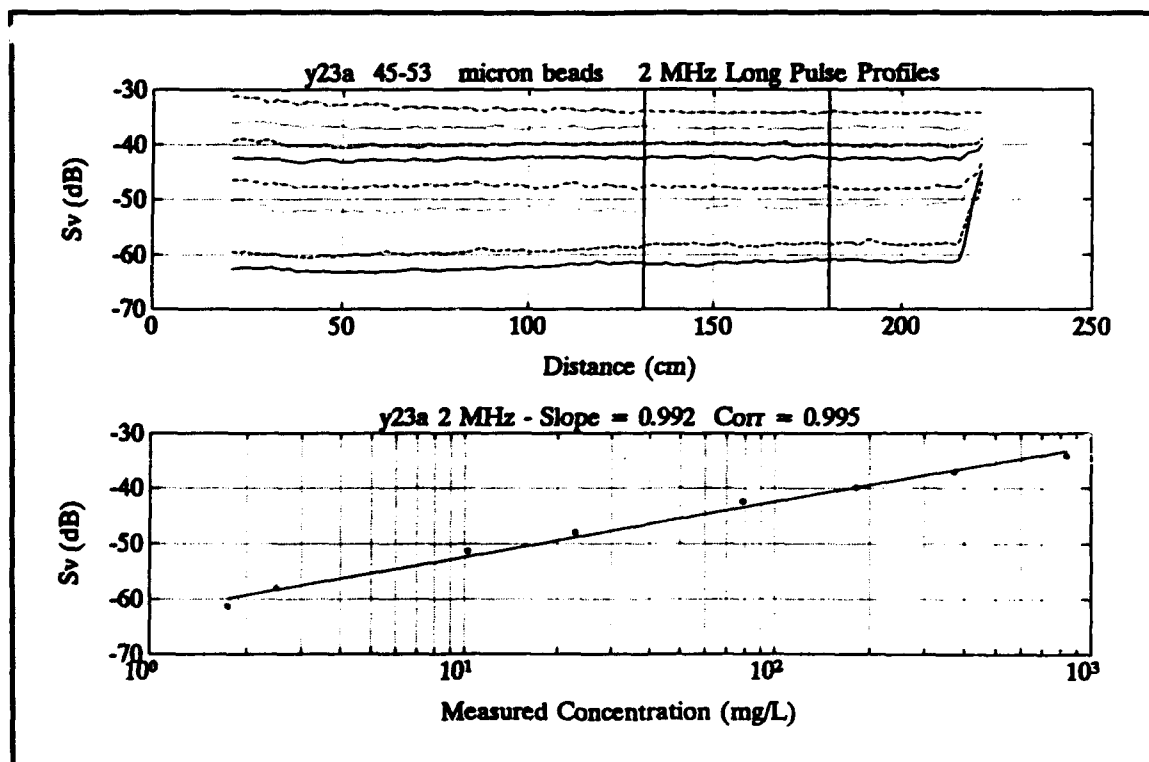
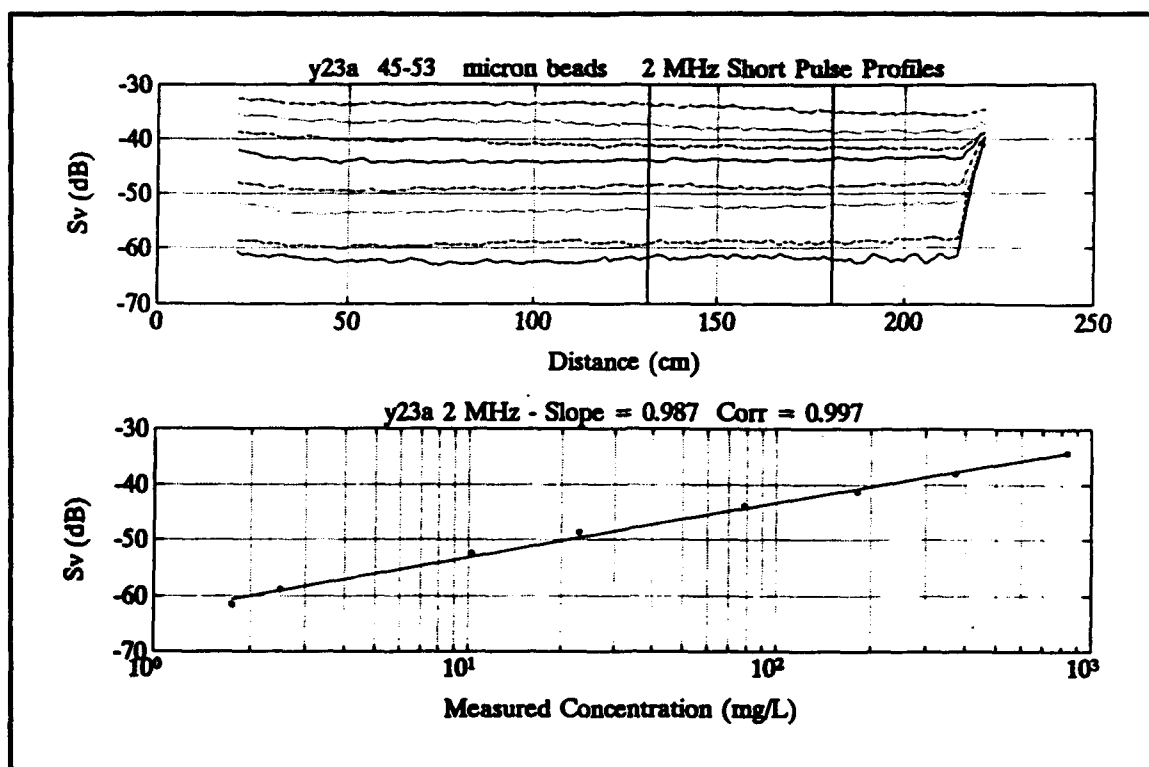


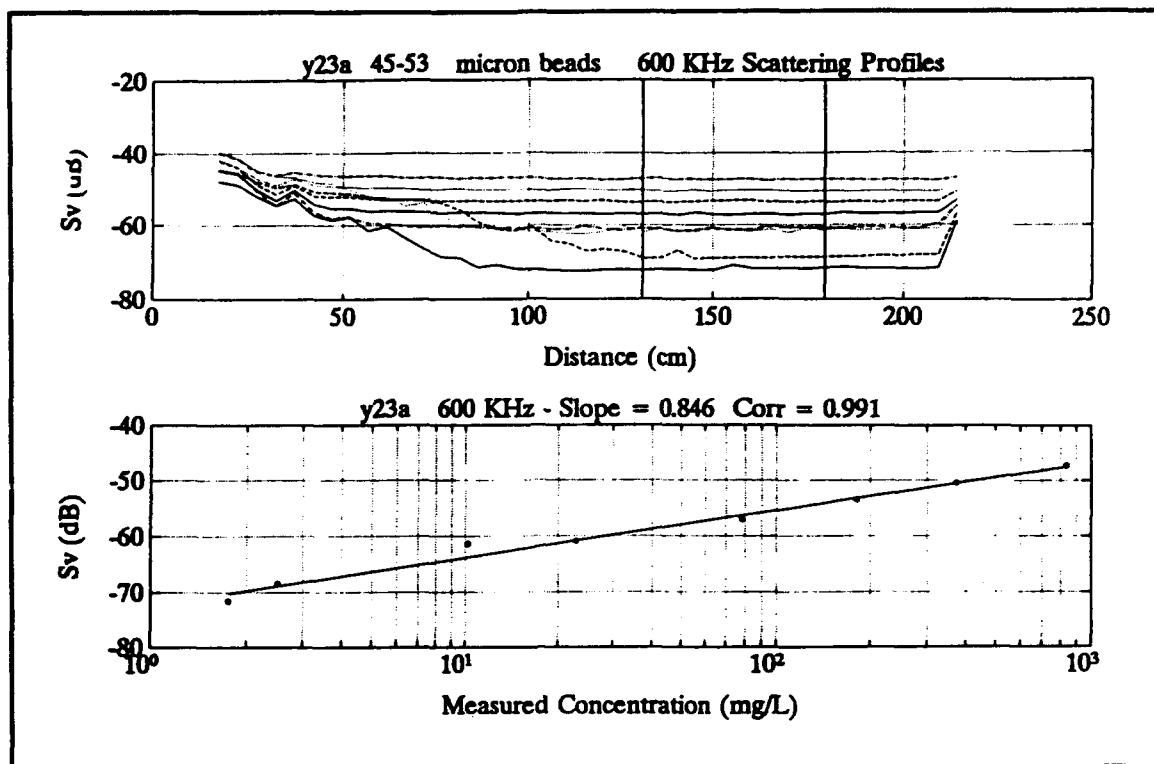


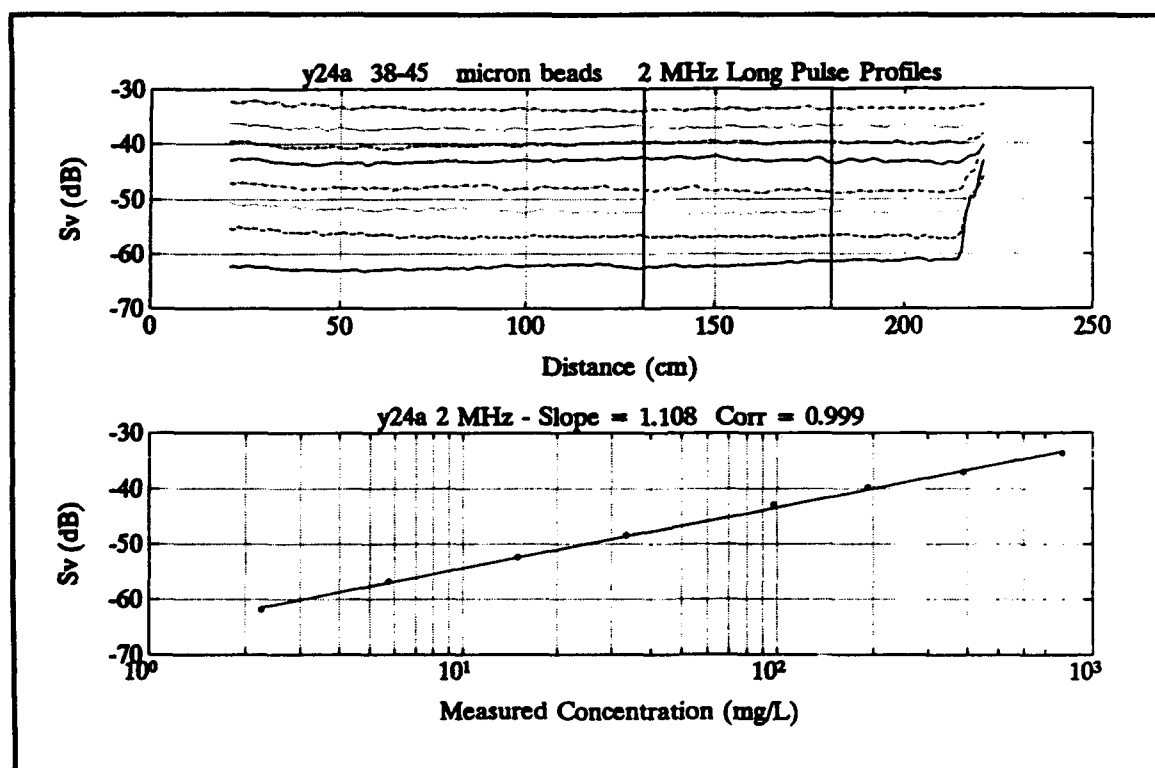
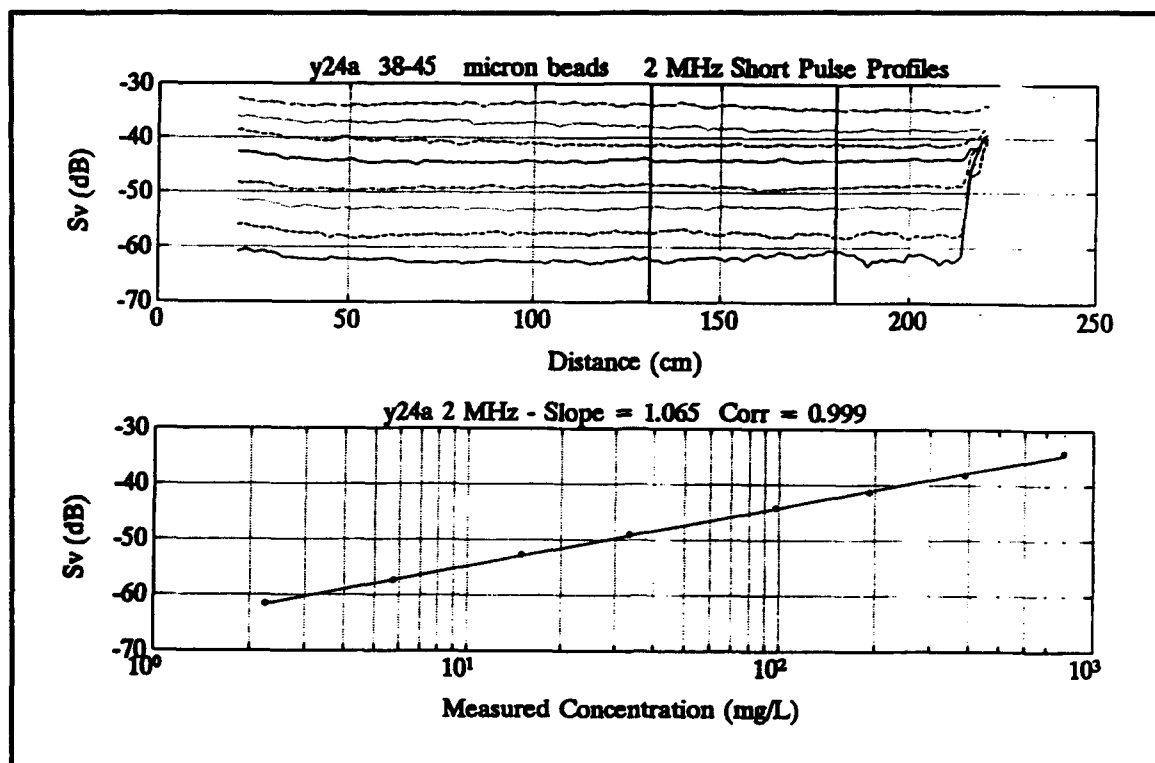


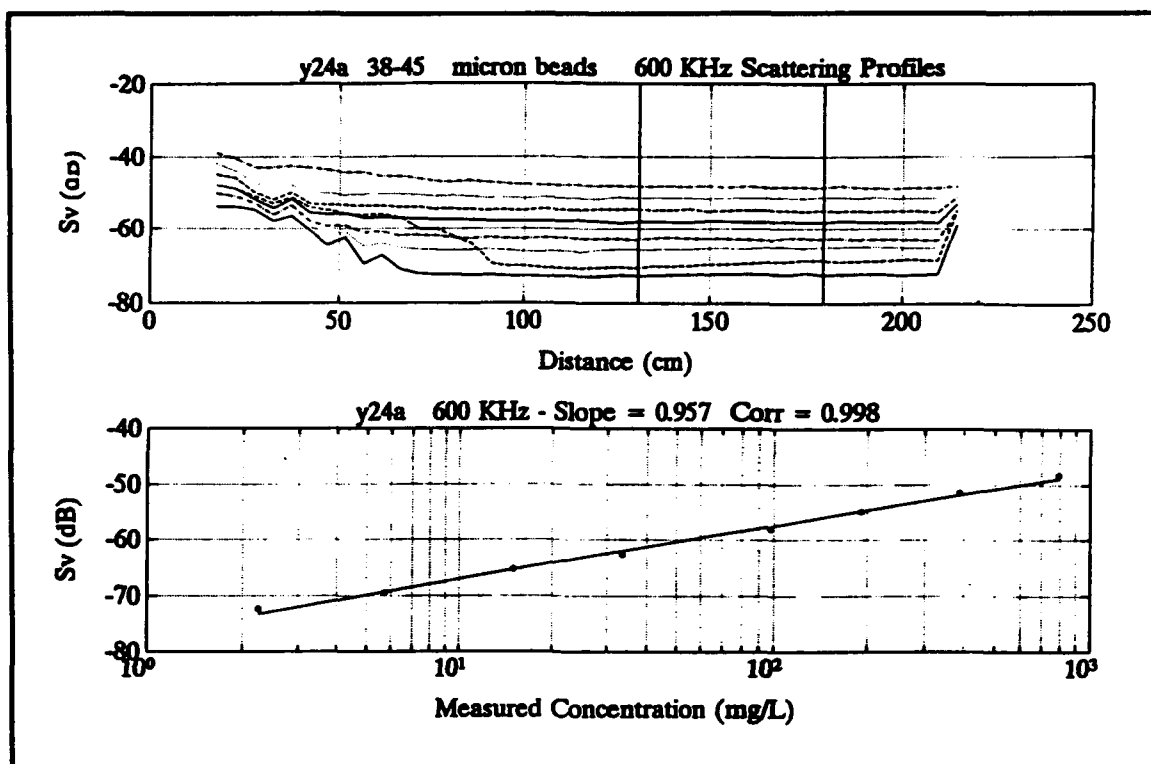


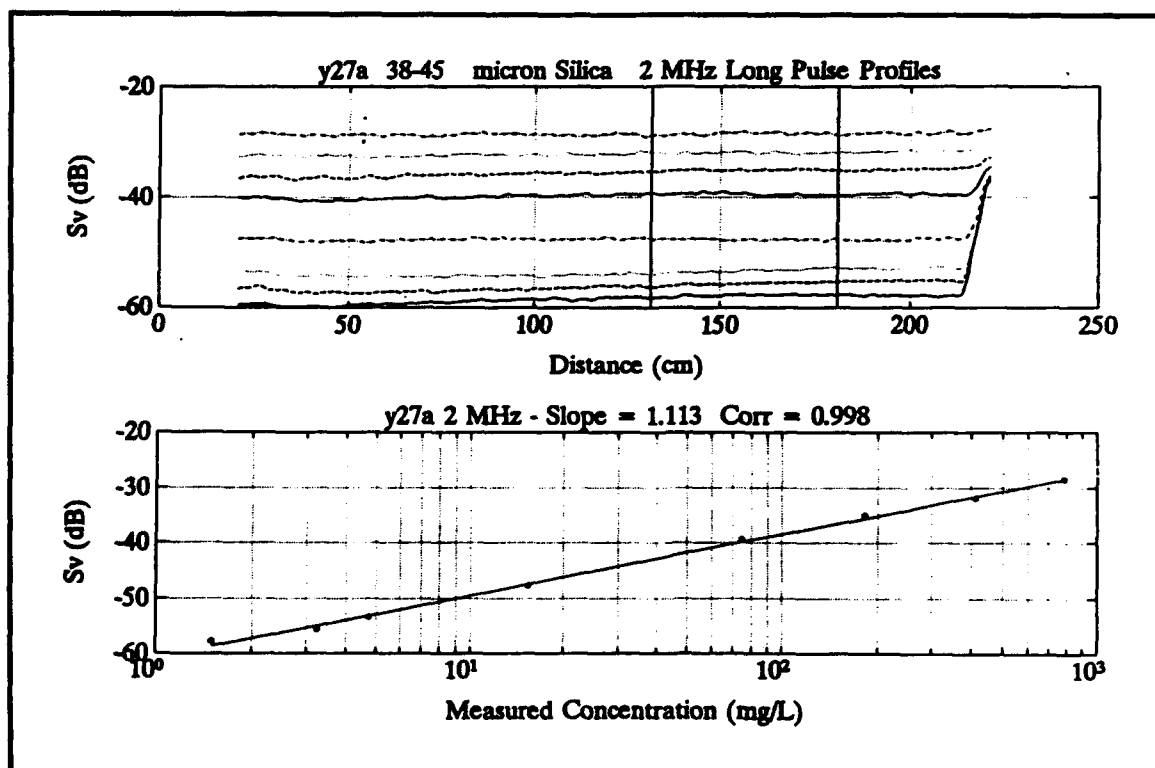
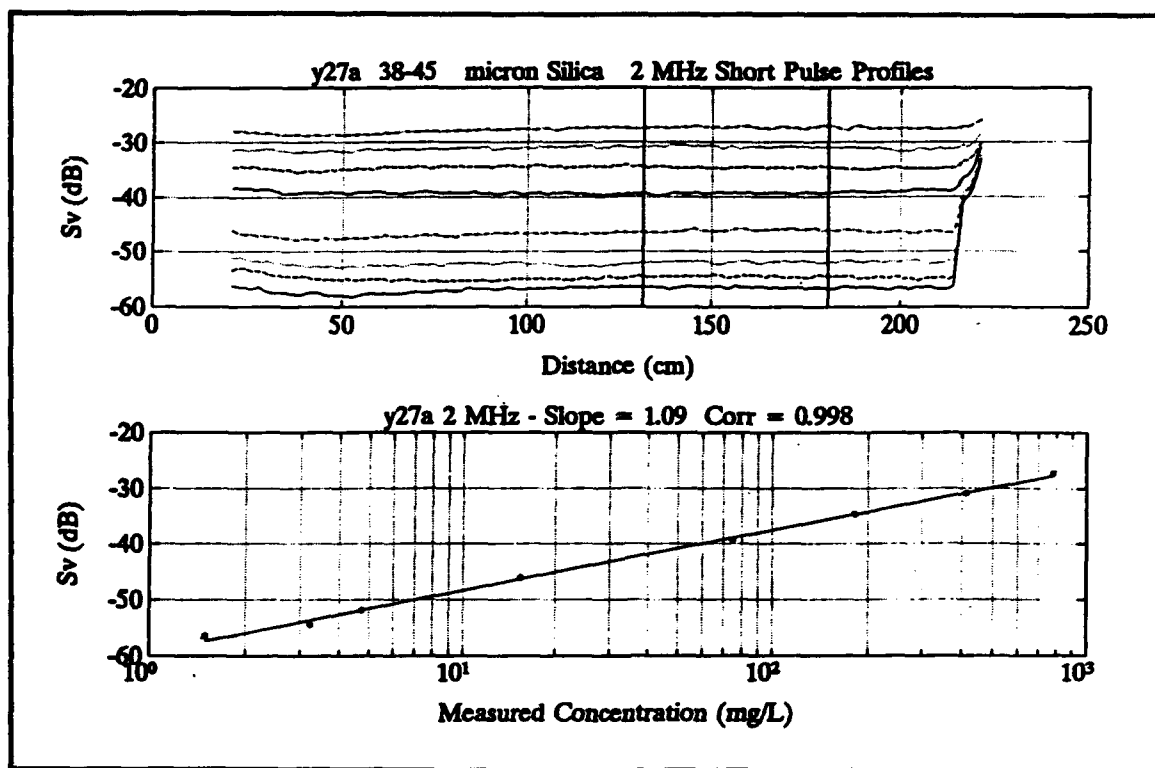


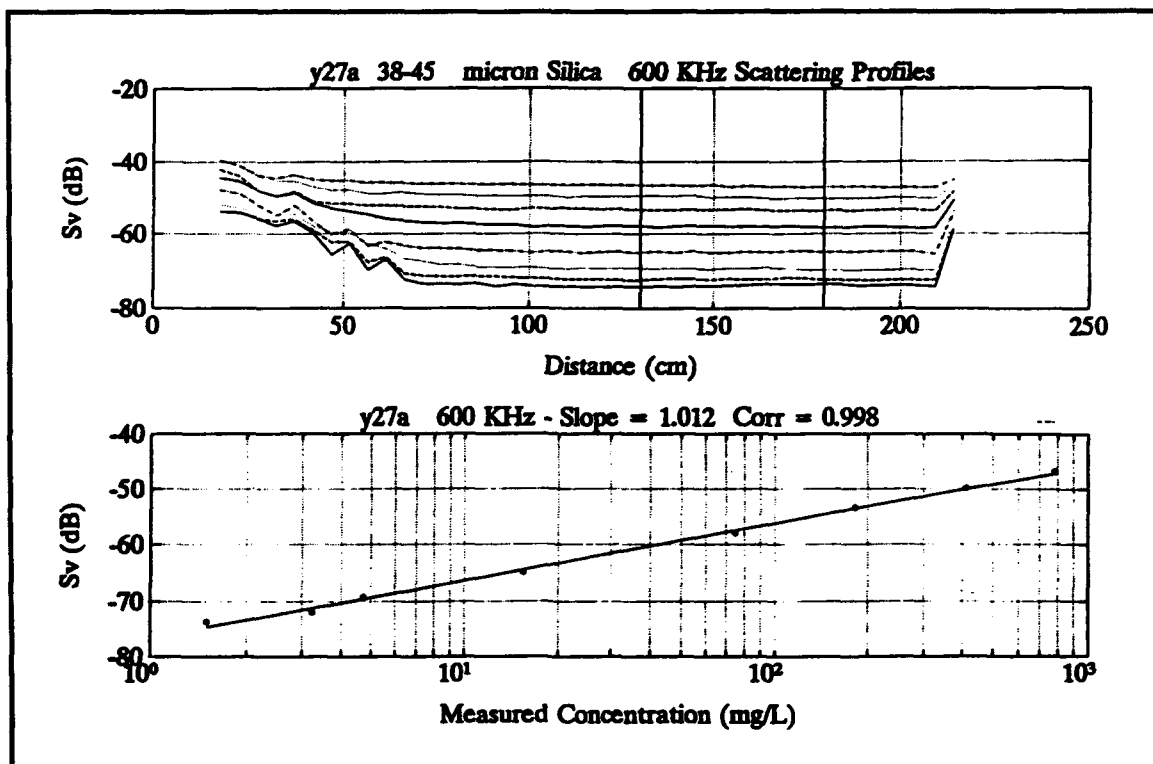


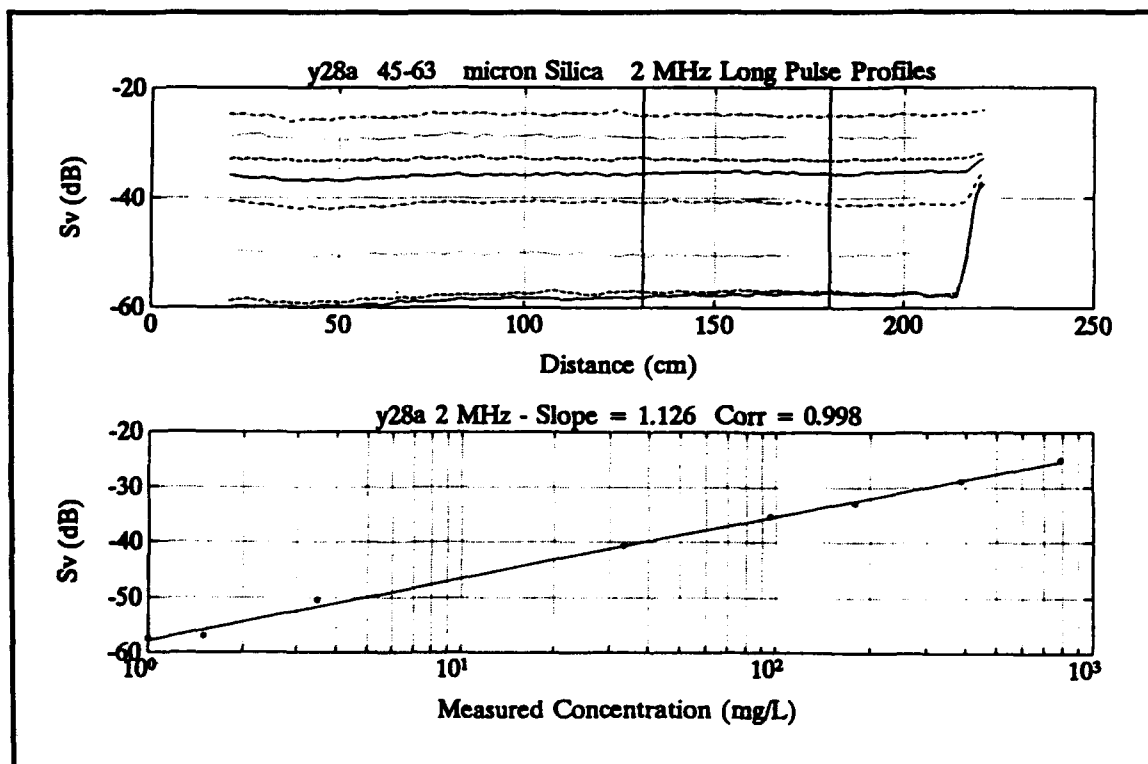
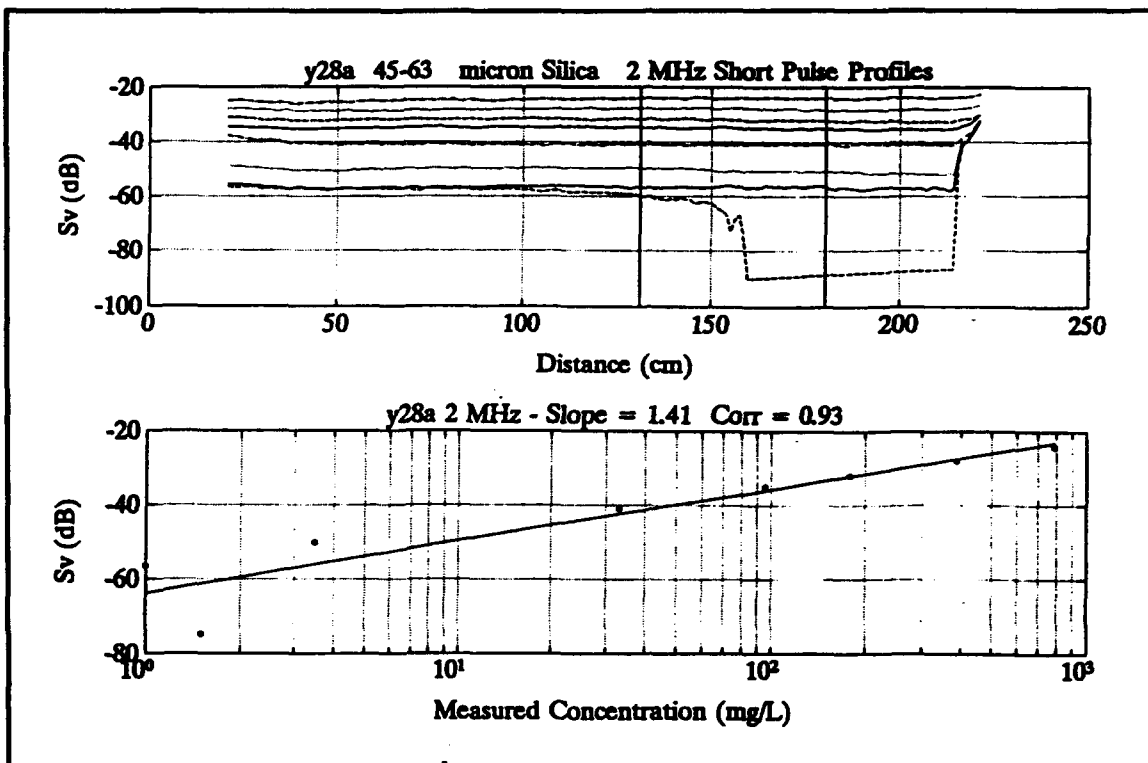


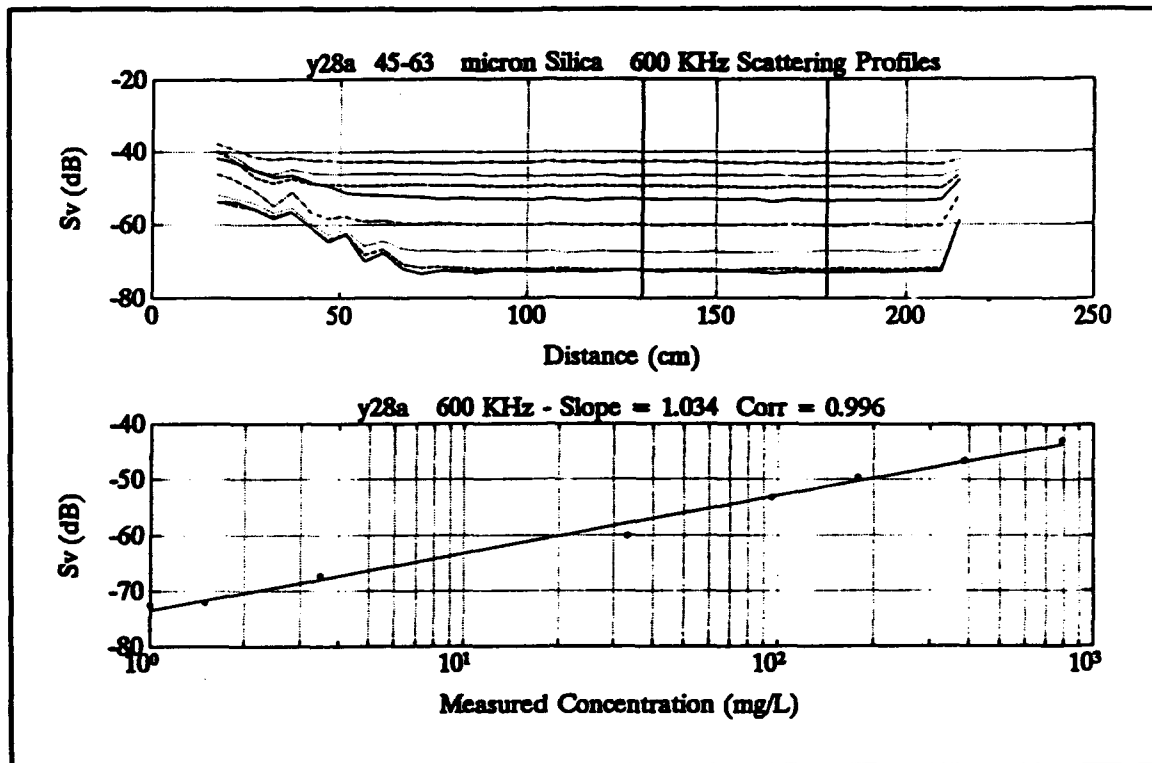


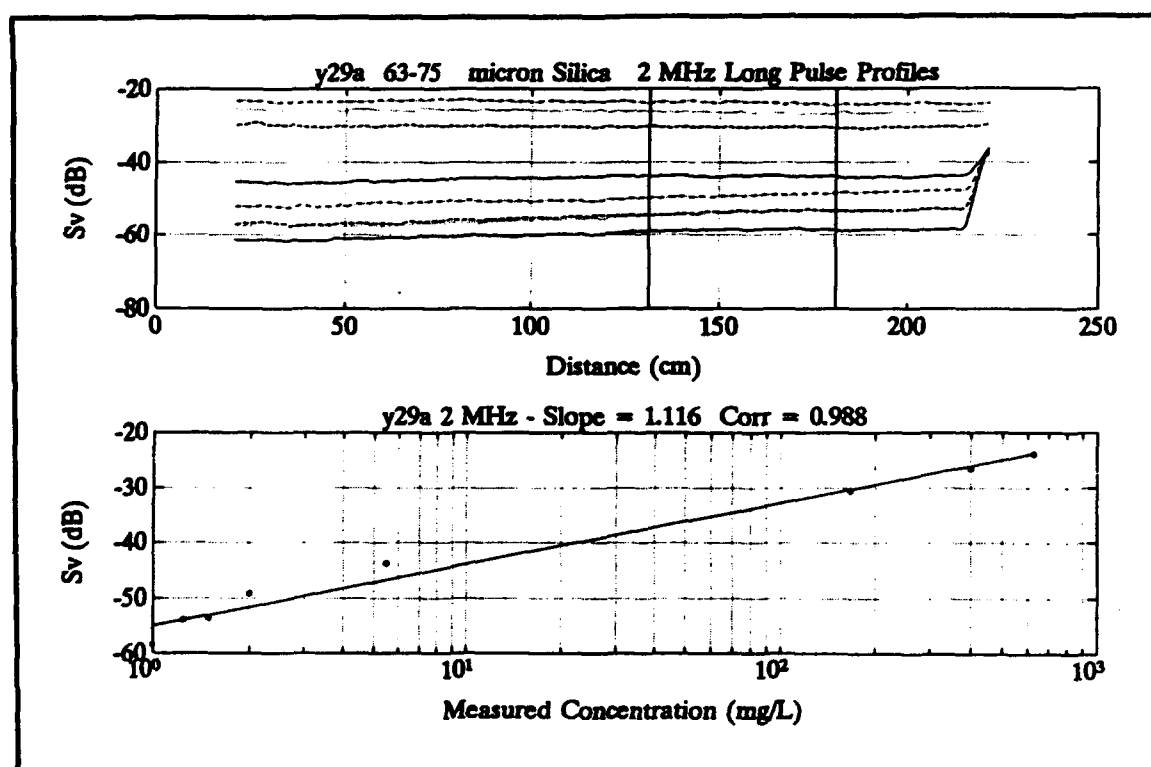
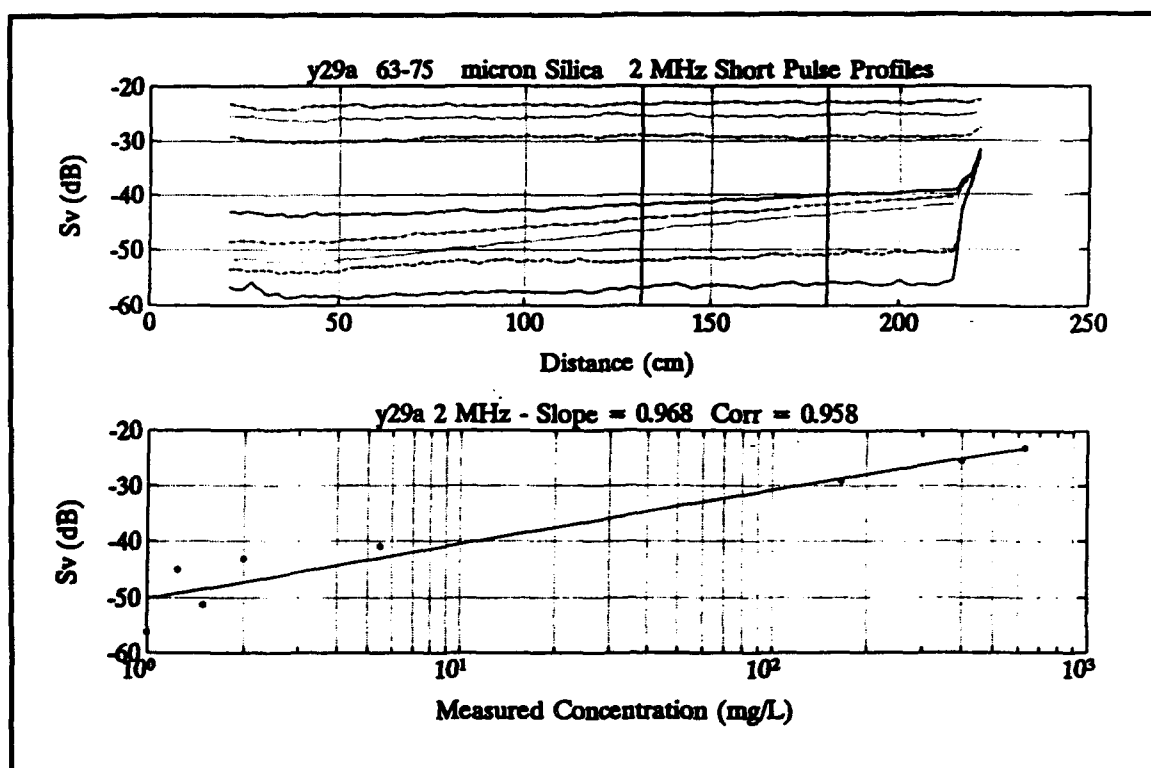


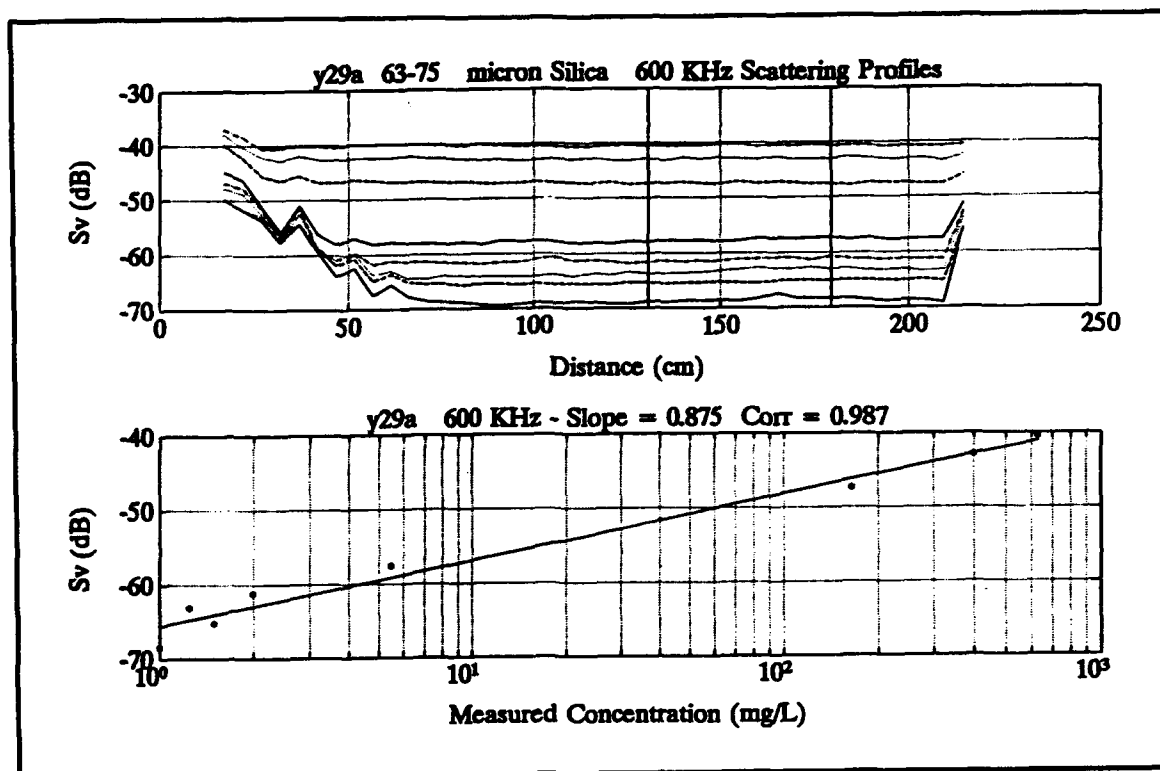


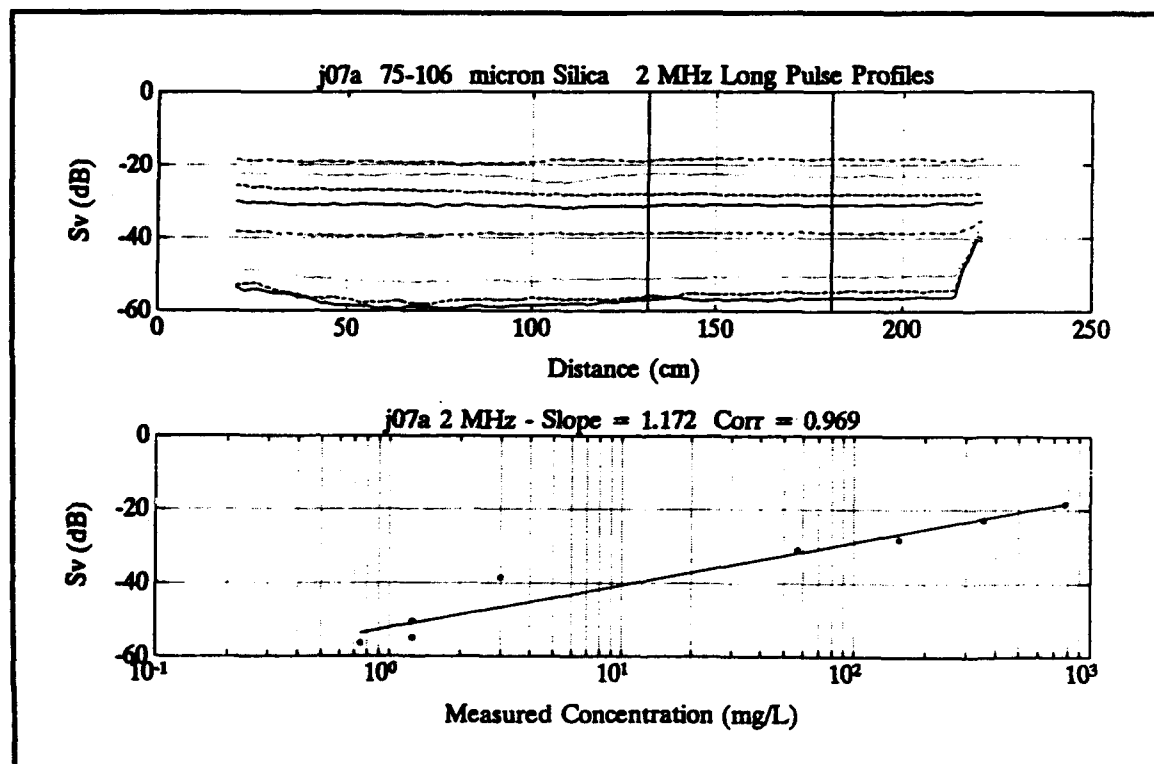
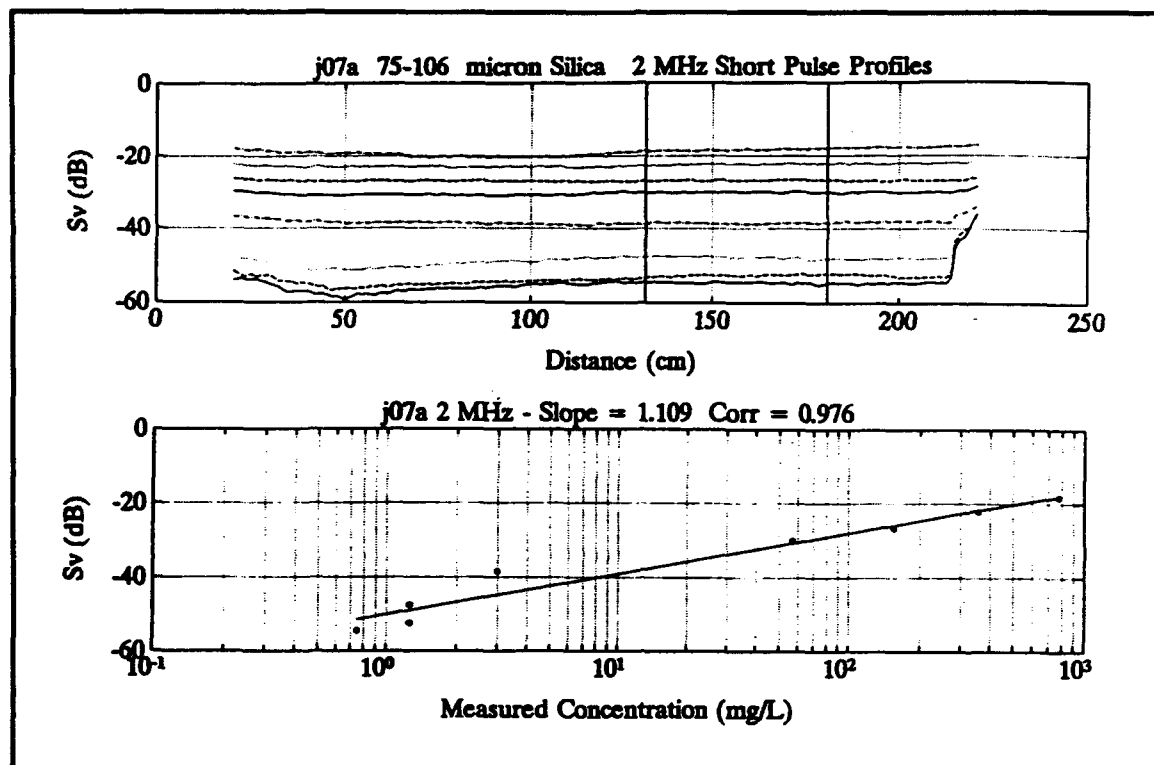


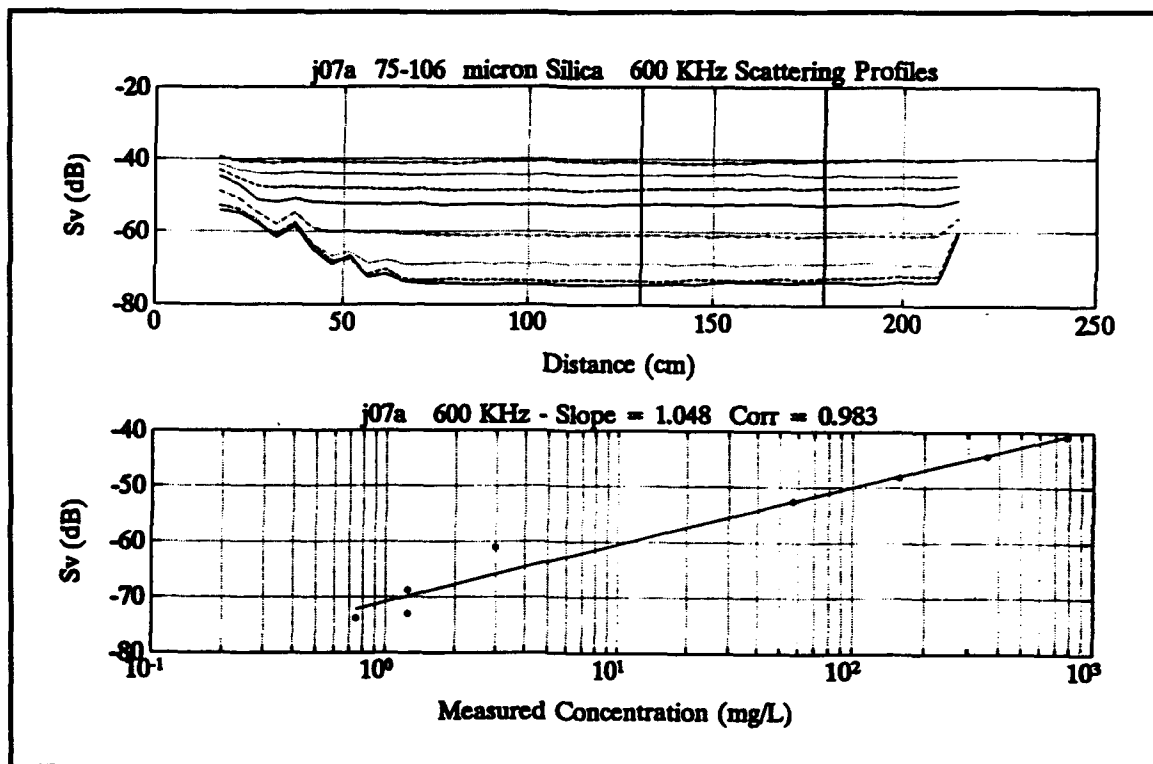


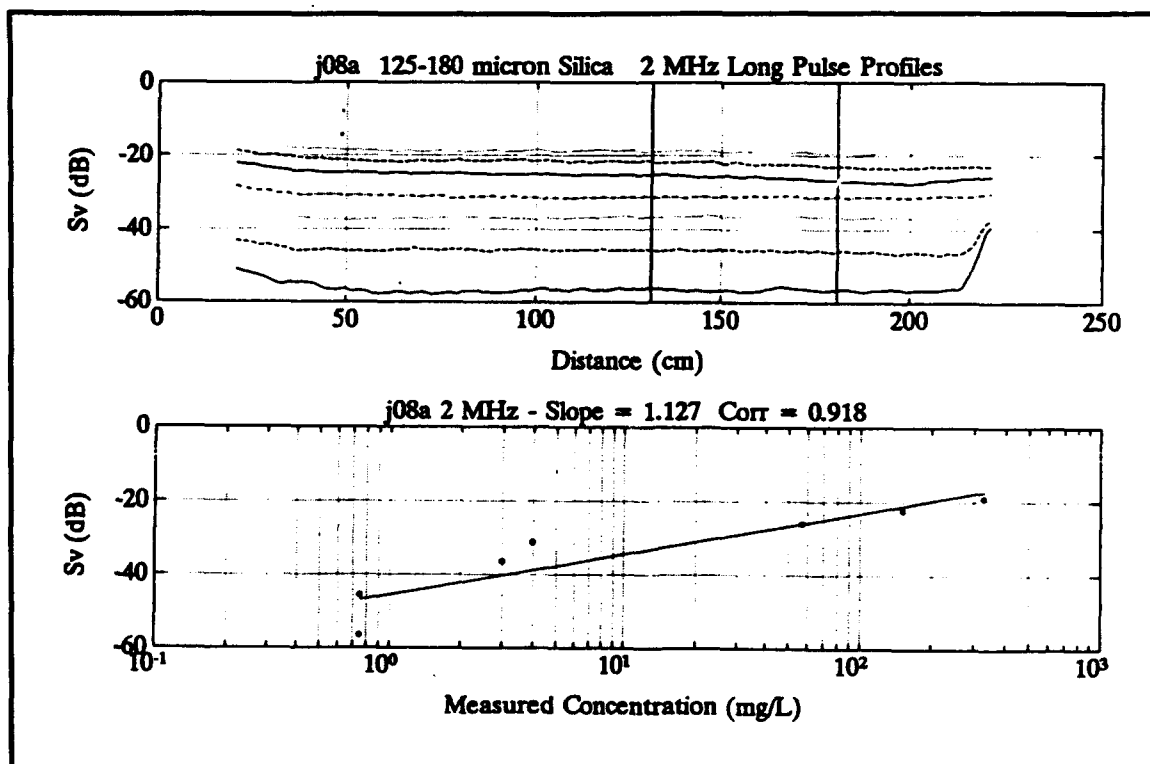
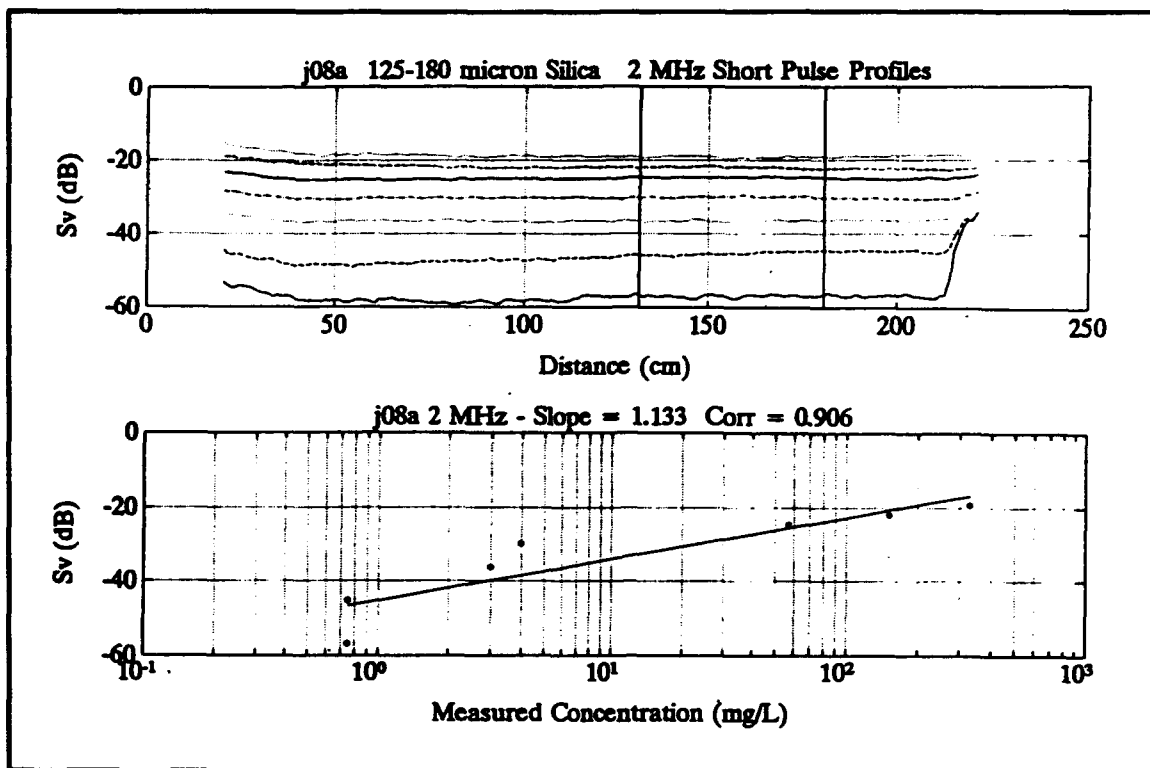


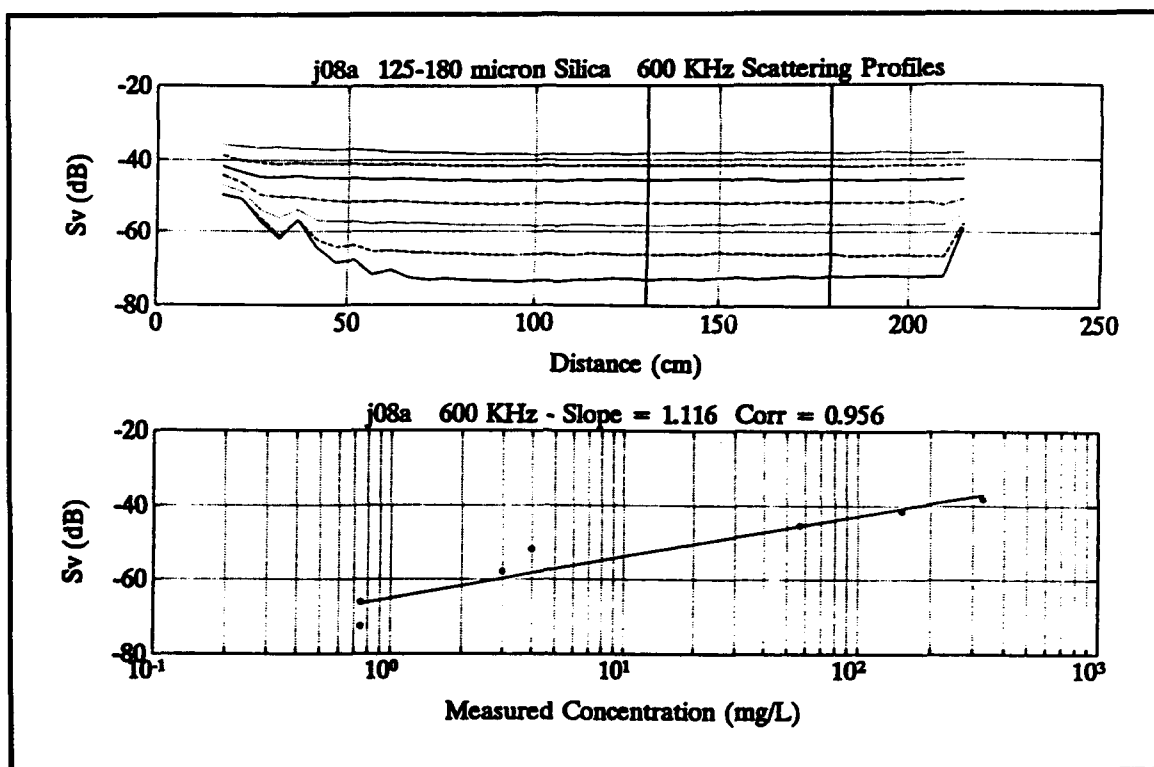


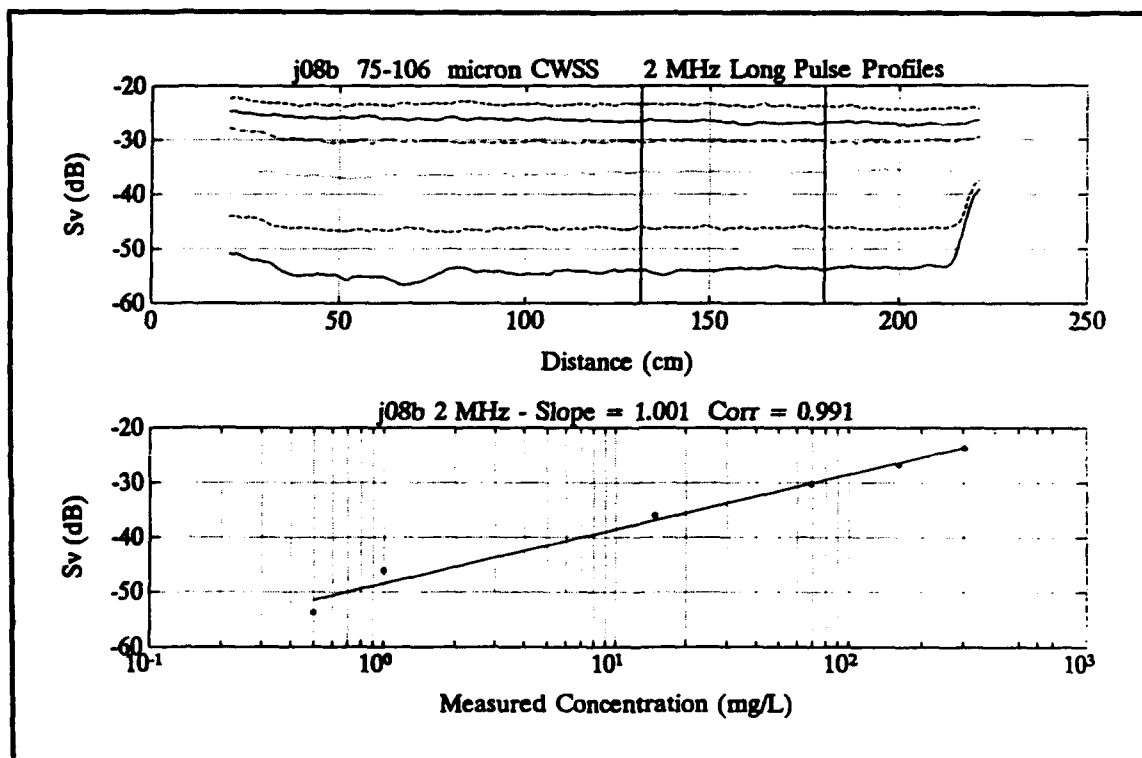
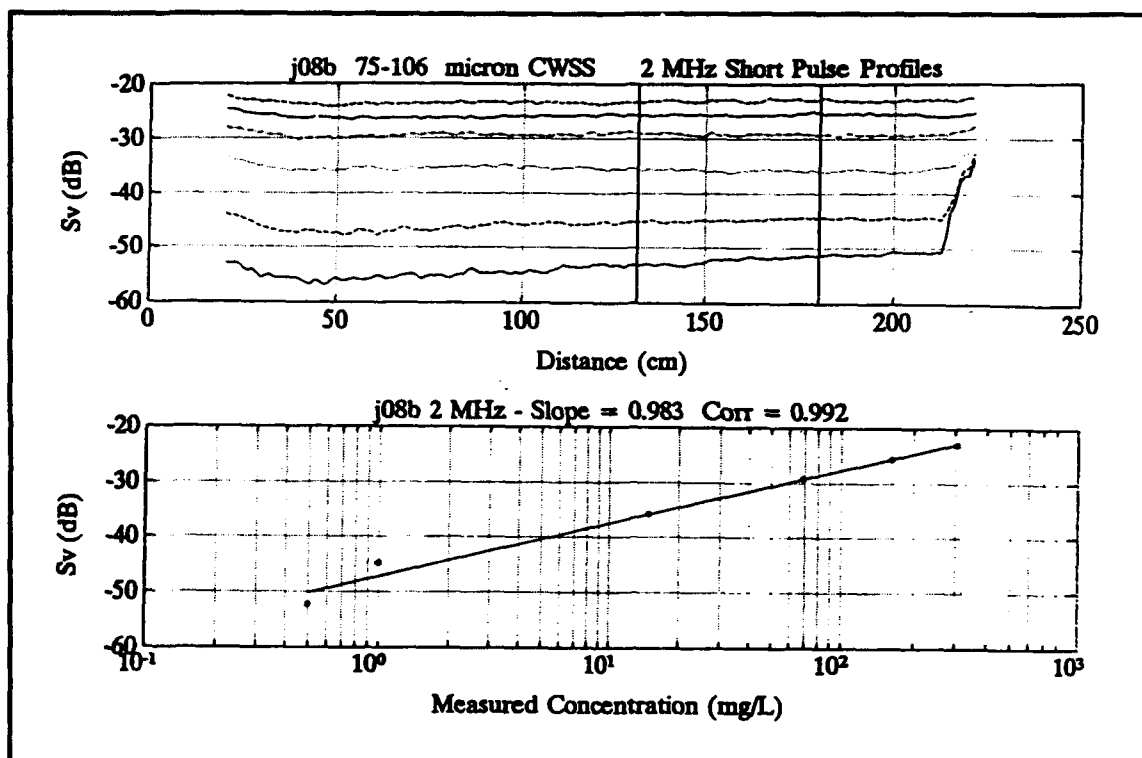


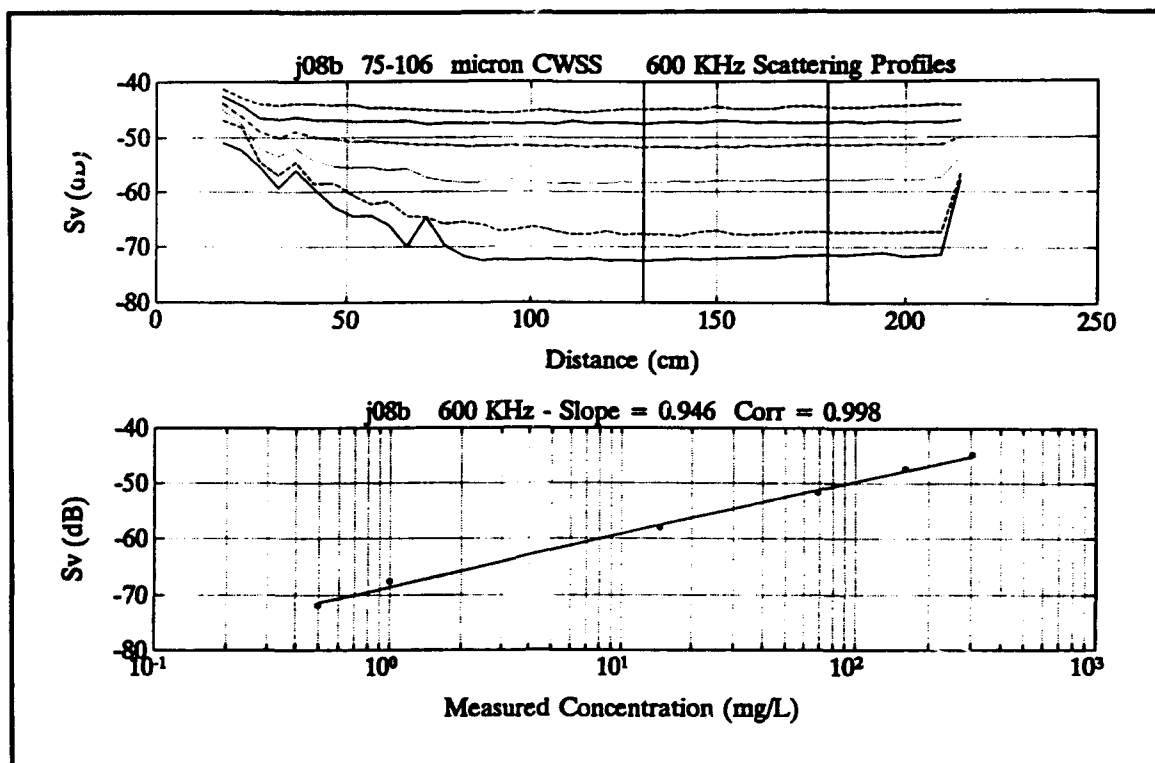


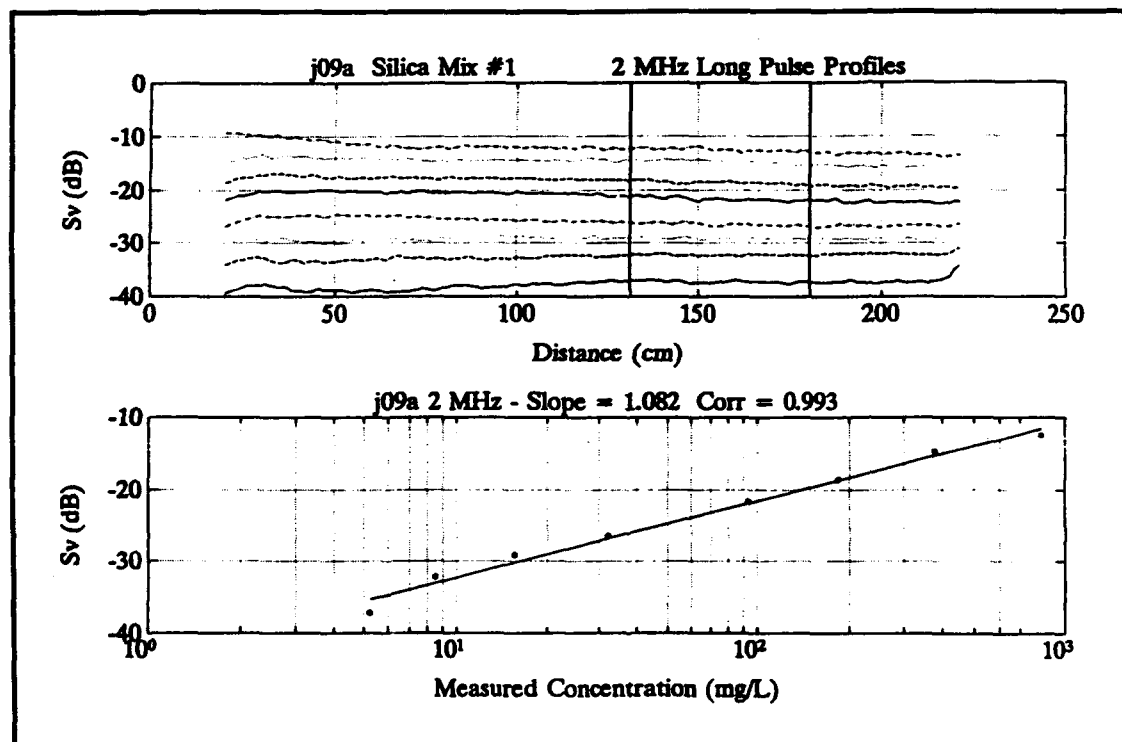
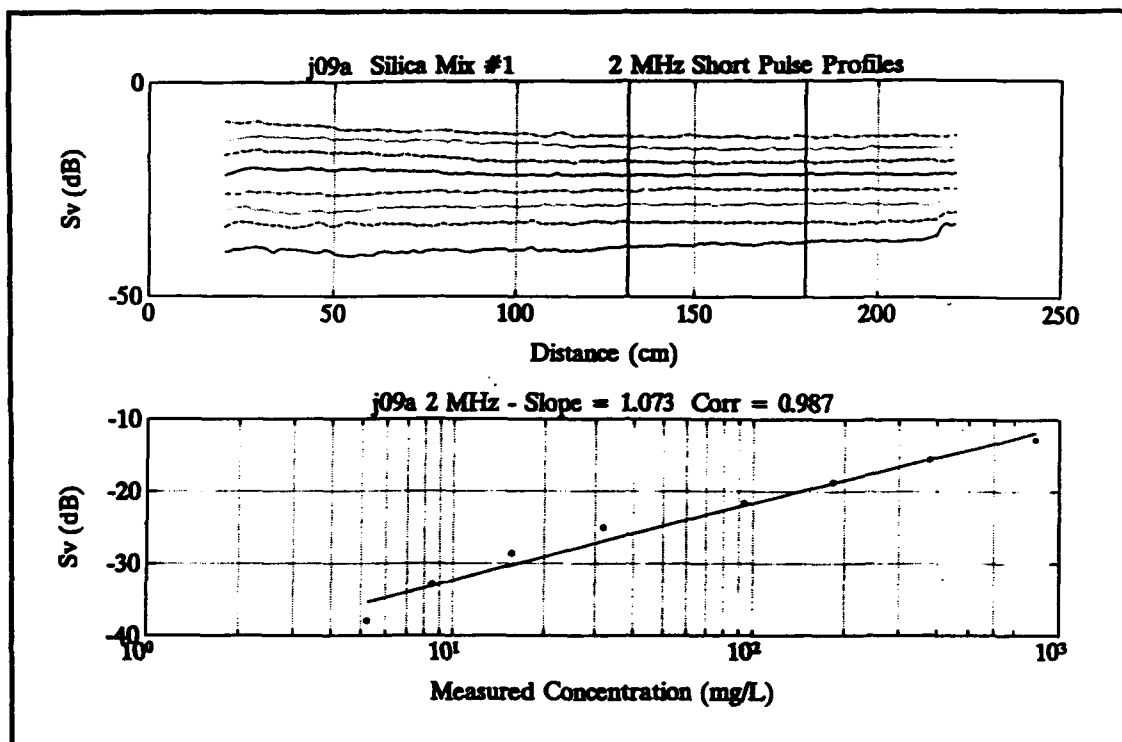


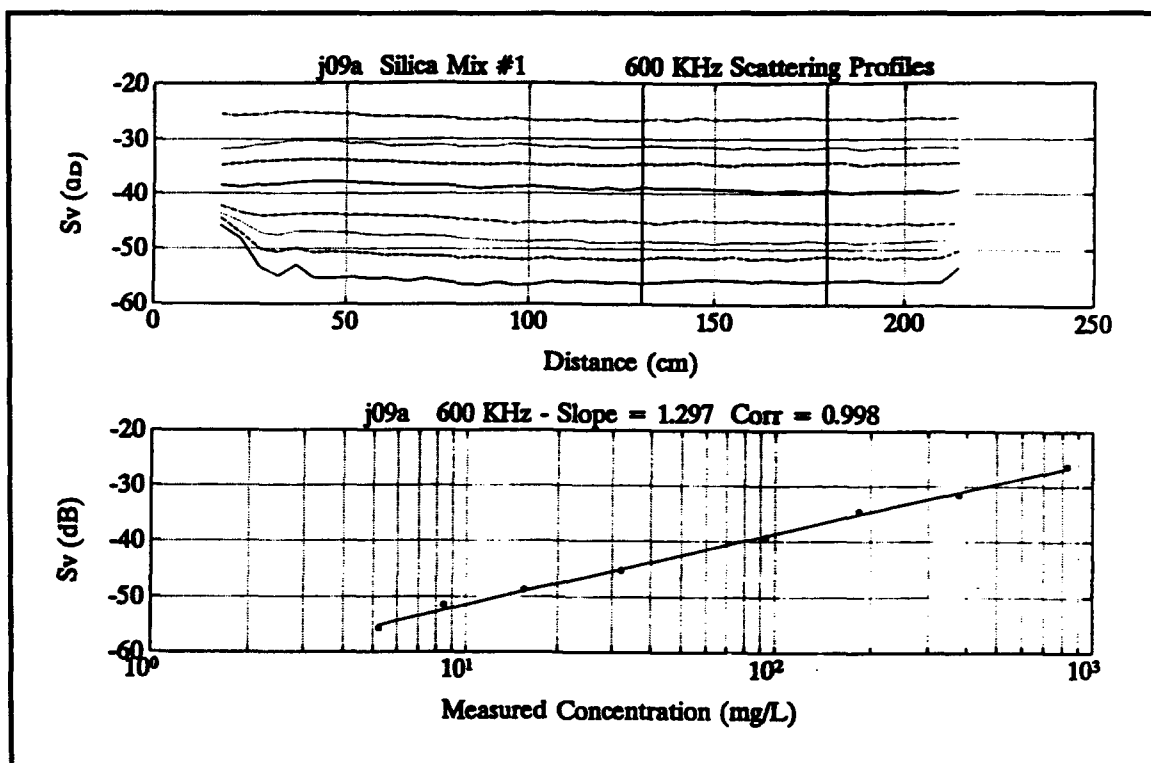


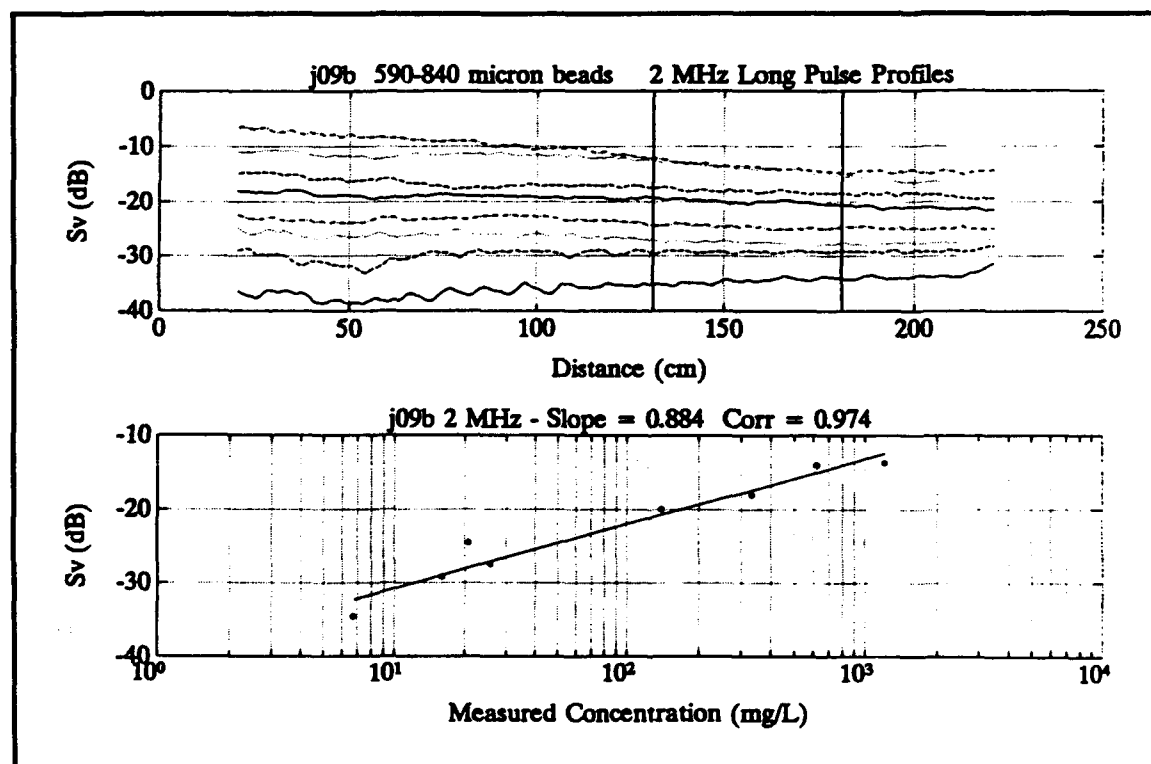
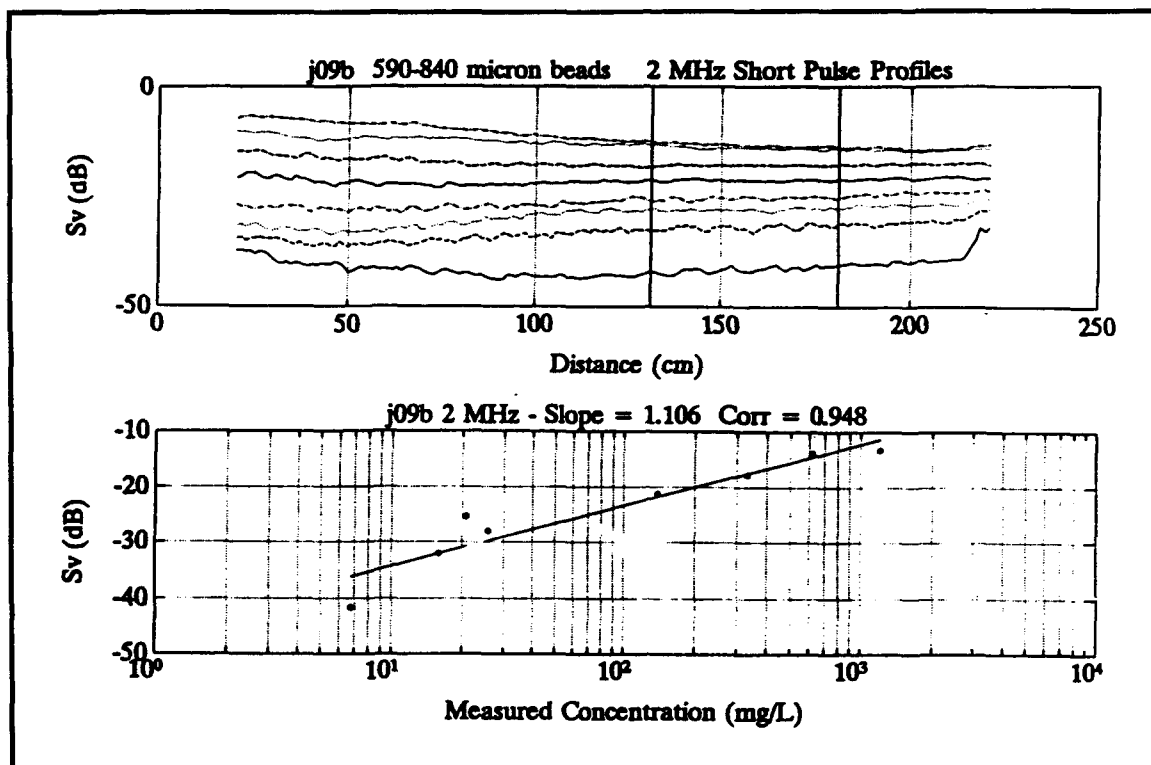


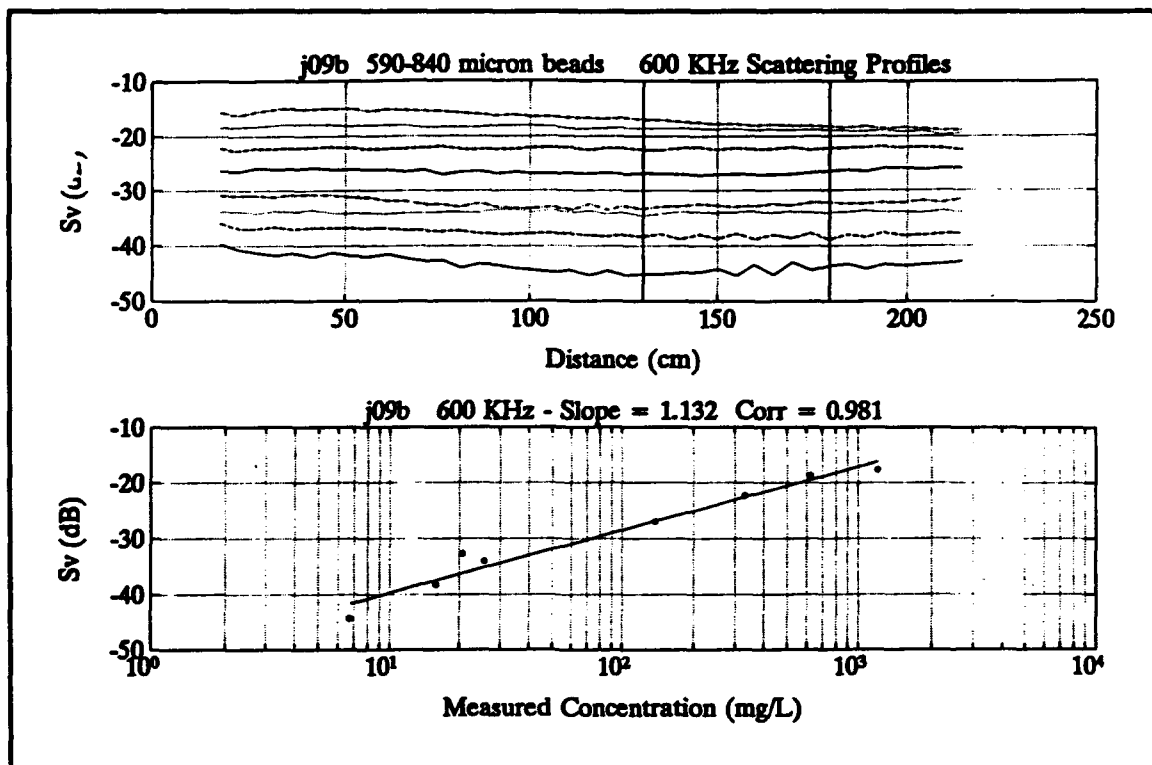


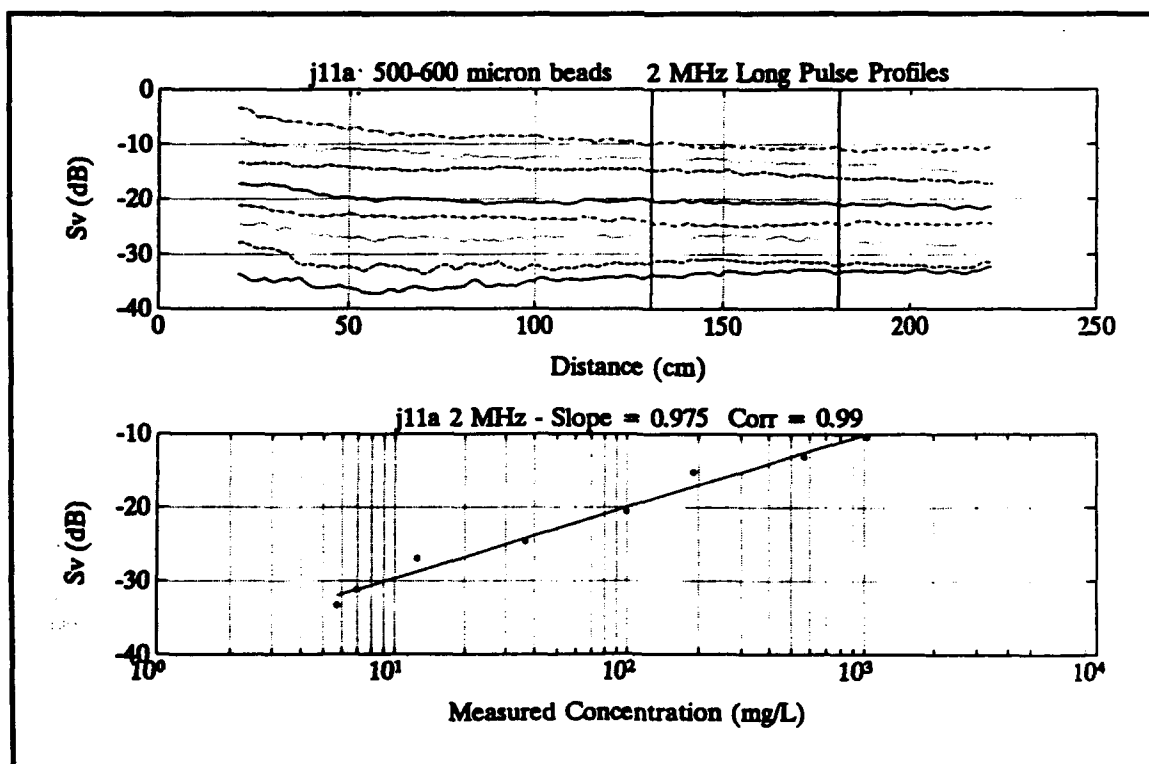
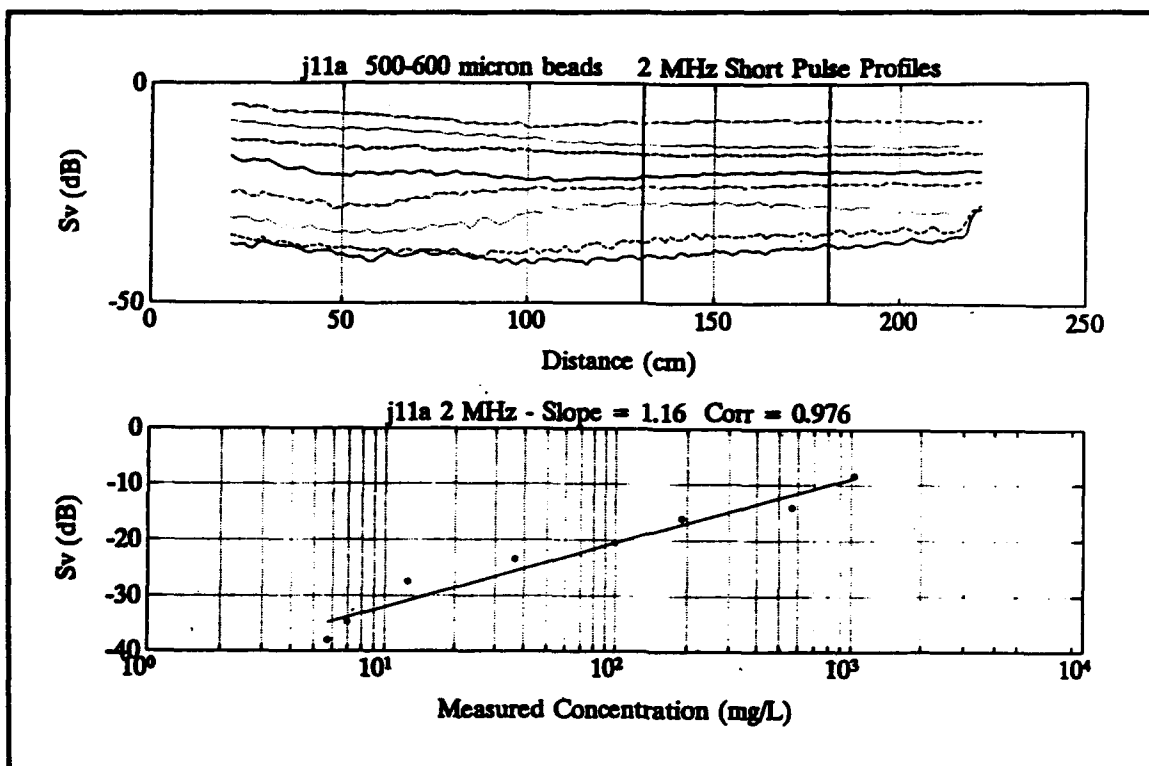


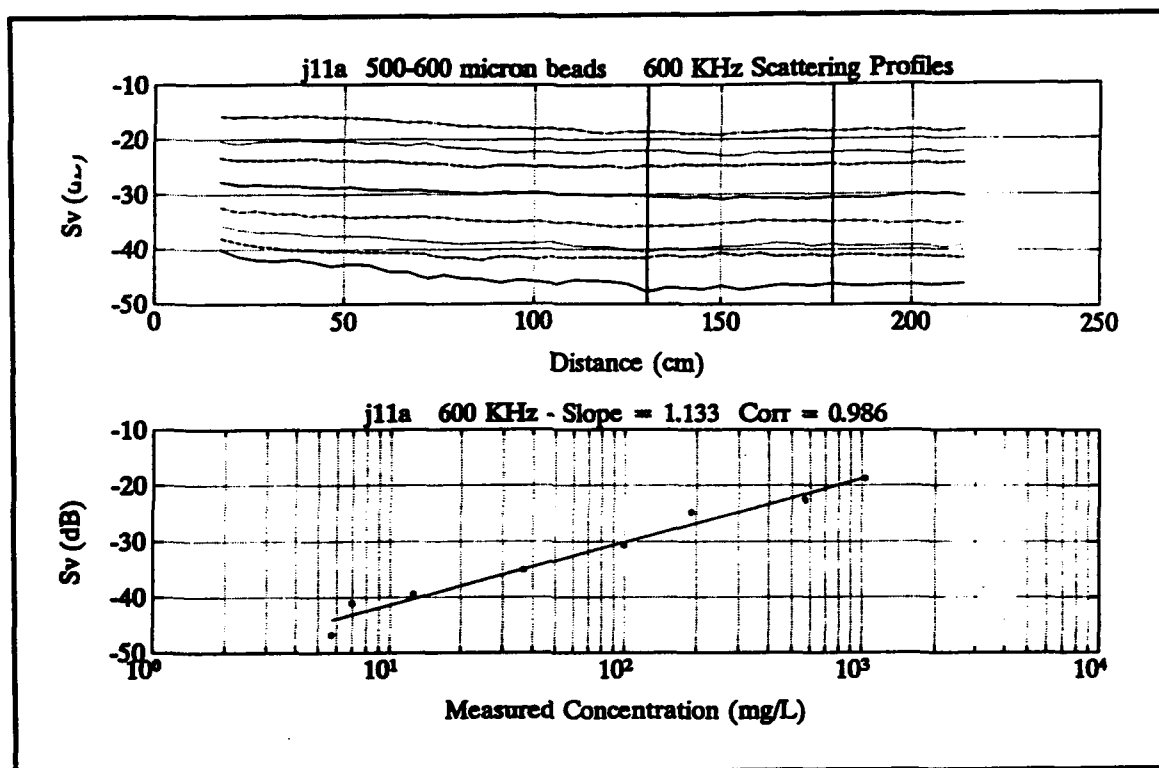


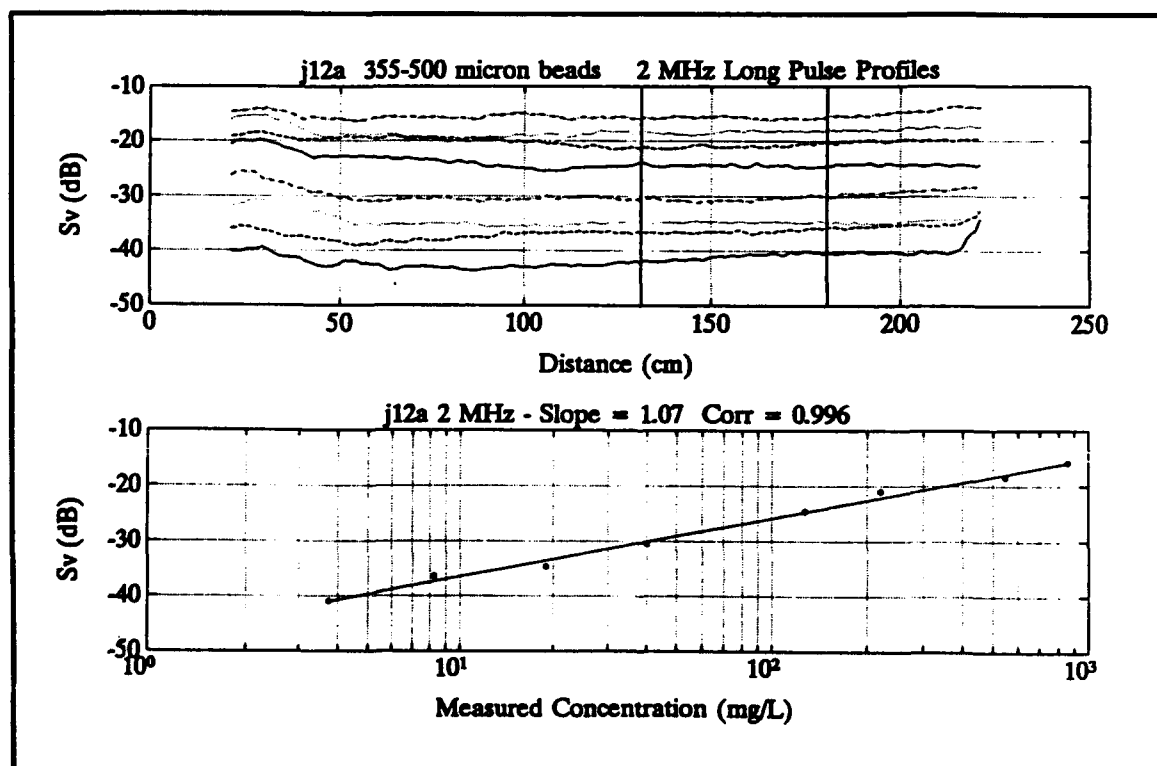
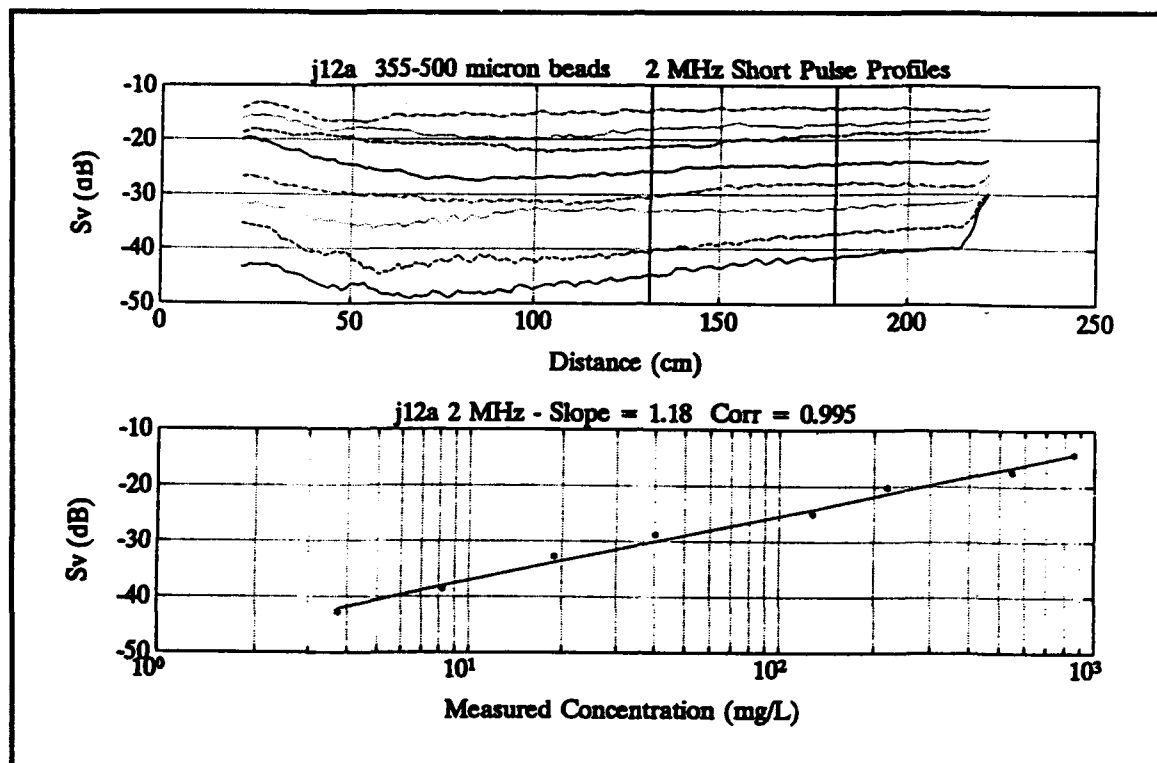


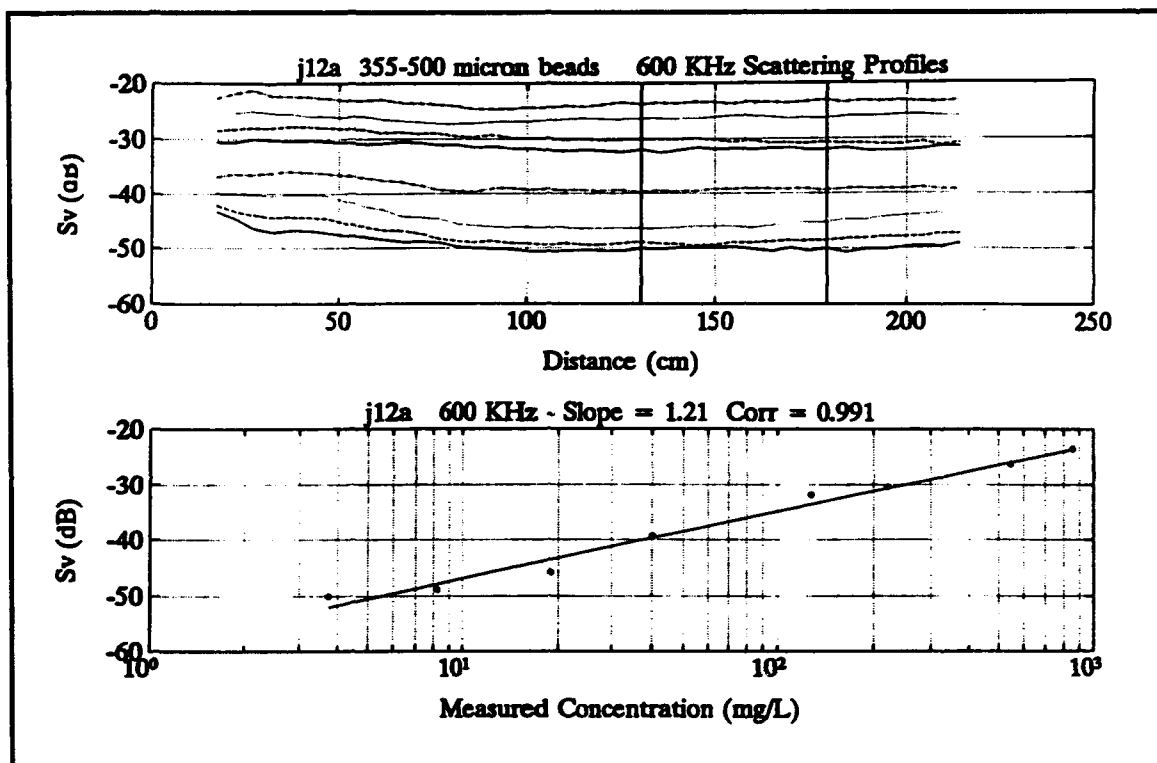


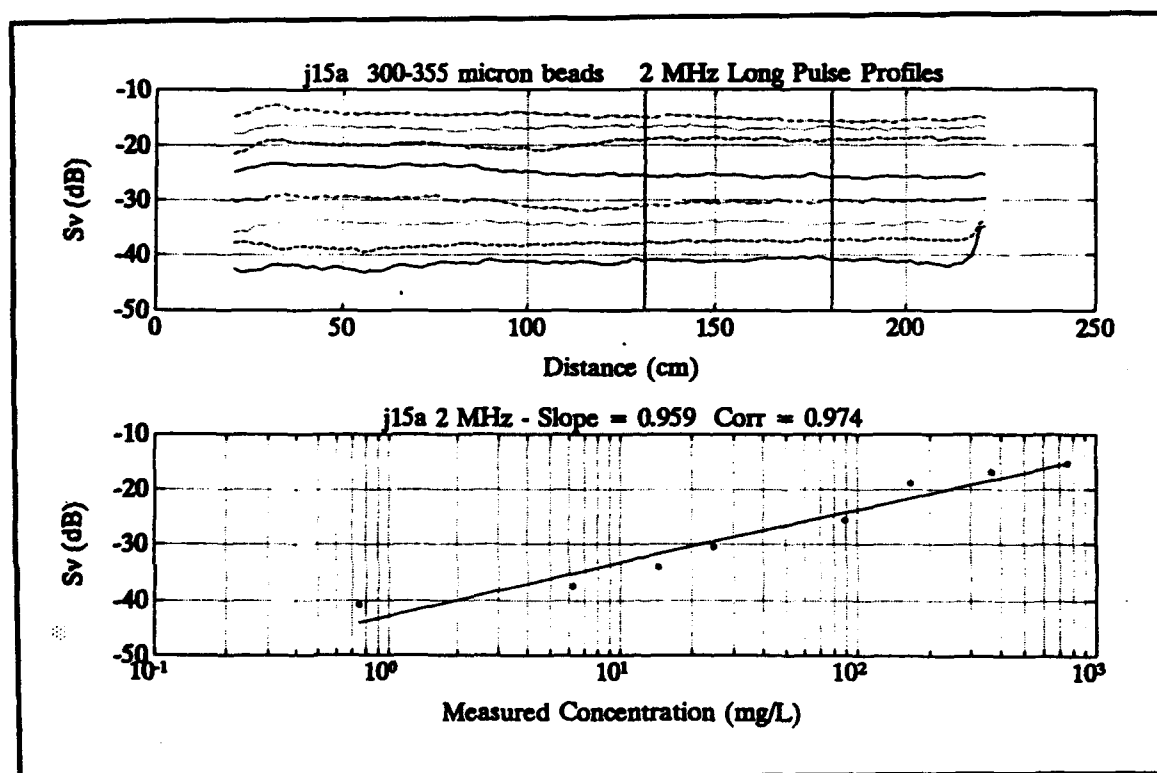
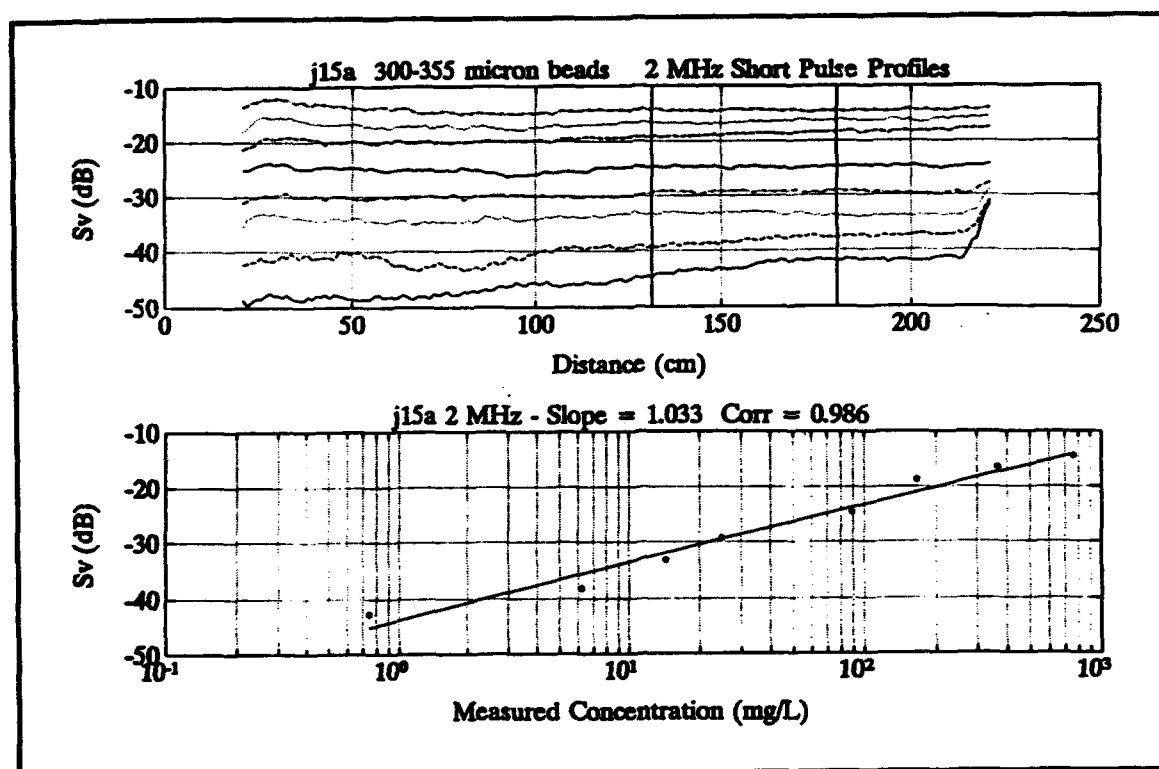


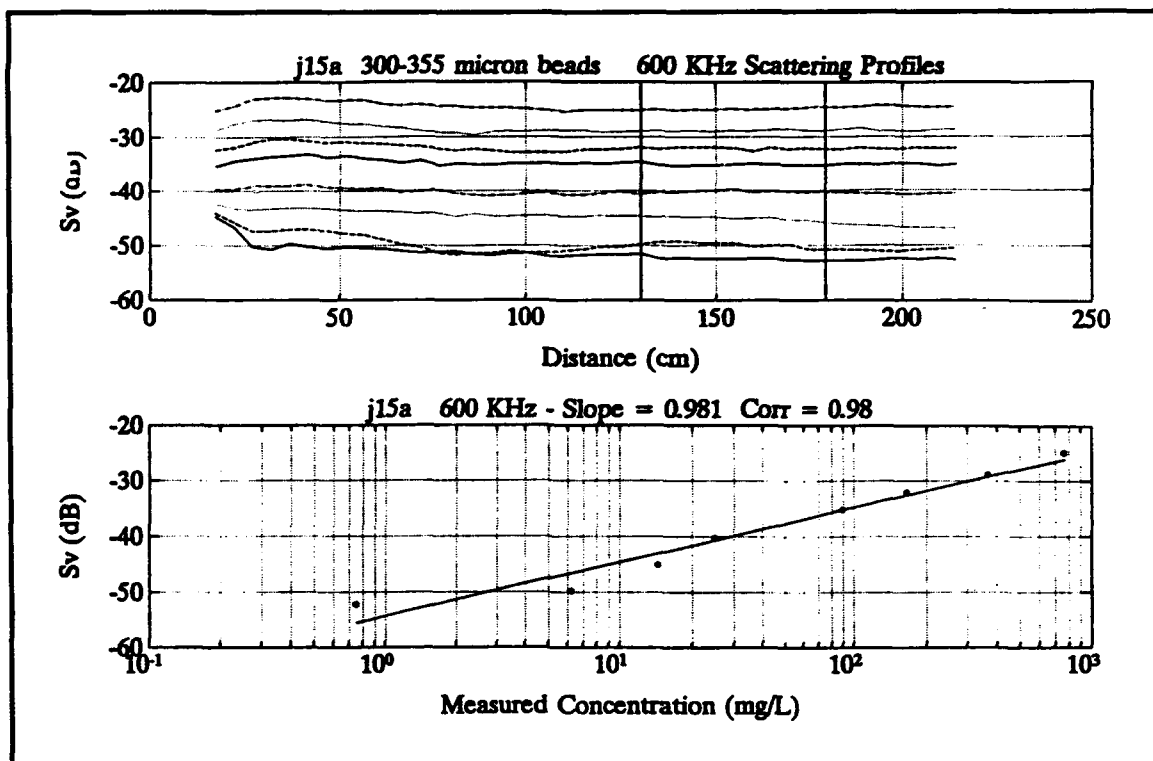


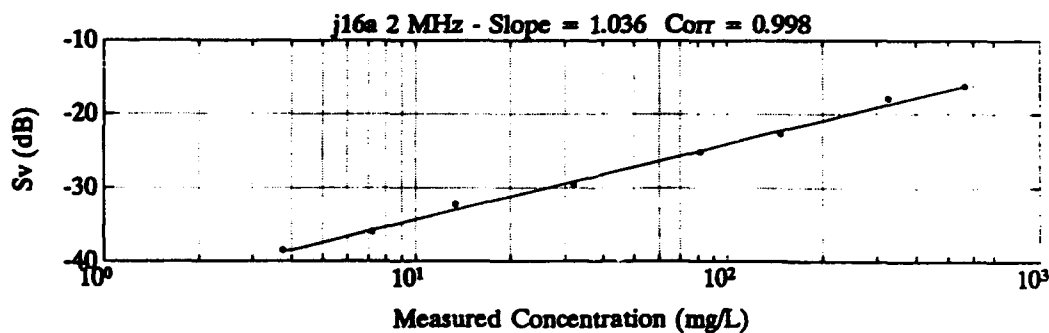
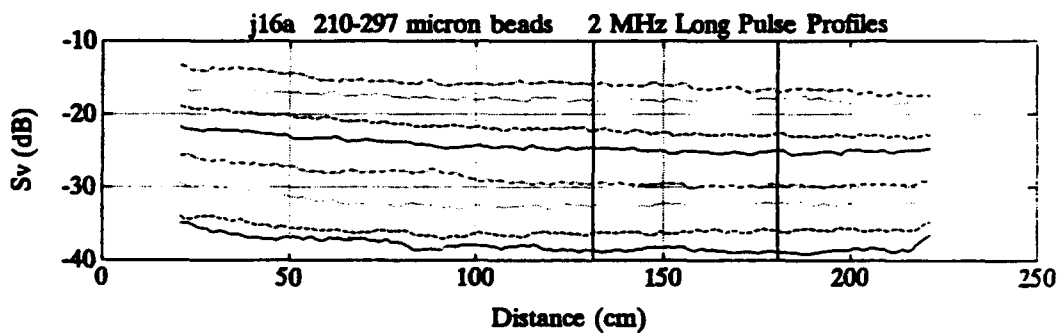
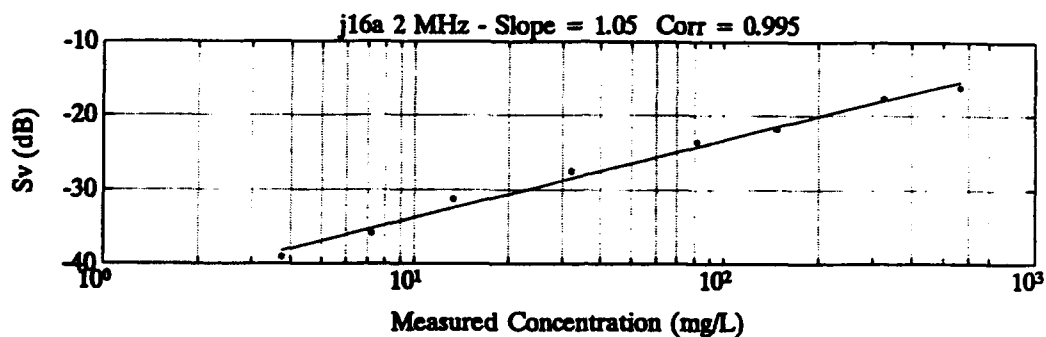
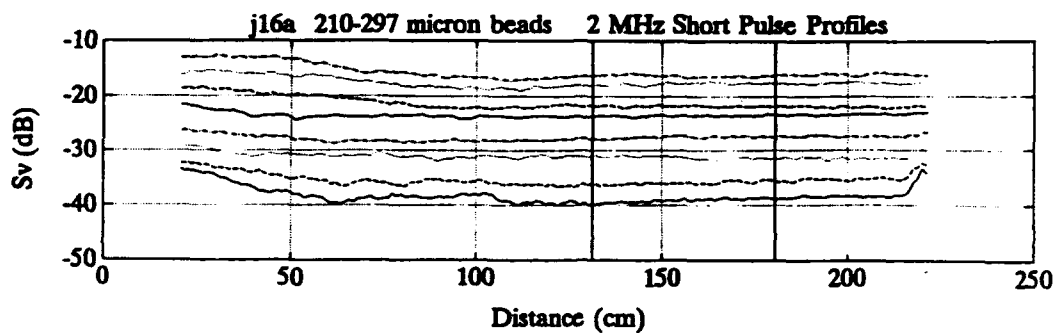


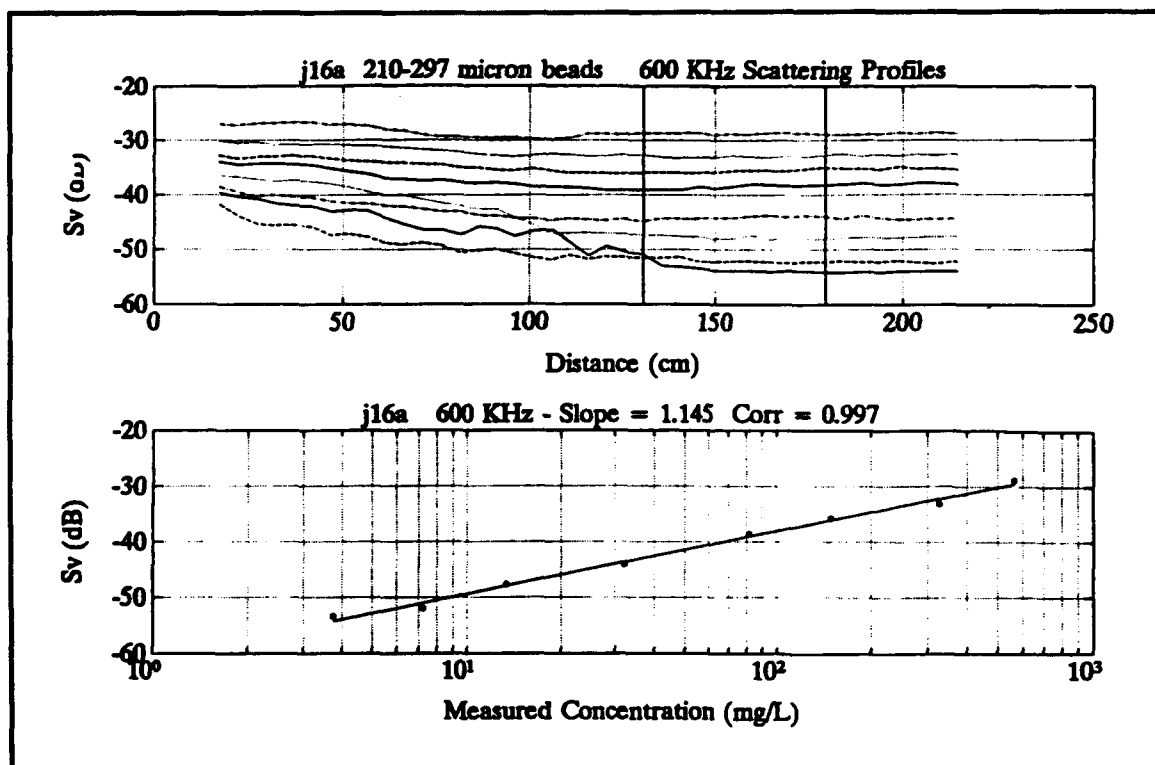


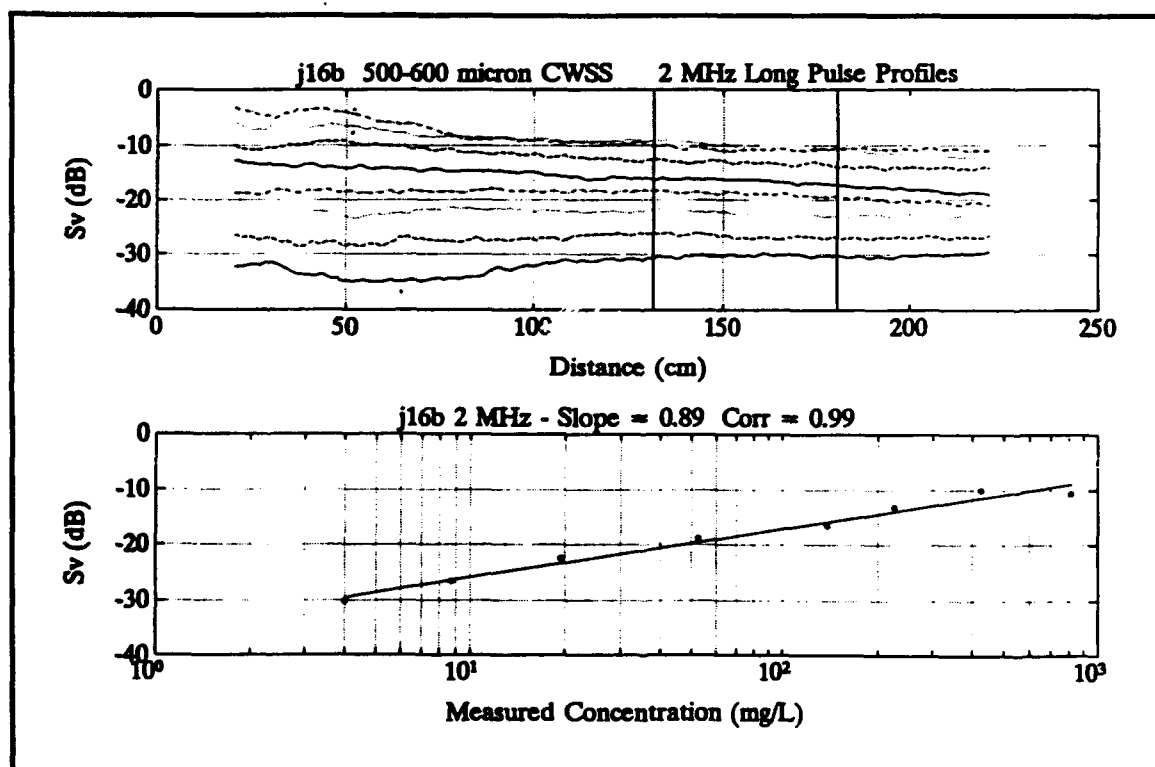
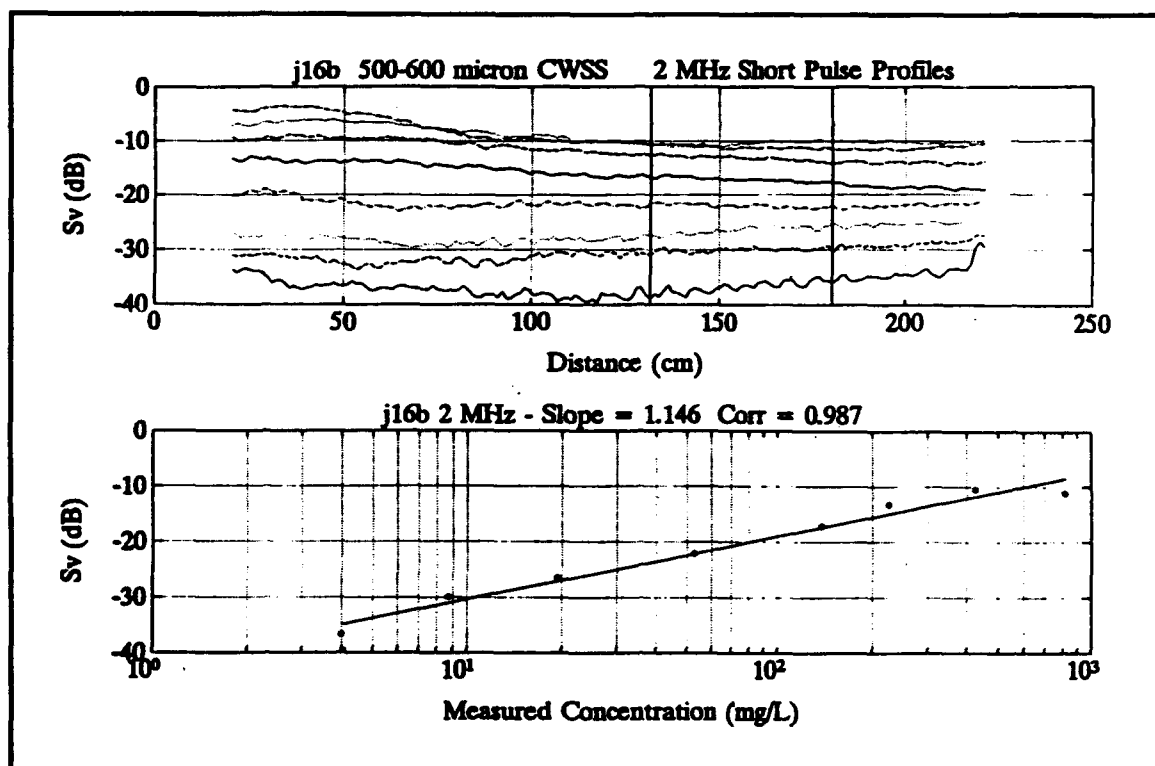


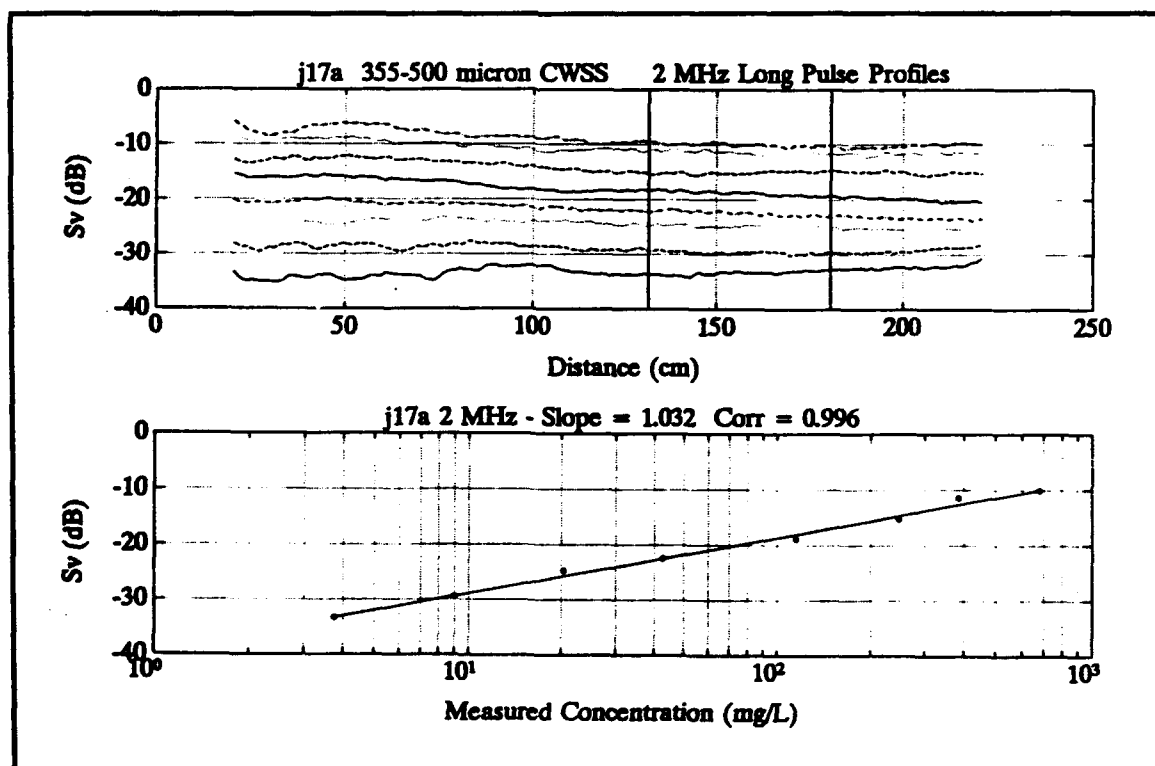
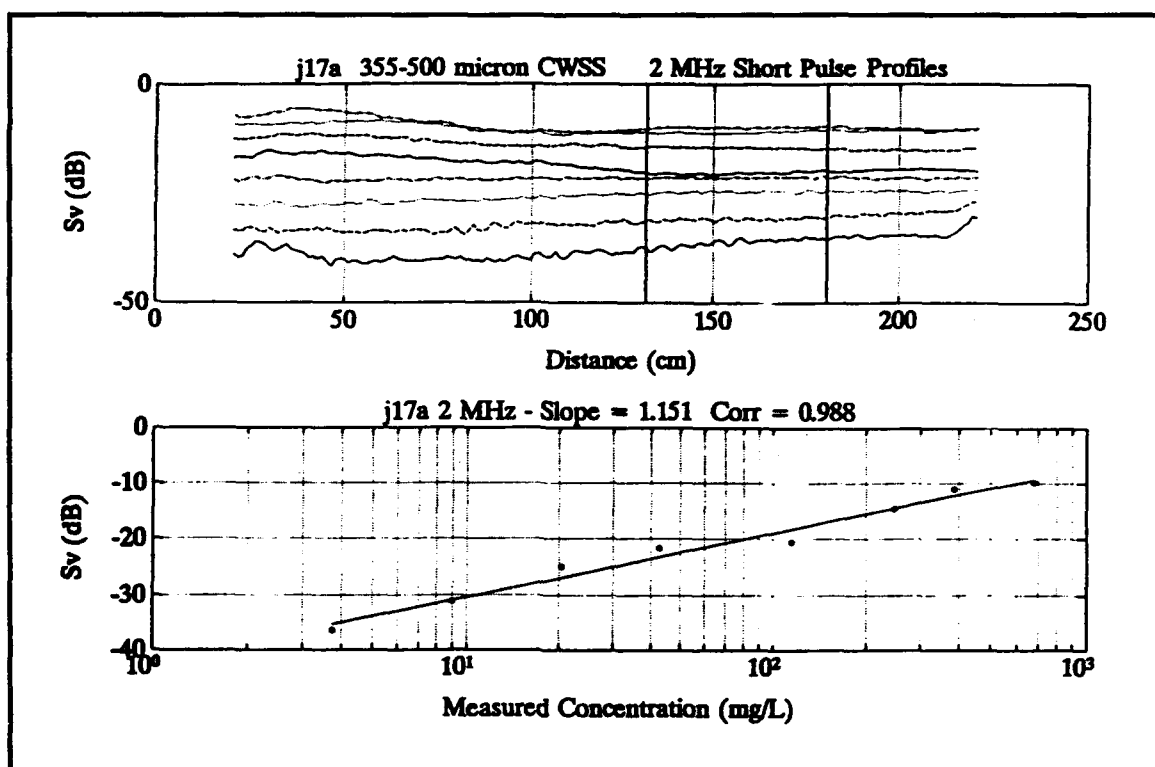


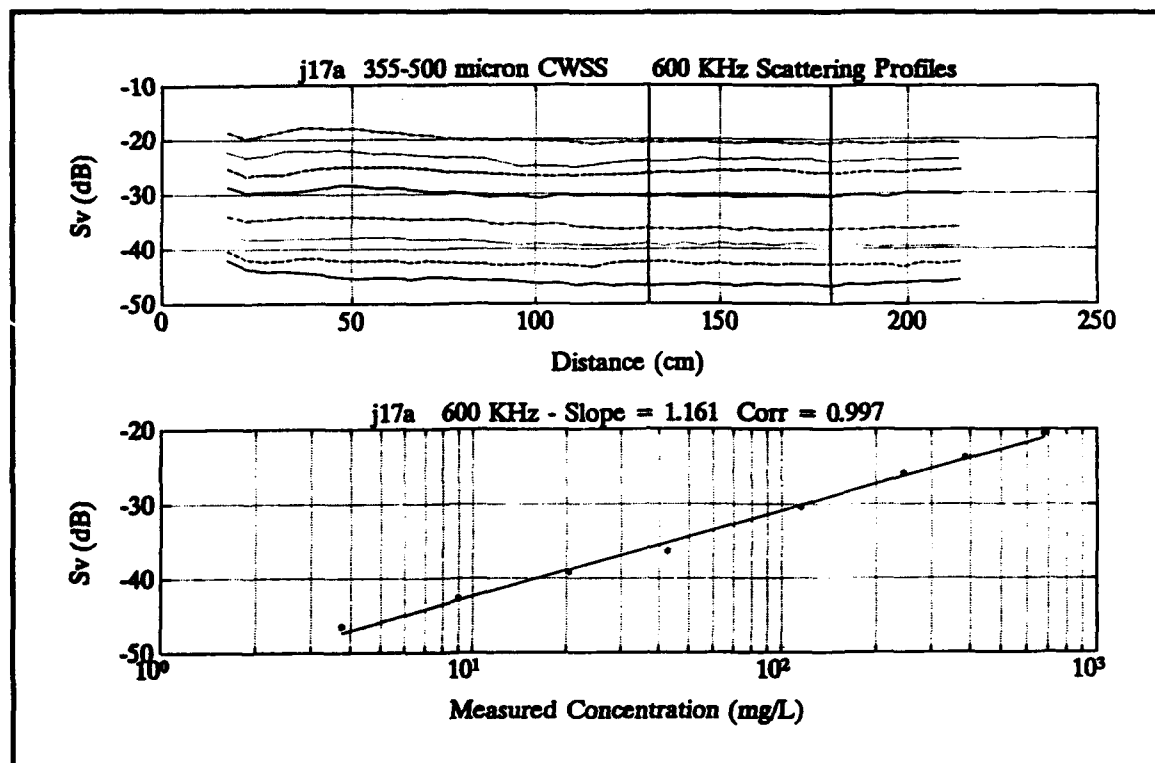












REPORT DOCUMENTATION PAGE

Form Approved
OMB No. 0704-0188

Public reporting burden for this collection of information is estimated to average 1 hour per response, including the time for reviewing instructions, searching existing data sources, gathering and maintaining the data needed, and completing and reviewing the collection of information. Send comments regarding this burden estimate or any other aspect of this collection of information, including suggestions for reducing this burden, to Washington Headquarters Services, Directorate for Information Operations and Reports, 1215 Jefferson Davis Highway, Suite 1204, Arlington, VA 22202-4302, and to the Office of Management and Budget, Paperwork Reduction Project (0704-0188), Washington, DC 20503.

1. AGENCY USE ONLY (Leave blank)	2. REPORT DATE August 1994	3. REPORT TYPE AND DATES COVERED Final report	
4. TITLE AND SUBTITLE Plume Measuring System (PLUMES) Calibration Experiment		5. FUNDING NUMBERS WU 32466	
6. AUTHOR(S) Atle Lohrmann, Craig Huhta			
7. PERFORMING ORGANIZATION NAME(S) AND ADDRESS(ES) SonTek, Inc., 7940 Silverton Avenue, No. 105, San Diego, CA 92126 JIMAR, University of Hawaii, Honolulu, HI 96822		8. PERFORMING ORGANIZATION REPORT NUMBER Technical Report DRP-94-3	
9. SPONSORING/MONITORING AGENCY NAME(S) AND ADDRESS(ES) U.S. Army Corps of Engineers, Washington, DC 20314-1000		10. SPONSORING/MONITORING AGENCY REPORT NUMBER	
11. SUPPLEMENTARY NOTES Available from National Technical Information Service, 5285 Port Royal Road, Springfield, VA 22161.			
12a. DISTRIBUTION/AVAILABILITY STATEMENT Approved for public release; distribution is unlimited.		12b. DISTRIBUTION CODE	
13. ABSTRACT (Maximum 200 words) <p>The Measurement of Entrainment and Transport work unit under the Dredging Research Program's Technical Area 1, entitled "Analysis of Dredged Material Placed in Open Water," developed the PLUMES MEasurement System (PLUMES) to monitor the transport of suspended sediment from dredging and dredged material disposal operations. This acoustic system can monitor nearly synoptically, both horizontally and vertically. To determine the relationship between PLUMES acoustic measurements and suspended sediment concentrations, a laboratory sediment calibration experiment was conducted. The experiment studied acoustic backscattering from particles equivalent in size to those commonly found at dredging and dredged material disposal sites. These particles were suspended in a calibration chamber built for the study. The experiment showed that backscatterance could be predicted and concentrations calculated using Rayleigh scattering theory and an acoustic calibration of PLUMES. This report describes the experiment and the results of the experiment. Data from each calibration run are presented in the Appendices.</p>			
14. SUBJECT TERMS Acoustic Acoustic backscatter intensity Laboratory calibration		15. NUMBER OF PAGES 152	
		16. PRICE CODE	
17. SECURITY CLASSIFICATION OF REPORT UNCLASSIFIED	18. SECURITY CLASSIFICATION OF THIS PAGE UNCLASSIFIED	19. SECURITY CLASSIFICATION OF ABSTRACT	20. LIMITATION OF ABSTRACT